Faculty of Aerospace Engineering

Incremental Nonlinear Flight Control for Fixed-Wing Aircraft

Design and Implementation of Incremental Nonlinear Flight Control Methods on the FASER UAV

Wim van Ekeren

December 15, 2016

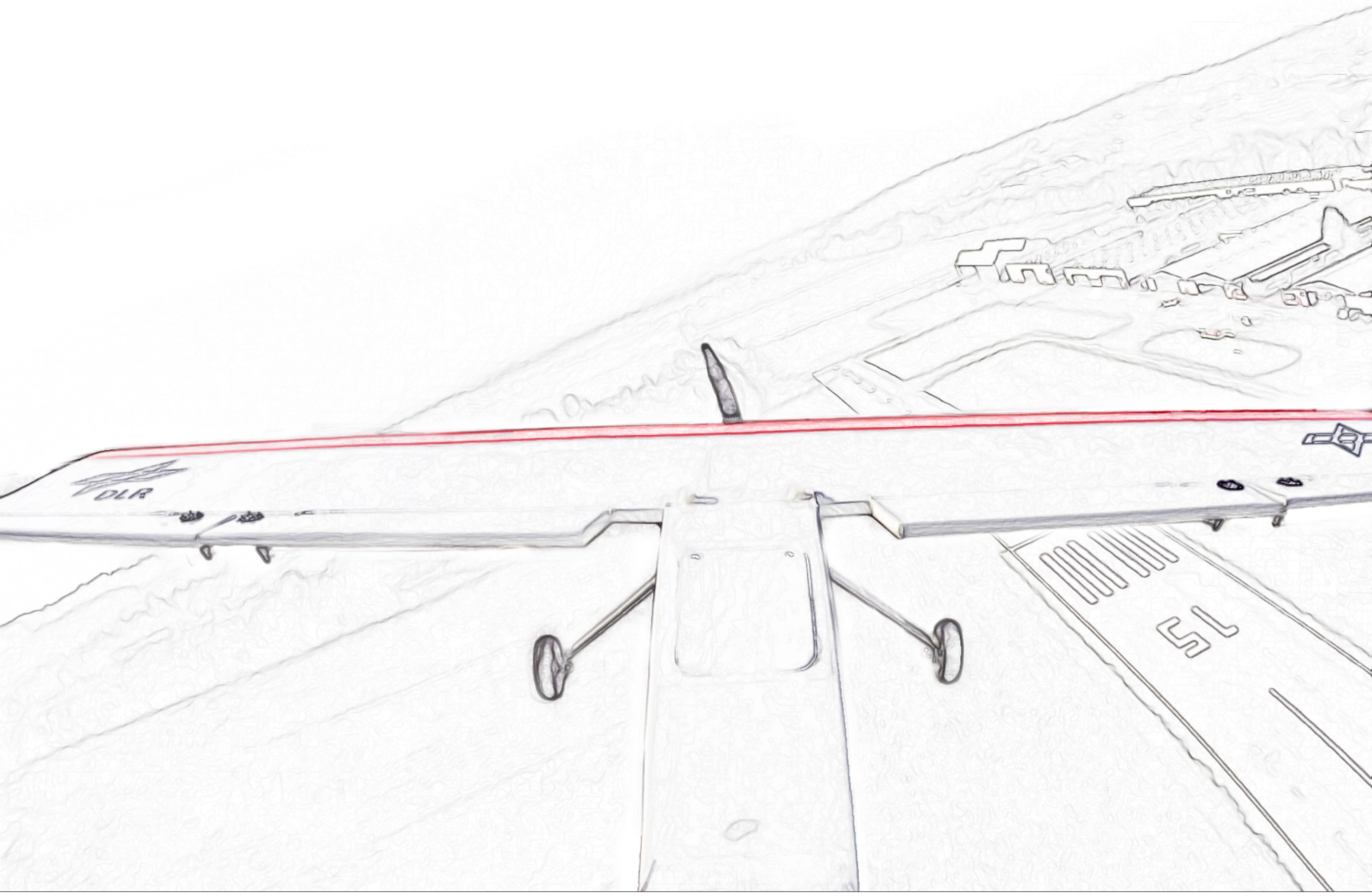

TU Delft Delft University of Technology

Challenge the future

Incremental Nonlinear Flight Control for Fixed-Wing Aircraft

Design and Implementation of Incremental Nonlinear Flight Control Methods on the FASER UAV

Master of Science Thesis

For obtaining the degree of Master of Science in Aerospace Engineering
at Delft University of Technology

Wim van Ekeren

December 15, 2016

Faculty of Aerospace Engineering · Delft University of Technology

Delft University of Technology

Delft University Of Technology
Department Of
Control and Simulation

The undersigned hereby certify that they have read and recommend to the Faculty of Aerospace Engineering for acceptance a thesis entitled **"Incremental Nonlinear Flight Control for Fixed-Wing Aircraft"** by **Wim van Ekeren** in partial fulfillment of the requirements for the degree of **Master of Science**.

Dated: December 15, 2016

Readers:

Dr. Q. P. Chu

Dr.ir. G. Looye

Dr.ir. D.M. Pool

Dr.ir. B.F. Lopes dos Santos

ir. E.J.J. Smeur

Acknowledgements

This thesis starts without any formula or use of words like 'nonlinear' or 'incremental'. I am thankful to many people that gave me feedback and inspiration during this thesis project and throughout my studies and therefore I am happy that there is a small place that I can use to mention at least some of them.

Regarding the thesis itself, I want to thank my supervisors for motivating me at all times. Meetings with Dr. Qiping Chu were always positive and motivating, which helped me to keep up the energy and inspiration that was necessary to deliver this result. I also have great respect for the knowledge and experience of my supervisor at the DLR, Dr. Gertjan Looye. It helped me to reflect on the practical aspects to test the different control laws in a meaningful way.

With respect to my time at the German Aerospace Center (DLR) at the department of System Dynamics and Control, I am very grateful for the support I received both from Gertjan himself, and from the other colleagues that made the flight tests happen. I want to thank Andreas Klöckner, Nir Kastner, Richard Kuchar and Reiko Müller for their persistance in all setbacks even though the delays and additional efforts conflicted with other projects at the institute.

The discussions I had with Paul Acquatella, researcher at DLR, on the more theoretical part of the work were extremely helpful. The thesis would not be at the same level if I did not get his valuable feedback. Furthermore, I feel very honored to be a contributer of his submitted paper.

As this thesis concludes my MSc studies at the department of Control and Simulation, I feel I have to acknowledge the people that were important over the entire course of the past three years. Among these, I especially want to mention Prof. Max Mulder and thank him for his extreme dedication to the department. Although professors are usually respected for their merits of research and Prof. Mulder and the entire department surely are well-known for high-quality work within the research community, I feel that the success is owed as much to the enthusiasm with which he teaches both in BSc and MSc courses. The complete atmosphere at the department is one in which people are motivated for the subjects and inspired to work on the topics they like. It holds for many of us, I think, that without the feeling to be an especially hard-working student, good quality research is delivered and high grades are obtained. I also want to thank Dr. Erik-Jan van Kampen, Dr. Coen de Visser and Dr. Qiping Chu and all other staff for their motivation and enthusiasm in teaching. It has been a great pleasure studying here.

Furthermore, I cannot let my parents and my two brothers go unmentioned, although they did not have much influence on the content of the work. Arie and Roel, if reading through this thesis makes you feel impressed, keep in mind that I do respect you much more. Don't fool yourself into being blown away by differential equations. Finally, I am also very thankful for all support of my parents. In the thesis of my cousin (Klamer, 2007), I noticed an excellent phrase from the book *'Pinkeltje en de raket'*, by Dick Laan. Regarding my studies, it applies just as much to the relation with me and my parents. So I happily share it over here as well. After Pinkeltje sees the rocket flying, the conversation between Pinkeltje and Pinkelprof reads:

> *'Wat geweldig knap van u om zoiets te maken!' riep Pinkeltje uit. Meneer Pinkelprof lachte en zei: 'Het is ook een heel werk geweest om de raket bestuurbaar te maken.' 'Wat zegt u? Bestuurbaar? Wat is dat eigenlijk?' vroeg Pinkeltje. 'Bestuurbaar,' antwoordde meneer Pinkelprof, 'wil zeggen dat ik de raket overal naar toe kan sturen, waar ik maar wil. Naar boven; naar beneden; naar rechts; naar links. Ik kan de raket zelfs in de lucht stil laten staan!' Pinkeltje wreef eens met zijn vinger langs zijn neus, en zei toen: 'Ik begrijp er niets van, maar ik vind u alleen heel, héél erg knap!'*

Summary

In the context of fault-tolerant flight control (FTFC), various types of incremental nonlinear control methods have been previously proposed that should overcome important challenges that are imposed by the use of nonlinear, model-based flight control systems. This work presents an analysis, design and implementation of promising incremental nonlinear dynamic inversion (INDI) and incremental backstepping (IBS) control laws for a fixed-wing aircraft. Flight tests on an Unmanned Aerial Vehicle (UAV) validate the control design and confirm many of the advantages of these methods. A summary of the contribution is split up into three parts.

First, an analysis is done on the performance of incremental nonlinear dynamic inversion for angular rate control. Incremental nonlinear dynamic inversion is shown to see great similarities with ordinary PI(D) control. When not including the actuators of the system, the gains of an incremental PI controller can be derived from the INDI control law, yielding an equivalent control law. In a similar manner, similarities can be derived between INDI and a non-incremental PI control law that does *not* need a feedback of the state derivative. Simulations on a model of the fixed-wing UAV support the findings. Besides a comparison with PI control, the validity of the assumptions of incremental methods are assessed for the case of angular rate control for fixed-wing aircraft. Steady state tracking errors in the inner control loop are caused by the assumption that the control-independent part of the acceleration does not change significantly. The steady state errors are directly related to the so-called increment delay, the effective time over which an incremental control action is given. Hence, the negative effect of neglecting the system dynamics increments can be mitigated by using faster actuators or by decreasing the acceleration measurement delay.

Secondly, integrated controller designs are presented for the attitude control of the aircraft. Control laws are designed for both the Euler attitude angles, as well as for the aerodynamic attitude. This is done using multi-loop nonlinear dynamic inversion and the Lyapunov-based backstepping procedure, yielding a multi-loop INDI and an IBS controller. Supported with model validation using flight data from open-loop experiments, the robustness of the controllers is demonstrated. Furthermore, the IBS aerodynamic attitude controller has been extended with an extra incremental backstepping loop to control the flight path angle and the airspeed.

Finally, flight tests are performed that validate the controller designs. Mainly qualitative conclusions can be drawn from the flight results. The INDI controller that controls the Euler attitude angles has been successfully tested in nominal flight. Simulated controller responses match closely with flight measurements. Also, a manually controlled flight with this INDI control law as augmented control has been performed. In the longest experiment, lasting 241 seconds, the longitudinal and lateral mode were excited with pitch angles of $\pm 22\,\mathrm{deg}$ and roll angles of $\pm 50\,\mathrm{deg}$. The IBS controller that controls the aerodynamic attitude was tested in both longitudinal and lateral mode, during separate maneuvers. Although results show a stable response to angle of attack commands, the lack of a good estimate of the angle of attack limits the applicability. The lateral mode of the aircraft was only tested with conservative, non-nominal gains. The results correspond to the expected response, but subsequent tests must be performed for a full validation.

Acronyms

ABS	adaptive backstepping
AIBS	adaptive incremental backstepping
BS	backstepping
CLF	control Lyapunov function
DLR	German Aerospace Center
DOF	degree-of-freedom
EKF	extended Kalman filter
FASER	free-flying aircraft for sub-scale experimental research
FBL	feedback linearization
FCS	flight control system
FDD	fault-detection and diagnosis
FTFC	fault-tolerant flight control
I&I	immersion & invariance
IBS	incremental backstepping
INDI	incremental nonlinear dynamic inversion
LMS	least mean squares
LOC-I	loss-of-control in-flight
LQR	linear-quadratic regulator
NDI	nonlinear dynamic inversion
NED	north-east-down
PI	proportional-integral
RFC	reconfigurable flight control
RMS	*root-mean-square*
TF	tuning functions
UAV	unmanned aerial vehicle
UMN	University of Minnesota
VLM	vortex lattice method

List of Symbols

Greek Symbols

α	Aerodynamic angle of attack
β	Aerodynamic angle of sideslip
δ_a	Aileron deflection
δ_e	Elevator deflection
δ_r	Rudder deflection
δ_t	Throttle level
ϕ	Body roll angle (third body Euler angle)
$\boldsymbol{\omega}$	Angular rate
ψ	Body yaw angle (first body Euler angle)
θ	Body pitch angle (second body Euler angle)

Roman Symbols

$\mathbf{A}_{x,y,z}$	Specific forces (non-gravitational forces divided by the mass)
b	Wing span (lateral reference length)
C	Stabilizing gain
$\bar{c}$	Mean aerodynamic chord (longitudinal reference length)
C_D	Nondimensional drag coefficient
C_L	Nondimensional lift coefficient
C_l	Nondimensional roll moment coefficient
C_m	Nondimensional pitch moment coefficient
C_n	Nondimensional yaw coefficient

C_Y	Nondimensional side force coefficient
χ	Tracking error compensation
χ	Aircraft course angle
e	Tracking error $x_r - x$
$\mathbf{F}$	Force
$\bar{\mathbf{F}}$	Aerodynamic force vector
F_T	Thrust force
$F(\cdot)$	System dynamics-related taylor series expansion term of the state derivative
$f(\cdot)$	Nonlinear control-independent dynamics
g	Gravitational acceleration
γ	Aircraft flight path angle
$G(\cdot)$	Control-related taylor series expansion term of the state derivative
$g(\cdot)$	Nonlinear control-dependent dynamics
K_d	Derivative gain
K_i	Integrator gain
K_p	Proportional gain
$\bar{L}$	Aerodynamic roll moment
$\bar{M}$	Aerodynamic pitch moment
m	Aircraft's mass
$\mathbf{M}$	Moment
$\bar{\mathbf{M}}$	Aerodynamic moment vector
$\bar{N}$	Aerodynamic yaw moment
p	Body roll rate
q	Body pitch rate
$\bar{q}$	Dynamic pressure, $\bar{q} = \frac{1}{2}\rho V^2$
r	Body yaw rate
$\mathbf{r_{cg}}$	Position of the center of gravity
$\mathbf{r_{cp}}$	Position of the center of pressure
$\mathbf{r_{np}}$	Position of the neutral point
S	Wing surface area (reference area)
$\mathbb{T}^{ji}$	Coordinate transformation matrix from frame i to frame j
T_s	Sampling time
V	Aircraft's total velocity

u	Control input
u	Aircraft's velocity, body x-component
v	Aircraft's velocity, body y-component
$\mathbf{V}$	Body inertial velocity
w	Aircraft's velocity, body z-component
$\bar{X}$	Aerodynamic force at C.G., x-component
x	System state
$\bar{Y}$	Aerodynamic force at C.G., y-component
$\bar{Z}$	Aerodynamic force at C.G., z-component
z	Tracking error $x - x_r$
$\bar{z}$	Compensated tracking error $z - \chi$

Subscripts

cg	Center of gravity
cp	Center of pressure

Superscripts

0	Raw control
a	Aerodynamic reference frame
b	Body reference frame
e	Earth fixed, North-East-Down reference frame
s	Stability reference frame
v	Velocity reference frame

Contents

List of Figures

List of Tables

Chapter 1

Introduction

Commercial airliners and advanced military aircraft nowadays are equipped with flight-control systems to provide augmented stability or to take over complete control tasks. During flight, major system failures may change the aircraft dynamics in such a way that the flight control system (FCS) is unable to provide the required stability and stops functioning, even though the main control effectors may still yield some level of performance. The research for this thesis aims to contribute to the development of adaptive and robust, nonlinear flight control laws that can cope with a wide variety of system faults. The thesis includes analysis, design and implementation of INDI and IBS flight control laws applied to fixed-wing aircraft. Flight tests are performed on a unmanned aerial vehicle (UAV) to validate the flight control methods.

The UAV platform that is used is part of a project named free-flying aircraft for sub-scale experimental research (FASER), initiated by the University of Minnesota (UMN). It entails the development of a small low-cost unmanned aircraft to be used for research on advanced flight control laws (Owens, Cox, & Morelli, 2006). An off-the-shelf aircraft platform has been used, on which a complete flight computer and sensors have been installed. A picture of this 7 kg, 2 m span aircraft is shown in Figure 1-1. Windtunnel tests are executed to create an accurate nonlinear model used for simulations. The German Aerospace Center (DLR) has acquired one FASER platform on which the presented control laws are tested.

The thesis consists of two parts. First, the final controller design and flight results are presented

Figure 1-1: The platform of the FASER project: the Ultrastick120. Image retrieved from `http://www.uav.aem.umn.edu/`.

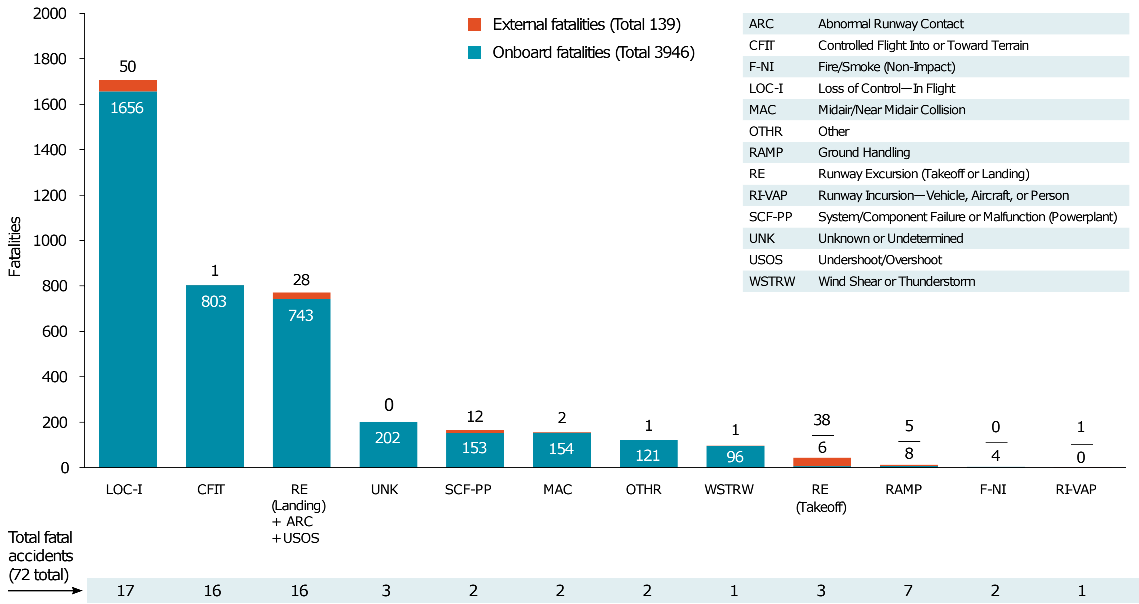

Figure 1-2: Classification of contributing factors to fatal accidents of commercial jet flights worldwide between 2005 and 2014 (Boeing Commercial Airplanes, 2010).

in a scientific paper. The subsequent chapters are part of the preliminary work done prior to the flight tests. It contains analysis of the control laws and describes the controller design in more detail. The remainder of this chapter will introduce the context, discusses the state-of-the-art in nonlinear flight control methods, it will discuss the current challenges, it presents the research objective of the thesis and finishes with a detailed outline of the thesis.

1-1 Research context

Since the advance of fly-by-wire actuation and control systems in aircraft, flight control systems have developed into systems that do not only translate control signals directly to actuator signals, but alter and create signals to augment stability characteristics and incorporate auto-pilot systems. It became possible to monitor the state of the aircraft and reconfigure flight control laws upon certain system faults. The integration of systems that perform these tasks is referred to as fault-tolerant flight control (FTFC) systems and should prevent a range of accidents that involve loss-of-control in-flight (LOC-I) events.

1-1-1 Loss of control in-flight

LOC-I events refer to all situations in which the aircraft cannot be controlled to the intended path. Prior to LOC-I events, other failures might cause the loss of control, but it can also be caused by an aircraft upset. LOC-I is still the largest contributing factor in all fatal aircraft accidents worldwide (Boeing Commercial Airplanes, 2010; European Aviation Safety

Agency (EASA), 2014). Figure 1-2 shows this clearly. Between 2005 and 2014, of all fatal accidents with commercial jet flights, 23% involved a LOC-I event. The number of fatalities due to accidents that involve a LOC-I is even more staggering: it contributed to more than 41% of all fatalities (Boeing Commercial Airplanes, 2010). In fact, loss of control accidents are still complex because there are often multiple events that finally lead up to a LOC-I accident. Therefore, no single intervention strategy can be designed to prevent these accidents. NASA (Belcastro & Foster, 2010) carried out an analysis to get insight into this sequence of events. The type of LOC-I events which are aimed to be prevented by FTFC system are those situations in which there is still enough controllability available to potentially stabilize the aircraft and keeping a certain degree of tracking performance, i.e. being able to follow some trajectory which could successfully land the aircraft.

1-1-2 Fault-tolerant flight fontrol

FTFC systems can be classified by the way in which the flight control system deals with faults. They can be subdivided into *passive* and *active* systems. Passive systems do not have an online reconfiguration of control laws: there are for example no adaptations of controller gains and the structure of the controller is not altered when certain faults are detected. Passive systems are merely designed to be robust to system faults. General disadvantages of passive systems are that the severity of the tolerated faults to be dealt with is limited and that the performance is lower compared to active systems, even for nominal conditions.

The adaptive control laws discussed in this research fall into the class of active FTFC systems. Active systems include some fault-detection and diagnosis (FDD) system in combination with a mechanism that reconfigures the control laws. The general structure of an active fault-tolerant control system is presented in Figure 1-3. The reconfiguration can be off-line projection based, in which the control laws are shaped according to predefined controllers. The reconfiguration can also be an online redesign. In this case control parameters are recalculated online and also the structure of the control law can be altered. Active, on-line reconfigurable flight control systems apply to a much wider range of system faults and are able to achieve higher performance than passive or off-line projection based methods. However, these methods often suffer from being computationally expensive (Edwards et al., 2010). Adaptive, on-line reconfigurable flight control techniques were already a topic of research in the 1980's, but only since the more recent advances in computational power and software in the 1990's, a rapid increase arose in the number of reconfigurable flight control approaches and complexity of the systems. Overviews of these developments can be found in Edwards et al. (2010); Steinberg (2005); Zhang and Jiang (2008).

Faults can be classified into three categories, displayed in Figure 1-3. Actuator faults are any faults that partially or completely change the control action. This includes actuator jamming, aerodynamic degradation of the control surfaces or any other case by which the desired control deflections do not correspond with the achieved signals because of some failure. Component faults refer to changes to the plant dynamics parameters, such as mass and aerodynamic coefficients. Lastly, sensor faults subdivide into total or partial faults. Total faults constitute those sensor faults in which the sensor readings are not related at all anymore to the physical quantity that is measured. Partial faults can be a scaling or constant bias in the sensor reading.

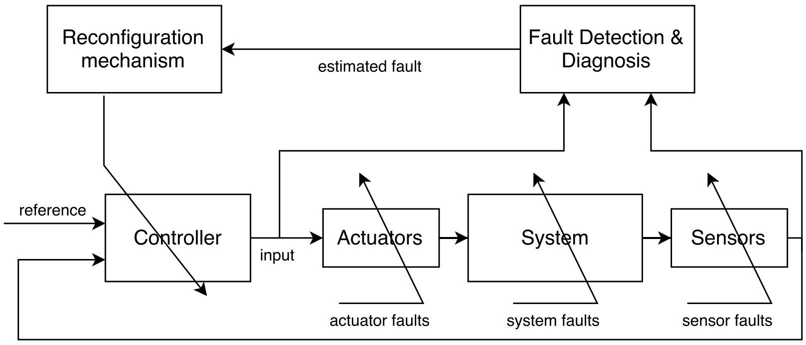

Figure 1-3: Main components of an active FTC system, adopted from Edwards et al. (2010) and Zhang and Jiang (2008).

The research in this thesis focuses on those situations in which the aircraft may encounter some system fault that changes the dynamics of the system, but still keeping full controllability. The typical control effectors considered are the elevator, aileron and rudder control surfaces. Hence, actuator failures are included only to such an extent that there is still some actuator action available in the original control structure so that aerodynamic moments can be generated that are large enough to bring the aircraft to a trimmed state, with some additional margin to achieve a satisfactory level of performance. Sensor failures are not considered although sensor dynamics, scaling and noise are included in the control law design. Component failures that alter the aerodynamic properties and its mass distribution are included.

1-2 Backstepping and nonlinear dynamic inversion control

Traditional flight control systems are most often based on linear systems and classical control theory. The typical techniques to develop control laws with desirable characteristics are root-locus techniques, frequency response analysis or more recent state space methods such as linear-quadratic regulator (LQR) control or robust H_∞ techniques (Stevens & Lewis, 2003). The advantage of using linear techniques is that the controllers are easy to analyze, and the control methods are well developed. However, these methods all suffer from being dependent on local linearization points and not being able to capture nonlinearities in the system dynamics or control action. Hence, control laws in the nonlinear region of the flight envelope, for example at high angles of attack, are more difficult to implement. Often, gain scheduling techniques must be used to create controllers that operate throughout the entire flight envelope. Interpolation can be performed between different linearization points. Nonlinear, model-based control methods solve this by formulating a control law that is applicable to the entire model. Hence, such control methods do not need gain scheduling techniques. NDI, a subset of Feedback Linearization, and the Backstepping method, a Lyapunov control method, are well-known nonlinear control methods based on a cancellation of the system dynamics.

Different topics and methods in the field of nonlinear control methods for aerospace applications are discussed in the next sections. This thesis focuses on incremental nonlinear control methods, which can be viewed as simplifications or special applications of nonlinear dynamic inversion or backstepping control. In Figure 1-4, it is shown how the discussed methods relate to each other in a general framework of nonlinear control methods.

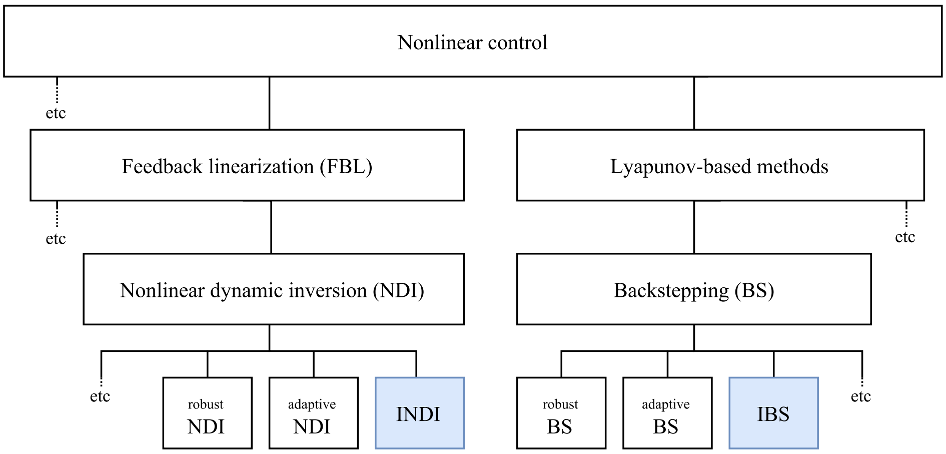

Figure 1-4: Categorization of nonlinear control methods used in this thesis. Adopted from Acquatella B. (2011).

1-2-1 Nonlinear dynamic inversion

Nonlinear control laws can capture the nonlinear dynamics and can provide a single solution that applies directly to the entire flight envelope. A well developed class of methods is feedback linearization, of which NDI is a subset that applies to first-order systems. The method involves a transformation of the system dynamics through a change of coordinates in such a way that the output is linearized with respect to a virtual input. The real input can be written in terms of the system states and this virtual input, so that the output can be controlled with linear methods. The limitations of these methods however are that it applies only to systems that can be written in lower triangular form. NDI cannot directly be applied to non-minimum phase systems because the virtual control uses the input that is separated from the output by the least amount of integrators. Furthermore, there are no robustness guarantees in the case of parametric uncertainties or unmodelled dynamics (Slotine, 1991). Since the early 1990's, nonlinear dynamic inversion has been successfully applied to many flight control problems(Bugajski, Enns, & Elgersma, 1990; da Costa, Chu, & Mulder, 2003; Doman & Ngo, 2002; Ochi & Kanai, 1991).

1-2-2 Backstepping control

With linear methods, stability can always be analyzed by looking at its poles. However, time responses of nonlinear systems do not have a general exponential solution and cannot be converted to the frequency domain or analysed with linear state space methods. Nonlinear systems do not have poles (in general) which characterize the overall stability of the system. Backstepping control is a nonlinear control technique which uses part of the concepts of feedback linearization, but the control laws are derived through Lyapunov stability concepts. As such, the developed control laws can be proven to be stable. Also, the control laws can easily be adapted to forms which account for parameter uncertainties. The theory originated from the 1990's, by P.V. Kokotović (Kokotovic, 1992). Since then, backstepping control has been widely used for a great variety of nonlinear control problems, and the control methods have been extended with command filters (J. Farrell, Polycarpou, & Sharma, 2003), tuning functions (Kanellakopoulos, Kokotovic, & Morse, 1991) and other techniques to increase its applicability to realistic nonlinear systems with uncertainties.

The basic idea of backstepping control is to bring the system into strict-feedback form:

$$
\begin{aligned}
\dot{\mathbf{x}} &= \mathbf{f}(\mathbf{x}) + \mathbf{g}(\mathbf{x})z_1 \\
\dot{z}_1 &= f_1(\mathbf{x}, z_1) + g_1(\mathbf{x}, z_1)z_2 \\
&\vdots \\
\dot{z}_i &= f_i(\mathbf{x}, z_1, \ldots, z_i) + g_i(\mathbf{x}, z_1, \ldots, z_i)z_{i+1} \quad \text{for } i = 1, \ldots, k-1 \\
&\vdots \\
\dot{z}_{k-1} &= f_{k-1}(\mathbf{x}, z_1, \ldots, z_{k-1}) + g_{k-1}(\mathbf{x}, z_1, \ldots, z_{k-1})z_k \\
\dot{z}_k &= f_k(\mathbf{x}, z_1, \ldots, z_k) + g_k(\mathbf{x}, z_1, \ldots, z_k)u
\end{aligned} \tag{1-1}
$$

Where $\dot{\mathbf{x}}$ is in $\mathbb{R}^n$, and $z_1, \ldots, z_k$ are scalars. In this form, the input is seperated from the output by several integrator states which in turn all act as an affine virtual control in the step closer to the output. In this way, a stabilizing virtual control can be designed at each integrator step to finally yield a stabilizing control law which brings the output signal to zero. Stability is proven by Lyapunov stability theory, based on the theorem of *LaSalle-Yoshizawa*, see for example Krstić (1995) or Khalil (1996) for an account of this theorem. Usually, the control Lyapunov functions (CLFs) are in the form:

$$
V_i = V_{i-1} + \tfrac{1}{2}z_i^2 \quad \text{for } i = 2, \ldots, k \tag{1-2}
$$

and $V_1 = \frac{1}{2}z_1^2$ in the case of scalar state x with a tracking error $z_1 = x - x_r$. The control laws are designed such that the time derivatives $\dot{V}_i$ are negative definite.

Next to its stability properties, a great advantage of backstepping control over NDI is that with backstepping control the designer has more freedom in the design of the control laws. This is due to the fact that the goal at each integrator step is to create a stabilizing control law that forces the derivative of the CLF to be negative definite. There are no further restrictions than that, so stabilizing terms do not have to be canceled by the control law. Also the Lyapunov function is usually chosen as the square of the error state itself, but in fact can take any form that will satisfy the requirements of a Lyapunov function (Krstić, 1995; Slotine, 1991).

Although the control laws developed through backstepping control have a theoretical stability proof, care must be taking when implementing these control techniques. In realistic systems, and especially for aircraft flight control, the basic assumptions for backstepping control are not valid. For example, the system is often not in a pure strict-feedback form when controlling attitude by the control surfaces. Also, noise and sensor dynamics make it impossible to know the true state. Furthermore, the sampling frequency must be sufficiently high to resemble the continuous system.

1-2-3 Adaptation methods

Apart from the nonlinear nature of backstepping control and NDI compared to traditional, linear flight control techniques, a second major difference is that both backstepping control and NDI are *model-based*, which means that the control laws depend on the model itself. In general, backstepping control laws depend on the functions f_i and g_i in Equation 1-1. This creates two challenges for real-life applications: first of all, the nominal model must somehow be identified to a certain accuracy, but cannot be known exactly. Hence, estimates $\hat{f}_i$ and $\hat{g}_i$ are used in the control laws. Secondly, when system dynamics change, the estimates must adapt to those or be robust to the estimation errors, but in either case one must make sure that changes in system dynamics do not destabilize the control laws. Usually, system dynamics are described as a function of a set of system parameters in such a way that $\hat{f}_i$ and $\hat{g}_i$ are found by estimating the system parameters. Referring back to the general active FTFC system scheme in Figure 1-3, one can see that the main task of the Fault Detection and Isolation block in this case is to identify the system parameters. The reconfiguration block updates these system parameters that are included in the control laws. Different techniques can be used to model-based control laws that use parameter estimates. We distinguish modular methods and integrated methods (Krstić, Kanellakopoulos, & Kokotovic, 1994).

Modular update law designs

Modular update law designs have a parameter update module that is separated from the control law design. Parameters that are used by the control law are identified by this module. Using this approach, the certainty equivalence principle is applied (Krstić, 1995). When applying this principle, one uses the parameter estimates in the control laws as if they were the true parameters. This separates the parameter estimation completely from the control law. When using this principle however, it becomes hard to prove that the derivative of the CLF is non-positive, hence stability proofs become difficult or even impossible with Lyapunov. However, because this principle allows the use of all well developed parameter estimation methods, it is still an attractive method. For example, some form of least squares parameter estimation method can be used when the model structure is linear in the parameters.

Integrated update law designs

The problem with applying the certainty equivalence principle is that the original Lyapunov functions do not exist any more, because the parameter estimation contains an uncertainty which is not taken into account in the stability analysis. Integrated approaches aim to include the parameter update laws in the Lyapunov-based control design method such that overall stability is still guaranteed. A way to integrate parameter updates in a way that still satisfies the Lyapunov stability proofs is by the Tuning Functions approach (Krstić, 1995). In this approach, dynamic parameter update laws are defined. These parameter update laws are incorporated in the control Lyapunov functions (CLFs) so that the input-to-state stability and parameter convergence is proved. A typical CLF then has the following form:

$$V_i = V_{i-1} + \frac{1}{2}z_i^2 + \frac{1}{2}\tilde{\boldsymbol{\theta}}_i^T \Gamma_i^{-1} \tilde{\boldsymbol{\theta}}_i \quad \text{for } i = 2, \ldots, k \tag{1-3}$$

Where $\tilde{\boldsymbol{\theta}}_i$ are the parameter errors in step i and Γ_i is a diagonal matrix with positive update gains. However, with the Tuning Functions approach the parameters do not converge to the true parameter but are only proven to converge to some point in the direction of the true parameters which guarantees stability of the overall system. The parameters update laws are dependent mainly on the tracking error. Hence, the parameter estimates are not really estimates of the model parameters anymore, but pseudo-estimates. Integrated approaches may be much more computationally expensive in the case of multiple dynamic update laws because the dynamic update laws need to be integrated by the control algorithm itself.

1-3 Incremental control methods

In the context of nonlinear control in aerospace applications, incremental control methods refer to a method whereby not the actual control u, but a control *increment* Δu is calculated, which is added to the previous control input. This representation of the control input is closely related to an integrator, but there are some important differences and advantages. The method can be integrated with NDI control, referred to as INDI. An application of such methods applied to fixed-wing aircraft was already described in Smith (1998) and Bacon, Ostroff, and Joshi (2001). A more general description of incremental NDI was given by Chen and Zhang (2008). In this reference, it is for the first time referred to as an incremental control method.

1-3-1 Incremental nonlinear dynamic inversion

The method is based on a Taylor series expansion of the system dynamics around a recent state in the past. Using this approach, the system is described as a locally linear system. By feeding back a measurement of the state derivative, only partial knowledge of the system dynamics is required. In fact, when applying NDI, only knowledge about the control effectiveness is necessary. As such, the control law is independent to any aerodynamic changes that do not affect the controls, and the sensitivity to the aircraft model is decreased (Chen & Zhang, 2008). As the control law is derived from a Taylor series expansion using only the first terms, the derived control structure is simple, even for more complex nonlinear systems.

The idea of an incremental description using Taylor series expansion for NDI was adopted by Delft University of Technology in Sieberling, Chu, and Mulder (2010) and referred to as INDI. The necessity for measurements of the angular accelerations was partially solved by estimating and predicting the angular accelerations using angular rate measurements. The predictive filter that is used is closely related to a simple n-point numerical differentiation for which the weightings of the measurements are tuned for the specific control law (Sieberling et al., 2010). Applying this INDI control law, the model dependency was greatly reduced compared to NDI and robustness was increased. Furthermore, the INDI control law profits from the usual advantages of nonlinear control methods.

Thereafter, more accounts of applications of nonlinear incremental control at Delft University of Technology have become available. In Smeur (2016), the control methods are applied to a small quad-rotor UAV. Furthermore, it is extended with adaptation methods to estimate the remaining model parameters to decrease its model-dependency and increase its flexibility to system faults. In Acquatella B., Falkena, van Kampen, and Chu (2012), the INDI method was succesfully applied to spacecraft attitude control and to the longitudinal control.

1-3-2 Incremental backstepping

One of the disadvantages faced by an application of NDI is that in general, stability of the overall system in combination with outer-loop control laws is not guaranteed. In his thesis and published article, Acquatella was the first to apply the incremental methods for backstepping control (Acquatella B., 2011; Acquatella B., van Kampen, & Chu, 2013). Using a backstepping procedure for the system to be controlled, an integrated control law is described which is proven to be stable for the system as a whole rather than for each individual control loop (Krstić, 1995). Incremental backstepping was then applied in adaptive forms by Ali, Chu, van Kampen, and de Visser (2014) and Van Gils (2015) for an F-16 aircraft model. Again, the strong robustness properties of incremental methods are shown, as well as the capability to deal with the lack of good angular acceleration measurements. Different adaptation methods are applied to further release the dependency on knowledge about the system dynamics.

1-4 Current challenges

Among others, one important challenge is to successfully implement and validate INDI and IBS flight control methods on a physical platform. INDI control laws have been shown to work well on quad-rotor UAVs (Smeur, 2016). It has also been applied to a fixed-wing UAV, but the results were never officially published (Vlaar, 2014). A big contribution to the ongoing research is to show the applicability of IBS methods and proof its validity by practical implementations with flight test results.

Secondly, incremental methods, and in particular INDI, have been presented primarily in forms that control angular rates in the inner loop of flight control systems. For fixed-wing aircraft, the typical cascaded control loop hierarchy follows a structure like what is shown in Figure 1-5. The structure relies on the fact that the velocity vector of any fixed-wing aircraft must be controlled by using the lift and thrust forces in appropriate directions and changing its magnitude. To achieve this, the aircraft's angle of attack α and bank angle μ are controlled. The total airspeed is usually controlled using the thrust. Attitude control is achieved by creating moments by the aerodynamic control surfaces. To control these outer loops, other control laws can be designed, resulting in a multi-loop NDI control structure. For this, one usually assumes a time-scale-separation between the different control loops. A drawback of this control structure is that it is not possible to proof the stability of the total controlled system. For this reason, the backstepping control method has been proposed, as it results in one integrated control law which is proven to be stable. In Van Gils (2015), a controller is described to control the aerodynamic attitude including the total airspeed. These control laws can be further extended for a control of the complete flight path described by the aircraft's course and vertical flight path angle.

Challenges that are not considered in this thesis are the adaptation of the remaining model parameters on-line and the optimization of stabilizing control laws. These two topics both support the goal to be able to apply incremental control methods in a systematic way on a wide variety of platforms, without the need to perform extensive model identification. Adaptation of INDI has been performed on quad-copter vehicles (Smeur, 2016). When using INDI for the stabilization of angular rates of a vehicle, the resulting control law only depends on the control effectiveness. Adaptation strategies then only need to consider a very limited set of model parameters.

Secondly, the optimization of gains spans a broad subject and particular solutions depend on the controller structure, optimization objectives and computational complexity. It may always be done off-line with the use of general constrained, zero-th order, direct search optimization methods such as genetic algorithms, Nelder-Mead simplex methods or combinations of multiple methods. Optimization may also refer to on-line optimal control in which optimization is integrated with the control law to maximize the performance.

Although adaptation and optimization of gains are not considered, this thesis does include an analysis on comparisons with classical PI control. Under certain restrictions, INDI can be used to derive gains of equivalent PI control laws. In this case, linear methods can be used for the analysis of the control laws. Hence, this comparison can help in the analysis of INDI in terms of the analysis of stability, parameter sensitivities and any other method for the optimization and adaptation of linear systems.

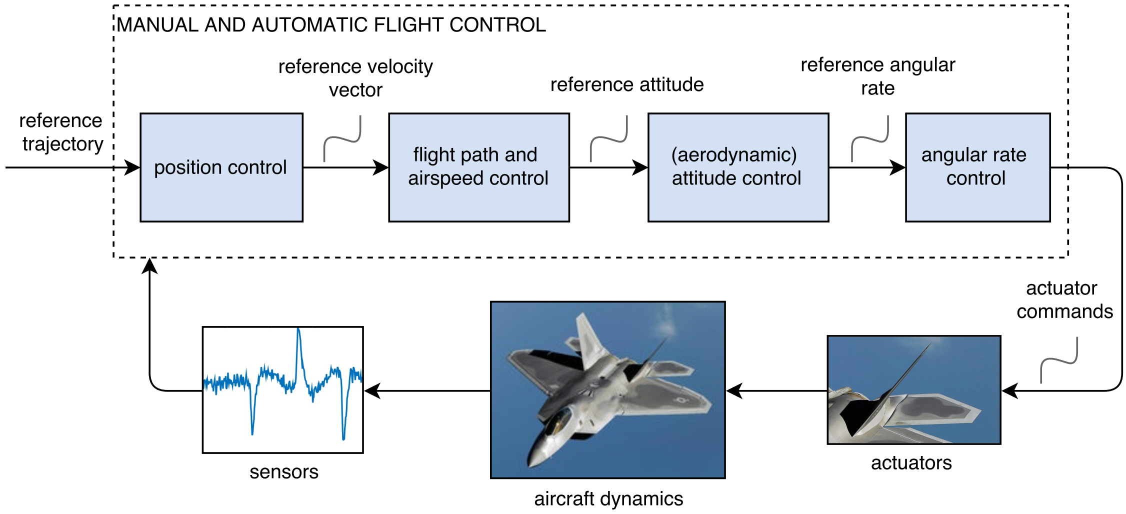

Figure 1-5: Typical cascaded flight control loop structure

1-5 Research objective and preliminary thesis outline

The research objective for this thesis is to analyze to what extent and in which forms incremental control laws, and in specific incremental backstepping control laws can be best applied to fixed-wing aircraft. Thereafter, the goal in this thesis project is to conduct real flight tests on the FASER UAV to proof the applicability of incremental nonlinear control methods. The research question is formulated as:

"How can IBS flight control methods be implemented for the flight path control of fixed-wing aircraft? How do IBS flight control methods perform on a small, fixed-wing UAV?"

The outline of the thesis is as follows. First, a final thesis paper is included, containing an outline of the most important analysis and results. The chapters thereafter govern the so-called 'preliminary thesis', which should be treated as preliminary studies executed prior to the final flight control design and flight testing that is presented in the paper. In chapter 2 the concepts of backstepping control, nonlinear dynamic inversion and incremental control are briefly discussed to introduce the methods mathematically before continuing to the actual controller design for fixed-wing aircraft. The chapter also contains a general discussion about the similarities between incremental nonlinear control and PI(D) control. Then, the aircraft model and equations of motion are introduced in chapter 3. It also contains a presentation of the polynomial model of the aerodynamics, that has been found by a model fitting on the look-up table interpolation data that was based on windtunnel tests. The next two chapters focus on the actual controller implementation on the FASER model and analysis of the control performance. Chapter 4 presents implementations of INDI control laws for angular rate and attitude control. Since the angular rate control loop is the most important part of the control laws, the major part of the chapter contains analyses and simulation results of the inner loop tracking response. Chapter 5 presents IBS control laws for the attitude and trajectory control, which use an inner loop control law that is in practice very similar to the discussed INDI control law. Not much attention is paid to the trajectory control; this control was also finally not tested on the FASER aircraft.

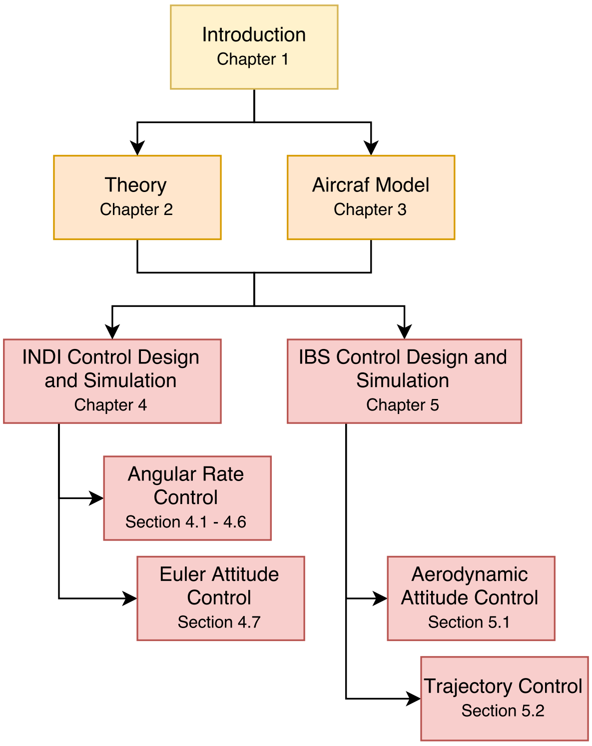

Figure 1-6: Structure of the preliminary thesis

Additionally, the thesis includes some appendices that support the results and analysis that is presented in the article and in the other chapter of the thesis. These appendices are:

A. Aerodynamic Model This appendix includes estimated coefficients of a polynomial fit for the aerodynamic model of the FASER aircraft. It also contains figures that display both the table look-up data and the polynomial fit.

B. Flight Results The article presents flight results of the INDI/IBS control laws. This appendix contains a more extensive overview of all flight test runs.

C. Model Validation Special maneuvers are performed to perform model validations. This is reported in the article. The appendix contains more detailed time responses of the performed maneuvers.

REMARK: It must finally be noted that there are differences in notation between the scientific paper and the remaining chapters (preliminary thesis). The most important difference is the numbering of the control loops. In the paper, the attitude loops and angular rate loop are numbered by subscripts 1 and 2, respectively. Because in the rest of the thesis also a flight path loop is considered, this loop is numbered with subscript 1, while the attitude and rate loop are designated by 2 and 3, respectively. The paper is provided with its own nomenclature at the first page. The list of symbols that is included at the start of this thesis applies to all other chapters.

Design, Implementation and Flight-Tests of Incremental Nonlinear Flight Control Methods

Wim van Ekeren [*], Gertjan Looye [†], Qiping Chu [‡]

Delft University of Technology, P.O. Box 5058, 2626HS Delft, The Netherlands

DLR, German Aerospace Center, 82234 Weßling, Germany

This paper presents the design and implementation of incremental nonlinear dynamic inversion (INDI) and incremental backstepping (IBS) methods for the attitude control and stabilization of a fixed-wing aircraft. The design consists of multiple functionalities such as command-filtered backstepping, angle of attack control and Euler angle control which are all based around an incremental control inner-loop that tracks the angular rates of the aircraft. The results include flight data of an integrated INDI/IBS design to support simulation results of incremental nonlinear flight control laws shown previously in literature. Furthermore, this paper contributes by showing that assumptions on neglecting system dynamics increments are not always valid for fixed-wing aircraft, although a successfull attitude control law can still be realized. Supported with model validation, the results show that it is possible to implement robust nonlinear flight control laws that are easy to tune and require only little knowledge about the system dynamics parameters.

Nomenclature

$C_{D,Y,L}$	Non-dimensional aerodynamic drag, lift and side force
C_i	Stabilizing control gain matrix in loop i
$C_{l,m,n}$	Non-dimensional aerodynamic roll, pitch and yaw moment
F_*	Model parameter scaling factor
F_T	Total propeller thrust, N
g	Gravitational acceleration, $^{m}/_{s^2}$
I	Aircraft inertia matrix
m	Aircrafts mass, m
$S(\cdot)$	Saturation function
$\mathbb{T}_{ij}$	Coordinate transformation matrix from frame j to frame i
T_s	Controller sample time, s
$\mathbf{V}$	Aircraft inertial velocity, $^{m}/_{s}$
V_i	Control Lyapunov Function in step i
$\mathbf{x}$	Total aircraft state including body velocities, attitude, aerodynamic angles and angular rates
z	Tracking error, $x - x_r$
α	Aerodynamic angle of attack, rad
β	Aerodynamic angle of sideslip, rad
$\boldsymbol{\omega}$	Body angular rates, $^{rad}/_{s}$
ω	Linear filter bandwidth or break frequency, $^{rad}/_{s}$

Subscripts

a	Aerodynamic
act	Actuator
p	Propeller+motor
i	Inertial
ref	Reference

Superscripts

0	Raw command
b	Body reference frame

I. Introduction

Since the advent of fly-by-wire actuation systems in aircraft, it became possible to intercept and manipulate pilot control inputs and add augmented stability based on sensor feedback. Although these flight

[*]Graduate Student, Faculty of Aerospace Engineering, Control and Simulation Division, Delft University of Technology
[†]Head, Department of Aircraft Systems Dynamics, Institute of System Dynamics and Control, German Aerospace Center
[‡]Associate Professor, Faculty of Aerospace Engineering, Control and Simulation Division, Delft University of Technology

control systems are designed to support the pilot and should improve the stability and performance in flight, loss-of-control in-flight (LOC-I) still remains the largest contributing factor in all fatal commercial aircraft accidents worldwide.[1,2] In many cases, major system failures change the aircraft dynamics in such a way that the FCS is unable to provide the required stability and stops functioning even though the main control effectors may still yield some level of performance.[3,4]

The majority of aircraft are inherently stable, so that in nominal cases a pilot could easily take over the control of the aircraft without requiring additional stability augmentation. However, system faults may cause the aircraft to become unstable and very difficult to control. Furthermore, high-performance aircraft are often inherently unstable and will always require flight control systems for additional stability. Therefore, to prevent LOC-I events, fault-tolerant flight control (FTFC) that can provide main functionalities in the event of system faults are essential.[5] One way in which FTFC systems could prevent these LOC-I events is by providing enough robustness to the control laws, often at the cost of performance in nominal flight. An alternative is to use active reconfiguration of the control laws in combination with a system that provides fault-detection and diagnosis (FDD).[6]

Conventional linear control laws always require gain scheduling methods to provide desired stability and performance characteristics over the entire flight envelope.[7,8] Reconfiguration upon system faults requires a re-scheduling of those control laws. For integrated, general approaches in which flight control laws provide the desired stability and performance criteria throughout the entire flight envelope, nonlinear model-based control laws have been developed, such as feedback linearization, nonlinear dynamic inversion or backstepping. These methods such attempt to cancel the system dynamics.[9–15] In effect, they highly rely on model parameters. Online identification and adaptation strategies are necessary to reconfigure the control laws.[16–20]

Incremental control methods attempt to solve the problem of the dependency on an accurate on-line available model of the plant. The methods refer to a technique applied to nonlinear model-based control laws that reduce their model-dependency by being more dependent on sensors and using actuator feedback.[21] By measuring the state derivatives and actuator positions, no knowledge of the control-independent system dynamics is necessary to apply control methods based on system dynamics cancellation. Incremental control methods are therefore promising because they need only little information about the plant while they still cancel the system dynamics to linearize the output with respect to a virtual control input. This makes the controller easy to implement and easy to tune.

Previous work

Incremental nonlinear dynamic inversion (INDI) is a method in which the dynamics are written in an incremental form. Dynamic inversion is applied to yield control law that is only dependent on the control-dependent part of the model. In Bacon et al.,[22] already an incremental, dynamic inversion based control law was proposed to control the aircraft attitude and angular rates. This was shown on a tailless aircraft model. Also in Smith[23] such a method was used. Both papers suggest a simplified approach to dynamic inversion by describing control increments and using angular acceleration feedback, but do assume that the angular accelerations are readily available from measurements. In Sieberling,[21] a study is done on the robustness to delays in the angular accelerations measurements. The references stated here consider the attitude or angular rate control of fixed-wing aircraft. Feedback linearization or nonlinear dynamic inversion is applied on the dynamics of angular accelerations in incremental form, thereby only requiring knowledge about the incremental control-dependent moments to linearize the output with respect to a virtual control. Because the core of these INDI control laws is based on an incremental description of the angular rate dynamics on which assumptions about the system dynamics are made, the method is not restricted to the application of dynamic inversion. It has also been applied as incremental backstepping (IBS) control by Acquatella et al.[24] for the attitude stabilization of spacecraft and for longitudinal flight control laws on a launch vehicle. IBS was also described for the attitude control of high-performance fixed-wing aircraft.[25,26] The backstepping control procedure is especially useful for the design of cascaded control systems for which stability must be guaranteed.

Figure 1. The FASER UltraStick120 aircraft. Image retrieved from `http://www.uav.aem.umn.edu/`.

In Smith et al.,[27] flight test results of a longitudinal pitch rate control law similar to INDI are presented. However, this article does not consider the effect of delays in the incremental control loop caused by actuator dynamics and synchronization with delayed acceleration measurements. Flight-tests of adaptive INDI attitude control laws on a small quad-copter vehicle have been performed recently by Smeur et al.,[28] showing the applicability of INDI as a novel, robust incremental control law. The dynamics of quad-copter rotorcraft are however significantly different, because the influence of aerodynamic damping is much lower. Real flight-tests of IBS control laws on aircraft or spacecraft has not been performed yet.

Contribution

The contribution of this paper consists of two parts. The first and major part is the presentation of the design, implementation and flight test results of novel INDI and IBS attitude control laws on a fixed-wing aircraft. The aircraft used for these flight-tests is the FASER UltraStick120 aircraft, a 2 m span UAV developed by the University of Minnesota.[29] Tests were performed on one of these platforms which is operated by the German Aerospace Center (DLR). The IBS and INDI methods are implemented as an integrated control design, in which different controller functions can be chosen. The longitudinal mode of the controllers can either track the pitch angle θ, suitable for manual flight, or the angle of attack α, which is more useful for an outer loop autopilot controller or high-performance aircraft. The lateral mode of the controllers will control the roll angle ϕ while minimizing the side slip angle β and the aerodynamic side force. The avionics components that are available on this aircraft are relatively cheap and widely available. Therefore, the INDI and IBS control laws presented in this paper proof its applicability as a robust, flexible and easy to tune control law.

Secondly, the paper includes an analysis on the system dynamics increments, showing that for fixed-wing aircraft the assumptions made to arrive at the simplified incremental control laws are not valid in general. System dynamics increments due to aerodynamic damping and due to changes in the angle of attack and angle of sideslip cause angular rate tracking errors. The size of these tracking errors is directly related to the total increment delay. This analysis was not done beore. It is furthermore shown that although assumptions are not valid for the system used in this paper, still a robust attitude control design can be achieved.

Outline

The structure of this paper is as follows. Section II presents the fixed-wing aircraft model that is used in the design. Also, flight test data of open-loop experiments are presented that is used for model validation. The incremental flight control laws are derived in section III. Thereafter, section IV discusses the final controller design used on the aircraft. Section V discusses the the assumptions on neglecting the system dynamics increments. In the remaining part of the paper, sections VI and VII the flight test experiments and results are presented. The paper is concluded in section VIII.

II. Aircraft model

The FASER project consists of multiple platforms that are equipped with similar software and hardware aiming to make the process of implementing and testing new flight control algorithms as simple as possible. Wind-tunnel tests are performed to generate a high-fidelity model, which is defined in MATLAB/Simulink. The platform used in this research is the UltraStick120, a 2 m span fixed-wing aircraft. Basic properties of the aircraft are listed in Tab. 1.

Table 1. Basic aircraft parameters of the UltraStick120 platform [1].

Parameter		
Mass (take-off weight)	m	8.13 kg
Length		1.26 m
C.G. from firewall	x_{cg}	0.315 m
Aero ref from firewall	x_a	0.320 m
Roll inertia	I_x	1.031 kgm^2
Pitch inertia	I_y	1.21 kgm^2
Yaw inertia	I_z	2.05 kgm^2
Roll-yaw inertia	I_{xz}	0.433
Chord	$\bar{c}$	0.433 m
Span	b	1.92 m
Wing Area	S	0.769 m^2

[1]Mass moment of inertia parameters were adopted from the already available model and scaled by the updated operational weight as used by the German Aerospace Center (DLR)

A. Equations of motion

The motion of the aircraft is described by rigid-body equations of motion in the body reference frame, as is common in most flight control problems. The most important assumptions made are:

- The aircraft is treated as a rigid body.
- The earth is flat and non-rotating, so that the north-east-down (NED) earth-fixed reference frame is inertial and the gravity vector always points downwards.
- The only forces and moments acting on the aircraft are aerodynamics, propulsive forces and moments and the aircraft's weight. The propeller thrust F_T acts purely in the direction of the body x-axis.
- The mass m of the aircraft is constant.

By applying Newton's equations of motion in the body reference frame, the time derivative of the body velocities $\mathbf{V}$ are defined as

$$\dot{\mathbf{V}} = \frac{\mathbf{F}_a}{m} + \frac{\mathbf{F}_p}{m} + \mathbf{g} - \boldsymbol{\omega} \times \mathbf{V} \tag{1}$$

where $\boldsymbol{\omega}$ are the rotational rates and $\mathbf{F}_a, \mathbf{F}_p$ are the aerodynamic and propeller/motor forces respectively, and $\mathbf{g}$ is the gravitational acceleration in body frame coordinates. The terms are given by

$$\mathbf{F}_a = \begin{bmatrix} \bar{X}^b \\ \bar{Y}^b \\ \bar{Z}^b \end{bmatrix} = \mathbb{T}_{bs}(\alpha)\bar{q}S \begin{bmatrix} -C_D \\ C_Y \\ -C_L \end{bmatrix}, \quad \mathbf{F}_p = \begin{bmatrix} F_T \\ 0 \\ 0 \end{bmatrix}, \quad \mathbf{g} = \mathbb{T}_{be}(\phi, \theta, \psi) \begin{bmatrix} 0 \\ 0 \\ g \end{bmatrix} = \begin{bmatrix} -g\sin\theta \\ g\cos\theta\sin\phi \\ g\cos\theta\cos\phi \end{bmatrix}, \tag{2}$$

where $\bar{q} = \frac{1}{2}\rho V_a^2 S$ is the dynamic pressure, S is the wing surface area, $\mathbf{C}_F = [C_D, C_Y, C_L]^T$ the non-dimensional aerodynamic force coefficients, g the gravitational acceleration and $\mathbb{T}_{bs}, \mathbb{T}_{be}$ are rotation matrices from the stability to the body frame and from the NED frame to the body frame, respectively. In scalar form, with $\mathbf{V} = [u, v, w]^T$ and $\boldsymbol{\omega} = [p, q, r]^T$, the equations can be written as

$$\begin{aligned} \dot{u} &= rv - qw - g\sin\theta + \tfrac{1}{m}\bar{X}^b + \tfrac{1}{m}F_T \\ \dot{v} &= pw - ru + g\cos\theta\sin\phi + \tfrac{1}{m}\bar{Y}^b \\ \dot{w} &= qu - pv + g\cos\theta\cos\phi + \tfrac{1}{m}\bar{Z}^b \end{aligned} \tag{3}$$

The time derivative of the angular rates $\boldsymbol{\omega}$ is described as

$$\dot{\boldsymbol{\omega}} = I^{-1}(\mathbf{M}_a + \mathbf{M}_p - \boldsymbol{\omega} \times I\boldsymbol{\omega}) \tag{4}$$

where I is the inertia matrix and $\mathbf{M}_p$ are the motor and propeller's reaction moments acting on the aircraft body due to the inertia of the motor and propeller. $\mathbf{M}_a$ is the aerodynamic moment, built up by non-dimensional force and moment coefficients in the body reference frame, defined as

$$\mathbf{M}_a = \bar{q}S \begin{bmatrix} b & & \\ & \bar{c} & \\ & & b \end{bmatrix} \mathbf{C}_M \tag{5}$$

with b the aircraft's wing span, $\bar{c}$ the mean chord length and $\mathbf{C}_M = [C_l, C_m, C_n]^T$ the aerodynamic moment coefficients. Note that the aerodynamic moment coefficients are defined in the body frame while the force coefficients are defined in the stability frame.

B. Aerodynamic model

Aircraft aerodynamic forces are described using non-dimensional force and moment coefficients, denoted as $\mathbf{C}_F = [C_D, C_Y, C_L]^T, \mathbf{C}_M = [C_l, C_m, C_n]^T$. The coefficients are modeled by look-up tables using wind-tunnel test data.[29,30] Coefficients are split up in a base part, depending on angle of attack and angle of sideslip α and β, a part dependent on control surface deflections and a part dependent on the rotational rates, so that

$$\begin{aligned} \mathbf{C}_F &= \mathbf{C}_{F,\text{base}}(\alpha, \beta) + \Delta\mathbf{C}_{F,\text{ctrl}}(\boldsymbol{\delta}, \alpha, \beta) + \Delta\mathbf{C}_{F,\text{rate}}(\hat{\boldsymbol{\omega}}, \alpha, \beta) \\ \mathbf{C}_M &= \mathbf{C}_{M,\text{base}}(\alpha, \beta) + \Delta\mathbf{C}_{M,\text{ctrl}}(\boldsymbol{\delta}, \alpha, \beta) + \Delta\mathbf{C}_{M,\text{rate}}(\hat{\boldsymbol{\omega}}, \alpha, \beta) \end{aligned} \tag{6}$$

with $\hat{\boldsymbol{\omega}} = [\frac{pb}{2V_a}, \frac{q\bar{c}}{2V_a}, \frac{rb}{2V_a}]^T$. Coefficients are measured at high angles of attack ($-2 \leq \alpha \leq 45$deg) and angles of sideslip ($-30 \leq \beta \leq 30$deg). Also, control moments $\mathbf{C}_M(\delta)$ and dynamic moments $\mathbf{C}_M(p, q, r)$ are incorporated for different angles of attack, for the complete range of control surface deflections and up to $150\,\mathrm{deg/s}$ (at $V = 25\,\mathrm{m/s}$).

To get estimates of the control effectiveness of the actuators, and to create a flexible, simplified model which is useful for simulation and controller design, the aerodynamic forces and moments are estimated by a polynomial model at angles of attack smaller than the stall angle ($\alpha < 12\,\text{deg}$) and low angles of sideslip ($\beta < 20\,\text{deg}$), according to

$$\begin{bmatrix} \mathbf{C}_F \\ \mathbf{C}_M \end{bmatrix} = \sum_{i=0}^{2}\sum_{j=0}^{2} \mathbf{c}_{\text{base}_{ij}} \alpha^i \beta^j + \mathbf{c}_{\text{base}_{03}} \beta^3 + \sum_{k=1}^{3}\sum_{i=0}^{2}\sum_{j=0}^{2} \mathbf{c}_{\text{ctrl}_{kij}} \delta_k \alpha^i \beta^j + \sum_{l=1}^{3}\sum_{j=0}^{2} \mathbf{c}_{\text{rate}_{lij}} \hat{\omega}_l \alpha^i \beta^j \tag{7}$$

Here, δ_k with $k = 1, 2, 3$ are the control surface deflections, and $\hat{\omega}_l$ with $l = 1, 2, 3$ are the non-dimensional angular rates. $\mathbf{c}_{(\dots)}$ are the polynomial coefficients. The basic estimated stability and control derivatives are stated in Tab. 2. In a paper by Klöckner,[31] a polynomial model of the Ultrastick120 unmanned aerial vehicle (UAV) has already been estimated using an aerodynamic dataset generated using the vortex lattice method (VLM), and mainly based on the geometrical information of the aircraft. Base coefficients $\mathbf{C}_{\text{base}}$ and dynamic coefficients $\mathbf{C}_{\text{rate}}$ match closely with the table data and for these coefficients, the polynomial coefficients also match closely with the polynomial model presented in this paper. The VLM dataset contained noticeable differences in the control coefficients. Therefore, also the polynomial model fit of the VLM data does not match for these coefficients.

Table 2. Most important estimated stability and control derivatives from the look-up table data.

C_{m_α}	C_{n_β}	C_{l_p}	C_{m_q}	C_{n_r}	$C_{l_{\delta_a}}$	$C_{m_{\delta_e}}$	$C_{n_{\delta_r}}$
-0.3025	0.0714	-0.397563	-7.8542	-0.13664	-0.186475	-0.689396	-0.0360641

C. Actuator model identification

The UltraStick120 in use at the DLR is equipped with JR DS8411 servos that control all control surfaces individually. Incremental control laws rely on a good actuator feedback. Because of practical reasons, the actuator position sensor data was not used in a closed-loop test. The electric signal was not reliable enough and in some cases the attachment of the potentiometer displaced over the duration of the experiment. However, the sensors could be used to gather open-loop step response data in order to identify the model. The dynamics were identified by commanding step inputs of different magnitude. The actuator dynamics are modeled with first-order dynamics with bandwidth ω_{act}, including rate limits and a time delay λ_{act}:

$$\dot{\delta}(t) = S_R\{-\omega_{act}\delta(t) + \omega_{act}u(t - \lambda_{act})\} \tag{8}$$

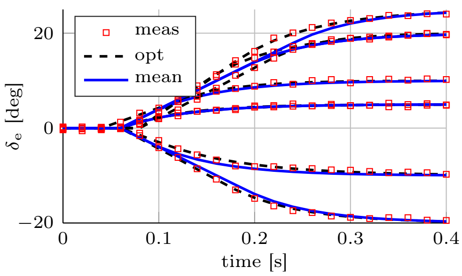

Figure 2. Measured elevator position (meas) for step commands, plotted with the identical step response of the individual optimal parameters (opt) for the response and the step response using the final identified (mean) parameter estimates

where S_R is a saturation function, defined as

$$S_R(x) = \begin{cases} R & \text{if} \quad x > M \\ x & \text{if} \quad |x| \leq M \\ -R & \text{if} \quad x < -M \end{cases} \tag{9}$$

Actuator time responses of the elevator deflections are shown in Fig. 2. For each step response, parameters R, λ_{act} and ω_{act} are found that minimize the root-mean-square (RMS) error between the measured and simulated response. The final estimates are the mean of those values, listed in Tab. 3.

Table 3. Identified (mean) actuator dynamics parameters, with standard deviation σ

ω_{act} [Hz]	R [deg/s]	λ_{act} [samples at 50 Hz]
2.35 ($\sigma = 0.44$)	99.6 ($\sigma = 30.4$)	2.25 ($\sigma = 0.707$)

D. Aircraft model validation

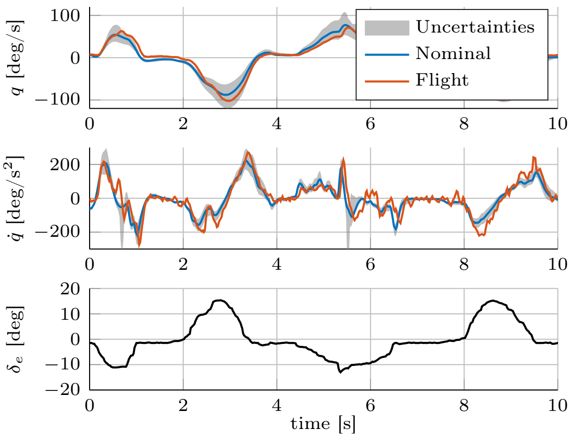

Figure 3. **Pitch maneuver angular rates and accelerations**

Open-loop, manually controlled flight tests have been performed for model validation purposes. Different maneuvers have been executed to excite the different modes of the system. For each maneuver, the pilot was instructed to give strong, aggressive inputs on a particular axis. Hence, executed maneuvers are pitch, yaw and roll maneuvers caused by elevator, rudder and aileron inputs, respectively. To validate the model, simulations are performed with the inputs as measured in-flight for each maneuver. First, a trim condition was calculated at the same airspeed. The simulation was then initialized at the initial non-trimmed state taken from the flight data. The simulation was thereafter performed by adding the measured input differences to the trim inputs. In this way, the problem of trim mismatches between the model and the flight tests was avoided.

Besides a simulation with the nominal model, simulations have been performed with scaled aerodynamic moments. Because the aerodynamics are modeled using look-up table data interpolation, scaling of stability derivatives has been implemented by scaling the respective moment component of part of the coefficient (such as the scaling of $C_{m,\text{base}}$ by F_{C_m}). Scaling factors are defined as

$$\begin{aligned} C_{i,\text{base,scaled}} &= F_{i,\text{base}} C_{i,\text{base}} \\ \Delta C_{i,\text{ctrl,scaled}} &= F_{i,\text{ctrl}} \Delta C_{i,\text{ctrl}} \qquad \text{for} \quad i = l, m, n \\ \Delta C_{i,\text{rate,scaled}} &= F_{i,\text{rate}} \Delta C_{i,\text{rate}} \end{aligned} \tag{10}$$

where F_* are scaling factors for each component of the aerodynamic model. By varying each scaling factor over a mimimum, nominal and maximum value, simulations of each possible combination set of factors is performed. In Figs. 3 to 5, measured and simulated responses are presented with scaling factors of $F_* = 25\%$. The bounds of the simulations with scaled parameters are plotted with gray areas. The figures show that the measured accelerations in flight can be explained by the model with the selected parameter offsets.

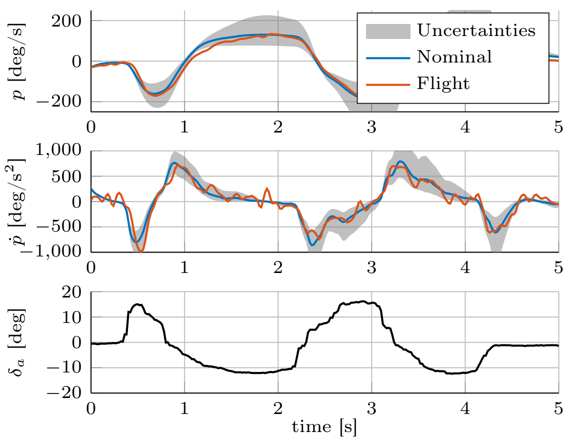

Figure 4. **Yaw maneuver angular rates and accelerations**

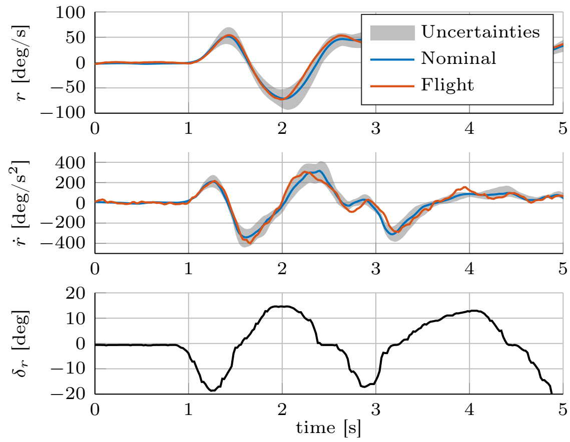

Figure 5. **Roll maneuver angular rates and accelerations**

III. Incremental nonlinear attitude control laws

This section presents the IBS and INDI control laws that are applied for two different control problems. In the first case, described in section A, the Euler attitude angles are the considered control variables. The external tracking commands are ϕ_{cmd} and θ_{cmd}, while the heading rate $\dot{\psi}$ is controlled such that coordinated turns are achieved. In the second task, described in section B, the angle of attack α is tracked instead of the pitch angle θ and the side slip angle β is controlled to zero. This makes this controller a lift-control device, which is more useful for outer loop flight path control tasks or for high-performance aircraft.[32,33]

A. Attitude control of Euler angles

The control task in this attitude control problem is to track references for the body Euler angles ϕ and θ, so that

$$\phi = \phi_{ref} \quad \text{and} \quad \theta = \theta_{ref}. \tag{11}$$

In this paper we specifically focus on the stabilization of the aircraft attitude angles ϕ and θ and we are not interested in the total heading ψ or course χ. Normally, the aircraft's heading is controlled by rolling the aircraft into a coordinated turn. Hence, although the total heading is not controlled, it is desired to keep a coordinated turn when performing a roll maneuver by commanding yaw rates. It will be shown that due to the kinematic relation between $\dot\phi, \dot\theta, \dot\psi$ and p, q, r, any reference $\dot\psi_{ref}$ can always be chosen so that a reference for p, q, r that tracks the pitch and roll references can be defined. At the end of this section, a reference for $\dot\psi_{ref}$ will be derived that controls the side force on the aircraft to zero and keeps the sideslip angle small. In this section, the output, tracking error, states and input are

$$\mathbf{y}_1 = \begin{bmatrix}\phi\\ \theta\end{bmatrix}, \quad \mathbf{y}_{1,ref} = \begin{bmatrix}\phi\\ \theta\end{bmatrix}_{ref}, \quad \mathbf{z}_1 = \mathbf{y}_1 - \mathbf{y}_{1,ref}, \quad \mathbf{x}_1 = \begin{bmatrix}\phi\\ \theta\\ \psi\end{bmatrix}, \quad \mathbf{x}_2 = \begin{bmatrix}p\\ q\\ r\end{bmatrix}, \quad \mathbf{u} = \begin{bmatrix}\delta_e\\ \delta_r\\ \delta_a\end{bmatrix}. \tag{12}$$

The references are outputs of a pre-filter to prevent unachievable commands that will saturate the actuators. The pre-filter also provides a time-derivative of the reference signal, which is used for feed-forward control.

1. *Dynamics*

The output $\mathbf{y}_1$ is related to the state $\mathbf{x}_1$ by

$$\mathbf{y}_1 = \begin{bmatrix}1 & 0 & 0\\ 0 & 1 & 0\end{bmatrix}\mathbf{x}_1 = H_1\mathbf{x}_1 \tag{13}$$

The dynamics of $\mathbf{x}_1$ are purely kinematic and we can write

$$\dot{\mathbf{x}}_1 = G_1(\mathbf{x}_1)\mathbf{x}_2 \tag{14}$$

with

$$G_1 = \begin{bmatrix}1 & \sin\phi\tan\theta & \tan\theta\cos\phi\\ 0 & \cos\phi & -\sin\phi\\ 0 & \sin\phi\sec\theta & \cos\phi\sec\theta\end{bmatrix} \tag{15}$$

The dynamics of the angular rates $\mathbf{x}_2$ are stated in Eq. (4). The aerodynamic moment $\mathbf{M}_a$ in Eq. (4) is split up in a control-dependent and a control-independent part, using Eq. (5) and Eq. (6)

$$\dot{\mathbf{x}}_2 = \mathbf{f}_2(\mathbf{x}) + \mathbf{g}_2(\mathbf{x}, \mathbf{u}) \tag{16}$$

with

$$\begin{aligned}\mathbf{f}_2(\mathbf{x}) &= I^{-1}\left(\bar{q}S\begin{bmatrix}b & & \\ & \bar{c} & \\ & & b\end{bmatrix}\mathbf{C}_{M,\text{base+rate}} + \mathbf{M}_p - \boldsymbol{\omega}\times\mathbf{V}\right)\\ \mathbf{g}_2(\mathbf{x}, \mathbf{u}) &= I^{-1}\bar{q}S\begin{bmatrix}b & & \\ & \bar{c} & \\ & & b\end{bmatrix}\mathbf{C}_{M,\text{ctrl}}\end{aligned} \tag{17}$$

Here, $\mathbf{x}$ denotes the total aircraft state which also includes aerodynamic speed and attitude. The dynamics of the angular rates can be written in incremental form by considering a Taylor series expansion around a previous point t_0 in the recent past[21,34,35]

$$\dot{\mathbf{x}}_2 = \dot{\mathbf{x}}_{2,0} + \underbrace{\left(\frac{\partial\mathbf{f}_2(\mathbf{x})}{\partial\mathbf{x}} + \frac{\partial\mathbf{g}_2(\mathbf{x},\mathbf{u})}{\partial\mathbf{x}}\right)\bigg|_{\substack{\mathbf{x}=\mathbf{x}_0\\ \mathbf{u}=\mathbf{u}_0}}}_{F_{2,0}}(\mathbf{x}-\mathbf{x}_0) + \underbrace{\frac{\partial\mathbf{g}_2(\mathbf{x},\mathbf{u})}{\partial\mathbf{u}}\bigg|_{\substack{\mathbf{x}=\mathbf{x}_0\\ \mathbf{u}=\mathbf{u}_0}}}_{G_{2,0}}(\mathbf{u}-\mathbf{u}_0) + \mathcal{O}\big((\mathbf{x}-\mathbf{x}_0)^2, (\mathbf{u}-\mathbf{u}_0)^2\big) \tag{18}$$

The second term contains the control derivatives. The estimate $\hat{G}_{2,0}$ is constructed as

$$\hat{G}_{2,0} = I^{-1}\bar{q}S \begin{bmatrix} 0 & bC_{l_{\delta_r}} & bC_{l_{\delta_a}} \\ \bar{c}C_{m_{\delta_e}} & 0 & 0 \\ 0 & bC_{n_{\delta_r}} & bC_{n_{\delta_a}} \end{bmatrix} \tag{19}$$

in which the non-dimensional control derivatives are obtained from the polynomial model fit described earlier. Eq. (18) is written in shorter form as

$$\dot{\mathbf{x}}_2 = \dot{\mathbf{x}}_{2,0} + F_{2,0}\Delta\mathbf{x} + G_{2,0}\Delta\mathbf{u} + \mathcal{O}(\Delta\mathbf{x}^2, \Delta\mathbf{u}^2). \tag{20}$$

Under the assumption that $\mathbf{f}_2(\mathbf{x})$ and $\mathbf{g}_2(\mathbf{x}, \mathbf{u})$ do not change significantly due to changes of $\mathbf{x}$ in the interval $[t_0, t]$, and that over this same interval the system is linear so that the higher order terms can be neglected, we can use the following approximation for the angular accelerations:

$$\dot{\mathbf{x}}_2 \cong \dot{\mathbf{x}}_{2,0} + G_{2,0}\Delta\mathbf{u} \tag{21}$$

This assumption is the fundamental step in the simplifications for incremental nonlinear control techniques. If this assumption cannot be made, the term $F_{2,0}\Delta\mathbf{x}$ cannot be neglected in Eq. (21). Because $F_{2,0}$ contains the major part of the system dynamics, neglecting this term makes any derived model-based control law only dependent on $G_{2,0}$. In section V, an analysis has been presented that shows that for fixed-wing aircraft steady state tracking errors in the angular rate loop are caused by system dynamics increments which are not cancelled because the term $F_{2,0}\Delta\mathbf{x}$ *is* significant. Fast actuators, high sample rate and a short measurement delay must be used to reduce the influence of system dynamics increments.

Using the incremental description for the system dynamics, control laws can be made for the incremental control input $\Delta\mathbf{u}$ instead of the total control input $\mathbf{u}$. This means that an incremental control $\Delta\mathbf{u}$ will be derived so that the total control is the sum of the increment and the input at a previous point in time, hence $\mathbf{u} = \Delta\mathbf{u} + \mathbf{u}_0$.

2. *Backstepping Procedure*

The idea of the backstepping procedure is to show that with appropriate choices for the inner loop command $\mathbf{x}_{2,ref}$ and input $\mathbf{u}$, the compensated tracking error is asymptotically stable. By defining the the tracking error $\mathbf{z}_1$, we convert the tracking problem into a stabilization problem. The system is proven to be asymptotically stable if it can be shown that a Lyapunov function can be derived for the equilibrium point at $\mathbf{z}_1, \mathbf{z}_2 = \mathbf{0}$. Command-filtered backstepping is implemented by using a linear, first-order command filter to calculate a smooth reference $\mathbf{x}_{2,ref}$ from the command value $\mathbf{x}_{2,cmd}$. This is obviates the need to calculate the time derivative $\dot{\mathbf{x}}_{2,ref}$ analytically. The bandwidth of this linear filter is high enough so that it is safe to assume for the derivation that $\mathbf{x}_{2,ref} = \mathbf{x}_{2,cmd}$. Therefore, in the derivation below only the final stabilizing reference $\mathbf{x}_{2,ref}$ is used.

The backstepping procedure is started by defining the first control Lyapunov function (CLF) as a radially unbounded function in the elements of $\mathbf{z}_1$ as

$$V_1(\mathbf{z}_1) = \frac{1}{2}\mathbf{z}_1^T\mathbf{z}_1. \tag{22}$$

Let the reference $\mathbf{x}_{2,ref}$ satisfy

$$\mathbf{x}_{2,ref} = G_1^{-1}\left(\begin{bmatrix} -C_1\mathbf{z}_1 - C_{1,d}\dot{\mathbf{z}}_1 \\ 0 \end{bmatrix} + \begin{bmatrix} \dot{\mathbf{x}}_{1,ref} \\ \dot{\psi}_{ref} \end{bmatrix}\right) \tag{23}$$

with C_1, $C_{1,d}$ being diagonal matrices with positive definite elements. The error dynamics $\dot{\mathbf{z}}_1$ yield

$$\begin{aligned} \dot{\mathbf{z}}_1 &= H_1G_1(\mathbf{z}_2 + \mathbf{x}_{2,ref}) - \dot{\mathbf{x}}_{1,ref} \\ &= H_1G_1\mathbf{z}_2 - C_1\mathbf{z}_1 - C_{1,d}\dot{\mathbf{z}}_1 \\ &= (I_{2\times2} + C_{1,d})^{-1}H_1G_1\mathbf{z}_2 - (I_{2\times2} + C_{1,d})^{-1}C_1\mathbf{z}_1 \end{aligned} \tag{24}$$

By substition of Eq. (24), the time derivative $\dot{V}_1$ yields

$$\begin{aligned}\dot{V}_1 &= \mathbf{z}_1^T \dot{\mathbf{z}}_1 \\ &= -\mathbf{z}_1^T (I_{2\times 2} + C_{1,d})^{-1} C_1 \mathbf{z}_1 + \mathbf{z}_1^T (I_{2\times 2} + C_{1,d})^{-1} H_1 G_1 \mathbf{z}_2\end{aligned} \tag{25}$$

Then, $\dot{V}_1$ is negative definite along $\mathbf{z}_1$, except for the second term due to $\mathbf{z}_2$. This term will be accounted for in the subsequent design step. To start the next and final step of the backstepping procedure, augment the CLF by a term that is radially unbounded in the elements of $\mathbf{z}_2$:

$$V_2(\mathbf{z}_1, \mathbf{z}_2) = V_1 + \frac{1}{2}\mathbf{z}_2^T \mathbf{z}_2 \tag{26}$$

The time derivative must be negative definite, in which we substitute for the system dynamics of $\mathbf{x}_2$ in incremental form:

$$\dot{V}_2 = \dot{V}_1 + \mathbf{z}_2^T \left\{ \dot{\mathbf{x}}_{2,0} + G_{2,0} \Delta \mathbf{u} - \dot{\mathbf{x}}_{2,ref} \right\} \tag{27}$$

If the incremental control satisfies

$$\Delta \mathbf{u} = G_{2,0}^{-1} \left(-C_2 \mathbf{z}_2 - \dot{\mathbf{x}}_{2,0} + \dot{\mathbf{x}}_{2,ref} + G_1^T H_1^T (I_{2\times 2} + C_{1,d})^{-1} \mathbf{z}_1 \right) \tag{28}$$

then the time derivative of the final CLF $\dot{V}_2$ yields

$$\dot{V}_2 = -\mathbf{z}_1^T C_1^\star \mathbf{z}_1 - \mathbf{z}_2^T C_2 \mathbf{z}_2, \tag{29}$$

with $C_1^\star = (I_{2\times 2} + C_{1,d})^{-1} C_1$ a diagonal matrix with positive definite elements. This shows that $\dot{V}_2$ is negative definite along $\mathbf{z}_1$ and $\mathbf{z}_2$. The result implies that with the given commands, the equilibrium $\mathbf{z}_1, \mathbf{z}_2 = 0$ is asymptotically stable, which implies that $\mathbf{z}_1, \mathbf{z}_2 \to \mathbf{0}$ when $t \to \infty$. Furthermore, the stabilization problem is exponentially stable in all terms with a decay rate determined by $C_1^\star$ and C_2, because a positive definite scalar η exists such that

$$\begin{aligned}\dot{V}_2 &= -\mathbf{z}_1^T C_1^\star \mathbf{z}_1 - \mathbf{z}_2^T C_2 \mathbf{z}_2 \\ &\leq -\eta \left(\frac{1}{2}\mathbf{z}_1^T \mathbf{z}_1 + \frac{1}{2}\mathbf{z}_2^T \mathbf{z}_2 \right) \\ &= -\eta V_2\end{aligned} \tag{30}$$

Control diagrams of the outer and inner loop are shown in Figs. 6 and 7.

3. Heading rate reference for coordinated turn maneuvers

From the derived intermediate control law in Eq. (23) it follows that an arbitrary reference $\dot{\psi}_{ref}$ may be defined without affecting the stability of the controlled variables. Usually, a desired heading rate $\dot{\psi}$ or course rate $\dot{\chi}$ determines the required roll angle ϕ. However, in the control problem presented in this paper we are only interested in the control of the roll and pitch angle. Therefore, the reference $\dot{\psi}_{ref}$ is determined by the actual roll angle to achieve a coordinated turn. Consider the course angle dynamics, using the sum of forces in the lateral direction of the horizontal plane

$$mV_c \cos\gamma_c \dot{\chi}_c = \bar{Y}^b \cos\beta \cos\mu_c + L \sin\mu_c + F_T (\sin\alpha_c \sin\mu_c - \cos\alpha_c \cos\mu_c \sin\beta_c) \tag{31}$$

Here, $V \cos\gamma_c$ is the total airspeed in the horizontal plane and L the aerodynamic lift. We aim to bring the body side force $\bar{Y}$ to zero to achieve a coordinated turn. Furthermore, we neglect the effect of the thrust in the lateral direction so that $F_T \sin\beta_c \approx 0$, and the reference course rate for a coordinated turn is set to

$$\dot{\chi}_{c,ref} = \frac{1}{mV_c \cos\gamma_c} \left(L \sin\mu_c + F_T (\sin\alpha \sin\mu_c) \right) \tag{32}$$

in which an approximation of the vertical specific force can be substituted, because $mA_z \approx L + F_T \sin\alpha$. The calculation of the bank angle μ involves quite complex kinematics, although in practice and for the experiments considered in this paper, it is very close to the roll angle ϕ. Furthermore, the reference $\dot{\chi}_{c,ref}$ is set by the reference roll angle ϕ_{ref} instead of the state ϕ. In this way, the course rate reference *anticipates* for roll angle to be tracked. We are interested in finding a reference for $\dot{\psi}_{ref}$ instead of $\dot{\chi}_{ref}$. When there

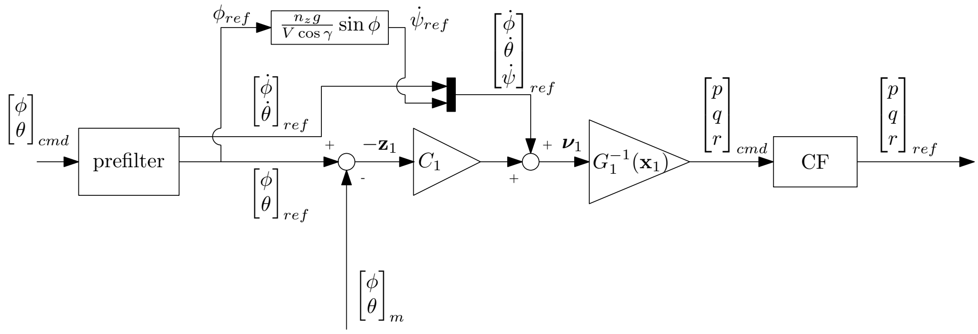

Figure 6. Outer loop control structure of the IBS Euler attitude control law. Angular rate references are passed to an inner-loop control law shown in Fig. 7.

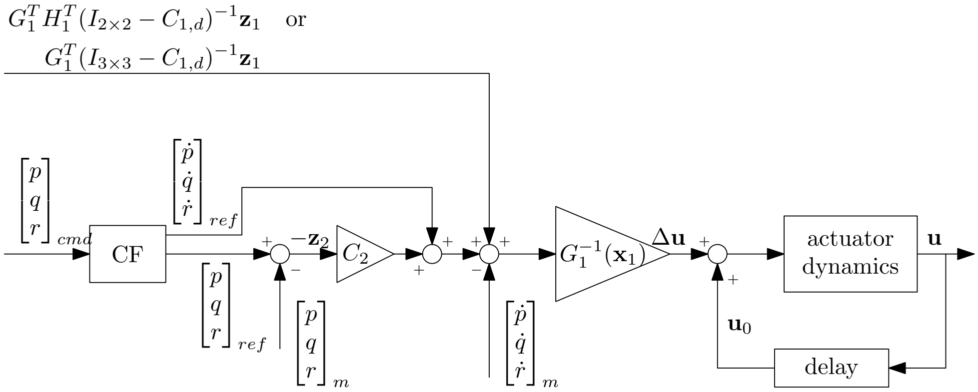

Figure 7. Inner loop control structure for both the IBS Euler attitude control law and IBS aerodynamic attitude control law

would be no wind, it holds that $\psi_{ref} = \chi_{ref}$, but with a constant wind, the aircraft heading deviates with a crab angle β_f, so that a reference for ψ_{ref} relates to the reference course angle by $\dot{\chi}_{ref} = \dot{\psi}_{ref} + \dot{\beta}_f$. A heading rate reference is therefore designed as

$$\begin{aligned}\dot{\psi}_{ref} &= \dot{\chi}_{c,ref} + \Delta\dot{\psi}_{ref} \\ &= \frac{mA_z \sin\phi_{ref}}{V_c \cos\gamma_c} + \Delta\dot{\psi}_{ref}\end{aligned} \tag{33}$$

with $\Delta\dot{\psi}_{ref}$ defined by a proportional control law on the side slip error that compensates for the effects of the crab angle β_f, as well as for all other deviations due to the assumptions made in this derivation, hence

$$\dot{\psi}_{ref} = \frac{mA_z \sin\phi_{ref}}{V_c \cos\gamma_c} + K_{p_\psi} A_y. \tag{34}$$

4. Multi-loop nonlinear dynamic inversion control law

In this section, a multi-loop nonlinear dynamic inversion (NDI) control law will be derived for the same control problem. It will be shown that the resulting control law is very similar. For a multi-loop NDI control structure, time-scale separation is assumed between the two control loops. This means that the dynamics of the inner loop, $\dot{\mathbf{x}}_2$, are assumed to be much faster than the outer loop dynamics $\dot{\mathbf{x}}_1$. It is hence assumed that in the outer loop, references for the angular rate are achieved immediately. Consider the outer loop dynamics:

$$\begin{aligned}\mathbf{y}_1 &= H_1\mathbf{x}_1 \\ \dot{\mathbf{x}}_1 &= G_1\mathbf{x}_2\end{aligned} \tag{35}$$

Applying the control law $\mathbf{x}_{2,ref} = G_1^{-1}\boldsymbol{\nu}_1$ yields $\dot{\mathbf{x}}_1 = \boldsymbol{\nu}_1$ (when assuming time-scale separation). By forcing the error dynamics to be exponentially stable, the virtual control is defined as

$$\boldsymbol{\nu}_1 = \begin{bmatrix} -C_1\mathbf{z}_1 - C_{1,d}\dot{\mathbf{z}}_1 \\ 0 \end{bmatrix} + \begin{bmatrix} \dot{\mathbf{z}}_{1,ref} \\ \dot{\psi}_{ref} \end{bmatrix} \tag{36}$$

By applying

$$\Delta\mathbf{u} = G_{2,0}^{-1}\left(\boldsymbol{\nu}_2 - \dot{\mathbf{x}}_{2,0}\right) \tag{37}$$

for the inner loop, where $\boldsymbol{\nu}_2$ is the virtual control law, set to

$$\boldsymbol{\nu}_2 = -C_2\mathbf{z}_2 + \dot{\mathbf{x}}_{2,ref}. \tag{38}$$

With appropriate choices for C_2 (in this case setting the elements positive definite), inner loop error dynamics $\dot{\mathbf{z}}_2$ are stable and decoupled. Hence, the final multi-loop INDI control laws are

$$\begin{aligned} \mathbf{x}_{2,ref} &= G_1^{-1}\left(\begin{bmatrix} -C_1\mathbf{z}_1 - C_{1,d}\dot{\mathbf{z}}_1 \\ 0 \end{bmatrix} + \begin{bmatrix} \dot{\mathbf{z}}_{1,ref} \\ \dot{\psi}_{ref} \end{bmatrix}\right) \\ \Delta\mathbf{u} &= G_{2,0}^{-1}\left(-C_2\mathbf{z}_2 + \dot{\mathbf{x}}_{2,ref} - \dot{\mathbf{x}}_{2,0}\right) \end{aligned} \tag{39}$$

with $C_1, C_{1,d}, C_2$ being diagonal matrices with positive definite elements. Comparing the terms with Eq. (23) and Eq. (28), one sees that the only difference is the compensation term $G_1^T H_1^T \mathbf{z}_1$.

B. Attitude control of aerodynamic angles

For the backstepping control procedure presented in this section, the aerodynamic attitude of the aircraft is controlled. Controlled variables are

$$\phi = \phi_{ref}, \quad \alpha = \alpha_{ref}, \quad \beta = \beta_{ref} \tag{40}$$

By controlling the aerodynamic attitude, one effectively controls the aerodynamic forces on the aircraft, since at given airspeeds the angle of attack is proportional to the vertical load. This type of control is useful for trajectory control or the attitude control of high-performance aircraft. Simulations with INDI and IBS aerodynamic attitude control laws are successfully shown previously in literature.[25,33,36] β_{ref} is set to zero to approximate a coordinated turn. This differs from the approach in the previous section where we aimed to control the side force $\bar{Y}$ to zero. The state $\mathbf{x}_1$ and tracking error $\mathbf{z}_1$ are now defined as

$$\mathbf{x}_1 = \begin{bmatrix} \phi \\ \alpha \\ \beta \end{bmatrix}, \quad \mathbf{x}_{1,ref} = \begin{bmatrix} \phi \\ \alpha \\ \beta \end{bmatrix}_{ref}, \quad \mathbf{z}_1 = \mathbf{x}_1 - \mathbf{x}_{1,ref} \tag{41}$$

1. *Dynamics*

While the time derivative of ϕ directly follows from the kinematic transformation presented in Eq. (14), the time derivative of α and β can be derived from a coordinate transformation of $[u, v, w] \Leftrightarrow [V_c, \alpha_c, \beta_c]$[25,33] and substitution in the equation for the linear accelerations in Eq. (3). A subscript c has been explicitly added to denote that the aerodynamic angles are with respect to the inertial constant-wind reference frame, because u, v, w in Eq. (3) are the inertial body velocities. Hence, they are not relative to the local wind. When considering an inertial frame fixed to the constant horizontal wind component, the equations for $\dot{\alpha}_c$ and $\dot{\beta}_c$ hold. The time derivatives for α_c and β_c yield

$$\begin{aligned} \dot{\alpha}_c &= q - p\cos\alpha_c\tan\beta_c - r\sin\alpha_c\tan\beta_c + \frac{1}{mV_c\cos\beta_c}\big(-A_x\sin\alpha_c + A_z\cos\alpha_c + mg_3\big) \\ \dot{\beta}_c &= p\sin\alpha_c - r\cos\alpha_c + \frac{1}{mV_c}\big(-A_x\cos\alpha_c\sin\beta_c + A_y\cos\beta_c - A_z\sin\alpha_c\sin\beta_c + mg_2\big) \end{aligned} \tag{42}$$

with A_x, A_y, A_z the specific forces and

$$\begin{aligned} g_2 &= g\left(\cos\alpha_c\sin\beta_c\sin\theta + \cos\beta_c\sin\phi\cos\theta - \sin\alpha_c\sin\beta_c\cos\phi\cos\theta\right) \\ g_3 &= g\left(\sin\alpha_c\sin\theta + \cos\alpha_c\cos\phi\cos\theta\right) \end{aligned} \tag{43}$$

The dynamics can be written in a more general form as

$$\dot{\mathbf{x}}_1 = \mathbf{f}_1(\mathbf{x}, \dot{\mathbf{x}}) + G_1(\mathbf{x})\mathbf{x}_2 \tag{44}$$

with

$$\begin{aligned}
\mathbf{f}_1(\mathbf{x}, \dot{\mathbf{x}}) &= \begin{bmatrix} 0 \\ \frac{1}{mV_c \cos\beta_c}\big(- A_x \sin\alpha_c + A_z \cos\alpha_c + mg_3\big) \\ \frac{1}{mV_c}\big(- A_x \cos\alpha_c \sin\beta_c + A_y \cos\beta_c - A_z \sin\alpha_c \sin\beta_c + mg_2\big) \end{bmatrix} \\
G_1(\mathbf{x}_1, \theta) &= \begin{bmatrix} 1 & \sin\phi \tan\theta & \tan\theta \cos\phi \\ -\cos\alpha_c \tan\beta_c & 1 & -\sin\alpha_c \tan\beta_c \\ \sin\alpha_c & 0 & -\cos\alpha_c \end{bmatrix}
\end{aligned} \tag{45}$$

$\mathbf{f}_1$ depends on the state derivative $\dot{\mathbf{x}}$, because accelerations appear in the equations for $\dot{\alpha}_c$ and $\dot{\beta}_c$. The structure differs from the outer loop dynamics in the previous section in Eq. (14) because of the extra system dynamics term $\mathbf{f}_1$. This term is measurable when $A_{x,yz}$ and the aerodynamic attitude $V_c\alpha_c, \beta_c$ are available and does only contain kinematic relationships.

2. Backstepping Procedure

The backstepping procedure for this control problem is very similar to the problem defined in the previous section. Again, a fast, unconstrained command filter is used for $\mathbf{x}_{2,ref}$ to obtain a time derivative $\dot{\mathbf{x}}_{2,ref}$. The control Lyapunov function (CLF) is again defined as $V_1 = \frac{1}{2}\mathbf{z}_1^T\mathbf{z}_1$, and the raw intermediate control is defined as

$$\mathbf{x}_{2,ref} = G_1^{-1}\left(-C_1\mathbf{z}_1 - C_{1,d}\dot{\mathbf{z}}_1 - \mathbf{f}_1 + \dot{\mathbf{x}}_{1,ref}\right) \tag{46}$$

with C_1 and $C_{1,d}$ diagonal matrices with positive definite elements. The error dynamics yield

$$\begin{aligned}
\dot{\mathbf{z}}_1 &= \mathbf{f}_1 + G_1\mathbf{x}_2 - \dot{\mathbf{x}}_{1,ref} \\
&= \mathbf{f}_1 + G_1(\mathbf{x}_{2,ref} + \mathbf{z}_2) - \dot{\mathbf{x}}_{1,ref} \\
&= -C_1\mathbf{z}_1 - C_{1,d}\dot{\mathbf{z}}_1 + G_1\mathbf{z}_2 \\
&= -(I_{3\times3} + C_{1,d})^{-1}C_1\mathbf{z}_1 + (I_{3\times3} + C_{1,d})^{-1}G_1\mathbf{z}_2
\end{aligned} \tag{47}$$

Taking the time derivative of V_1 and substituting Eq. (47) yields

$$\begin{aligned}
\dot{V}_1 &= \mathbf{z}_1^T\dot{\mathbf{z}}_1 \\
&= -(I_{3\times3} + C_{1,d})^{-1}C_1\mathbf{z}_1 + (I_{3\times3} + C_{1,d})^{-1}G_1\mathbf{z}_2
\end{aligned} \tag{48}$$

The second step of the backstepping is identical to the previous section, except that one has to compensate a different term from the first step, because $\mathbf{z}_1^TG_1$ refers to different physical variables. Hence, augmenting the CLF as $V_2 = V_1 + \frac{1}{2}\mathbf{z}_2^T\mathbf{z}_2$ and selecting the raw incremental control law as

$$\Delta\mathbf{u} = G_{2,0}^{-1}\left(-C_2\mathbf{z}_2 + \dot{\mathbf{x}}_{2,ref} + G_1^T(I_{3\times3} + C_{1,d})^{-1}\mathbf{z}_1\right) \tag{49}$$

yields

$$\dot{V}_2 = -\mathbf{z}_1^TC_1^\star\mathbf{z}_1 - \mathbf{z}_2^TC_2\mathbf{z}_2 \tag{50}$$

with $C_1^\star = (I_{3\times3} + C_{1,d})^{-1}C_1$. This implies again that $\mathbf{z}_1, \mathbf{z}_2 \to 0$ when $t \to \infty$, and asymptotic stability is obtained. Furthermore, the stabilization problem is exponentially stable in all terms with a decay rate determined by $C_1^\star$ and C_2, because a positive definite scalar η exist such that

$$\begin{aligned}
\dot{V}_2 &= -\mathbf{z}_1^TC_1^\star\mathbf{z}_1 - \mathbf{z}_2^TC_2\mathbf{z}_2 \\
&\leq -\eta\left(\frac{1}{2}\mathbf{z}_1^T\mathbf{z}_1 + \frac{1}{2}\mathbf{z}_2^T\mathbf{z}_2\right) \\
&= -\eta V_2
\end{aligned} \tag{51}$$

A schematic of the outer loop control law is shown in Fig. 8. The schematic of the inner loop already shown in the previous section in Fig. 7 also applies to the currently presented control law.

3. Multi-loop nonlinear dynamic inversion control law

Like the Euler attitude control laws presented in the previous section, also the aerodynamic attitude backstepping control laws can be compared to a multi-loop nonlinear dynamic inversion control law by ignoring some of the compensation terms that are introduced by the Lyapunov procedure. When considering again time-scale separation between both integrator steps, the reference $\mathbf{x}_2$ that linearizes the output $\mathbf{x}_1$ with respect to a virtual control $\boldsymbol{\nu}_1$ is:

$$\mathbf{x}_{2,ref} = G_1^{-1}\left(\boldsymbol{\nu}_1 - \mathbf{f}_1\right) \tag{52}$$

The virtual control law can be defined such that the error dynamics are exponentially stable:

$$\boldsymbol{\nu}_1 = -C_1\mathbf{z}_1 - C_{1,d}\dot{\mathbf{z}}_1 + \dot{\mathbf{x}}_{ref} \tag{53}$$

The inner loop INDI control law is identical to Eq. (39), hence the final multi-loop nonlinear dynamic inversion control laws are

$$\begin{aligned} \mathbf{x}_{2,ref} &= G_1^{-1}\left(-C_1\mathbf{z}_1 - C_{1,d}\dot{\mathbf{z}}_1 - \mathbf{f}_1 + \dot{\mathbf{x}}_{ref}\right) \\ \Delta\mathbf{u} &= G_{2,0}^{-1}\left(-C_2\mathbf{z}_2 + \dot{\mathbf{x}}_{2,ref} - \dot{\mathbf{x}}_{2,0}\right) \end{aligned} \tag{54}$$

Again, the multi-loop NDI control law only differs from the backstepping control design by the term $G_1^T(I_{3\times 3} + C_{1,d})^{-1}\mathbf{z}_1$

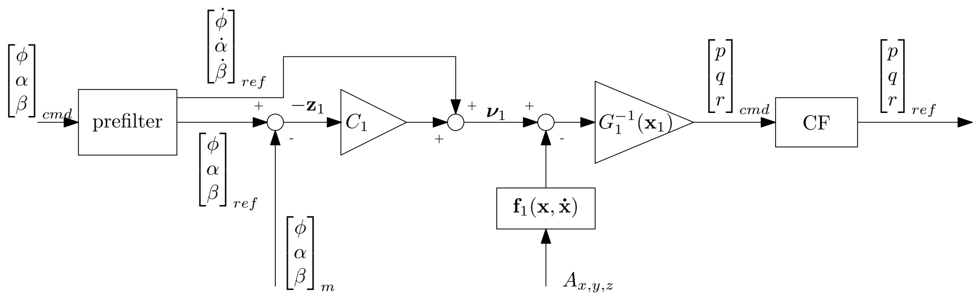

Figure 8. Outer loop control structure of the IBS aerodynamic attitude control law

C. Actuator dynamics

In the derivation for the backstepping and NDI control laws, the actuator dynamics have not been considered. If the actuator dynamics would be considered as part of the plant, this would have created at least one extra integrator step. Consequently, this would require to perform an extra step in the backstepping procedure, which means one would need a feedback for $\ddot{\mathbf{x}}_2$ in the control design.

In practise, actuator dynamics are considered to be time-scale separated from the controller, hence we assume that commands are reached instantaneously. With incremental control however, one relies on a synchronization of the inputs with the feedback of the state derivative. Therefore, $\mathbf{u}_0$ should be the delayed real control surface deflection. Furthermore, the feedback of the actuator position includes filters and delays that match the delays in the feedback of the state derivative $\dot{\mathbf{x}}_2$. It was already shown previously that this is a corret way to implement the incremental control law when including actuator dynamics with delayed acceleration measurements.[28] In Fig. 7, the general control scheme of the incremental control loop as part of the inner angular rate control loop has been depicted.

D. Parameter uncertainties

Thusfar, the derived control laws use a true inversion of $G_{2,0}$, i.e., the control derivatives are supposed to be perfectly known. Consider now the estimate $\hat{G}_{2,0}$ and the estimation error $\widetilde{G}_{2,0}$, related to each other by

$$G_{2,0} = \hat{G}_{2,0} + \widetilde{G}_{2,0} \tag{55}$$

and the overestimation factor matrix Γ

$$\hat{G}_{2,0} = \Gamma G_{2,0}. \tag{56}$$

For the inner loop angular rate stabilization, applying the control law

$$\Delta \mathbf{u} = \hat{G}_{2,0}^{-1} \left(-C_2 \mathbf{z}_2 + \dot{\mathbf{x}}_{2,ref} - \dot{\mathbf{x}}_{2,0} \right) \tag{57}$$

yields

$$\begin{aligned}
\dot{\mathbf{z}}_2 &= \dot{\mathbf{x}}_{2,0} + G_{2,0} \Delta \mathbf{u} - \dot{\mathbf{x}}_{2,ref} \\
&= \dot{\mathbf{x}}_{2,0} + \hat{G}_{2,0} \hat{G}_{2,0}^{-1} \left(-C_2 \mathbf{z}_2 + \dot{\mathbf{x}}_{2,ref} - \dot{\mathbf{x}}_{2,0} \right) - \dot{\mathbf{x}}_{2,ref} + \widetilde{G}_{2,0} \hat{G}_{2,0}^{-1} \left(-C_2 \mathbf{z}_2 + \dot{\mathbf{x}}_{2,ref} - \dot{\mathbf{x}}_{2,0} \right) \\
&= -C_2 \mathbf{z}_2 + (I_{3\times3} - \Gamma)\Gamma^{-1} \left(-C_2 \mathbf{z}_2 + \dot{\mathbf{x}}_{2,ref} - \dot{\mathbf{x}}_{2,0} \right) \\
&= -\Gamma^{-1} C_2 \mathbf{z}_2 + (\Gamma - I_{3\times3})\Gamma^{-1} \left(\dot{\mathbf{x}}_{2,0} - \dot{\mathbf{x}}_{2,ref} \right)
\end{aligned} \tag{58}$$

where we used

$$\begin{aligned}
\widetilde{G}_{2,0} \hat{G}_{2,0}^{-1} &= (G_{2,0} - \Gamma G_{2,0}) \hat{G}_{2,0}^{-1} \\
&= (I_{3\times3} - \Gamma) G_{2,0} (\Gamma G_{2,0})^{-1} \\
&= (I_{3\times3} - \Gamma) G_{2,0} G_{2,0}^{-1} \Gamma^{-1} \\
&= (I_{3\times3} - \Gamma)\Gamma^{-1}.
\end{aligned} \tag{59}$$

For a more intuitive insight in the result, assume Γ to be a diagonal matrix, of which all elements on the diagonal equal a constant factor $1/\gamma$, so that Eq. (58) simplifies to

$$\dot{\mathbf{z}}_2 = -\gamma C_2 \mathbf{z}_2 + (1 - \gamma) \left(\dot{\mathbf{x}}_{2,0} - \dot{\mathbf{x}}_{2,ref} \right). \tag{60}$$

Note that γ now resembles an estimation factor such that $\gamma > 1$ implies an *underestimation.* Also note that this notation of the uncertainty of the inner loop control effectiveness estimate by γ corresponds to the definition used by Lu et al.[37] The following conclusions can be drawn for result in Eq. (60):

- The first term in Eq. (60) shows that the decay rate of the error is scaled by γ. This implies a slower convergence in the case of overestimation, i.e. when $\gamma < 1$,
- Comparing with the first equation of Eq. (58), the second term in Eq. (60) represents the untracked accelerations when $\gamma < 1$ (overestimation) or the overcompensated accelerations when $\gamma > 1$ (underestimation).
- When γ is very small, the control input will be very small and the error dynamics approach the open-loop dynamics.

In various previous studies on INDI and IBS, incremental angular rate control was combined with online parameter estimation methods to adapt the matrix $G_{2,0}$.[26,28,38] A simple way to implement adaptation is to use the certainty equivalence principle[11] by treating the estimate $\hat{G}_{2,0}$ in the control law as the true parameter. On-line identification of $\hat{G}_{2,0}$ can then be done in a separate, modular way. Because this type of adaption does still violate the Lyapunov stability proof, one can use integrated methods such as adaptive backstepping using tuning functions[11] or immersion and invariance[39,40] so that asymptotic stability is guaranteed. This paper does not focus on the estimation of $\hat{G}_{2,0}$. The control laws will use the best off-line estimated control derivatives to construct $\hat{G}_{2,0}$.

IV. Controller design and implementation

For a complete controller design, the control laws prented in section III are implemented with additional subsystems in the flight control software. These systems include state estimation and filtering modules, an auto-throttle system and functions dedicatated to the controller configuration. A functional overview of the implemented systems can be found in Fig. 9. The software has been designed such that control laws can be reconfigured quickly, for example to switch between the two different attitute control laws, or to switch between NDI and backstepping (BS) control laws.

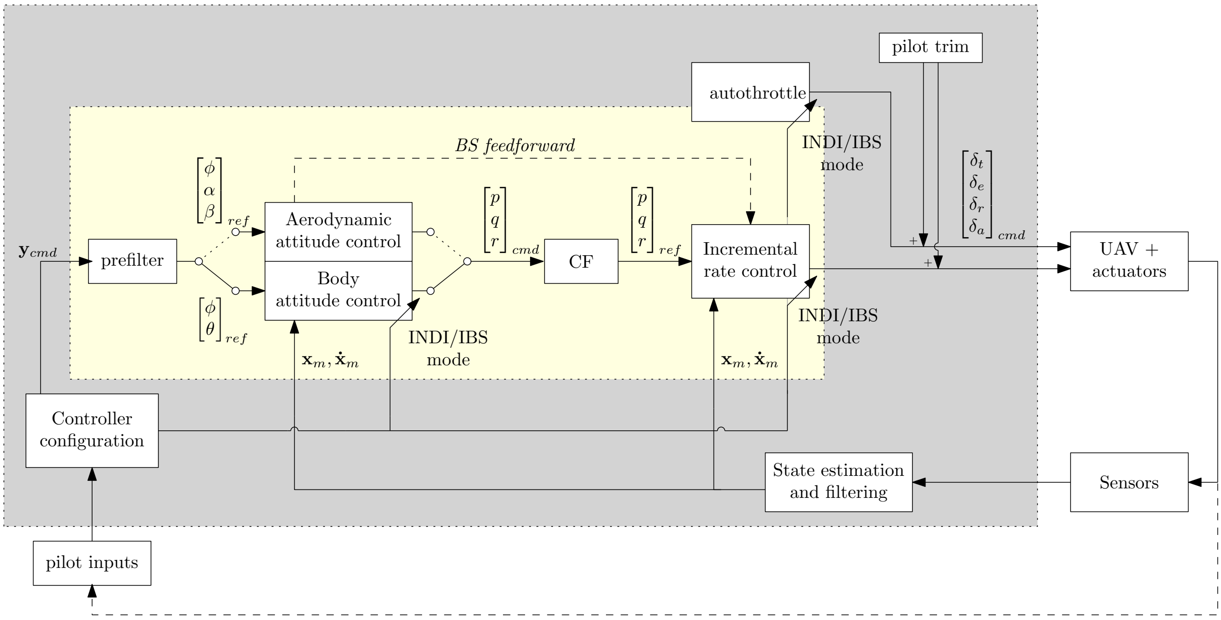

Figure 9. General controller structure at a functional level.

The software is implemented on the "Goldy flight control system (FCS)", of which the most important hardware components are listed in Tab. 4. The control laws run at a rate of 50 Hz. Implementing control laws on a flight computer that runs at discrete samples means that all integrators appearing in the control law must be discretized.

Table 4. Aircraft avionics and hardware components[1]

Component	Description
Flight Computer	Phytec MPC5200B Tiny (400 MHz, 64MB DDR DRAM, controller sample rate 50 Hz)
GPS Receiver	Novatel OEM Star
IMU	Analog Devices ADIS16405
Servos	DS8411 (1.55 Nm @4.8 V)
Pressure sensors	AMS5812

A. Subsystems

1. Pre-filters and command filters

The system dynamics and platform specifications have been assessed and simulated to design a suitable controller that matches the capabilities and limitations of the platform. Pre-filters for the attitude commands are second-order linear filters with rate and position limits, so that the dynamics for each reference signal are described by

$$\begin{aligned}\begin{bmatrix} q_1(k+1) \\ q_2(k+1) \end{bmatrix} &= \begin{bmatrix} S_M\{q_1(k) + T_s q_2(k)\} \\ q_2(k) + T_s S_R \left\{ 2\zeta\omega_n \left(\frac{\omega_n^2}{2\zeta\omega_n} \left[y_{cmd}(k) - q_1(k) \right] - q_2(k) \right) \right\} \end{bmatrix} \\ y_{ref} &= q_1 \\ \dot{y}_{ref} &= q_2 \end{aligned} \tag{61}$$

with ζ, ω_n the damping and natural frequency of the filter, and S_R and S_M the magnitude and rate limits. The dynamics of the prefilter have been set such that no unachievable references are passed to the controller. Estimates of maximum achievable angular rates and accelerations are used to verify that the pre-filter parameters have conservative settings. Estimates for maximum angular rates and accelerations are calculated using basic estimates of the stability derivatives, e.g.

$$\hat{p}_{max} = \frac{2V}{b} \frac{C_{l_{\delta_a}}}{C_{l_p}} \delta_{a_{max}}, \qquad \hat{\dot{p}}_{max} = -\frac{\bar{q}S}{I_{xx}} C_{l_{\delta_a}} \tag{62}$$

The derivative for α depends both on the pitch rate q and the load factor n_z (see Eq. (42)). The maximum rate $\dot{\alpha}_{ref}$ has been determined empirically by finding a conservative limit that yields achievable commands.

[1] For a detailed list see Owens (2006)[29] or the web page of the UAV Laboratory of the University of Minnesota: `http://uav.aem.umn.edu/`

The dynamics of the command-filters for the angular rate references are a first-order linear filter to limit the delays caused by each discrete integrator

$$x_{ref}(k+1) = x_{ref}(k) + T_s S_R \left\{\omega_n[x_{cmd}(k) - x_{ref}(k)]\right\} \tag{63}$$

Table 5. Pre-filter parameters and estimated maximum angular rates and accelerations

Ref	ω_n[rad/s]	$\zeta[-]$	rate limit [deg/s]	$\hat{\omega}_{max}$[deg/s]	$\hat{\dot{\omega}}_{max}$[deg/s²]
ϕ_{ref}	4	0.7	60	146.8	500.8
θ_{ref}	4	0.7	60	121.5	1571.4
α_{ref}	4	0.7	4		

2. *State estimation*

The flight software is equipped with a main state estimation module that fuses the sensor data from the linear accelerometers, rate gyros and GPS velocity using an extended Kalman filter (EKF) and estimates sensor biases to yield the best possible state estimate. The Kalman filter is based on a standard kinematic model, hence no detailed knowledge of the model is necessary for state estimation. The update rate is limited by the GPS model to about 1 Hz. The velocity and attitude estimations at intermediate samples are obtained from integration of linear accelerations and angular rates after substraction of the estimated bias. Standard deviations of the observed noise these sensors are 0.045 m/s² (accelerations) and 0.021 deg/s (angular rates), respectively.

3. *Aerodynamic attitude estimation and filtering*

On this UAV, no angle of attack or angle of sideslip measurements were available. This is problematic for the aerodynamic attitude controller, since it relies on a feedback of α and β. For this reason, the aerodynamic angles are estimated using the available aerodynamic model. For the angle of attack the simplified aerodynamic lift model is used to estimate α using vertical acceleration measurements:

$$\hat{C}_L = C_{L_0} + C_{L_\alpha}\alpha + C_{L_{\delta_e}}\delta_e, \quad \text{with} \quad \hat{C}_L\bar{q}S \cong -mA_z\cos\alpha \tag{64}$$

This equation is solved for α. For β, lateral accelerations A_y are used:

$$\hat{C}_Y = C_{Y_\beta}\beta + C_{Y_r}\frac{rb}{2V_a}, \quad \text{with} \quad \hat{C}_Y\bar{q}S \cong mA_y \tag{65}$$

When used in real flight, the estimations $\hat{\alpha}$ and $\hat{\beta}$ will contain the experienced turbulence at each particular moment. To prevent the aircraft to compensate for this turbulence and create unneccessary control effort, a complementary filter is used that complements low-pass filtered estimates $\hat{\alpha}$ and $\hat{\beta}$ with high-pass filtered measurements of the inertial angle of attack α_i and angle of sideslip β_i, calculated using the inertial (ground) velocity. The inertial velocity as estimated by the EKF is converted body frame coordinates by

$$\begin{bmatrix} u \\ v \\ w \end{bmatrix}_i = \mathbb{T}_{be}(\phi,\theta,\psi)\begin{bmatrix} V_N \\ V_E \\ V_D \end{bmatrix} \tag{66}$$

Then, angles α_i and β_i are calculated as

$$\alpha_i = \arctan\frac{w_i}{u_i}, \quad \beta_i = \arcsin\frac{v_i}{V_i} \tag{67}$$

The output of the complementary filter can be described by the discrete transfer function

$$\alpha_f(z) = \frac{\omega_{n,c}T_s}{z + \omega_{n,c}T_s - 1}\alpha_a(z) + \frac{z-1}{z + \omega_{n,c}T_s - 1}\alpha_i(z) \tag{68}$$

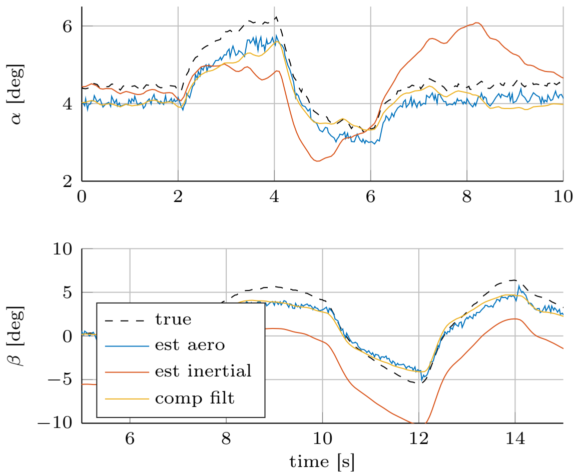

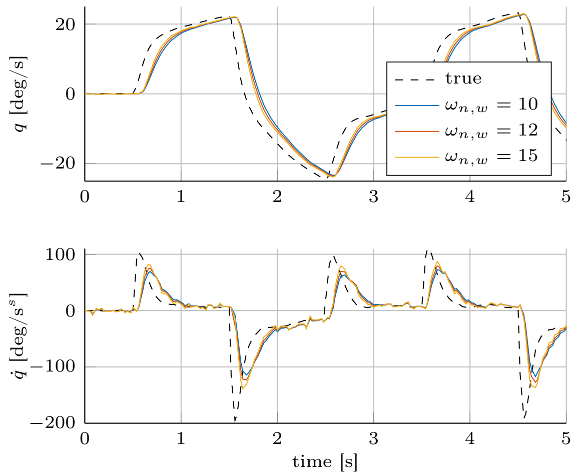

Figure 10. Simulated angle of attack (left) and angle of sideslip (right) estimation responses: aerodynamic estimate from accelerometers, inertial estimate from GPS velocity and complementary filtered angle.

Figure 11. Filtered pitch accelerations for different washout filter bandwidths $\omega_{n,w}$[deg/s].

where $\omega_{n,c}$ is the bandwidth of the filter, set to a frequency such that the turbulence is filtered out in α_f. This is implemented as

$$\begin{aligned} x_1(k) &= \alpha_i(k) - \alpha_i(k-1) + x_1(k-1) - \omega_{n,c} T_s x_1(k-1) \\ x_2(k) &= (1 - \omega_{n,c} T_s)\, x_2(k-1) + \omega_{n,c} T_s \alpha_a(k-1) \\ \alpha_f(k) &= x_1(k) + x_2(k) \end{aligned} \tag{69}$$

A complementary filter for β_f is implemented similarly. Fig. 10 shows simulated output of the filters under the presence of noise, turbulence and a constant horizontal wind, while executing a simultaneous pitch and roll maneuver.

4. Angular acceleration estimation

Because no sensors for angular acceleration are available, the accelerations are estimated from the angular rates. This is done using a washout filter. It is shown previously in literature that the use of a washout filter is a simple way to obtain estimates of the angular accelerations that can be used for an incremental control law.[25,28] In discrete time the washout filter is implemented as

$$\begin{aligned} \boldsymbol{\omega}_f(k+1) &= \boldsymbol{\omega}_f(k) + T_s \omega_{n,w} \left[\boldsymbol{\omega}_m(k) - \boldsymbol{\omega}_f(k)\right] \\ \dot{\boldsymbol{\omega}}_f(k) &= \omega_{n,w} \left[\boldsymbol{\omega}_{m,k} - \boldsymbol{\omega}_f(k)\right] \end{aligned} \tag{70}$$

with $\boldsymbol{\omega}_m = [p, q, r]_m^T$ the measured angular rates, $\boldsymbol{\omega}_f = [p, q, r]_f^T$ the filtered angular rates and $\dot{\boldsymbol{\omega}} = [\dot{p}, \dot{q}, \dot{r}]_f^T$ the filtered angular accelerations. $\omega_{n,w}$ denotes the bandwidth of the washout filter in rad/s, which has been set to 12 rad/s. It was determined minimizing by the phase lag caused by this filter while keeping acceptable noise levels on the final control surface commands. Fig. 11 shows the simulated output of the washout filter for three different bandwidth settings during a pitch up maneuver.

5. Auto-throttle

During the experiments, executed maneuvers will have an immediate effect on the airspeed. However, it is desired to keep the airspeed at the same level during each executed experiment run, because the airspeed as a great effect on the aerodynamic effectiveness of each control surface. A proportional-control auto-throttle system is integrated in the flight software to keep airspeed within an acceptable range. The control law is

$$\delta_t = S_M\{\delta_{t,trim} + K_{p,t}(V_a - V_{a,trim})\} \tag{71}$$

where the *trim* point refers to the state at which the experiment run was started so that only differences are commanded with respect to the initial state. The saturation levels of the throttle command are $[0, 1]$. During the executed experiments, the control gain was set to $K_{p,t} = 0.15$.

B. Controller gain tuning

Within the backstepping procedure, the only requirement that is imposed on the value of the gains to provide Lyapunov stability is that the gains are positive definite. In the case of multi-loop NDI control, time-scale separation is assumed. To guarantee time-scale separation, the controlled bandwidth of the outer loop, which is determined by the loop gain, should be lower than the inner loop so that the inner loop dynamics are much faster than the outer loop dynamics. Since actuator dynamics are not considered as part of the plant during the control law derivation, the bandwidth of the inner loop must respect the bandwidth of the actuators. Controller gains are tuned manually, by considering bandwidth limits for each control loop.

Table 6. Controller gains for body and aerodynamic attitude control

Aero			Body			
C_1	C_{1d}	C_2	C_1	C_{1d}	C_2	ω_{act}[rad/s]
3	1	6	4	1.5	8	12
5	0	8	4	2	8	12
1	0	2	-	-	8	12

During the control tuning it appeared that extra damping gains C_{1d} in the outer loop were required to decrease the overshoot. Tracking performance was improved by adding damping gains in the outer loop controller. The damping gains were only added in the euler attitude variables, hence not in the feedback for α and β.

Another parameter that can be tuned is the control effectiveness $G_{2,0}$. To perfectly cancel the system dynamics and to force the error dynamics stable and decoupled, the best estimate of the control effectiveness $\hat{G}_{2,0}$ should be used. However, the total control aggressiveness can be scaled by scaling this matrix. An overestimation of $G_{2,0}$ will result in a slower tracking response, similar to decreasing the proportional gain of a PID controller. In Acquatella et al.[41] it is already shown that by comparing INDI/IBS control laws with PID control, the proportional gain of the PID controller is directly related to $\hat{G}_{2,0}^{-1}$. For this reason, control laws can configured to a conservative setting by an overestimation of $G_{2,0}$. This corresponds with our findings in section D

C. Incremental control loop with actuator position feedback

Reliable actuator position measurements were not available for closed-loop experiments. Therefore, actuator positions are estimated using an on-line (discrete) model denoted by $\mathbf{A}(z)$, identified as a first-order linear system with rate limits:

$$\mathbf{u}(k+1) = \mathbf{u}(k) + T_s S_R \left\{\omega_{act}[\mathbf{u}_c(k) - \mathbf{u}(k)]\right\} \tag{72}$$

Here $\mathbf{u}_c$ are the commanded actuator positions. Furthermore, to synchronize the actuator feedback $\mathbf{u}_0$ with the angular acceleration feedback $\dot{\boldsymbol{\omega}}_0$, a controller time delay and a linear filter with the same bandwidth $\boldsymbol{\omega}_f$ as the washout filter has been incorporated in the incremental control loop (denoted by $\mathbf{H}(z)$. Finally, the controller command has been added to a constant initial command $\mathbf{u}_{trim}$, which correspond to the last actuator commands before the controller is switched on. This ensures a smooth transition when switching from manual to automatic control during flight. An overview of the final incremental control loop is displayed in Fig. 16.

D. Simulation and controller robustness

With the specified controller parameters for the loop gains, pre-filters, command-filters and total controller delay, series of simulations are performed to assess the robustness of the controllers. In these simulations, aerodynamic model parameters are varied by scaling the stability derivatives of the model by specific uncertainty factors F_* as defined earlier in section D. Simulations with only the inner loop angular rate tracking are also performed. Results of these simulations can be found in Figs. 12 and 13. A comparison is made with faster control actions, by increasing the bandwidth of the actuators to 5 Hz and increasing the washout filter bandwidth to 24 rad/s. The controller gain was increased by 50%. This shows the advantage of the systematic control structure; by only improving the controller specifications, the tracking response can be greatly improved without additional tuning of controller parameters.

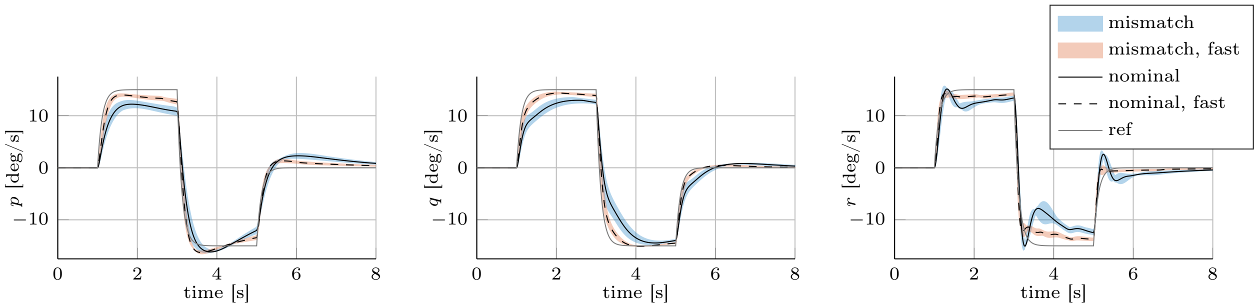

Figure 12. Tracking response of the INDI inner angular rate control loop, simulated separately for each different mode (roll/pitch/yaw), with the actual system specifications and with faster system specifications. Colored areas depict the simulated bounds with control effectiveness model mismatches affecting $\mathbf{g}_2$ only with $F_{i,\mathbf{ctrl}} = \pm 25\%$.

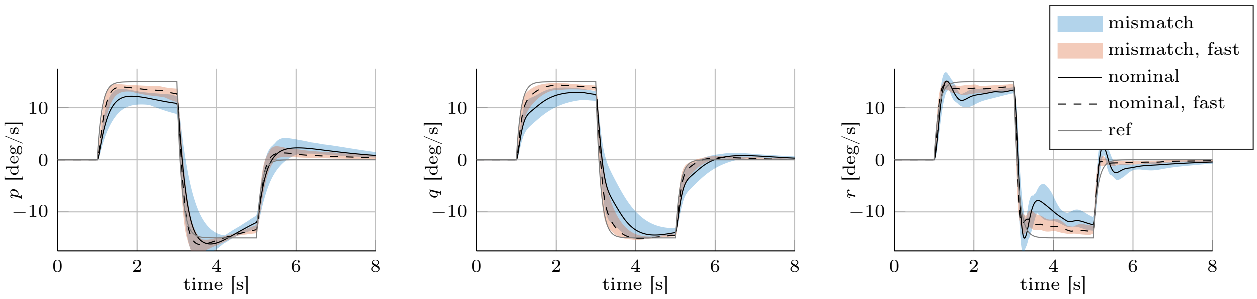

Figure 13. Tracking response of the INDI inner angular rate control loop, simulated separately for each different mode (roll/pitch/yaw), with the actual system specifications and with faster system specifications. Colored areas depict the simulated bounds with system dynamics model mismatches affecting both $\mathbf{f}_2$ and $\mathbf{g}_2$ by using parameter scaling factors $F_{i,\mathbf{base}}, F_{i,\mathbf{ctrl}}, F_{i,\mathbf{rate}} = \pm 25\%$.

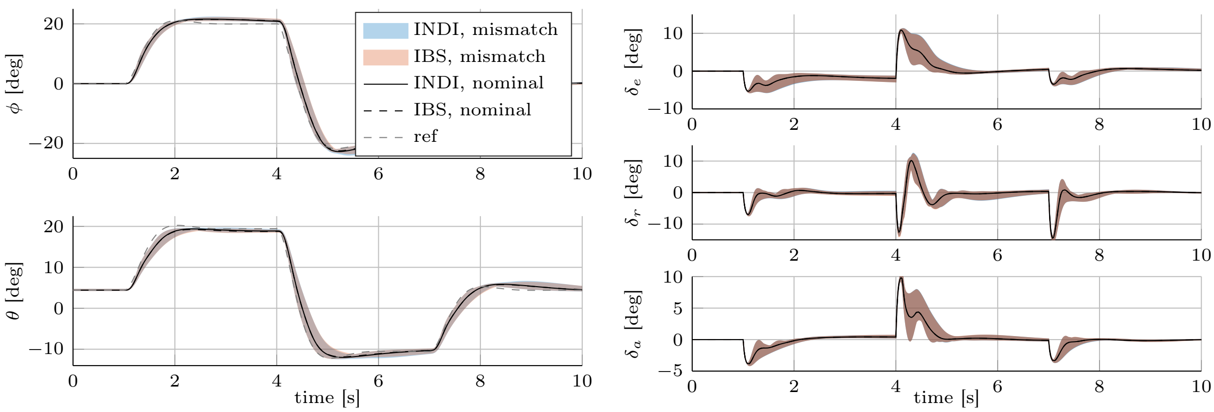

Figure 14. Tracking response of the INDI/IBS euler attitude controllers. Colored areas depict bounds of the simulations with control effector model mismatches of $F_{i,\mathbf{ctrl}} = \pm 25\%$

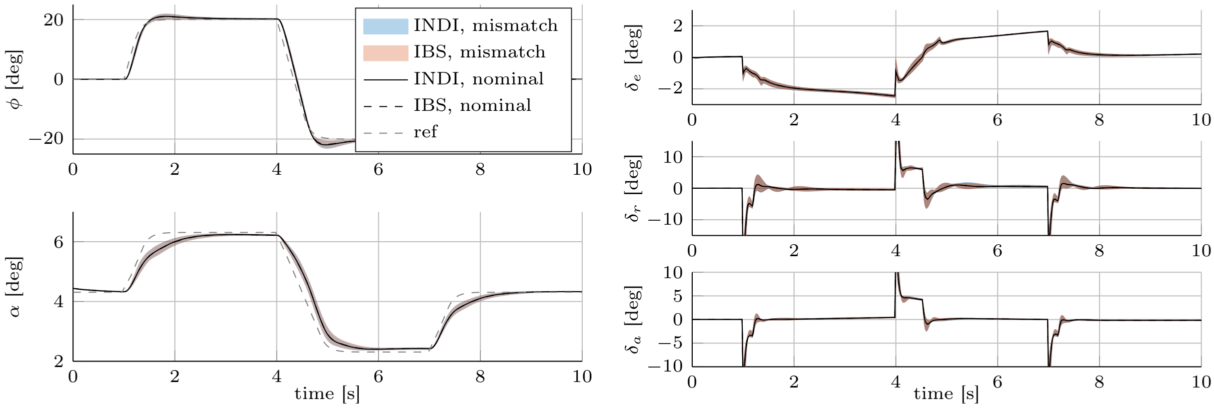

Figure 15. Tracking response of the INDI/IBS aerodynamic attitude controllers. Colored areas depict bounds of the simulations with control effector model mismatches of $F_{i,\mathbf{ctrl}} = \pm 25\%$

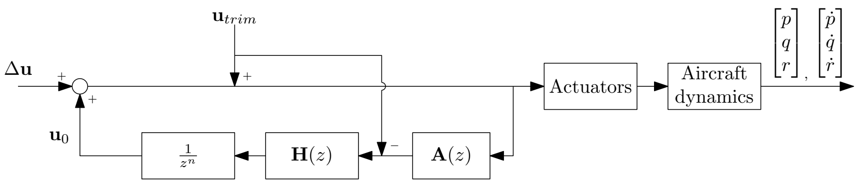

Figure 16. Incremental control loop with actuator model $\mathbf{A}(z)$, linear filter $\mathbf{H}(z)$ and delay.

Simulation results for the IBS and INDI euler attitude controllers are presented in Fig. 14. Simulation results of IBS and INDI aerodynamic attitude controllers are presented in Fig. 15. In both attitude control simulations, the estimation error of the control derivatives is varied by varying $F_{i,\text{ctrl}}$ over $\pm 25\%$. For both control laws, the tracking response of the IBS controller is almost identical to INDI. Hence, in the current tracking task the stabilizing term $G_1^T \mathbf{z}_1$ has little effect. The simulation results show that the system is highly robust to variations in model parameters.

V. Effects of system dynamics increments and total increment delay

We will now show that the assumption on neglecting system dynamics increments is not always valid, especially for fixed-wing aircraft. Consider again the first-order Taylor-series expansion of the state derivative around a previous point in time, as presented in Eq. (18):

$$\dot{\mathbf{x}}_2 = \dot{\mathbf{x}}_{2,0} + F_{2,0}\Delta\mathbf{x} + G_{2,0}\Delta\mathbf{u} + \mathcal{O}(\Delta\mathbf{x}^2, \Delta\mathbf{u}^2) \tag{73}$$

Neglecting increments caused by system dynamics and assuming a locally linear model, this equation is simplified to

$$\dot{\mathbf{x}}_2 \cong \dot{\mathbf{x}}_{2,0} + G_{2,0}\Delta\mathbf{u} \tag{74}$$

Previous papers on INDI and IBS have not discussed the validity of this assumption in detail, but usually mentioned the assumption of time-scale separation. It is argued that the control input $\mathbf{u}$ can change very fast and that the incremental time step is very fast, so that it can be assumed that $\Delta\mathbf{x} = 0$.[21,25,28,34] In the paper by Sieberling et al.,[21] the development of states other than the angular rates is not even considered. Also, most papers refer only to the development of the state, instead of the entire system dynamics increment $F_{2,0}\Delta\mathbf{x}$. In this section it will be shown that tracking errors in the angular rates arise due to these system dynamics increments. The size of those tracking errors is directly related to the so-called increment delay of the incremental control loop, which is smaller for faster actuator dynamics, for smaller acceleration measurement delays and for smaller overall controller delays.

Validation of the assumptions can be done by grouping the neglected terms into $\Delta\mathcal{F}$ and calculating this term by

$$\Delta\mathcal{F} = F_{2,0}\Delta\mathbf{x} + \mathcal{O}(\Delta\mathbf{x}^2, \Delta\mathbf{u}^2) = \dot{\mathbf{x}}_2 - \dot{\mathbf{x}}_{2,0} - G_{2,0}\Delta\mathbf{u} \tag{75}$$

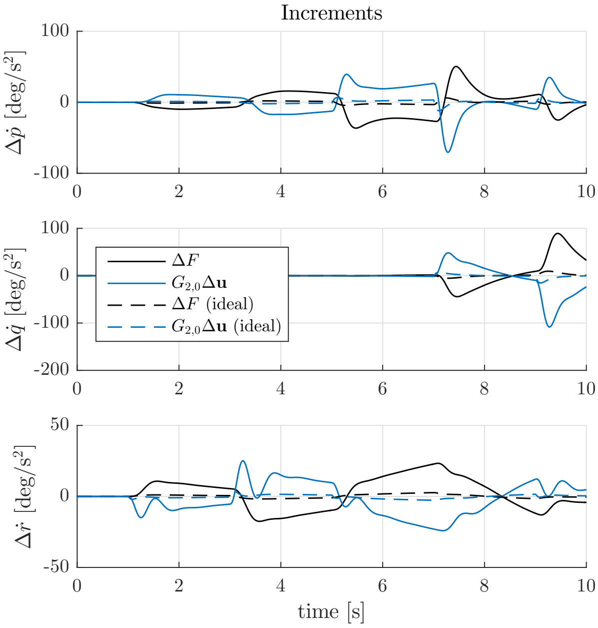

Figure 17. Comparison of incremental terms $\Delta\mathcal{F}$ and $G_{2,0}\Delta\mathbf{u}$ from Equation 73 while tracking angular rate references with the nominal INDI controller (solid) and the ideal controller (dashed).

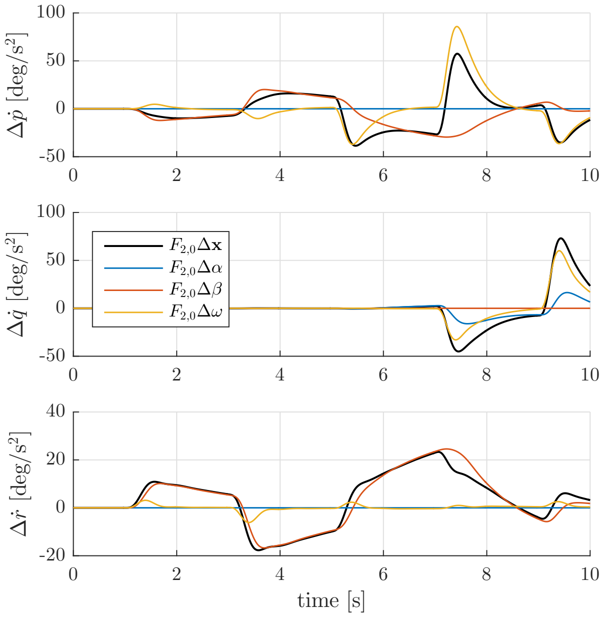

Figure 18. Breakdown of incremental term $F_{2,0}\Delta\mathbf{x}$ from Equation 73 while tracking angular rate references with the nominal INDI controller.

For the remainder of this discussion, we will refer to $\Delta\mathcal{F}$ as the system dynamics increments. Simulations have been performed to calculate this term. Results are shown in Fig. 17 and Fig. 19. Simulations are done both for the nominal model and for a system without actuator dynamics and with perfect angular acceleration feedback. The nominal system includes filters, delays and actuator dynamics that match the expected specifications of the FASER UAV. The ideal system does not include actuator dynamics and uses perfect and angular acceleration feedback without delays. In these figures, it can be seen that at almost any moment the control is applied, the system dynamics increment is not small. The system dynamics increments do damp out quite quickly in the pitch axis, but in the yaw and roll axes increments achieve a steady state value and are continuously counteracted by a control increment. The tracking response contains both transient and steady state tracking errors.

When the aerodynamics are simulated with a simplified linear polynomial model, the higher order terms in Eq. (73) can be neglected and the calculation of $\Delta\mathcal{F} = F_{2,0}\Delta\mathbf{x}$ becomes straightforward. From Eqs. (16) and (17) it follows that

$$F_{2,0}\Delta\mathbf{x} = \bar{q}S\begin{bmatrix} b & & \\ & \bar{c} & \\ & & b \end{bmatrix}\begin{bmatrix} & C_{l_\beta} & \frac{2V}{b}C_{l_p} & & \\ C_{m_\alpha} & & & \frac{2V}{c}C_{m_q} & \\ & C_{n_\beta} & & & \frac{2V}{b}C_{n_r} \end{bmatrix}\begin{bmatrix} \Delta\alpha \\ \Delta\beta \\ \Delta p \\ \Delta q \\ \Delta r \end{bmatrix}. \tag{76}$$

The effect of the cross-product of the angular rates generally is small and can be neglected. A breakdown of the different system dynamics increments is plotted in Fig. 18. From this the following can be concluded: during the tracking of step responses, the transient system dynamics increments are dominated by terms related to the angular rates, which are damping terms, whereas steady state increments are dominated by the aerodynamic angles; in the longitudinal dynamics, the angle of attack has only little effect on the system dynamics increment and the sideslip has no effect at all. However, in the lateral dynamics, the increment related to the sideslip angle is non-negligible. Hence, the aerodynamic damping and stability coefficients in Eq. (76) influence the size of the system dynamics increments.

Simulations are performed in which the specific stability derivatives $C_{m_\alpha}, C_{n_\beta}, C_{l_\beta}$ and dynamic damping coefficients $C_{n_p}, C_{m_q}, C_{l_r}$ are reduced. The tracking results are plotted in Figure 20. It can be seen that the

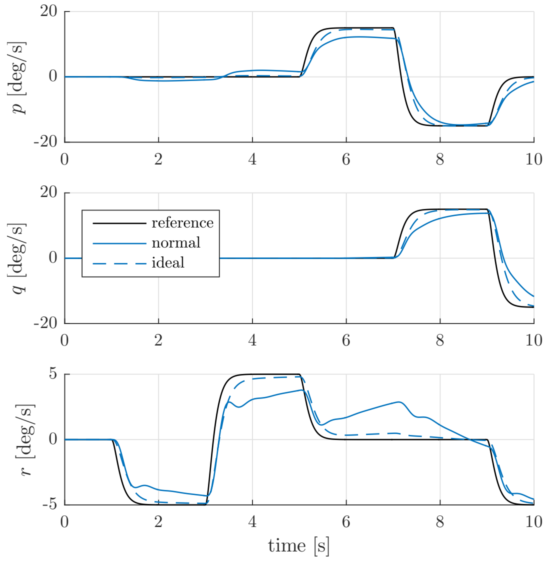

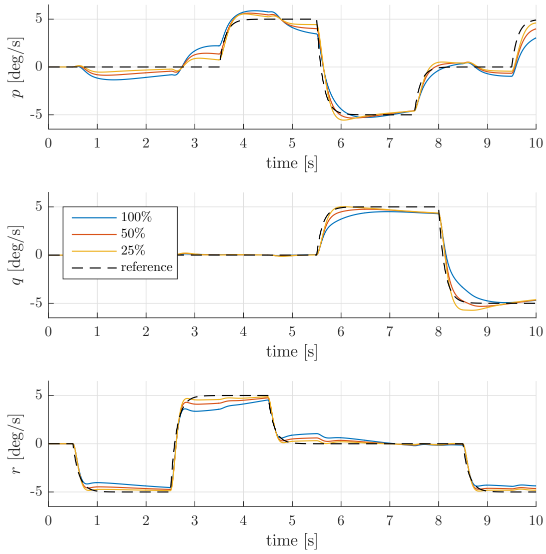

Figure 19. Angular rate tracking response of the nominal INDI controller (solid) and the ideal INDI controller without actuator dynamics and with perfect angular acceleration feedback (dashed).

Figure 20. INDI angular rate response with reduced system dynamics coefficients C_{m_α}, C_{n_β}, C_{l_β}, C_{n_p}, C_{m_q}, C_{l_r}.

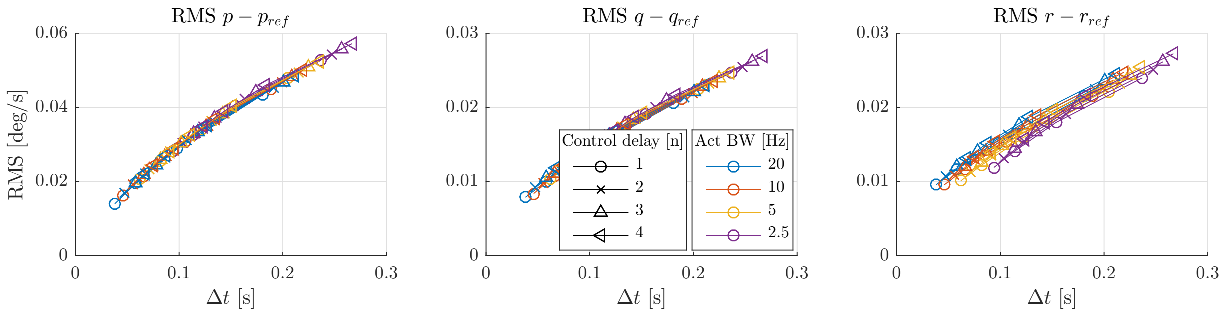

Figure 21. RMS angular rate tracking error versus increment delay, for discrete controller delays of $n = 1, 2, 3, 4$ (at 50 Hz), actuator bandwidths from $2.5 - 20\,\text{Hz}$ and washout filter bandwidths of $6.125 - 50\,{}^{\text{rad}}/_{\text{s}}$.

tracking errors are reduced when the aerodynamic coefficients are reduced.

Fig. 19 already indicates that the effect of system dynamics increments is also related to the bandwidth of the actuators and the delay of the filter to obtain angular accelerations from the angular rates. We will show that this is related to the total estimated delay in the incremental control loop. Consider the estimated increment delay Δt as an estimate of the time interval over which the Taylor series expansion of Eq. (73) is performed. In reality, t_0 is not related to a definite moment in time because $\dot{\mathbf{x}}_{2,0}$ and $\mathbf{u}_0$ are filtered states. The estimated increment delay is defined as

$$\Delta t = nT_s + \tau_{act} + \frac{1}{\omega_{f,n}} \tag{77}$$

Hence, the delay of the actuator and the filter are defined to be the modeled time constants. Simulations are performed in which the discrete delay n, the actuator bandwidth and the washout filter bandwidth $\omega_{f,n}$ are varied. The RMS tracking error is plotted against the increment delay Δt in Fig. 21. The result clearly presents the relationship between the tracking error and the increment delay and shows the relevance to consider a total increment delay Δt to compare effects of varied filter bandwidths, actuator bandwidths and discrete controller delays.

Concluding, Fig. 17 and Fig. 18 show that the assumption of neglecting the system dynamics increments is not valid in general and causes steady state tracking errors in the angular rates. Furthermore, Fig. 21

Table 7. List of sequentially executed experiments

#	Controller configuration	Tracking tasks
INDI Euler attitude control experiments		
1A	Pitch control only, manual roll/yaw and velocity control. conservative parameters	Stabilization Pitch angle doublets (± 10 deg)
1B	Add auto-throttle control	
1C	Add roll/yaw control (fully automatic control)	Stabilization Roll angle doublets ($\pm 20, \pm 30$ deg)
2	Fully automatic control, nominal gains	Stabilization Pitch angle doublets ($\pm 10, \pm 15$ deg) Roll angle doublets ($\pm 20, \pm 45$ deg)
3	Augmented manual control	Pilot commands
IBS aerodynamic attitude control experiments		
4	Pitch and velocity control only, manual roll/yaw control. conservative parameters	Stabilization α doublets ($\pm\pm 1, \pm 2$ deg)
5	Fully automatic control, nominal gains	Stabilization α doublets ($\pm 1, \pm 2$ deg)
6	Add roll/yaw control (fully automatic control)	Stabilization Roll angle doublets (± 15 deg)

shows that a reduction of the increment delay caused by the discrete control delay, filters and actuator dynamics reduces the effect of the system dynamics increments. By compensating for the system dynamics increments in the control law, the tracking errors could potentially be eliminated. However, compensating for system dynamics increments requires knowledge of extra model parameters.

VI. Experiment set-up

After the validation of the model and analysis of the controller robustness in simulation, real flight tests were executed to validate the implementation of the controllers. Experiments were executed as follows. Each flight is controlled by an experienced safety pilot that manually gives direct inputs to the control surfaces of the aircraft. During manual flight, speed is only roughly controlled by the throttle level. When the the aircraft is in a trimmed horizontal flight condition, the safety pilot switches from 'manual' to 'automatic' flight mode to iniate an experiment run. In automatic mode, the flight computer can take over complete control authority of all control surfaces. One flight can contain about 12 experiment runs, each of about 12 seconds. Each experiment consists of a controlled maneuver, in which the attitude commands are pre-programmed doublet signals.

Figure 22. The FASER aircraft during one of the experiments.

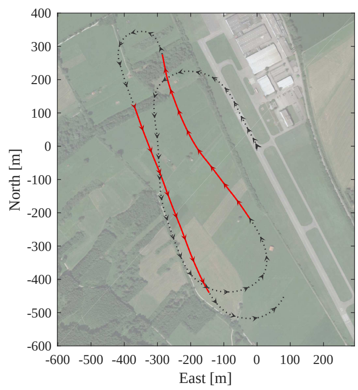

Figure 23. Trajectory of flight during the first two runs of experiment 1A.

The different experiments that have been executed are listed in Tab. 7. Each experiment defines a different controller configuration. Within each experiment, different tracking tasks are executed. The first runs of each experiment consist of a simple stabilization task in which the initial attitude needs to be held. When stable responses are observed, doublet signals with increasing magnitude are commanded in the subsequent tasks of most experiments. During the last flight of the Euler attitude control experiments, the control law is used as an augmented control law in which the pilot gives commands for the roll and pitch angle that are tracked by the control system.

The experiments are executed in the order as listed so that the total controller design is verified with each step of increasing complexity and intensity. No on-line controller tuning was performed. Instead, control laws are first tested with a set of conservative parameters. The conservative parameters are set by multiplying the control effectiveness parameters

$G_{2,0}$ with a factor 2. The experiments are all done for multiple runs, at flight speeds between 20 and 35 m/s and between 100 and 200 m above ground. On total, a number of 68 successfully controlled runs are flown. As an example, Fig. 23 shows the horizontal flight trajectory of the flight in which experiments 1A and 1B were executed.

With the listed experiments, we aim to *validate* the simulation results of the presented control laws. A trade-off was made to gain the highest value from the experiments. Due to time and resources constraints, the following experiments therefore have *not* been executed:

- Actuator failures
- IBS Euler attitude control
- INDI aerodynamic attitude control
- Lateral IBS aerodynamic attitude control with nominal gains

An on-board camera was mounted on the vertical tail to capture all experiments. Videos are uploaded and publicly available[a]. Fig. 22 shows a movie frame as an example.

Finally, the following two notes concerning the experiment execution of the experiments with the IBS aerodynamic attitude flight controller must be made:

1. The complementary filter for α_f and β_f as described in section 3 was finally not used during the executed experiments due to practical implementation issues that were not yet solved when executing the flight tests. Instead the unfiltered estimate, $\hat{\alpha}_a$ was used as feedback.

2. The lateral mode of the IBS aerodynamic attitude controller was only tested with conservative parameters and without derivative gains $C_{1,d}$ in the roll angle feedback. Furthermore, in the IBS aerodynamic attitude controller experiments, a simplified sideslip control was used. The sideslip control was a simple proportional control added to the yaw rate command, with a feedback from the measured lateral acceleration. Therefore, the value of the flight results of the lateral mode is limited.

VII. Results

A. INDI Euler attitude control flight results

During the execution of experiments 1-3 (see Tab. 7), a total of 44 successful runs lasting about 10 seconds each have been flown with the presented INDI Euler attitude controller. In Figs. 24 and 25, flight data of the pitch angle tracking responses are shown. Roll angle tracking results are shown in Figs. 26 and 27. A manually controlled flight with augmented INDI controller was performed and lasted on total 241 seconds. Results of a typical part of the flight are shown in Fig. 28. All runs resulted in the stable and accurate responses with a low tracking error, matching our expectations from simulation results. Both the experiments with nominal parameters and the experiments with conservative parameters are very consistent and correspond with the physics of the system. The tracking response during the manually augmented controlled flight is very similar to the response of the other experiments.

Both for the longitudinal and lateral experiments, simulations with matched initial conditions were performed. These simulation results are plotted in the same figures. The initial condition of the experiment was considered to be a trim condition with some small offset. Therefore, the simulation starts from a trimmed condition at the same altitude and airspeed and attitude. In some cases, an initial trim offset needed to be matched experimentally. All observed controller responses could be replicated in simulation and show a very similar tracking response and control behavior. We see that the simulation response matches well with the response measured in-flight. The elevator input is slightly less damped in simulation. This indicates an underestimation of the pitch damping in the model. Looking at the aileron input for the lateral experiments, this difference is not visible. However, by looking at the angular rate response, these experiments show relatively more disturbance effects. Disturbances from turbulence are not simulated here.

RMS of the tracking errors are shown in Fig. 32. The experiments with nominal parameters show a low overall RMS error, following the same trends as observed in simulation. In flight, the RMS error is slightly larger for all experiments. In the time responses, this is visible as a slight delayed tracking response. Because the control surface commands show the same small delay, this is likely due to a different controller delay.

[a]A selection of the experiment runs can be viewed at `https://youtu.be/PRnHx8323Ts`.

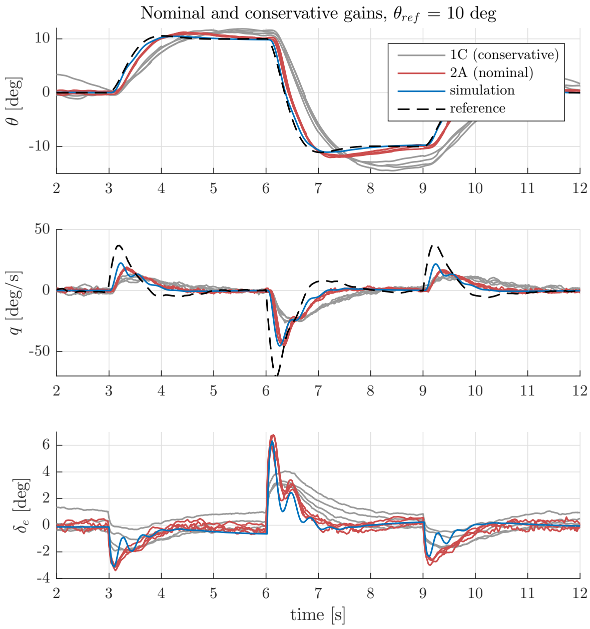

Figure 24. INDI longitudinal tracking response for pitch angle commands of 10 deg (experiment 1B, 2), showing pitch angle, pitch rate and elevator deflection. Pitch angles and elevator deflections are deviations from the initial state.

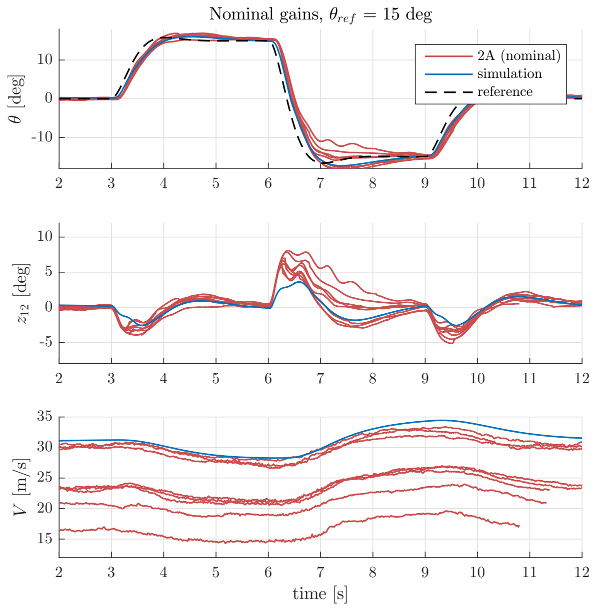

Figure 25. INDI longitudinal tracking response for pitch angle commands of 15 deg (experiment 2), showing pitch angle, tracking error and airspeed. Pitch angles are deviations from the initial state.

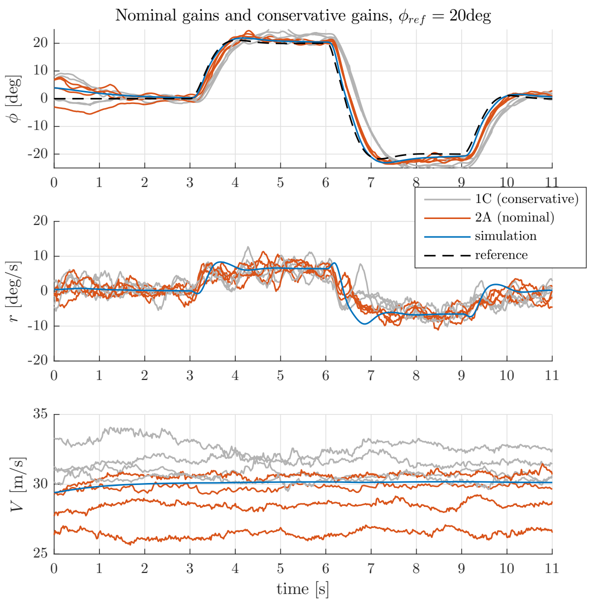

Figure 26. INDI lateral tracking response, with roll angle commands of 20 deg (experiment 1C and 2), showing roll angle, yaw rate and airspeed.

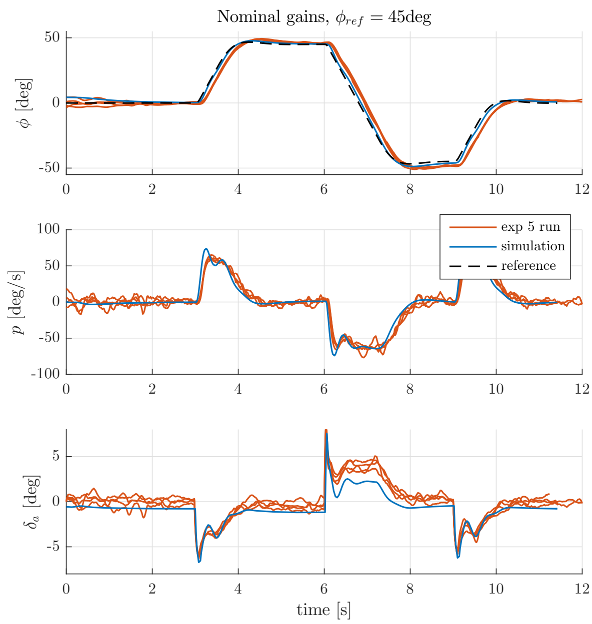

Figure 27. INDI lateral tracking response, with roll angle commands of 45 deg (experiment 2), showing roll angle, roll rate and aileron deflection.

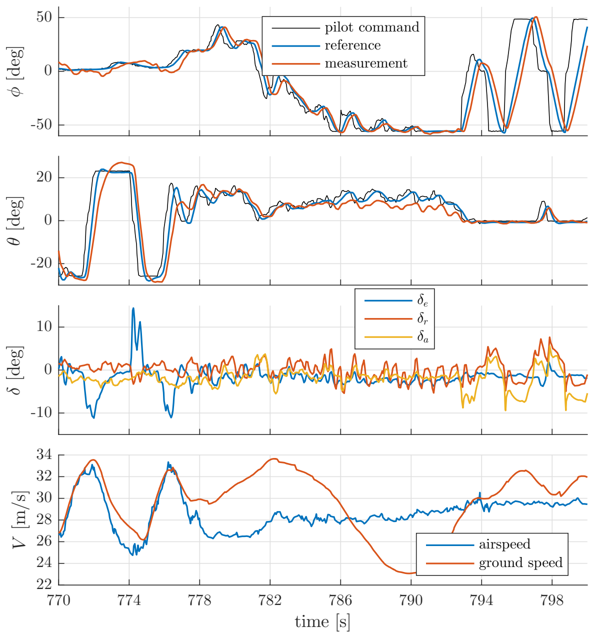

Figure 28. Tracking response of augmented manual flight (experiment 3) with INDI Euler attitude control.

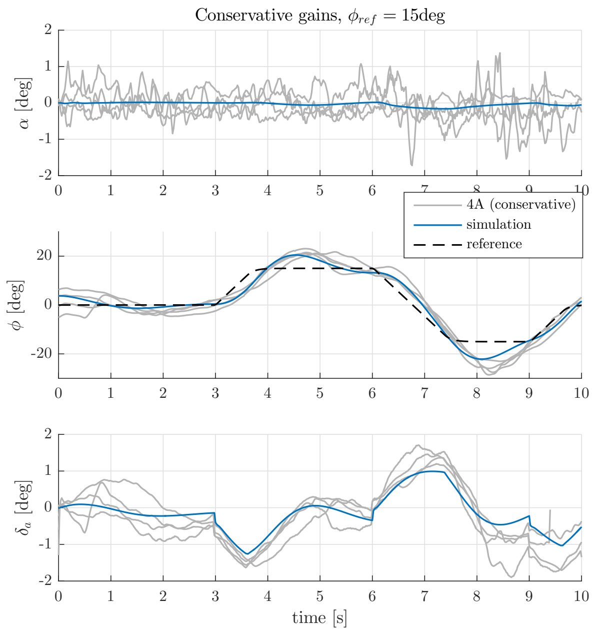

Figure 29. IBS aerodynamic attitude control lateral tracking response with conservative parameters only (experimentn 6), comparing flight data and simulated data, with roll angle commands of 15 deg. Aileron deflections are deviations from the initial value.

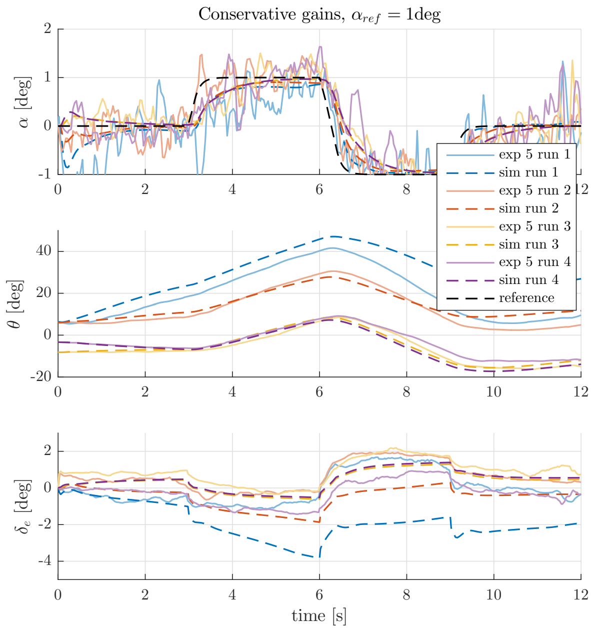

Figure 30. IBS aerodynamic attitude control tracking response, comparing flight data with simulations. α commands of 1 deg with both nominal and conservative parameters are shown (experiment 4 and 5), showing angle of attack, pitch angle and elevator deflection. Angles of attack and control surface deflections are deviations from the initial state.

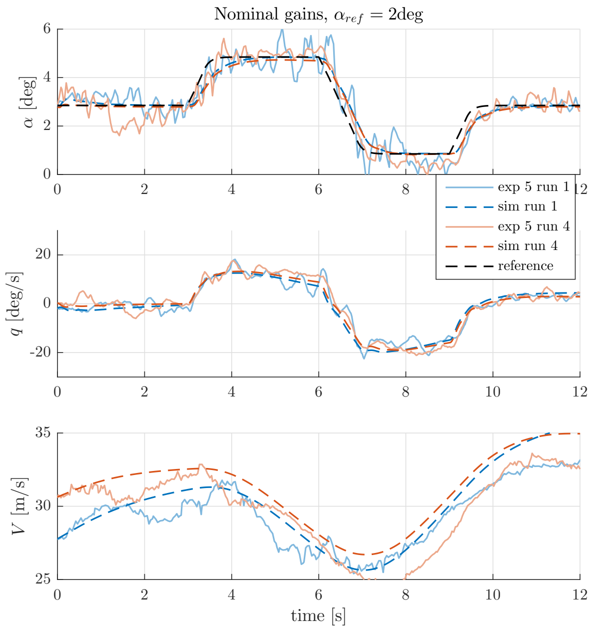

Figure 31. IBS aerodynamic attitude control tracking response, comparing flight data with simulations. α commands of 2 deg with nominal parameters are shown (experiment 5), showing angle of attack, pitch rate and airspeed. Angles of attack are deviations from the initial state.

Overall, the results clearly show that the flight control laws function well over a variety of airspeeds ($V > 20\,\text{m/s}$). Figure 24 shows that at lower speeds the elevator inputs contain more oscillations due to a decreased elevator effectiveness. Due to the variety of airspeeds that are tested and the two different parameter settings (nominal and conservative) that are chosen, the results demonstrate that the controller is able to impose specified reference with desired error dynamics.

B. IBS aerodynamic attitude control flight results

For experiments 4 and 5 (see Tab. 7), on total 22 runs each of about 10 seconds were executed. Results of the longitudinal tracking of the IBS aerodynamic attitude controller are shown in Figs. 30 and 31. Results of the lateral IBS aerodynamic attitude control with conservative parameters and simplified sideslip controller are shown in Fig. 29. RMS tracking errors can be found in Fig. 32.

A clear tracking of the reference α_{ref} is visible. The results show that the controller functions well between airspeeds of 25 and 35 m/s. Furthermore, the observed response in-flight matches with the simulation results. The difference in RMS error between simulation and flight can be partly attributed to the additional turbulence measured in flight which was not included in simulation. Since a direct estimate of the angle of attack α was used as feedback, the signal included the turbulence. As can be seen in the results, especially when tracking doublets with a magnitude of 1 deg, the variance of the turbulence is quite big compared to the reference signal. Nevertheless, the observed effect of the turbulence propagating in the elevator deflection is small, the response is stable and damped and tracking is fast.

An issue with using the unfiltered estimate of α is that upon initiation of the controller, the angle of attack reference α_{ref} is set to its actual estimate which includes the measured turbulence. This results in tracking a non-zero vertical load as reference offset and causes the aircraft to follow this reference, thereby initially pitching either up or down. This effect can be seen in the pitch angle response in Figs. 30 and 31. During certain runs, not shown in the figures, the offset was large enough to let the aircraft climb up to pitch angles of about 70 degrees. Airspeeds dropped to about 10 m/s. This resulted in heavy elevator oscillations at its minimum speed, which stabilized and damped out again when the airspeed was above about 15 m/s.

Looking at the roll angle response in Fig. 29, a clear tracking is observed. Since conservative parameters are used for this mode and since the damping parameter $C_{1,d}$ was set to zero, the response is slow and contains overshoot. Simulation results match closely with the observed response. The yaw rate response and the rudder input (not shown here) contained oscillations that were only marginally damped.

Overall, the responses show that the IBS aerodynamic attitude controller follows the imposed dynamics and performs as expected. Especially the longitudinal mode is showing that the controller can be used for stable, accurate tracking of an imposed reference signal by cancelling all system dynamics while requiring only little knowledge of model parameters.

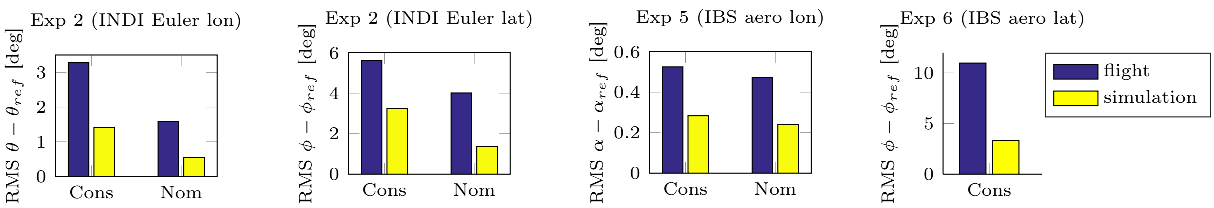

Figure 32. RMS tracking error results over all runs of the separate experiments with the INDI Euler attitude controller and IBS aerodynamic attitude controller.

VIII. Conclusion

The paper presents the design and implementation of incremental nonlinear control laws on a fixed-wing aircraft. Qualitative flight tests are performed to validate simulation results presented in this paper and shown in previous studies on incremental nonlinear flight control methods. In particular, a successful application of INDI and command-filtered IBS methods on a fixed-wing aircraft are shown, which was not done before in practice. We presented a complete design for the attitude control of fixed-wing aircraft which can be used for multiple purposes. By implementing control laws either for controlling pitch angle or angle of attack, we showed the applicability of these results for manual augmented attitude control, outer loop flight path control or vertical load control. The UAV that is considered contains basic, relatively cheap and widely available avionics components and actuators. Simulations show that robustness to system aerodynamic changes can be greatly increased if faster actuators are used and if a better acceleration measurement with a smaller delay is available.

Through repeated experiments, flight data results of the INDI and IBS attitude controllers show that accurate tracking is achieved and system dynamics are canceled well without requiring much knowledge of model parameters. Simulation results with identical controller configurations match closely with the observed response. Hence, the results in this paper validate the applicability of the control methods under the presence of parameter uncertainties, delayed measurements and turbulence disturbances.

Furthermore, we presented an analysis on the validity of neglecting the control-independent system dynamics related to the incremental control laws, which was also not done before. System dynamics increments create tracking errors related to the aerodynamic damping and stability properties of the aircraft. The size of the tracking errors is related to the total increment delay.

Control laws proposed in this paper require little knowledge about the system dynamics, yet they result in an input-to-output linearized (INDI) and exponentially stable system (IBS) by being more dependent on sensor measurements. Advantages compared to classical methods are that they are easy to tune and propose one control design that is valid over the entire flight envelope. These properties together make it very easy to implement high-performance, robust fault-tolerant flight control systems.

Acknowledgements

We acknowledge Andreas Klöckner, Nir Kastner, Richard Kuchar and Reiko Müller at the department of System Dynamics and Control at the DLR, in their the support in executing the experiments on the FASER UAV. Paul Acquatella is acknowledged for his valuable review of the work.

References

[1]European Aviation Safety Agency (EASA), "Annual Safety Review 2013," Tech. rep., European Aviation Safety Agency, 2014.

[2]Boeing Commercial Airplanes, "Statistical Summary of Commercial Jet Airplane Accidents," Tech. rep., 2010.

[3]Smaili, H., Breeman, J., Lombaerts, T., and Stroosma, O., "A Benchmark for Fault Tolerant Flight Control Evaluation," *AIAA Modeling and Simulation Technologies Conference and Exhibit*, 2006.

[4]Lombaerts, T. J., Smaili, M. H., Stroosma, O., Chu, Q. P., Mulder, J. A., and Joosten, D. A., "Piloted Simulator Evaluation Results of New Fault-Tolerant Flight Control Algorithm," *Journal of Guidance, Control, and Dynamics*, Vol. 32, No. 6, 2009, pp. 1747–1765.

[5]Zhang, Y. and Jiang, J., "Bibliographical review on reconfigurable fault-tolerant control systems," *Annual Reviews in Control*, Vol. 32, No. 2, 2008, pp. 229–252.

[6]Edwards, C., Lombaerts, T., and Smaili, H., *Fault Tolerant Flight Control*, Springer, 2010.

[7]Blakelock, J., *Automatic Control of Aircraft and Missiles*, Wiley, New York, 2nd ed., 1991.

[8]Stevens, B. L. and Lewis, F. L., *Aircraft Control and Simulation*, Wiley, 2003.

[9]da Costa, R. R., Chu, Q. P., and Mulder, J. A., "Reentry Flight Controller Design Using Nonlinear Dynamic Inversion," *Journal of Spacecraft and Rockets*, Vol. 40, No. 1, 2003, pp. 64–71.

[10]Snells, S., Enns, D. F., and William, W., "Nonlinear Inversion Flight Control for a Supermaneuverable Aircraft," *Journal of Guidance, Control, and Dynamics*, Vol. 15, No. 4, 1992, pp. 976–984.

[11]Krstić, M., *Nonlinear and Adaptive Control Design*, Wiley, 1995.

[12]Slotine, L., *Applied Nonlinear Control*, Prentice Hall, 1991.

[13]Ochi, Y. and Kanai, K., "Design of Restructurable Flight Control Systems Using Feedback Linearization," *Journal of Guidance, Control, and Dynamics*, Vol. 14, No. 5, 1991, pp. 903–911.

[14]Bugajski, D. J., Enns, D. F., and Elgersma, M. R., "A Dynamic Inversion Based Control Law With Application To The High Angle-of-Attack Research Vehicle," *Guidance, Navigation and Control Conference*, 1990, pp. 826–839.

[15]Enns, D., Bugajski, D., Hendrick, R., and Stein, G., "Dynamic inversion: an evolving methodology for flight control design," *International Journal of Control*, Vol. 59, No. 1, 1994, pp. 71–91.

[16]Kanellakopoulos, I., Kokotovic, P., and Morse, A., "Systematic Design of Adaptive Controllers For Feedback Linearizables Systems," *IEEE Transactions on Automatic Control*, Vol. 36, No. 11, 1991, pp. 1241–1253.

[17]Krstic, M., Kanellakopoulos, I., and Kokotovic, P., "Adaptive Nonlinear Control Without Overparametrization," *Systems & Control Letters*, Vol. 19, 1992, pp. 177–185.

[18]Farrell, J., Polycarpou, M., and Sharma, M., "Adaptive Backstepping With Magnitude, Rate, and Bandwidth Constraints: Aircraft Longitude Control," *Proceedings of the 2003 American Control Conference, 2003.*, Vol. 5, 2003, pp. 3898–3904.

[19]Sonneveldt, L., Chu, Q. P., and Mulder, J. a., "Nonlinear Flight Control Design Using Constrained Adaptive Backstepping," *Journal of Guidance, Control, and Dynamics*, Vol. 30, No. 2, 2007, pp. 322–336.

[20]Sonneveldt, L., Van Oort, E., Chu, Q., and Mulder, J., "Nonlinear Adaptive Trajectory Control Applied to an F-16 Model," *Journal of Guidance, Control, and Dynamics*, Vol. 32, No. 1, 2009, pp. 25–39.

[21]Sieberling, S., Chu, Q. P., and Mulder, J. A., "Robust Flight Control Using Incremental Nonlinear Dynamic Inversion and Angular Acceleration Prediction," *Journal of Guidance, Control, and Dynamics*, Vol. 33, No. 6, 2010, pp. 1732–1742.

[22]Bacon, B., Ostroff, A. J., and Joshi, S., "Reconfigurable NDI Controller Using Inertial Sensor Failure Detection & Isolation," *Aerospace and Electronic Systems, IEEE Transactions on*, Vol. 37, No. 4, 2001, pp. 1373–1383.

[23]Smith, P. R., "A Simplified Approach to Nonlinear Dynamic Inversion Based Flight Control," *AIAA Atmospheric Flight Mechanics Conference and Exhibit*, 1998, pp. 762–770.

[24]Acquatella B., P., van Kampen, E.-j., and Chu, Q., "Incremental Backstepping for Robust Nonlinear Flight Control," *Proceedings of the EuroGNC 2013, 2nd CEAS Specialist Conference on Guidance, Navigation & Control*, 2013, pp. 1444–1463.

[25]Van Gils, P., "Adaptive Incremental Backstepping Flight Control for a High-Performance Aircraft with Uncertainties," *AIAA Guidance, Navigation, and Control Conference*, 2015.

[26]Ali, A., Chu, Q., van Kampen, E., and de Visser, C., "Exploring Adaptive Incremental Backstepping using Immersion and Invariance for an F-16 aircraft," *AIAA Guidance, Navigation, and Control Conference*, 2014.

[27]Berry, A., Smith, P., "Flight Test Experience of a Non-linear Dynamic Inversion Control Law on the VAAC Harrier," *AIAA Atmospheric Flight Mechanics Conference*, 2000, pp. 132–142.

[28]Smeur, E. J. J., "Adaptive Incremental Nonlinear Dynamic Inversion for Attitude Control of Micro Aerial Vehicles," *Journal of Guidance, Control, and Dynamics*, Vol. 39, No. 3, 2016, pp. 450–461.

[29]Owens, B., Cox, D. E., and Morelli, E. A., "Development of a Low-Cost Sub-Scale Aircraft for Flight Research: The FASER Project," *AIAA Aerodynamic Measurement Technology and Ground Testing Conference*, 2006, pp. 1–11.

[30]Hoe, G., Owens, D. B., and Denham, C., "Forced Oscillation Wind Tunnel Testing for FASER Flight Research Aircraft," *AIAA Atmospheric Flight Mechanics Conference*, 2012, pp. 1–12.

[31]Klöckner, A., "Geometry Based Flight Dynamics Modelling of Unmanned Airplanes," *AIAA Modeling and Simulation Technologies (MST) Conference*, 2013.

[32]Farrell, J., Sharma, M., and Polycarpou, M., "Backstepping-Based Flight Control with Adaptive Function Approximation," *Journal of Guidance, Control, and Dynamics*, Vol. 28, No. 6, 2005, pp. 1089–1102.

[33]Sonneveldt, L., *Adaptive Backstepping Flight Control For Modern Fighter Aircraft*, PhD Thesis, Delft University of Technology, 2010.

[34]Simplício, P., Pavel, M. D., van Kampen, E., and Chu, Q. P., "An Acceleration Measurements-Based Approach For Helicopter Nonlinear Flight Control Using Incremental Nonlinear Dynamic Inversion," *Control Engineering Practice*, Vol. 21, No. 8, 2013, pp. 1065–1077.

[35]Acquatella B., P., Falkena, W., van Kampen, E.-J., and Chu, Q. P., "Robust Nonlinear Spacecraft Attitude Control using Incremental Nonlinear Dynamic Inversion," *AIAA Guidance, Navigation, and Control Conference*, , No. August, 2012.

[36]Lu, P., van Kampen, E.-J., de Visser, C., and Chu, Q., "Aircraft Fault-Tolerant Trajectory Control Using Incremental Nonlinear Dynamic Inversion," *Control Engineering Practice*, Vol. 57, 2016, pp. 126–141.

[37]Lu, P., van Kampen, E., and Chu, Q., "Robustness and Tuning of Incremental Backstepping Approach," *AIAA Guidance, Navigation and Control Conference*, 2015.

[38]Van Gils, P., *Adaptive Incremental Backstepping Flight Control*, MSc thesis, Delft University of Technology, 2015.

[39]Astolfi, A. and Ortega, R., "Immersion and Invariance: A New Tool for Stabilization and Adaptive Control of Nonlinear Systems," *IEEE Transactions on Automatic Control*, Vol. 48, No. 4, 2003, pp. 590–606.

[40]Sonneveldt, L., van Oort, E., Chu, Q., and Mulder, J., "Immersion and Invariance Based Nonlinear Adaptive Flight Control," *AIAA Guidance, Navigation, and Control Conference*, , No. August, 2010.

[41]Acquatella B., P., van Ekeren, W., and Chu, Q., "PI(D) tuning for Flight Control Systems via Incremental Nonlinear Dynamic Inversion (unpublished)," *20th International Federation of Automatic Control (IFAC) World Congress*, 2017.

Chapter 2

Backstepping and Nonlinear Dynamic Inversion Control Theory

In this chapter, the basic tools that are used to build up the control laws of this research will be presented. These tools inlcude backstepping control, nonlinear dynamic inversion control, command filters, parameter adaptation methods and incremental control methods. In the following sections these methods will be briefly explained, using examples to support the explanation.

The purpose of this chapter is to give an overview of the methods used. For a more detailed, theoretical reference, the reader is adviced to conduct the references mentioned in this chapter. For a good understanding of (adaptive) nonlinear control methods such as Feedback Linearization and Backstepping, the books written by Khalil (1996); Krstić (1995); Slotine (1991) are good references.

2-1 Lyapunov-based backstepping control

To derive stable control laws by means of the backstepping control laws, control Lyapunov functions (CLFs) need to be set op. Lyapunov functions are used in nonlinear systems to assess the stability or convergence to a set. The theorem of Lasalle and Yoshizawa is used for this and is stated below. The formulation of the theorem is adopted from Krstić (1995) and Klamer (2007). The theorem is stated as follows:

> *Let $x = 0$ be the equilibrium point of the time-varying system $\dot{x} = f(x,t)$ and suppose f is locally Lipschitz and x uniformly in t. Let $V : \mathbb{R}^n \rightarrow \mathbb{R}_+$ be a continuously differentiable, positive definite and radially unbounded function $V(x)$ such that*

$$\dot{V} = \frac{\partial V}{\partial x} f(x,t) \leq -W(x) \leq 0, \quad \forall t \geq 0, \quad \forall x \in \mathbb{R}^n \tag{2-1}$$

Where W is a continuous function. Then, all soluations $\dot{x} = f(x,t)$ are globally uniformly bounded and satisfy

$$\lim_{x \to 0} W(x(t)) = 0 \tag{2-2}$$

In addition, if $W(x)$ is positive definite, then the equilibrium $x = 0$ is globally uniformly asymptotically stable.

In normal words, the theorem says that a system can be proven to be globally uniformly asymptotically stable, if a scalar function $V(x)$ can be found that greater than zero for every non-zero state x and approaches infinity if x approaches infinity. Furthermore, its time derivative must be negative definite. As an analogy one can look at the Lyapunov function as a description of the energy of the error to be controlled. As long as the energy decreases at any possible state, the system will return to its equilibrium point.

A backstepping control law can be defined for systems in strict-feedback form using control Lyapunov functions (CLFs). control Lyapunov functions (CLFs) are candidates for Lyapunov functions and control laws must be designed such that the CLF satisfies the constraints of a Lyapunov function. Consider a system in strict-feedback form, which was already presented in a slightly different form in Equation 1-1:

$$\begin{aligned}
\dot{x}_1 &= f_1(x_1) + g_1(x_1)x_2 \\
&\vdots \\
\dot{x}_i &= f_i(\bar{x}_i) + g_i(\bar{x}_i)x_{i+1} \quad \text{for } i = 1, \ldots, k-1 \\
&\vdots \\
\dot{x}_{k-1} &= f_{k-1}(\bar{x}_{k-1}) + g_{k-1}(\bar{x}_{k-1})x_k \\
\dot{x}_k &= f_k(\bar{x}_k) + g_k(\bar{x}_k)u
\end{aligned} \tag{2-3}$$

Where the bar symbol in $\bar{x}_j$ denotes collection of states $x_1, \ldots, x_j$. The property of a system in strict-feedback form is that the state derivatives $\dot{x}_i$ only depend on states that are separated by more integrators from the output signal x_1 to be tracked. So $\dot{x}_i$ only depends on $x_i, x_{i+1}, x_{i+2}, \ldots$. The control task for this system is to track a reference y_r by the output x.

2-1-1 Backstepping design for scalar systems without uncertainties

The backstepping design procedure starts by considering the subsystem that is closest to the output, and defining the tracking error dynamics:

$$\begin{aligned}
z_1 &= x_1 - y_r \\
\dot{z}_1 &= f_1(x_1) + g_1(x_1)x_2 - \dot{y}_r
\end{aligned} \tag{2-4}$$

Subsystem 1

Stable tracking is achieved when the tracking error z_1 converges to zero. Therefore, we define the first control Lyapunov function as:

$$V_1 = \frac{1}{2}z_1^2 \tag{2-5}$$

of which its derivative must be rendered negative definite for asymptotic stability:

$$\dot{V}_1 = z_1\big(f_1(x_1) + g_1(x_1)x_2 - \dot{y}_r\big) \tag{2-6}$$

A stabilizing function α_1 can be designed for x_2:

$$\alpha_1 = g_1^{-1}\big(-C_1 z_1 - f_1(x_1) + \dot{y}_r\big) \tag{2-7}$$

When x_2 perfectly tracks the stabilizing function α_1, $\dot{V}_1$ is rendered negative definite:

$$\dot{V}_1 = -C_1 z_1^2 \quad \text{if} \quad x_2 = \alpha_1 \tag{2-8}$$

Because x_2 is a state and not an input, we must define a second tracking error:

$$z_2 = x_2 - \alpha_1 \tag{2-9}$$

And the initial derivative of the CLF, $\dot{V}_1$ then equals:

$$\begin{aligned} \dot{V}_1 &= z_1\big(f_1(x_1) + g_1(x_1)(z_2 + \alpha_1) - \dot{y}_r\big) \\ \dot{V}_1 &= -c_1 z_1^2 + z_1 g_1(x_1) z_2 \end{aligned} \tag{2-10}$$

With $c_1 > 0$. The remaining destabilizing term $z_1 g_1(x_1) z_2$ must be cancelled in the subsequent step.

Subsystem i

For all subsequent subsystems $i = 2, \ldots, k-1$, the procedure in each step is as follows. Define the tracking error dynamics in subsystem i:

$$\begin{aligned} z_i &= x_i - \alpha_{i-1} \\ \dot{z}_i &= f_i(\bar{x}_i) + g_i(\bar{x}_i)(z_{i+1} + \alpha_i) - \dot{\alpha}_{i-1} \end{aligned} \tag{2-11}$$

Augment the previous CLF:

$$V_i = V_{i-1} + \frac{1}{2} z_i^2 \tag{2-12}$$

Then, the derivative must be rendered negative definite:

$$\begin{aligned} \dot{V}_i &= \dot{V}_{i-1} + z_i\big(f_i + g_i(z_{i+1} + \alpha_i) - \dot{\alpha}_{i-1}\big) \\ &= -\sum_{j=1}^{i-1} C_j z_j^2 + z_{i-1} g_{i-1} z_i + z_i\big(f_i(\bar{x}_i) + g_i(z_{i+1} + \alpha_i) - \dot{\alpha}_{i-1}\big) \end{aligned} \tag{2-13}$$

The stabilizing function α_i is defined as:

$$\alpha_i = g_i^{-1}\big(-C_i z_i - f_i + \dot{\alpha}_{i-1} - z_{i-1} g_{i-1}\big) \tag{2-14}$$

With $c_i > 0$. This yields:

$$\dot{V}_i = -\sum_{j=1}^{i} c_j z_j^2 + z_i g_i z_{i+1} \tag{2-15}$$

Subsystem k

In the last design step, the control law for the input is finally derived. The error dynamics are:

$$\begin{aligned} z_k &= x_k - \alpha_{k-1} \\ \dot{z}_k &= f_k(\bar{x}_k) + g_k(\bar{x}_k)u - \dot{\alpha}_{k-1} \end{aligned} \tag{2-16}$$

The CLF is augmented:

$$V_k = V_{k-1} + \frac{1}{2}z_k^2 \tag{2-17}$$

And its derivative is:

$$\dot{V}_k = -\sum_{j=1}^{k-1} c_j z_j^2 + z_k\big(f_k + g_k u - \dot{\alpha}_{k-1}\big) \tag{2-18}$$

A control law which renders $\dot{V}_k$ negative definite is:

$$u = g_k^{-1}\big(-c_k z_k - f_k + \dot{\alpha}_{k-1} - z_{k-1}g_{k-1}\big) \tag{2-19}$$

With $c_k > 0$. The final derivative CLF equals:

$$\dot{V} = \dot{V}_k = -\sum_{j=1}^{k} c_j z_j^2 \tag{2-20}$$

In each design step of the backstepping procedure that is shown, all system dynamics f_i are cancelled out. This is often not a necessary condition to proof stability. Damping terms which have a stabilizing effect do not have to be cancelled. This can prevent the necessity of large control inputs.

Backstepping control in vector form

The backstepping control law can be extended easily to dynamical systems described in vector form. The Lyapunov functions must still be scalar and derive to:

$$V_i = V_{i-1} + \frac{1}{2}\mathbf{z}_i^T\mathbf{z}_i \tag{2-21}$$

Intermediate stabilizing functions derive to:

$$\boldsymbol{\alpha}_i = G_i^{-1}\big(-C_i\mathbf{z}_i - \mathbf{f}_i + \dot{\boldsymbol{\alpha}}_{i-1} - G_{i-1}^T\mathbf{z}_{i-1}\big) \tag{2-22}$$

Here, G_i is the control effectiveness matrix, analogous to its scalar version g_i. It must be full rank so that its inverse exists and controllability is provided. The control gain matrices C_i are positive diagonal matrices.

2-1-2 Example: backstepping control and nonlinear dynamic inversion

To show how both a backstepping and a NDI control law are defined for a simple problem, an example control task is presented in this section. Consider the a system described by:

$$\begin{aligned} \dot{x}_1 &= -x_1^3 + a \sin x_1 + x_2 \\ \dot{x}_2 &= bu \end{aligned} \tag{2-23}$$

And suppose $x_1 = y$ is the output which should track the reference y_r. Nonlinear dynamic inversion can be applied to track y_r, by means of feedback linearisation. In this process, the output signal y is differentiated analytically until the control input u is appears explicitly. The number of differentiations that are necessary equals the relative degree r of the system. In this case this yields:

$$\begin{aligned} y &= x_1 \\ \dot{y} &= -x_1^3 + a \sin x_1 + x_2 \\ \ddot{y} &= (-3x_1^2 + a \cos x_1)\dot{x}_1 + \dot{x}_2 \\ &= (-3x_1^2 + a \cos x_1)(-x_1^3 + x_2) + bu \end{aligned} \tag{2-24}$$

The control input can be defined in terms of a virtual control v:

$$u = \frac{1}{b}\big(v - (-3x_1^2 + a\cos x_1)(-x_1^3 + x_2)\big) \tag{2-25}$$

so that:

$$\ddot{y} = v \tag{2-26}$$

And the result it a linear system of states $y, \dot{y}$ with a virtual control v, for which a stabilizing control law can be defined. When the error is defined as $z_1 = x_1 - y_r$, the error dynamics must be stabilized to a form like:

$$z_1 + k_1\dot{z}_1 + k_2\ddot{z}_1 = 0 \tag{2-27}$$

with $\ddot{z} = v - \ddot{y}_r$, this yields a stabilizing virtual control:

$$v = \ddot{y}_r - \frac{k_1}{k_2}\dot{z}_1 - \frac{1}{k_2}z_1 \tag{2-28}$$

which can be redefined as:

$$v = \ddot{y}_r - d_1\dot{z}_1 - d_2 z_1 \tag{2-29}$$

and can be substituted in (2-25) to yield the complete control law:

$$u_{\text{ndi}} = \frac{1}{b}\big(- d_1\dot{z}_1 - d_2 z_1 + (3x_1^2 - a\cos x_1)\dot{x}_1 + \ddot{y}_r\big) \tag{2-30}$$

To derive the control law with a backstepping procedure, the derivative of the first CLF derives to:

$$\dot{V}_1 = z_1(-x_1^3 + a\sin x_1 + z_2 + \alpha_1 - \dot{y}_r) \tag{2-31}$$

with:

$$\alpha_1 = -c_1 z_1 + x_1^3 - a \sin x_1 + \dot{y}_r \tag{2-32}$$

The derivative of the second CLF derives to:

$$\dot{V}_2 = -c_1 z_1^2 + z_1 z_2 + z_2\big(bu - \dot{\alpha}_1\big) \tag{2-33}$$

which yields:

$$\begin{aligned} u_{\text{bs}} &= \frac{1}{b}\big(- c_2 z_2 + \dot{\alpha}_1 - z_1\big) \\ &= \frac{1}{b}\big(- c_2 z_2 - c_1 \dot{z}_1 + (3x_1^2 - a\cos x_1)\dot{x}_1 + \ddot{y}_r - z_1\big) \end{aligned} \tag{2-34}$$

Note that, because

$$\begin{aligned} z_2 &= x_2 - \alpha_1 \\ &= x_2 + c_1 z_1 - x_1^3 + a \sin x_1 - \dot{y}_r \\ &= \dot{y} - \dot{y}_r + c_1 z_1 \\ &= (1 + c_1) z_1 \end{aligned} \tag{2-35}$$

it yields that

$$u_{\text{bs}} = \frac{1}{b}\big(- c_2(1+c_1) z_1 - c_1 \dot{z}_1 + (3x_1^2 - a\cos x_1)\dot{x}_1 + \ddot{y}_r - z_1\big) \tag{2-36}$$

Comparing u_{ndi} in (2-30) with u_{bx} above, it can be seen that the two results are very similar. There are only a two differences: first of all, with backstepping, feedback is performed on the state errors instead of the output errors. Comparing (2-36) with (2-30), we see that the control laws are equivalent for $d_2 = c_2(1 + c_1)$ and $d_1 = c_1$. Secondly, in the backstepping control law, the term z_1 is added to guarantee stability of the outer loop. Tracking results are displayed in Figure 2-1.

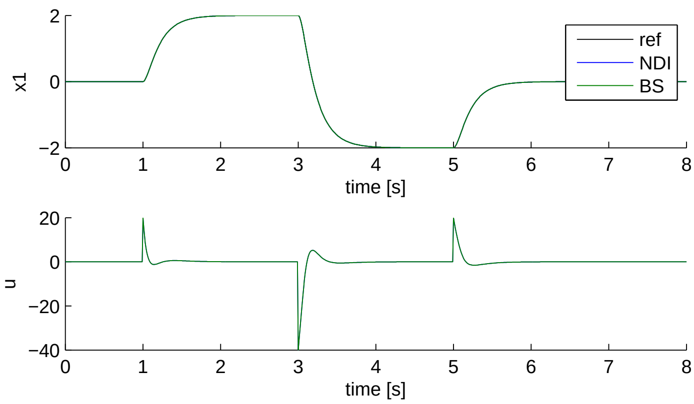

Figure 2-1: Tracking results of the example problem. The reference can be tracked perfectly by both the NDI and the Backstepping (BS) controller.

If the problem is converted to a regulation problem, then the stabilizing term x_1^3 does not need to be cancelled by the backstepping controller. So when $y_r = 0$ so that $z_1 = x_1$, the first stabilizing function can be defined as $\alpha_1 = -c_1 z_1 + \dot{y}_r$. The results of all three control laws (NDI, full backstepping, reduced backstepping) for the regulation problem are given in Figure 2-2.

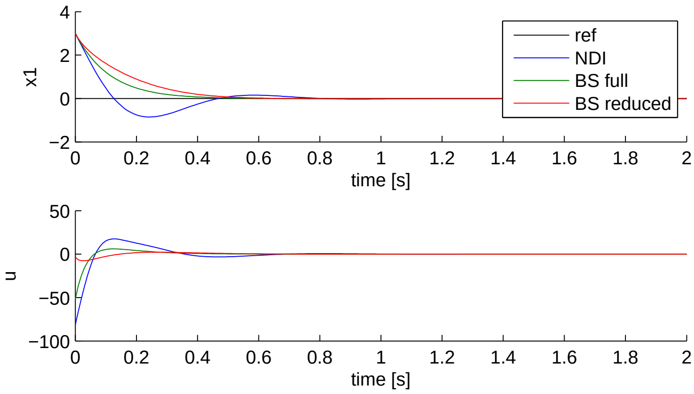

Figure 2-2: Regulation results of the example problem. The reduced backstepping controller needs considerably smaller inputs than the NDI and full backstepping controller.

2-2 Adaptive backstepping

Adaptive control structures in Backstepping control can be devided into two classes. They are distinguished by the way in which the parameter estimations or updates are combined with the controller: this can be of an integrated or modular nature (Krstić et al., 1994). The modular techniques are of a certainty-equivalence type: the estimated parameters $\hat{\theta}$ are assumed to be the true parameters and the control law uses them as such. Any parameter estimation method can be used in a modular adaptive control method. The tuning functions method however is an integrated, Lyapunov based method: the parameter update laws are integrated in the Lyapunov function.

The essence of the tuning functions approach lies in the fact that not the true parameters are not really estimated. The parameter estimates that are used in the control law adapt using special parameter update laws which are designed such that asymptotic stability of the entire system is guaranteed. Hence, the parameter errors are incorporated in the control Lyapunov functions (CLFs) to proof the stability. The basic approach to derive the update laws can be shown as follows.

Consider integrator step i of a dynamical system in strict-feedback form, like in Equation 2-3:

$$\dot{x}_i = f_i(\bar{x}_i) + g_i(\bar{x}_i)x_{i+1} \tag{2-37}$$

and express f_i and g_i as a product of function regressors with parameters, such that the dynamical equations are linear in the parameters:

$$\dot{x}_i = \phi_{f_i}^T(\bar{x}_i)\boldsymbol{\theta}_{f_i} + \phi_{g_i}^T(\bar{x}_i)\boldsymbol{\theta}_{g_i}x_{i+1} \tag{2-38}$$

Describe the parameter values as the sum of the estimate and the error:

$$\boldsymbol{\theta}_j = \hat{\boldsymbol{\theta}}_j + \tilde{\boldsymbol{\theta}}_j \tag{2-39}$$

and assume constant parameters $\boldsymbol{\theta}_j$ so that $\dot{\hat{\boldsymbol{\theta}}}_j = -\dot{\tilde{\boldsymbol{\theta}}}_j$. Then, include the parameter estimation errors in the CLF:

$$V_i = V_{i-1} + \frac{1}{2}z_i^2 + \frac{1}{2}\tilde{\boldsymbol{\theta}}_{f_i}^T\Gamma_{f_i}^{-1}\tilde{\boldsymbol{\theta}}_{f_i} + \frac{1}{2}\tilde{\boldsymbol{\theta}}_{g_i}^T\Gamma_{g_i}^{-1}\tilde{\boldsymbol{\theta}}_{g_i} \tag{2-40}$$

so that its derivative at step i can be split up into the control error and the estimation error as follows (compare it with (2-13)):

$$\begin{aligned}
\dot{V}_i &= \dot{V}_{i-1} + z_i\big(\phi_{f_i}^T\boldsymbol{\theta}_{f_i} + \phi_{g_i}^T\boldsymbol{\theta}_{g_i}(z_{i+1}+\alpha_i) - \dot{\alpha}_{i-1}\big) + \dots \\
&\quad + \tilde{\boldsymbol{\theta}}_{f_i}^T\Gamma_{f_i}^{-1}\dot{\tilde{\boldsymbol{\theta}}}_{f_i} + \dots \\
&\quad + \tilde{\boldsymbol{\theta}}_{g_i}^T\Gamma_{g_i}^{-1}\dot{\tilde{\boldsymbol{\theta}}}_{g_i} \\
&= \dot{V}_{i-1} + z_i\big(\phi_{f_i}^T\hat{\boldsymbol{\theta}}_{f_i} + \phi_{g_i}^T\hat{\boldsymbol{\theta}}_{g_i}(z_{i+1}+\alpha_i) - \dot{\alpha}_{i-1}\big) + \dots \\
&\quad + \tilde{\boldsymbol{\theta}}_{f_i}^T\Gamma_{f_i}^{-1}\big(\dot{\tilde{\boldsymbol{\theta}}}_{f_i} + \Gamma_{f_i}\phi_{f_i}z_i\big) + \dots \\
&\quad + \tilde{\boldsymbol{\theta}}_{g_i}^T\Gamma_{g_i}^{-1}\big(\dot{\tilde{\boldsymbol{\theta}}}_{g_i} + \Gamma_{g_i}\phi_{g_i}z_i x_{i+1}\big)
\end{aligned} \tag{2-41}$$

Then, because $\dot{\hat{\boldsymbol{\theta}}}_j = -\dot{\tilde{\boldsymbol{\theta}}}_j$ we can define the dynamic parameter update laws as:

$$\begin{aligned}
\dot{\hat{\boldsymbol{\theta}}}_{f_i} &= \Gamma_{f_i}\phi_{f_i}z_i \\
\dot{\hat{\boldsymbol{\theta}}}_{g_i} &= \Gamma_{g_i}\phi_{g_i}z_i x_{i+1}
\end{aligned} \tag{2-42}$$

and the virtual control laws of step i equal to those showed already in (2-14), but based on the parameter estimates:

$$\alpha_i = \hat{g}_i^{-1}\big(- C_i z_i - \hat{f}_i + \dot{\alpha}_{i-1} - z_{i-1}\hat{g}_{i-1}\big) \tag{2-43}$$

Then, the CLF can be rendered negative definite in z_i and negative semi-definite in $\tilde{\boldsymbol{\theta}}_{f_i}$ and $\tilde{\boldsymbol{\theta}}_{f_i}$, because the derivative $\dot{V}_i$ equals:

$$\dot{V}_i = -\sum_{j=1}^{i} c_j z_j^2 + z_i\hat{g}_i z_{i+1} \tag{2-44}$$

The example from subsection 2-1-2 can be extended with parameter uncertainties for the parameters a and b, by writing update laws for those parameters:

$$\begin{aligned}
\dot{\hat{a}} &= \Gamma_a z_1 \sin x_1 \\
\dot{\hat{b}} &= \Gamma_b z_2 u
\end{aligned} \tag{2-45}$$

Results are shown in Figure 2-3. We can see from the differential equations in Equation 2-23 that uncertainties in parameter estimates for $\hat{a}$ and $\hat{b}$ do not directly have a destabilizing effect. This is because the error terms $\tilde{a}\sin x_1$ and $\tilde{b}u$ are not destabilizing terms. However, consider an extra parameter c that scales the damping in the first integrator:

$$\begin{aligned}
\dot{x}_1 &= -cx_1^3 + a\sin x_1 + x_2 \\
\dot{x}_2 &= bu
\end{aligned} \tag{2-46}$$

Then, the estimation error dynamics for this parameter are defined by the term $\tilde{c}x_1^3$ which really is destabilizing for a negative error. The parameter update law with the tuning functions approach that should guarantee stability equals:

$$\dot{\hat{c}} = -\Gamma_c z_1 x_1^3 \tag{2-47}$$

Results with estimation errors $\tilde{c}$ are shown in Figure 2-4. The normal, non-adaptive controllers are unstable and the tuning functions controller still provides stability.

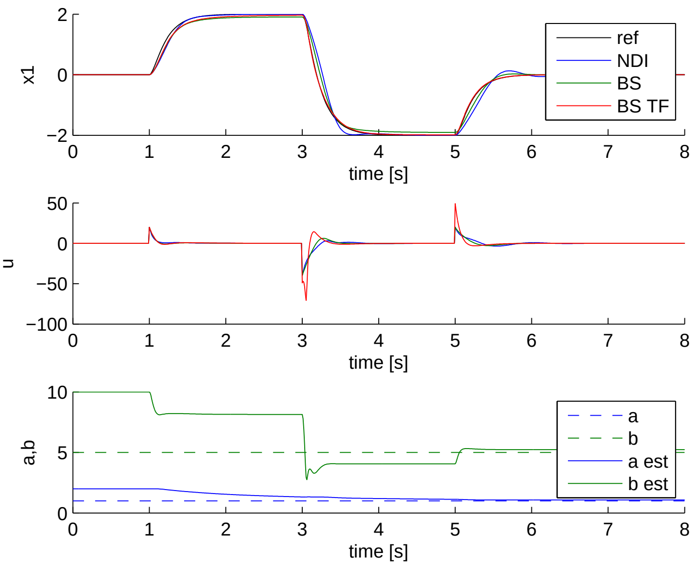

Figure 2-3: Performance of Backstepping control with tuning functions for parameters a and b.

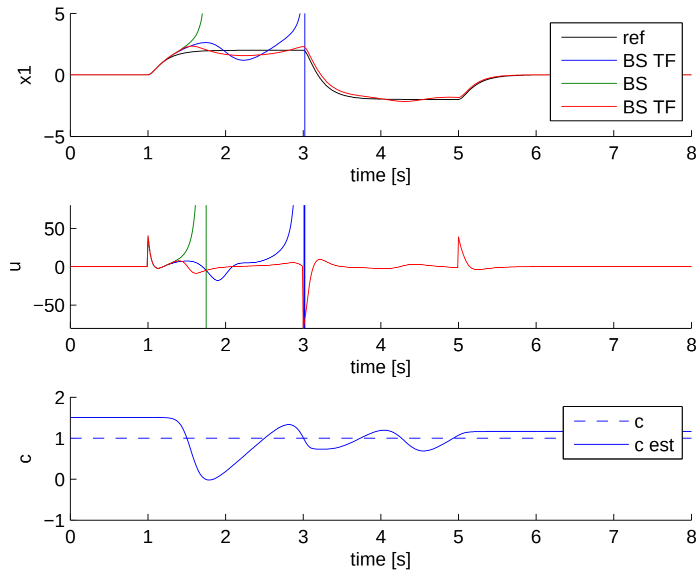

Figure 2-4: Performance of Backstepping control with tuning functions for parameter c.

2-3 Command filtering

Looking at the control laws derived in Equation 2-34, one can see that time derivatives of the virtual control, $\dot{\alpha}_1$ must be known. It can often become difficult to come up with analytical expressions for these derivatives, as these virtual controls contain parts of the system dynamics. Command filtering is a way to circumvent this problematic property of backstepping control. In command filtered backstepping, the raw intermediate reference signals are passed through a filter before it is used as the final reference. In this way, the filtered time derivate is retrieved.

Command filters can also be used to impose position, rate limit and bandwidth constraints on the reference signals at each step. The command filters need to be integrated with a backstepping control procedure so that global asymptotic stability is still guaranteed. This was desribed by Dong, Farrell, Polycarpou, Djapic, and Sharma (2012); J. A. Farrell, Polycarpou, Sharma, and Dong (2008). A modified tracking error is introduced to prove stability and to implement valid parameter update laws in the presence of command saturation. In this thesis, command filtering is only used to obtain time derivatives of the intermediate reference signals. Only a brief overview of the theory is therefore described in this section, by using a command filters for a second-order system.

Consider a second-order system in strict-feedback form with a relative degree of 2:

$$\begin{aligned} \dot{x}_1 &= f_1(x_1) + g_1(x_1)x_2 \\ \dot{x}_2 &= f_2(x_1, x_2) + g_2(x_1, x_2)u \end{aligned} \tag{2-48}$$

Of which the x_1 is the output command variable. Tracking errors are defined as:

$$\begin{aligned} z_1 &= x_1 - x_{1,r} \\ z_2 &= x_2 - x_{2,r} \end{aligned} \tag{2-49}$$

The references $x_{1,r}, x_{2,r}$ and the output u are the final, filtered and limited references. Raw, unfiltered commands are denoted as $x^0_{1,r}, x^0_{2,r}$ and u^0. Now define the *modified* tracking errors as:

$$\begin{aligned} \bar{z}_1 &= z_1 - \chi_1 \\ \bar{z}_2 &= z_2 - \chi_2 \end{aligned} \tag{2-50}$$

The variables χ_1, χ_2 are an estimation of the effect that the command filter limits has on the tracking error. The dynamics of those variables are defined by stable linear filters:

$$\dot{\chi_1} = -c_1\chi_1 + g_1(x_1)\big(x_{1,r} - x^0_{1,r}\big)\dot{\chi_2} = -c_2\chi_2 + g_2(x_2)\big(u - u^0\big) \tag{2-51}$$

and control Lyapunov functions (CLFs) are set up for the modified tracking errors. Consider the first CLF:

$$V_1 = \frac{1}{2}\bar{z}_1^2 \tag{2-52}$$

of which the time derivative must be rendered negative definite:

$$\begin{aligned} \dot{V}_1 &= \bar{z}_1\big\{f_1 + g_1x_2 - \dot{x}_{1,r} - \dot{\chi}_1\big\} \\ &= \bar{z}_1\big\{f_1 + g_1x_{2,r} + z_2) - \dot{x}_{1,r} + c_1\chi_1 - g_1\big(x_{2,r} - x^0_{2,r}\big)\big\} \\ &= \bar{z}_1\big\{f_1 + g_1(x_{2,r} + z_2) - \dot{x}_{1,r} + c_1\chi_1 - g_1\big(x_{2,r} - x^0_{2,r}\big)\big\} \\ &= \bar{z}_1\big\{f_1 + g_1z_2 - \dot{x}_{1,r} + c_1\chi_1 + g_1x^0_{2,r}\big\} \end{aligned} \tag{2-53}$$

A possible choice for $x_{2,r}^0$ is:

$$x_{2,r}^0 = g_1^{-1}\big(- c_1 z_1 - f_1 + \dot{x}_{1,r}\big) - \chi_2 \tag{2-54}$$

which yields:

$$\begin{aligned} \dot{V}_1 &= \bar{z}_1\big\{g_1 z_2 + c_1\chi_1 - c_1 z_1 - g_1\chi_2\big\} \\ &= \bar{z}_1\big\{g_1\bar{z}_2 - c_1\bar{z}_1\big\} \\ &= -c_1\bar{z}_1^2 + \bar{z}_1 g_1 \bar{z}_2 \end{aligned} \tag{2-55}$$

For the second step, augment the V_1 with a term that is radially unbounded in $\bar{z}_2$:

$$V_2 = V_1 + \bar{z}_2^2 \tag{2-56}$$

The time derivate should be rendered negative definite:

$$\begin{aligned} \dot{V}_2 &= \dot{V}_1 + \bar{z}_2\big\{f_2 + g_2 u - \dot{x}_{2,r} - \dot{\chi}_2\big\} \\ &= \dot{V}_1 + \bar{z}_2\big\{f_2 + g_2 u - \dot{x}_{2,r} + c_2\chi_2 - g_2(u - u^0)\big\} \\ &= -c_1\bar{z}_1^2 + \bar{z}_1 g_1\bar{z}_2 + \bar{z}_2\big\{f_2 - \dot{x}_{2,r} + c_2\chi_2 + g_2 u^0\big\} \end{aligned} \tag{2-57}$$

A possible choice for u^0 is:

$$u = g_2^{-1}\big(- c_2 z_2 + - f_2 + \dot{x}_{2,r} - g_1 z_1\big) \tag{2-58}$$

which yields:

$$\begin{aligned} \dot{V}_2 &= -c_1\bar{z}_1^2 + \bar{z}_1 g_1\bar{z}_2 + \bar{z}_2\big\{c_2\chi_2 - c_2 z_2 - g_1 z_1\big\} \\ &= -c_1\bar{z}_1^2 - c_2\bar{z}_2^2 \end{aligned} \tag{2-59}$$

Which proofs global asymptotic stability of the modified tracking errors at the equilibrium $\bar{z}_1, \bar{z}_2 = 0$. According to J. Farrell, Sharma, and Polycarpou (2005), if there are no constraints of the command filters in effect, χ_1, χ_2 will approach zero with an exponential decay rate c_1 and c_2, respectively. This implies therefore that because $\bar{z}_1, \bar{z}_2$ are asymptotically stable, also z_1, z_2 are stable. During a period where the implemented limits come into effect, it follows from Equation 2-51 that χ becomes non-zero. But because the input to this stable linear filter is bounded, also χ is bounded. Because $\bar{z}_1, \bar{z}_2$ are asymptotically stable, from Equation 2-50 it follows that also z_1, z_2 are bounded.

2-4 Incremental nonlinear control

This section covers a brief derivation of the INDI and IBS control laws applied to general first-order nonlinear system dynamics. It highlights the similarity between the derived NDI and backstepping control laws when the CLF is chosen to have a simple quadratic form, and when all system dynamics are canceled in the control law. Furthermore, it will be shown that the resulting incremental control law is under some conditions similar to classical PI-control. These similarities are not yet published in literature. In subsection 2-4-3, various similarities with PID control have been derived for continuous-time implementations. In subsection 2-4-4, incremental nonlinear control has been compared with incremental PID control. An equivalence is presented for discrete implementations of the control laws. This has been performed both for INDI, as well for a second-order feedback linearizable system. Therefore, the latter section presents a more general approach.

The idea that this incremental control method can be compared with classical PI(D)-control is not entirely new; in a paper by Chang and Jung (2009), a similarity is shown in order to tune the gains of a PI(D)-controller in a systematic way. This was done by comparing incremental PID with time-delayed nonlinear dynamic inversion control, a control strategy very similar to INDI. The result in subsection 2-4-4 in this report is contained in greater detail in a submitted paper that is currently under review(Acquatella B., van Ekeren, & Chu, 2017). The author of this report is also one of the contributors to this paper. The paper is included at the end of this report as an appendix.

2-4-1 Incremental nonlinear dynamic inversion

INDI applies to any system on which normal dynamic inversion can be applied, but can also be applied to systems that are non-affine in control. Because the derivation is based on a first-order taylor series expansion about a previous point in the recent past, the system is assumed to be locally linear, hence the control needs to be locally affine-in-control. For a meaningfull result, it must furthermore be assumed that the variation of the system dynamics contained in $f(x)$ do not vary significantly over the time increment considered. Let us first derive the simplified, incremental dynamics.

$$\begin{aligned} \dot{x} &= f(x) + g(x,u) \\ y &= h(x) \end{aligned} \tag{2-60}$$

Taking the first taylor series expansion of $\dot{x}$ at t_0 yields:

$$\dot{x} = \dot{x}_0 + \underbrace{\left(\frac{\partial f(x)}{\partial x} + \frac{\partial g(x,u)}{\partial x} \right)\Bigg|_{x_0}}_{A_0} (x - x_0) + \underbrace{\frac{\partial g(x,u)}{\partial u}\Bigg|_{x_0,u_0}}_{B_0} (u - u_0) + \underbrace{\mathcal{O}(\Delta x^2, \Delta u^2)}_{\epsilon} \tag{2-61}$$

in which we defined $\Delta x = x - x_0$ and $\Delta u = u - u_0$. The equation can be written in short as:

$$\dot{x} = \dot{x}_0 + A_0 \Delta x + B_0 \Delta u + \epsilon \tag{2-62}$$

For locally linear systems, the higher order terms gathered in ϵ may be neglected. The derivation of a general INDI control law is shown for a first-order system with a relative degree of one and without hidden dynamics, but can be applied to any system in lower-triangular form. As long as the system behaves linear between two samples, the overall system does not even need to be affine in control, contrary to usal NDI. We start by taking the first derivative of the output y and substituting (2-61). For the sake of simplicity in this example, consider the output to equal the state, $y = x$.

$$\begin{aligned} \dot{y} &= \frac{\partial h(x)}{\partial x} \dot{x} \\ &= f(x) + g(x,u) \\ &= \dot{x}_0 + A_0 \Delta x + B_0 \Delta u \end{aligned} \tag{2-63}$$

By setting

$$\Delta u = B_0^{-1} \left(-\dot{x}_0 - A_0 \Delta x + \nu \right) \tag{2-64}$$

A linear input-to-ouput map is described between y and the virtual input ν:

$$\begin{aligned} y &= h(x) \\ \dot{y} &= \nu \end{aligned} \tag{2-65}$$

When defining the tracking error as:

$$\begin{aligned} e &= y_r - y \\ \dot{e} &= \dot{y}_r - \dot{y} \end{aligned} \tag{2-66}$$

we are able to select the virtual control as:

$$\nu = K_p e + \dot{y}_r \tag{2-67}$$

Such that the error dynamics yield by substitution of (2-65) in (2-66):

$$\begin{aligned} \dot{e} &= \dot{y}_r - \nu \\ &= \dot{y}_r - K_p e - \dot{y}_r \\ &= -K_p e \end{aligned} \tag{2-68}$$

Then, we can design a value for K_p to achieve the desired error dynamics. The final control law for Δu is:

$$\begin{aligned} \Delta u &= B_0^{-1} \left(-\dot{x}_0 - A_0 \Delta x + \nu \right) \\ &= B_0^{-1} \left(-\dot{x}_0 - A_0 \Delta x + K_p e + \dot{y}_r \right) \end{aligned} \tag{2-69}$$

In (2-69), the terms $K_p e + \dot{y}_r$ represent the desired acceleration (or desired time derivative), $\dot{y}_{\text{des}}$. The other terms, $\dot{x}_0 + A_0 \Delta x$ is the compensation to the actual acceleration at the current state and input, $\dot{y}_{\text{cur}}$. The factor A_0 still contains model parameters from the system dynamics. When the sampling time is high, the increment $A_0 \Delta x$ could be neglected, to release this model-dependency. The assumption implies that the system dynamics are slow such that it all system dynamics increments are measured using the feedback of the state derivative $\dot{x}_0$. With this assumption the incremental control law yields:

$$\Delta u = B_0^{-1} \left(-\dot{x}_0 + K_p e + \dot{y}_r \right) \tag{2-70}$$

The final total control command at the current time step then equals the previous control input plus the control increment:

$$u = u_0 + \Delta u \tag{2-71}$$

If actuator dynamics are present between the commanded input u_c and the actual input u_f, the actual actuator position u_0 can be used as feedback, as illustrated in Figure 2-6. This method is used for example by Smeur (2016); Van Gils (2015); Vlaar (2014). It justifies Equation 2-61 better, because in this equation u_0 refers to the physical input at a previous point in time. The advantage of applying the incremental control method presented in this section is that the control is less dependent on system dynamics at the cost of a higher dependency on sensors, as the state derivative $\dot{x}_0$ needs to be known. Furthermore, actuator positions have to be fed back.

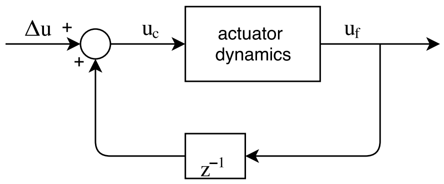

Figure 2-5: Implementation of incremental control law under the presence of actuator dynamics: the control increment is added to the previous final actuator position.

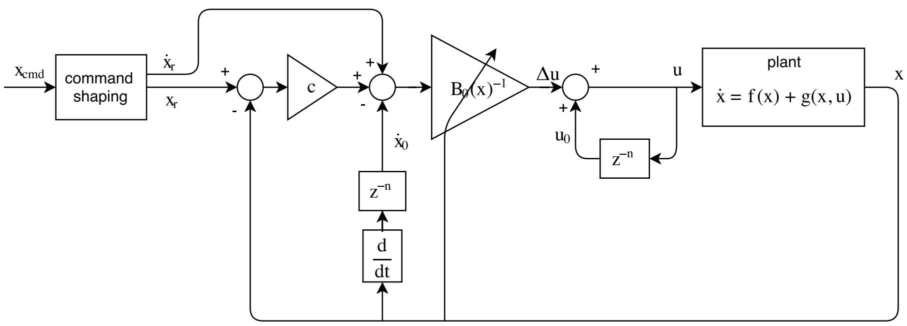

Figure 2-6: Schematic of the general incremental control law as derived in this section.

2-4-2 Incremental backstepping

Backstepping control laws can be extended with incremental forms at any integration step of the backstepping controller design process described in subsection 2-1-1.

Comparing (2-60) and (2-62), it can be seen that the nonlinear, non-affine in control system has been converted to a locally linear, affine in control system. The input is now described by means of its increment Δu. Describe a CLF by

$$V = \frac{1}{2}z^2 \tag{2-72}$$

with $z = y - y_r$ is the error between the state and the reference signal. Note that $e = -z$. Both notations are used to be consistent with literature both for feedback linearization as backstepping control. The derivative must be renedered negative definite which yields the following control law:

$$\begin{aligned} \dot{V} &= z\big(\dot{x} - \dot{y}_r\big) \\ &= z\big(\dot{x}_0 + A_0\Delta x + B_0\Delta u - \dot{y}_r\big) \end{aligned} \tag{2-73}$$

$$\Delta u = {B_0}^{-1}\big(-cz - \dot{x}_0 - A_0\Delta x + \dot{y}_r\big) \tag{2-74}$$

With $c > 0$. Again, if we assume system dynamics increments $A_0\Delta x$ are small, this yields:

$$\Delta u = {B_0}^{-1}\big(-cz - \dot{x}_0 + \dot{y}_r\big) \tag{2-75}$$

Comparing with (2-70), it can be seen that the resulting control laws are equivalent, with $K_p = c$. A diagram of this general incremental control law is depicted in Figure 2-6.

2-4-3 Similarities with classical Proportional-Integral control

It can be shown that the INDI and IBS control law for systems with a relative degree of 1 show a large similarity with well-known classical proportional-integral (PI) control. First, we consider system dynamics without actuator dynamics. Next, they will be included.

Without actuator dynamics

Consider the incremental control law (2-71) in discrete time with a total increment delay that equals its sample time T_s:

$$u_{k+1} = u_k + \Delta u_k \tag{2-76}$$

When considering low sampling times, this control law is comparable with a continuous integrator:

$$u(t) = \int_0^t \frac{\Delta u}{T_s} d\tau \tag{2-77}$$

Substituting for the incremental control and taking terms outside the integrator term yields:

$$\begin{aligned} u(t) &= \int_0^t \frac{B_0^{-1}(x)}{T_s} \Big(-cz(\tau) - \dot{x}(\tau - T_s) + \dot{y}_r(\tau) \Big) d\tau \\ &= \frac{B_0^{-1}(x)}{T_s} \left(-c \int_0^t z(\tau) d\tau - x(t - T_s) + y_r(t) \right) \\ &= \frac{B_0^{-1}(x)}{T_s} \left(-c \int_0^t z(\tau) d\tau - z(t) \right) \end{aligned} \tag{2-78}$$

when assuming that the state x changes slow enough compared to the sample time so that the tracking error $z(t) \approx x(t - T_s) - y_r(t)$. Now we can see the similarity with a classical PI-controller. Equation 2-78 can written as:

$$u(t) = -K_p z(t) - K_i \int_0^t z(t) dt \tag{2-79}$$

with:

- $K_p = \frac{1}{T_s} B_0^{-1}(x)$, acting as proportional gain
- $K_i = c\frac{1}{T_s} B_0^{-1}(x) = cK_p$, acting as integral gain

The control scheme of such a controller is presented in Figure 2-7. This is quite a remarkable result: the derivation shows how a non-linear controller which is capable of (in theory) a perfect tracking of the reference signal by an inversion of the system dynamics, is under certain conditions equivalent to a linear PI-controller (although parameter-varying by $B_0(x)$). The conditions under which this can be compared are:

- Absence of feedback delays: Looking at Figure 2-6, there is no additional delay in the feedback of the angular accelerations. Hence, the moment t_0 in Equation 2-61 refers to one sample back in time. However, the incremental controllers applied so far in literature all use filtered estimates of the angular accelerations which causes some delay. See (Sieberling et al., 2010; Smeur, 2016; Van Gils, 2015).

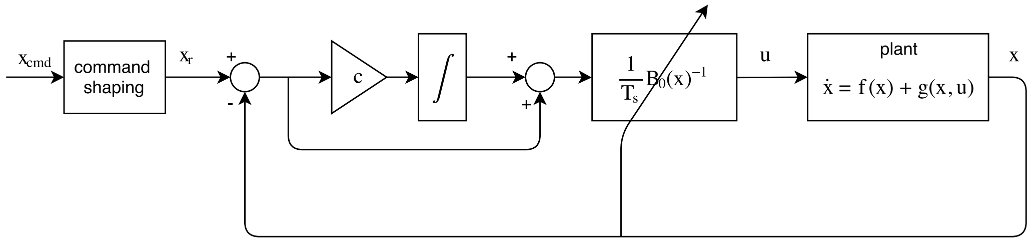

Figure 2-7: Control diagram in continuous time for the derived PI-controller from an INDI controller with low sampling times and without delays.

- High sample rates: The sample rate must be high enough to make the assumption that $u_{k+1} = u_k + \Delta u_k$ resembles a pure integrator which yields the continuous time integrator in Equation 2-77. In this way, the feedback of angular accelerations results in a feedback of normal angular rates after this integration.

With actuator dynamics

Now, let us consider first-order actuator dynamics with a time constant τ_a in the system and feedback the actuator position to the incremental controller, as shown in Figure 2-5. From the actuator dynamics we derive:

$$\begin{aligned} \dot{u}_f &= -\frac{1}{\tau_a}u_f + \frac{1}{\tau_a}u_c \\ &= -\frac{1}{\tau_a}u_f + \frac{1}{\tau_a}(u_f + \Delta u) \\ &= \frac{1}{\tau_a}\Delta u \end{aligned} \tag{2-80}$$

when the actuator limits are not reached, so that:

$$u_f = \frac{1}{\tau_a}\int_0^t \Delta u d\tau \tag{2-81}$$

Comparing this with (2-77), we see that by substitution, the result for the final actuator position is similar:

$$\begin{aligned} u_f(t) &= \int_0^t \frac{B_0^{-1}(x)}{\tau_a}\Big(- cz(\tau) - \dot{x}(\tau - T_s) + \dot{y}_r(\tau)\Big)d\tau \\ &= \frac{B_0^{-1}(x)}{\tau_a}\left(-c\int_0^t z(\tau)d\tau - x(t - T_s) + y_r(t)\right) \\ &= \frac{B_0^{-1}(x)}{\tau_a}\left(-c\int_0^t z(\tau)d\tau - z(t)\right) \end{aligned} \tag{2-82}$$

again, under the consideration of a high sample rate and without feedback delays included. This can be compared with a PI-control with the following gains:

- $K_p = \frac{1}{\tau_a} B_0^{-1}(x)$, acting as proportional gain
- $K_i = c \frac{1}{\tau_a} B_0^{-1}(x)$, acting as integral gain

This is the result when considering the final actuator position u_f as comparison. The resulting PI-controller is in this case not an actual controller that can be directly implemented as such. This is because does not specify the commanded control u_c, but the final actuator position u_f. This result is hence more useful as a reference for the incremental control. From the result in (2-82) and (2-79), some important observations can be made:

- The inversed control effectiveness B_0^{-1} scales the proportional gain in the controller. Hence, more agressive control is reached by an under-estimation of B_0, while, over-estimation, yields a safer and lower response.
- The time constant T_s or actuator time constant tau_a also has a proportional effect on the proportional gain. Hence, faster control is reached by lowering the sampling time.
- The parameter c, which is the linear control parameter to reduce the tracking error, acts as an integral gain. Hence, removing c will result in steady state errors.

When considering the commanded control u_c instead of the actuator position u_f, a different result is obtained:

$$\begin{aligned} u_c &= u_f + \Delta u \\ &= \frac{1}{\tau_a} \int_0^t \Delta u d\tau + \Delta u \end{aligned} \tag{2-83}$$

This is not a pure integrator; the control also contains a direct feed-through of Δu. Writing out the control law gives:

$$\begin{aligned} u_c(t) &= \int_0^t \frac{B_0^{-1}(x)}{\tau_a} \Big(- cz(\tau) - \dot{x}(\tau - \tau_a) + \dot{y}_r(\tau) \Big) d\tau + \dots \\ &\qquad \dots + B_0^{-1}(x) \big(- cz(t) - \dot{x}(t - T_s) + \dot{y}_r(t) \big) \\ &= \frac{B_0^{-1}(x)}{\tau_a} \left(-c \int_0^t z(\tau) d\tau - z(t) \right) + B_0^{-1}(x) \big(- cz(t) - \dot{z} \big) \\ &= B_0^{-1}(x) \left(- \frac{c}{\tau_a} \int_0^t z(\tau) d\tau - \left(\frac{1}{\tau_a} + c \right) z(t) - \dot{z} \right) \end{aligned} \tag{2-84}$$

which compares with a PID-controller for which:

- $K_p = -B_0^{-1}(x) \left(\frac{1}{\tau_a} + c \right)$ is the proportional gain
- $K_i = -B_0^{-1}(x) \frac{c}{\tau_a}$ is the integral gain
- $K_d = -B_0^{-1}(x)$ is the derivative gain

Note that this result is only valid for first-order actuator dynamics of which the model is accurately known, so that it can be integrated in the gains of the PID controller.

An important difference between the PI-control and the incremental control technique is that the latter leaves the possibility to feedback actual actuator positions, and hence integrate actuator constraints and dynamics into the controller. Furthermore, in practical implementations, usually some non-negligible delay will be present. The incremental control techniques provide a systematic way to compensate for this delay, because it is based on a taylor series expansion about a previous point in time. In any case, however, the results obtained in this section, especially those in Equation 2-78 and Equation 2-82, are usefull as a *comparison*.

In section 4-4, simulations are presented to show the similarity between both controllers.

2-4-4 Equivalence of incremental feedback linearization with incremental proportional-integral-derivative control

In this section, a comparison with the gains of a PID control law is presented that is based on Acquatella B. et al. (2017). A discrete formulation of both a feedback linearization control law and an incremental PID control law is used to compare the terms and show the equivalence between both.

Consider a tracking problem with a reference y_r of which $\dot{y}_r$ and $\ddot{y}_r$ are defined available and consider a tracking error $e = y_r - y$. Furthermore, consider the system to be controlled to be a general, affine-in-control, lower-triangular second order system with a relative degree r of 2:

$$\begin{aligned} y &= h(z_1, z_2) \\ \dot{z}_1 &= \phi_1(z_1) + \gamma_1(z_1)z_2 \\ \dot{z}_2 &= \phi_2(z_1, z_2) + \gamma_2(z_2)u \end{aligned} \tag{2-85}$$

On which a state transformation can be made to yield a triangular second-order system (Chu, 2014; Slotine, 1991):

$$\begin{aligned} y &= x_1 \\ \dot{x}_1 &= x_2 \\ \dot{x}_2 &= f(x_1, x_2) + g(x_1, x_2)u \end{aligned} \tag{2-86}$$

The system dynamics can be inverted and the output can be linearized with respect to a virtual control ν:

$$u = g^{-1}(\nu - f) \tag{2-87}$$

The virtual control can be defined such that the error dynamics are exponentially stable:

$$\nu = P_{\text{fl}}e(t) + D_{\text{fl}}\dot{e}(t) + \ddot{y}_r \tag{2-88}$$

where P_{fl} are D_{fl} are constants. To apply feedback linearization in incremental form, take a first order taylor series expansion of $\ddot{y} = \dot{x}_2$ around a previous point t_0 in time:

$$\ddot{y} = \ddot{y}_0 + \frac{\partial}{\partial \bar{x}}\bigg(f(x_1, x_2) + g(x_1, x_2)u\bigg)\bigg|_{\bar{x}=\bar{x}_0}(\bar{x} - \bar{x}_0) + \frac{\partial}{\partial u}g(x_1, x_2)\bigg|_{\bar{x}=\bar{x}_0}(u - u_0) \tag{2-89}$$

with $\bar{x} = [x_1, x_2]^T$. If then, it can be assumed that f and g do not change significantly over $t - t_0$, so that:

$$\begin{aligned} \epsilon_1(t) &= f\big(x_1(t), x_2(t)\big) - f\big(x_1(t_0), x_2(t_0)\big) \cong 0 \\ \epsilon_2(t) &= g\big(x_1(t), x_2(t)\big) - g\big(x_1(t_0), x_2(t_0)\big) \cong 0 \end{aligned} \tag{2-90}$$

Then it can be assumed that:

$$\ddot{y} \cong \ddot{y}_0 + G_0 \Delta u \tag{2-91}$$

with:

$$\begin{aligned} G_0 &= \frac{\partial}{\partial u} g(x_1, x_2)\bigg|_{\bar{x}=\bar{x}_0} \\ \Delta u &= u - u_0 \end{aligned} \tag{2-92}$$

and feedback linearization can be applied similar to the non-incremental case in (2-87):

$$\Delta u = G_0^{-1}\big(\nu - \ddot{y}_0\big) \tag{2-93}$$

with:

$$\nu = P_{\text{ifl}} e(t) + D_{\text{ifl}} \dot{e}(t) + \ddot{y}_r \tag{2-94}$$

where P_{ifl} are D_{ifl} again are constants that yield exponentially stable error dynamics. We will look now at a discrete implementation of the control laws. To that end, consider the increment delay to sample time T_s, the smallest possible delay. We apply a numerical differentiation to obtain time derivatives:

$$\begin{aligned} \dot{e}_k &= \frac{1}{T_s}(e_k - e_{k-1}) \\ \ddot{e}_k &= \frac{1}{T_s^2}(e_k + e_{k-2}) \end{aligned} \tag{2-95}$$

with T_s the sample time. With $\ddot{y}_0 = \ddot{y}_k$, Equation 2-93 yields:

$$\begin{aligned} u_k &= u_{k-1} + G_0^{-1}\big(P_{\text{ifl}} e_k + D_{\text{ifl}} \dot{e}_k + \ddot{e}_k\big) \\ &= u_{k-1} + G_0^{-1}\left(P_{\text{ifl}} e_k + D_{\text{ifl}} \frac{1}{T_s}(e_k - e_{k-1}) + \frac{1}{T_s^2}(e_k + e_{k-2})\right) \end{aligned} \tag{2-96}$$

Now, consider a discrete PID control law:

$$u_k = P_{\text{pid}} e_k + I_{\text{pid}} \sum_{i=1}^{k} T_s e_i + D_{\text{pid}} \dot{e}_k \tag{2-97}$$

where $P_{\text{pid}}, I_{\text{pid}}, D_{\text{pid}}$ are the gains of the PID controller. The derivative term can be written out as a numerical differentiation of e. Then subtract the previous PID command from the current command to yield a PID control law in incremental form:

$$\begin{aligned} u_k &= u_{k-1} + P_{\text{pid}}(e_k - e_{k-1}) + I_{\text{pid}} T_s e_k + D_{\text{pid}}(\dot{e}_k - \dot{e}_{k-1}) \\ &= u_{k-1} + P_{\text{pid}}(e_k - e_{k-1}) + I_{\text{pid}} T_s e_k + D_{\text{pid}} \frac{1}{T_s}(e_k + e_{k-2}) \end{aligned} \tag{2-98}$$

The result can be compared term by term with Equation 2-96, so that the gains of the PID controller can be written in terms of the gains of the incremental feedback linearization control law:

$$\begin{aligned} P_{\text{pid}} &= G_0^{-1}\frac{D_{ifl}}{T_s} \\ I_{\text{pid}} &= G_0^{-1}\frac{P_{ifl}}{T_s} \\ D_{\text{pid}} &= G_0^{-1}\frac{1}{T_s} \end{aligned} \tag{2-99}$$

The same process can be followed for a first order system with a relative degree of 1, so that feedback linearization reduces to non-linear dynamic inversion. So, consider the tracking problem of a first-order, nonlinear affine-in-control system, on which the same assumptions can be made with respect to the increment of inner loop:

$$\begin{aligned} e &= y - y_r \\ y &= x \\ \dot{x} &= f(x) + g(x)u \\ \dot{x} &\cong \dot{x}_0 + G_0\Delta u \end{aligned} \tag{2-100}$$

the incremental control law that yields exponentially stable and decoupled error dynamics is:

$$\Delta u = G_0^{-}1\big(P_{\text{indi}}e(t) + -\dot{y}_0 + \dot{y}_r\big) \tag{2-101}$$

In a discrete implementation, this yields:

$$u_k = u_{k-1} + G_0^{-1}\big(P_{\text{indi}}e_k + \frac{1}{T_s}(e_k - e_{k-1})\big) \tag{2-102}$$

The result can be compared again with the incremental PID controller in Equation 2-98. By comparing terms, we find:

$$\begin{aligned} P_{\text{pid}} &= G_0^{-1}\frac{1}{T_s} \\ I_{\text{pid}} &= G_0^{-1}\frac{P_{\text{ifl}}}{T_s} \\ D_{\text{pid}} &= 0 \end{aligned} \tag{2-103}$$

It can be seen that the result is equivalent to what has been derived in Equation 2-79. The way the simililarity is derived in this section is different in that it is based on a discrete formulation through which an exact equivalence with incremental PID is shown, whereas in the previous section the assumption had to be made that the continuous

Chapter 3

Fixed-Wing Aircraft Model

Up to this point, all the basic tools that are need to present the flight control laws have been presented. Before the control designs are discussed, the aircraft model will be presented. As the control laws are implemented and tested on a real fixed-wing aircraft, first this platform will be introduced. Subsequent sections discuss equations of motion, the aerodynamic model and actuator dynamics

The FASER project consists of multiple platforms that are equipped with similar software and hardware aiming to make the process of implementing and testing new flight control algorithms as simple as possible. Wind-tunnel tests are performed to generate a high-fidelity model, which is defined in MATLB/Simulink. The platform used in this research is the UltraStick120, a 2 m span fixed-wing aircraft. Basic properties of the aircraft are listed in Tab. 3-1. A schematic of the hardware communications of the Flight Computer and the hardware compontents is presented in Figure 3-1

3-1 Assumptions and reference frames

Multiple reference frames are used to the define equations of motion as well as variables that are used in the control laws, like the acceleration components and aerodynamic forces. The reference frames are consistent with the common conventions used in aircraft flight dynamics Mulder et al. (2011); Stevens and Lewis (2003). To set up the equations of motion in the next chapter, the most important assumptions made are:

- The aircraft is treated as a rigid body. No structural vibrations or aeroelastic effects are considered.
- The mass of the aircraft is constant.
- The north-east-down is an inertial reference frame, hence it is assumed that the earth is flat and non-rotating.

Table 3-1: Basic aircraft parameters of the UltraStick120 platform.

Parameter		
Mass (take-off weight)	m	8.13 kg
Length		1.26 m
C.G. from firewall	x_{cg}	0.315 m
Aero ref from firewall	x_a	0.320 m
Roll inertia	I_x	1.031 kgm^2
Pitch inertia	I_y	1.21 kgm^2
Yaw inertia	I_z	2.05 kgm^2
Roll-yaw inertia	I_{xz}	0.433
Chord	$\bar{c}$	0.433 m
Span	b	1.92 m
Wing Area	S	0.769 m^2

Table 3-2: Aircraft avionics and hardware components.

Component	Description
Flight Computer	Phytec MPC5200B Tiny (400 MHz, 64MB DDR DRAM, controller sample rate 50 Hz)
GPS Receiver	Novatel OEM Star
IMU	Analog Devices ADIS16405
Servos	DS8411 (1.55 Nm @4.8 V)
Pressure sensors	AMS5812

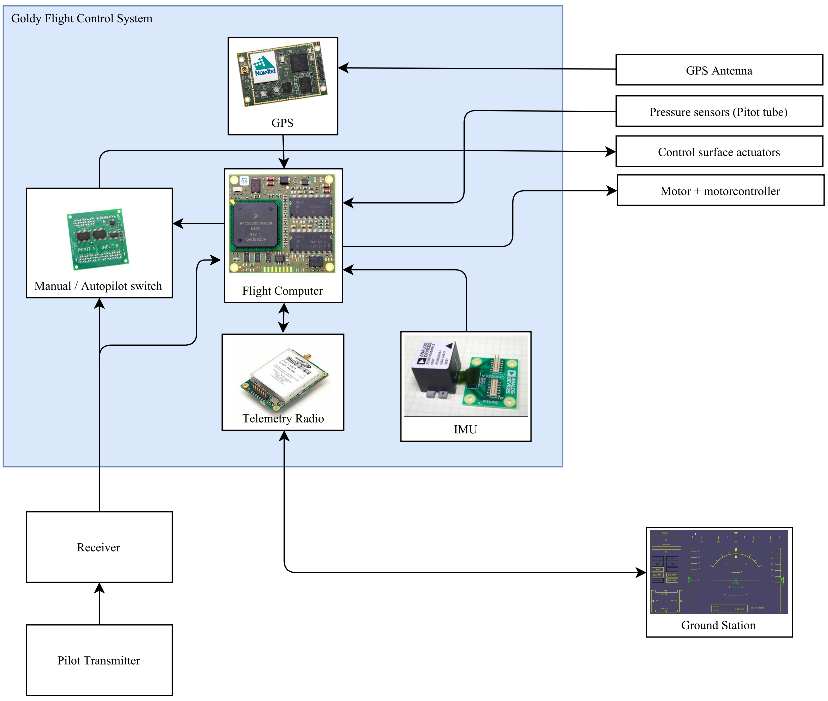

Figure 3-1: FASER sensors and actuators communication signals structure

- The gravitational acceleration g is constant and always points in the vertical direction.
- Steady flow is considered. Hence, the aircrafts attitude with respect to the free-stream velocity completely determine the aerodynamic forces acting on the aircraft.

Earth-fixed, north-east-down reference frame The north-east-down (NED) reference frame is considered to be the inertial reference frame. Its origin coincides with the aircraft's center of gravity. The x-axis is pointing in north direction, the y-axis is pointing to the east and the z-axis is pointing downward.

Body reference frame The body reference frame is fixed to the aircraft's body and originates in its center of gravity. The x-axis points in the nose direction, the z-axis points downward, and the y-axis points in the starboard direction. Accelerations, body velocities and angular rates are usually defined in this reference frame. The transformation from the NED to the body reference frame can be defined in terms of three Euler angles:

$$\begin{aligned}\mathbb{T}^{be}(\phi,\theta,\psi) &= \mathbb{T}_x(\phi)\mathbb{T}_y(\theta)\mathbb{T}_z(\psi) \\ &= \begin{bmatrix} \cos\psi\cos\theta & \cos\theta\sin\psi & -\sin\theta \\ \cos\psi\sin\phi\sin\theta - \cos\phi\sin\psi & \cos\phi\cos\psi + \sin\phi\sin\psi\sin\theta & \cos\theta\sin\phi \\ \sin\phi\sin\psi + \cos\phi\cos\psi\sin\theta & \cos\phi\sin\psi\sin\theta - \cos\psi\sin\phi & \cos\phi\cos\theta \end{bmatrix}\end{aligned} \tag{3-1}$$

Stability reference frame The stability reference frame has its origin in the aircraft's center of gravity and is defined such that the xz-plane is aligned with the xz-plane of the body reference frame, with the x-axis pointing in the direction of the aircraft's velocity relative to the wind. Hence, the reference frame is obtained by rotating the body reference frame over an angle α around the negative y-axis. In this frame, the aerodynamic lift, drag and side force acting on the aircraft are defined. The lift points in the *negative* z-direction, the drag points in the *negative* x-direction and the side force points in the *positive* y-direction of the stability reference frame. The transformation from the body to the stability reference frame is:

$$\mathbb{T}^{sb}(\alpha) = \mathbb{T}_y(-\alpha) = \begin{bmatrix} \cos\alpha & 0 & \sin\alpha \\ 0 & 1 & 0 \\ -\sin\alpha & 0 & \cos\alpha \end{bmatrix} \tag{3-2}$$

Aerodynamic reference frame The aerodynamic reference frame has its origin in the center of gravity. The frame is defined such that the x-axis points in the direction of the aircraft's aerodynamic velocity. It is obtained by rotating the stability reference frame over an angle β around the positive z-axis. The transformation from the stability to the aerodynamic frame of reference is hence given by:

$$\mathbb{T}^{as}(\beta) = \mathbb{T}_z(\beta) = \begin{bmatrix} \cos\beta & \sin\beta & 0 \\ -\sin\beta & \cos\beta & 0 \\ 0 & 0 & 1 \end{bmatrix} \tag{3-3}$$

Velocity frame The velocity frame becomes more usefull in outer loop, trajectory control problems when the total inertial velocity of the aircraft needs to be controlled. It is defined by 3 Euler angles from the NED reference frame: the aircraft course χ, the flight path angle χ, and the aircraft bank angle μ. When there is no wind, the velocity frame is aligned with the aerodynamic reference frame. When wind is considered, this is not the case as the aircraft's velocity considered in the velocity frame is the inertial velocity, whereas the velocity considered for the aerodynamic reference frame is the local velocity relative to the moving air.

3-2 Equations of motion

Following Newton's laws of motion applied to rigid bodies with a constant mass, the translational equations of motion in the body reference frame can be defined:

$$\dot{\mathbf{V}} = \frac{\mathbf{F}^b}{m} - \boldsymbol{\omega} \times \mathbf{V} \tag{3-4a}$$

$$\dot{\boldsymbol{\omega}} = I^{-1}(\mathbf{M}^b - \boldsymbol{\omega} \times I\boldsymbol{\omega}) \tag{3-4b}$$

Where $\mathbf{V} = [u, v, w]^T$ are the translational velocities, $\mathbf{F}^b = [F_x^b, F_y^b, F_z^b]^T$ are the total of forces and $\boldsymbol{\omega} = [p, q, r]^T$ are the rotational rates, all in body frame components. The aircraft's mass is denoted by m and its inertia matrix by:

$$I = \begin{bmatrix} I_x & 0 & I_{xz} \\ 0 & I_y & 0 \\ -I_{xz} & 0 & I_z \end{bmatrix} \tag{3-5}$$

Differential equations for kinematic motion can be derived by first writing the time derivative of each Euler angle in (3-1) in body frame components. The sum must equal the rotational rates in the body frame, because the NED frame is an inertial frame. So:

$$\begin{aligned} \begin{bmatrix} p \\ q \\ r \end{bmatrix} &= \mathbb{T}_x(\phi)\mathbb{T}_y(\theta) \begin{bmatrix} 0 \\ 0 \\ \dot{\psi} \end{bmatrix} + \mathbb{T}_x(\phi) \begin{bmatrix} 0 \\ \dot{\theta} \\ 0 \end{bmatrix} + \begin{bmatrix} \dot{\phi} \\ 0 \\ 0 \end{bmatrix} \\ &= \begin{bmatrix} 1 & 0 & -\sin\theta \\ 0 & \cos\phi & \cos\theta\sin\phi \\ 0 & -\sin\phi & \cos\theta\cos\phi \end{bmatrix} \begin{bmatrix} \dot{\phi} \\ \dot{\theta} \\ \dot{\psi} \end{bmatrix} \end{aligned} \tag{3-6}$$

Inverting this equation gives the equations for kinematic motion of the rotating body frame of reference:

$$\begin{bmatrix} \dot{\phi} \\ \dot{\theta} \\ \dot{\psi} \end{bmatrix} = \begin{bmatrix} 1 & \sin\phi\tan\theta & \tan\theta\cos\phi \\ 0 & \cos\phi & -\sin\phi \\ 0 & \sin\phi\sec\theta & \cos\phi\sec\theta \end{bmatrix} \begin{bmatrix} p \\ q \\ r \end{bmatrix} \tag{3-7}$$

The three scalar translational equations are found by writing out (3-4a) and splitting up the total force acting on the airplane, $\mathbf{F}^b$ into aerodynamic forces $\bar{X}^b, \bar{Y}^b, \bar{Z}^b$, a propeller thrust

F_T acting purely in x-direction and gravitational force $m\mathbf{g}$:

$$\dot{u} = rv - qw - g\sin\theta + \frac{\bar{X}^b}{m} + \frac{F_T}{m} \tag{3-8a}$$

$$\dot{v} = pw - ru + g\cos\theta\sin\phi + \frac{\bar{Y}^b}{m} \tag{3-8b}$$

$$\dot{w} = qu - pv + g\cos\theta\cos\phi + \frac{\bar{Z}^b}{m} \tag{3-8c}$$

where $\bar{X}^b, \bar{Y}^b, \bar{Z}^b$ are the aerodynamic forces at the cg in body frame components. The rotational equations are derived from (3-4b):

$$\dot{p} = (c_1 r + c_2 p)q + c_3\bar{L}^b + c_4\bar{N}^b \tag{3-9a}$$

$$\dot{q} = c_5 pr - c_6(p^2 - r^2) + c_7\bar{M}^b \tag{3-9b}$$

$$\dot{r} = (c_8 p - c_2 r)q + c_4\bar{L}^b + c_9\bar{N}^b \tag{3-9c}$$

where $\bar{L}^b, \bar{M}^b, \bar{N}^b$ are the aerodynamic moments around the cg in body frame components and c_i are inertia terms defined as:

$$\Gamma c_1 = (I_y - I_z) - I_{xz}^2 \qquad \Gamma c_4 = I_{xz} \qquad c_7 = \frac{1}{I_y} \tag{3-10a}$$

$$\Gamma c_2 = (I_x - I_y + I_z)I_{xz} \qquad c_5 = \frac{I_z - I_x}{I_y} \qquad \Gamma c_8 = I_x(I_x - I_y) + I_{xz}^2 \tag{3-10b}$$

$$\Gamma c_3 = I_z \qquad c_6 = \frac{I_{xz}}{I_y} \qquad \Gamma c_9 = I_x \tag{3-10c}$$

and $\Gamma = I_x I_z - I_{xz}^2$. The following assumptions are made when defining the equations of motion like above:

- The NED reference frame is an inertial reference frame, which implies that the earth is flat and non-rotating.
- The aircraft is a rigid body with constant mass.
- $I_{xy} = I_{yx} = 0$, which implies that the aircraft is symmetrical in the xy-plane.
- The body reference frame is defined such that the thrust force only has a component in the x-axis.
- The gravitational acceleration points in the positive z-direction of the NED reference frame.

Furthermore, no assumptions about the wind have been made. The equations of motion are given in inertial velocity components and a variable wind must be included when defining the angle of attack as a function of the aircrafts velocity components. When a constant wind is assumed, and the velocity $\mathbf{V}$ is defined relative to the constant wind, the equations of motions do not change because the constant wind can be seen as a different inertial reference frame.

3-3 Aerodynamical forces and moments

Extensive wind tunnel tests were performed on the particular model considered in this thesis Hoe, Owens, and Denham (2012); Owens et al. (2006). Because of this, an accurate aerodynamic model is available for simulations. The windtunnel test measurements are captured in look-up tables of the aerodynamic coefficients on which interpolation methods can be used to calculate the aerodynamic coefficients on a continuous domain. The aerodynamic forces and moments are measured in and around the center of pressure $\mathbf{r}_{\text{cp}}$, so that the measured aerodynamic forces also create a moment around the *cg*.

3-3-1 Aerodynamic model

The aerodynamic force coefficients are defined in the stability reference frame with its origin at the *cp*. The dimensional aerodynamic forces are defined in terms of their coefficients as:

$$\bar{\mathbf{F}}^{s,\text{cp}} = \bar{q}S \begin{bmatrix} -C_D \\ C_Y \\ -C_L \end{bmatrix} \tag{3-11}$$

and in body frame components at the *cg* as:

$$\bar{\mathbf{F}}^{b,\text{cg}} = \mathbb{T}^{bs}\bar{\mathbf{F}}^{s,\text{cp}} \tag{3-12}$$

so:

$$\begin{bmatrix} \bar{X}^b \\ \bar{Y}^b \\ \bar{Z}^b \end{bmatrix} = \mathbb{T}^{bs}\bar{q}S \begin{bmatrix} -C_D \\ C_Y \\ -C_L \end{bmatrix} \tag{3-13}$$

where $\bar{q}$ is the dynamic pressure, S is the reference (wing surface) area and C_D, C_Y, C_L are the drag, side force and lift coefficients, respectively. $\mathbb{T}^{bs}$ is the rotation matrix from the stability to the body reference frame. The dimensional aerodynamic coefficients are defined in the body reference frame with its origin at the *cp*. The dimensional aerodynamic moments are defined in terms of their non-dimensional coefficients as:

$$\bar{\mathbf{M}}^{b,\text{cp}} = \bar{q}S \begin{bmatrix} bC_{l,\text{cp}} \\ \bar{c}C_{m,\text{cp}} \\ bC_{n,\text{cp}} \end{bmatrix} \tag{3-14}$$

where b and $\bar{c}$ are the lateral and longitudinal reference lengths (wing span and mean aerodynamic chord) and C_l, C_m, C_n are the non-dimensional moment coefficients.

$$\bar{\mathbf{M}}^{b,\text{cg}} = \bar{\mathbf{M}}^{b,\text{cp}} + (\mathbf{r}_{\text{cp}} - \mathbf{r}_{\text{cg}}) \times \mathbb{T}^{bs}\bar{\mathbf{F}}^{s,\text{cp}} \tag{3-15}$$

Written out, this gives:

$$\begin{bmatrix} \bar{L}^b \\ \bar{M}^b \\ \bar{N}^b \end{bmatrix} = \bar{q}S \left(\begin{bmatrix} bC_{l,\text{cp}} \\ \bar{c}C_{m,\text{cp}} \\ bC_{n,\text{cp}} \end{bmatrix} + (\mathbf{r}_{\text{cp}} - \mathbf{r}_{\text{cg}}) \times \mathbb{T}^{bs} \begin{bmatrix} -C_D \\ C_Y \\ -C_L \end{bmatrix} \right) \tag{3-16}$$

For simplicity, we can define the moment coefficients around the center of gravity to avoid cross product with force-terms. Hence we can define:

$$\begin{bmatrix} \bar{L}^b \\ \bar{M}^b \\ \bar{N}^b \end{bmatrix} = \bar{q}S \begin{bmatrix} bC_{l,\mathrm{cg}} \\ \bar{c}C_{m,\mathrm{cg}} \\ bC_{n,\mathrm{cg}} \end{bmatrix} \tag{3-17}$$

with:

$$\begin{bmatrix} C_{l,\mathrm{cg}} \\ C_{m,\mathrm{cg}} \\ C_{n,\mathrm{cg}} \end{bmatrix} = \begin{bmatrix} C_{l,\mathrm{cp}} \\ C_{m,\mathrm{cp}} \\ C_{n,\mathrm{cp}} \end{bmatrix} + \begin{bmatrix} 0 & 0 & 0 \\ -{}^{\Delta x_{cp}}/_{c} \sin\alpha & 0 & -{}^{\Delta x_{cp}}/_{c} \cos\alpha \\ 0 & {}^{\Delta x_{cp}}/_{b} & 0 \end{bmatrix} \begin{bmatrix} -C_D \\ C_Y \\ -C_L \end{bmatrix} \tag{3-18}$$

under the assumption that $\mathbf{r}_{\mathrm{cp}} - \mathbf{r}_{\mathrm{cg}} = [\Delta x_{\mathrm{cp}}, 0, 0]^T$. This can be simplified to:

$$\begin{bmatrix} C_{l,\mathrm{cg}} \\ C_{m,\mathrm{cg}} \\ C_{n,\mathrm{cg}} \end{bmatrix} = \begin{bmatrix} C_{l,\mathrm{cp}} \\ C_{m,\mathrm{cp}} + {}^{\Delta x_{\mathrm{cp}}}/_{c} C_L \\ C_{n,\mathrm{cp}} + {}^{\Delta x_{\mathrm{cp}}}/_{b} C_Y \end{bmatrix} \tag{3-19}$$

This holds under the assumptions that $C_D \sin\alpha \ll C_L \cos\alpha$ and $\cos\alpha \approx 1$. Note that even when the assumptions are violated by more than, for instance 10%, this still does not have a large effect on the dynamics, as ${}^{\Delta x_{\mathrm{cp}}}/_{c} = 0.012$ is small. It can be compared with the position of the neutral point:

$$\frac{r_{\mathrm{cp},x} - r_{\mathrm{np},x}}{c} = -\frac{C_{m_\alpha,\mathrm{cp}}}{C_{L_\alpha}} = 0.068 \tag{3-20}$$

which is larger than Δx_{cp} by about a factor 5.

The aerodynamic coefficients are split up in three parts: a base coefficient C_{base}, a control part C_{ctrl} and a dynamic part dependent on the (non-dimensional) angular rates, C_{rate}. All three parts in turn depend on the aerodynamic angles α and β. So force and moment coefficients are split up as:

$$C_i = C_{i,\mathrm{base}}(\alpha,\beta) + \Delta C_{i,\mathrm{ctrl}}(\alpha,\beta,\delta_e,\delta_r,\delta_a) + \Delta C_{i,\mathrm{rate}}(\alpha,\beta,\hat{p},\hat{q},\hat{r}) \tag{3-21}$$

The non-dimensional angular rates are defined as:

$$\hat{p} = \frac{pb}{2V_a}, \quad \hat{q} = \frac{q\bar{c}}{2V_a}, \quad \hat{r} = \frac{rb}{2V_a} \tag{3-22}$$

where V_a is the total aerodynamic velocity. For each force/moment coefficient and each part, a look-up table exist. The specific dependencies are listed in Table 3-3.

3-4 Polynomial estimation of aerodynamic coefficients

The advantage of look-up tables is that all nonlinearities that are measured in windtunnel tests can be captured well and high-fidelity simulations can be performed. A disadvantage is that the tables act like a black-box model: no real insight can be gained about the behavior of the model and the strengths of the nonlinearities. Furthermore, it is less straightforward to design model-based control laws with table-lookup models. For instance, if the aerodynamic pitching moment was described as an analytical equation like $C_m = C_{m_0} + C_{m_\alpha}\alpha + C_{m_{\delta_e}}\delta_e$, then it would be easier to define a control law for the elevator that compensates a pitching moment for a disturbance of α. Besides this, it was desirable to have an analytical aerodynamic model which could be simplified easily to verify different control laws.

The look-up tables are therefore estimated by polynomials using a least-squares approach. The goal was to create a model which was easy to work with and which approximates the look-up table model well up to moderate angles of attack and angles of sideslip ($\alpha = 10\,\text{deg}, \beta = 20\,\text{deg}$).

Base coefficients are modelled by a polynomial of the form:

$$C_{i,\text{base}} = \sum_{k=0}^{2}\sum_{j=0}^{2} c_{jk}\alpha^j\beta^k \tag{3-23}$$

The elements in Table 3-3 that represent the different parts of the control and angular rate coefficients are modeled by a polynomial of the form:

$$\Delta C_i = \sum_{k=0}^{2}\sum_{j=0}^{2} c_{jk1}\alpha^j\beta^k\delta + c_{jk2}\alpha^j\beta^k\delta^2 \tag{3-24}$$

in which δ represents the control deflection or rotational rate. On page 71, the estimated polynomial model as well as the table look-up values of some relevant coefficients are plotted. For a more detailed overview, the reader is referred to Appendix A.

3-4-1 Model simplifications

In order to see the effect of nonlinearities in the model and to have a simple basis to test the control laws, the polynomial model has been simplified by only keeping the most important coefficients of the polynomial model. The simplified model is affine-in-control, so the squared terms like $\alpha^j\beta^k\delta_a^2$ are set to zero. Furthermore, longitudinal coefficients are made independent of β and all other insignificant higher order terms of α and β are left out. The final simplified model is given as:

$$\begin{aligned}
C_D &= C_{D_0} + C_{D_1}\alpha + C_{D_2}\alpha^2\\
C_Y &= C_{Y_1}\beta + C_{Y_2}\delta_r + C_{Y_3}\hat{r}\\
C_L &= C_{L_0} + C_{L_1}\alpha + C_{L_2}\delta_e\\
C_l &= C_{l_1}\beta + C_{l_2}\delta_a + C_{l_3}\hat{p}\\
C_m &= C_{m_0} + C_{m_1}\alpha + C_{m_2}\delta_e + C_{m_3}\hat{q}\\
C_n &= C_{n_1}\beta + C_{n_2}\delta_r + C_{n_3}\hat{r}
\end{aligned} \tag{3-25}$$

Open-loop step-responses of the different models are plotted in Figure 3-8. The most important difference with the table-lookup model is in the behavior of the side slip angle β. Appearantly the side force is not modeled well.

3-5 Actuators

The UltraStick120 in use at the DLR are equipped with JR DS8411 servos which control all control surfaces individually. Incremental control laws rely on a good actuator feedback.

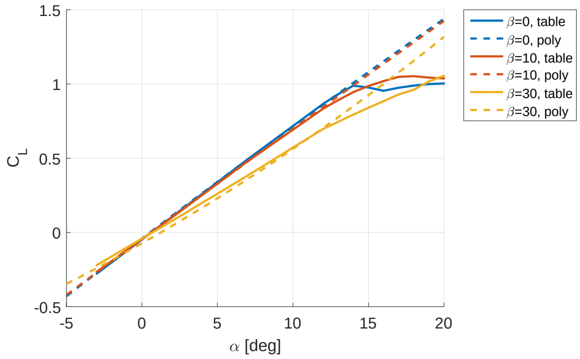

Figure 3-2: C_L vs. α

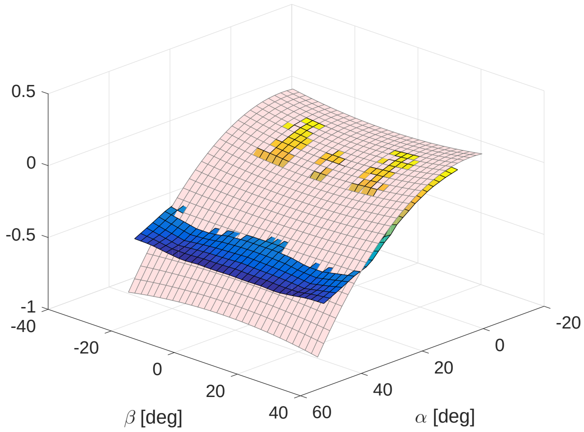

Figure 3-3: C_m vs. α and β

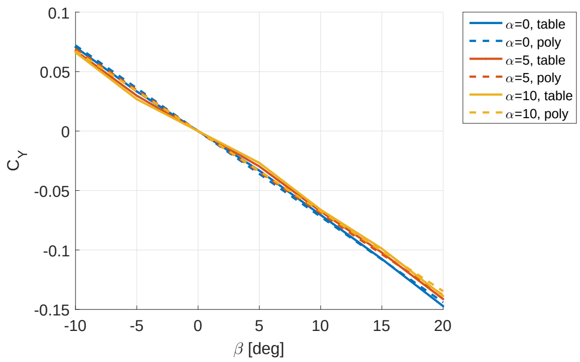

Figure 3-4: C_Y vs. β

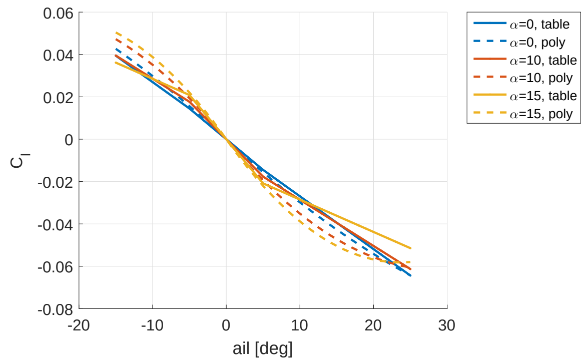

Figure 3-5: C_l vs. δ_a and α

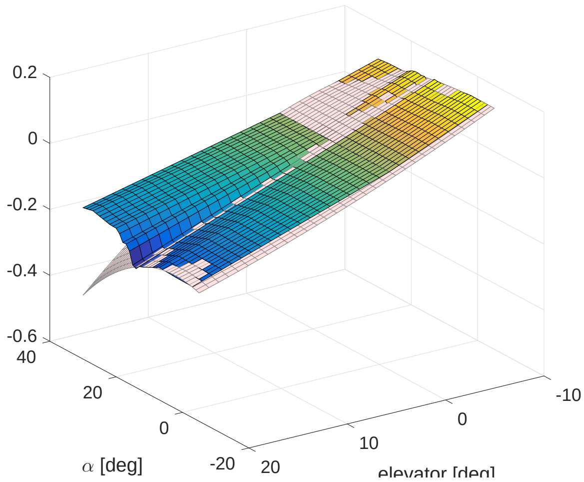

Figure 3-6: C_m vs. δ_e and α

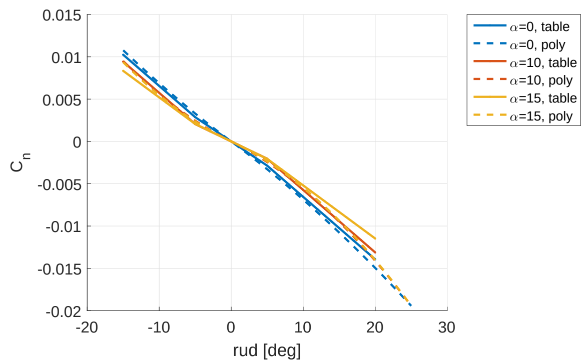

Figure 3-7: C_n vs. δ_r and α

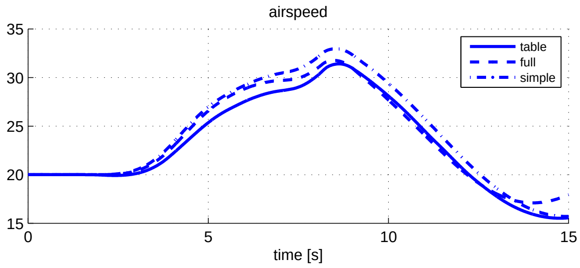

(a) Velocity

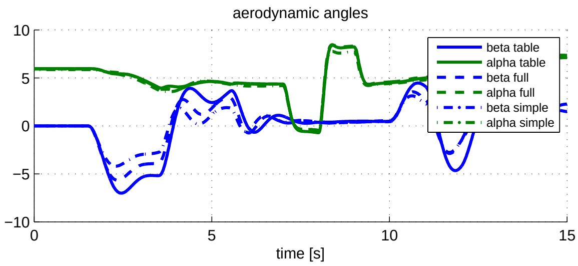

(c) Aerodynamic angles

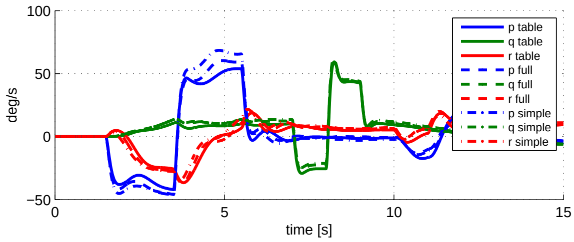

(b) Angular rates

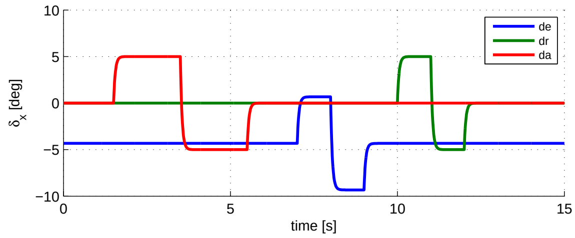

(d) Control surface deflections

Figure 3-8: Open-loop step-responses for different aerodynamic models: look-up tables (solid), full polynomial model (dash) and simplified polynomial model (dash dot).

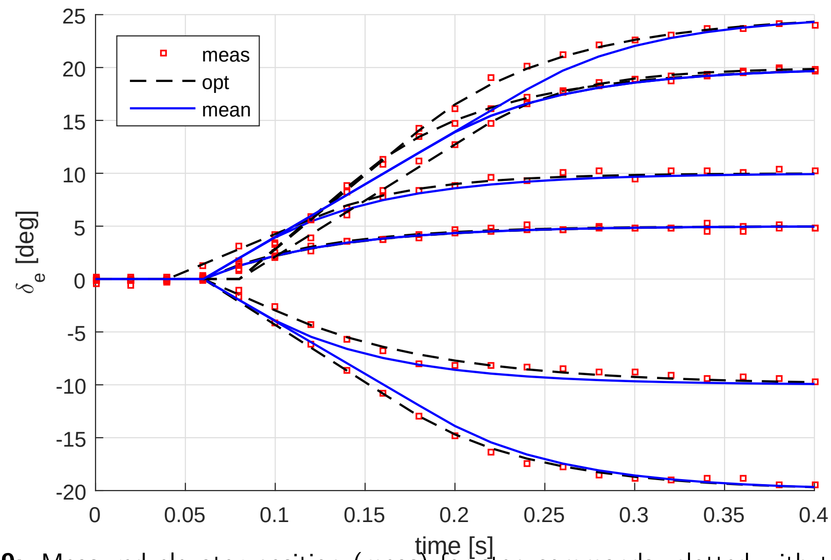

Figure 3-9: Measured elevator position (meas) for step commands, plotted with the identical step resonse of the individual optimal parameters (opt) for the response and the step response using the final identified (mean) parameter estimates

Table 3-3: Overview of dependency of the different force and moment coefficients on the aircraft states in the aerodynamic look-up tables.

coefficient	C_D	C_Y	C_L	C_l	C_m	C_n
base C_{base}	α, β	α, β	α, β	α, β	α, β	α, β
elevator C_{base,δ_e}	α, δ_e		α, δ_e		α, δ_e	
rudder C_{base,δ_r}		α, β, δ_r				α, β, δ_r
aileron C_{base,δ_a}				α, β, δ_a		
roll rate $C_{\text{rate},\hat{p}}$		$\alpha, \beta, \hat{p}$				$\alpha, \beta, \hat{p}$
pitch rate $C_{\text{rate},\hat{q}}$					fixed C_{m_q}	
yaw rate $C_{\text{rate},\hat{r}}$		$\alpha, \beta, \hat{r}$				$\alpha, \beta, \hat{r}$

Table 3-4: Identified (mean) actuator dynamics parameters, with standard deviation σ

ω_{act} [Hz]	R [deg/s]	λ_{act} [samples at 50 Hz]
2.35 ($\sigma = 0.44$)	99.6 ($\sigma = 30.4$)	2.25 ($\sigma = 0.707$)

Because a reliable actuator position measurement was not available, an online model of the actuators was required. The original available model does not have an accurate estimation for the complete actuator dynamics. Therefore, the dynamics were identified by commanding step inputs of different magnitude. The actuator dynamics are modelled with first order dynamics with bandwith ω_{act}, including rate limits and a time delay λ_{act}:

$$\dot{\delta}(t) = S_R\{-\omega_{act}\delta(t) + \omega_{act}u(t - \lambda_{act})\} \tag{3-26}$$

where S_R, a saturation function, is defined as

$$S_R(x) = \begin{cases} R & \text{if} \quad x > M \\ x & \text{if} \quad |x| \leq M \\ -R & \text{if} \quad x < -M \end{cases} \tag{3-27}$$

Actuator time responses of the elevator deflections are shown in Figure 3-9. For each step response, parameters R, λ_{act} and ω_{act} that minimize the *root-mean-square* (RMS) error between the measured and simulated response are found. The final estimates are the mean of those values, listed in Table 3-4.

Chapter 4

Incremental NDI for Angular Rate and Attitude Flight Control

This chapter elaborates on two control problems, for which both INDI control laws are used. First, the angular rates are controlled with a single dynamic-inversion loop. Secondly, two attitude control laws are presented, a multi-loop INDI control law (with an inner loop identical to the former angular rate control law), and an integrated, single loop INDI controller, which in fact uses feedback linearization for the second order system.

section 4-1 until section 4-6 discuss the angular rate control laws, with extensive analysis using simulation results of multiple controller configurations. Because these sections cover a fairly large part of the analysis of this thesis, it is concluded with an interim summary in section 4-6. Thereafter, section 4-7 presents the derivation and simulation results of the attitude control laws. The chapter is concluded in section 4-8

Introduction to INDI for angular rate control

The goal of an angular rate controller is to track the angular rates p, q, r using the aerodynamic control devices. In fixed-wing aircraft, these three rates are normally controlled using the elevator, rudder and aileron control surfaces. The longitudinal dynamics are often well decoupled from the lateral dynmics, so the pitch rate q can be controlled by mainly using the elevator δ_e. Due to dutch roll dynamics, the roll and yaw rate p and r are coupled and must be decoupled by the control law.

First, both a NDI and a INDI control law are formulated. This makes the derivation of the incremental control law more insightfull. After the formulation, simulation results on the FASER model are presented.

4-1 Nonlinear dynamic inversion angular rate controller

For this control problem, the state and input is defined as:

$$\mathbf{x}_3 = \boldsymbol{\omega} = \begin{bmatrix} p \\ q \\ r \end{bmatrix}, \quad \mathbf{x}_{3,ref} = \begin{bmatrix} p \\ q \\ r \end{bmatrix}_{ref}, \quad \mathbf{u} = \begin{bmatrix} \delta_e \\ \delta_r \\ \delta_a \end{bmatrix} \tag{4-1}$$

and use the subscript 3 to keep consistent with the notation for the angular rates in subsequent outer loop control structures.

The dynamics, derived in section 3-2, can be described as:

$$\dot{\mathbf{x}}_3 = \mathbf{f}_3(\mathbf{x}) + \mathbf{g}_3(\mathbf{x}, \mathbf{u}) \tag{4-2}$$

with:

$$\mathbf{f}_3 = I^{-1}(\mathbf{M}_0(\mathbf{x}) - \mathbf{x}_3 \times I\mathbf{x}_3) \tag{4-3a}$$

$$\mathbf{g}_3 = I^{-1}\mathbf{M}_\delta(\mathbf{x}, \mathbf{u}) \tag{4-3b}$$

where $\mathbf{x}$ describes the entire aircraft state, $\mathbf{M}_0$ is the control independent part of the moment, and $\mathbf{M}_\delta$ is the control dependent part of the moment. The aerodynamic moments can be written out in terms of their coefficients and be split up in a control dependent and a control independent part, using Equation 3-21:

$$\mathbf{M}_0 = \bar{q}S \begin{bmatrix} bC_{l,\text{base+rate}} \\ cC_{m,\text{base+rate}} \\ bC_{n,\text{base+rate}} \end{bmatrix} \tag{4-4a}$$

$$\mathbf{M}_\delta = \bar{q}S \begin{bmatrix} b\Delta C_{l,\text{ctrl}} \\ c\Delta C_{m,\text{ctrl}} \\ b\Delta C_{n,\text{ctrl}} \end{bmatrix} \tag{4-4b}$$

A NDI control law requires that the system is affine in control, so we must assume simplified aerodynamics for which $\mathbf{M}_\delta$ can be written as:

$$\mathbf{M}_\delta = \bar{q}S \begin{bmatrix} b & & \\ & c & \\ & & b \end{bmatrix} C_{\mathbf{M}_\delta} \begin{bmatrix} \delta_e \\ \delta_r \\ \delta_a \end{bmatrix} \tag{4-5}$$

with $C_{\mathbf{M}_\delta}$ a constant matrix of control effectiveness coefficients. For the simplified model in Equation 3-25 this clearly holds. Then Equation 4-2 can be written as:

$$\dot{\mathbf{x}}_3 = \mathbf{f}_3(\mathbf{x}) + G_3(\mathbf{x})\mathbf{u} \tag{4-6}$$

with:

$$G_3(\mathbf{x}) = I^{-1}\bar{q}S \begin{bmatrix} b & & \\ & c & \\ & & b \end{bmatrix} C_{\mathbf{M}_\delta} \tag{4-7}$$

The control input $\mathbf{u}$ selected as:

$$\mathbf{u} = G_3^{-1}(\mathbf{x}) \left(\boldsymbol{\nu}_3 - \mathbf{f}_3(\mathbf{x}) \right) \tag{4-8}$$

yields a system dynamics of which the output has a linear relationship with the virtual control $\boldsymbol{\nu}_3$:

$$\dot{\mathbf{x}}_3 = \boldsymbol{\nu}_3 \tag{4-9}$$

By selecting this virtual control as:

$$\boldsymbol{\nu}_3 = C_3\mathbf{e} + \dot{\mathbf{x}}_{3,ref} \tag{4-10}$$

the error dynamics yield:

$$\dot{\mathbf{e}}_3 + C_3\mathbf{e}_3 = 0 \tag{4-11}$$

so that the linear control gain C_3 can be designed to yield error dynamics as desired. Hence, the final NDI control law is:

$$\mathbf{u} = G_3^{-1}(\mathbf{x})\left(C_3\mathbf{e}_3 + \dot{\mathbf{x}}_{3,ref} - \mathbf{f}_3(\mathbf{x})\right) \tag{4-12}$$

The general control scheme to be implemented on the Ultrastick UAV is shown in Figure 4-1. In this block, a prefilter is present to provide the controller with the time derivative of the reference signal $\dot{x}_3$. It is a linear, second order filter for all 3 channels of $x_{3,des}$ with natural frequency ω_n and damping ζ:

$$\begin{bmatrix}\dot{q}_1\\ \dot{q}_2\end{bmatrix} = \begin{bmatrix}0 & 1\\ -\omega_n^2 & -2\zeta\omega_n\end{bmatrix}\begin{bmatrix}q_1\\ q_2\end{bmatrix} + \begin{bmatrix}0\\ \omega_n^2\end{bmatrix}u \tag{4-13}$$

Where $q_1 = x_{3,ref,i}$, $q_2 = \dot{x}_{3,ref,i}$ and $u = x_{3,des,i}$, for $i = 1, 2, 3$.

4-2 Incremental nonlinear dynamic inversion angular rate controller

We apply incremental control to the systemd described by (4-2). To derive the equations in incremental form, we perform the first taylor series expansion from a point in the recent past, denoted by $\mathbf{x}_0, \mathbf{u}_0, t_0$:

$$\dot{\mathbf{x}}_3 \approx \dot{\mathbf{x}}_{3,0} + \underbrace{\left(\frac{\partial \mathbf{f}_3(\mathbf{x})}{\partial \mathbf{x}} + \frac{\partial \mathbf{g}_3(\mathbf{x},\mathbf{u})}{\partial \mathbf{x}}\right)\bigg|_{\mathbf{x}_0,\mathbf{u}_0}}_{A_{3,0}}(\mathbf{x}-\mathbf{x}_0) + \underbrace{\frac{\partial \mathbf{g}_3(\mathbf{x},\mathbf{u})}{\partial \mathbf{u}}\bigg|_{\mathbf{x}_0,\mathbf{u}_0}}_{B_{3,0}}(\mathbf{u}-\mathbf{u}_0) \tag{4-14}$$

Which is written in a shorter form as:

$$\dot{\mathbf{x}}_3 \approx \dot{\mathbf{x}}_{3,0} + A_{3,0}\Delta\mathbf{x} + B_{3,0}\Delta\mathbf{u} \tag{4-15}$$

The advantage of writing the dynamics in this incremental form becomes apparent when assuming that the incremental term caused by the control input, $B_{3,0}\Delta\mathbf{u}$ is much larger than the increment caused by the system dynamics, $A_{3,0}\Delta\mathbf{x}$. If this holds, then the incremental control law can be derived as:

$$\Delta\mathbf{u} = B_{3,0}^{-1}\left(\boldsymbol{\nu}_3 - \dot{\mathbf{x}}_{3,0}\right) \tag{4-16}$$

which yields a linear relationship between the output and the virtual control $\boldsymbol{\nu}_3$:

$$\dot{\mathbf{x}}_3 = \boldsymbol{\nu}_3 \tag{4-17}$$

By selecting the virtual control as

$$\boldsymbol{\nu}_3 = C_3\mathbf{e} + \dot{\mathbf{x}}_{3,ref} \tag{4-18}$$

the error dynamics result as:

$$\dot{\mathbf{e}}_3 + C_3\mathbf{e}_3 = 0 \tag{4-19}$$

and we can select the gain C_3 to yield the desired error dynamics. The total control is given by:

$$\begin{aligned} \mathbf{u} &= \mathbf{u}_0 + \Delta\mathbf{u} \\ &= \mathbf{u}_0 + B_{3,0}^{-1}\left(C_3\mathbf{e} + \dot{\mathbf{x}}_{3,ref} - \dot{\mathbf{x}}_{3,0}\right) \end{aligned} \tag{4-20}$$

Here, u_0 refers to the control deflection in the recent past. Any calculated increment $\Delta\mathbf{u}$ should hence be added to this deflection. When the system includes actuator dynamics, we are therefore feeding back the actuator position.

With this control law, the only required knowledge about the model is the (current) control effectiveness matrix $B_{3,0}$. As long as the model is locally linear, so that the first order taylor series expansion in Equation 4-14 holds, the system can be steered accurately towards the reference signal $\mathbf{x}_{3,ref}$. This advantage goes at the cost of dependence on angular acceleration measurements $\dot{\mathbf{x}}_{3,0}$.

The general control scheme of the INDI angular rate controller is displayed in Figure 4-2. Again, the reference signal is pre-filtered. Because this layout includes sensors to measure the aircraft state, the angular accelerations must be obtained from the angular rates using a filter which estimates $\dot{\mathbf{x}}_{3,0}$. This could be a second order washout filter with the following transfer function H:

$$H(s) = \frac{\omega_n^2 s}{s^2 + 2\zeta\omega_n s + \omega_n^2} \tag{4-21}$$

with a damping $\zeta = 1$ and a bandwith ω_n which is high enough to keep the delay small. The incremental controller strongly depends on a good synchronization of the inputs and measured state derivative, because the calculated control increment $\Delta\mathbf{u}$ is based on a taylor series expansion at a given point in time t_0, see (4-14). Therefore $\Delta\mathbf{u}$ must be added to the input that corresponds to $\dot{\mathbf{x}}_{3,0}$ in the controller. For this reason, the control increment must be added to the delayed control deflection δ_0 instead of the delayed commanded deflection u_0. Furthermore, for the same reason the measured control deflection must be filtered with a filter that has the same delay as the washing filter that is used to obtain the angular accelerations.

4-3 Simulation results

4-3-1 NDI controller

With perfect knowledge of the model and states, a continuous-time NDI controller should yield a response that exactly corresponds to the commands given, as long as the control is not saturated. Any uncertainties in the system dynamics should result in imperfections in the

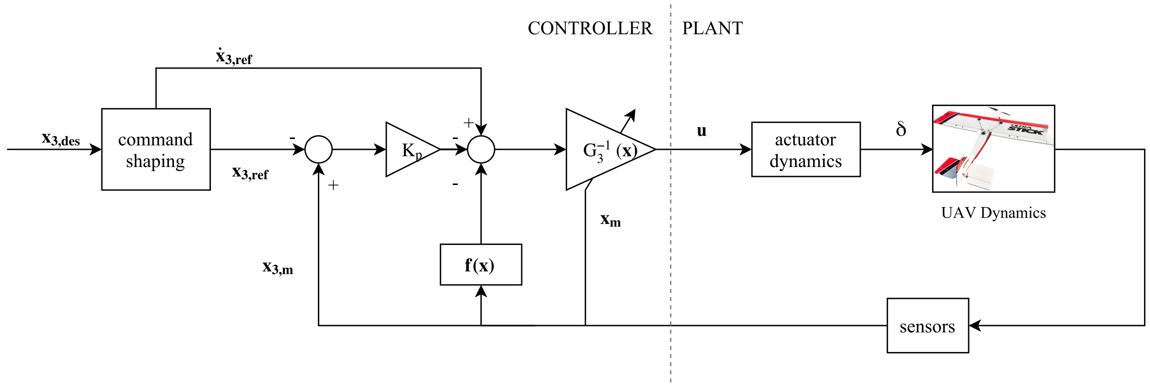

Figure 4-1: General NDI angular rate control scheme

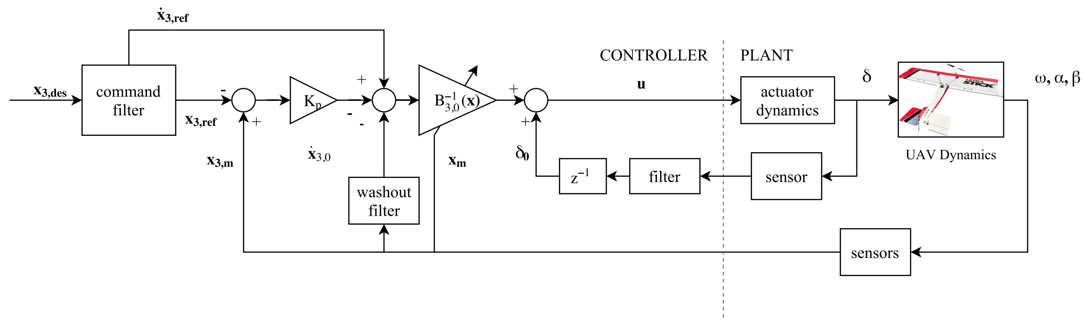

Figure 4-2: General INDI angular rate control scheme

tracking response. To show the effect of model uncertainties on the performance of the NDI controller, multiple simulations results are presented.

The simulations in this section are done with continuous-time controllers that are as close to the derived control laws as possible. The following propierties apply to the simulation, model and controller set-up:

- A continuous-time controller has been simulated, i.e., continuous time control signal $u(t)$ has been calculated using a ode45 (Dormand-Prince) solver for the entire simulation, with a sample time of 0.01 s unless stated otherwise.
- The aerodynamic model of the UAV has the simplified, affine-in-control aerodynamics, so that the system dynamics can be fully known by the controller, and feedback linearization is possible. Furthermore, the motor dynamics are not modeled, so that there are no gyroscopic effects due to the motor and propeller inertia.
- No actuator dynamics are incorporated
- Controller gains are set to $K_p = 5$ in nominal cases to have first-order error dynamics with a time constant of $1/K_p = 0.2\,\text{s}$.
- The simulation is initialized with a non-zero angular rate, to show the controller's response to a tracking error.

Table 4-1: Parameters used for the simulations in Figure 4-3

Parameter	Value
Solver	ode3 Bogacki-Shampine
Sample time	0.01 s
Trim velocity	20 m/s
Aerodynamics	Simplified polynomial model
Motor and propeller inertia	no
Actuator dynamics	no
Sensor noise	no
Sensor dynamics	no
Control law	NDI angular rate control, Equation 4-12
Command shaping	$\omega_n = 10$ rad/s, rate limit 30 deg/s

Table 4-2: Changed aerodynamic parameters for case A (small uncertainties) and case B (to mimic an asymmetrical damage in the horizontal stabilizer).

parameter	old value	case A	case B
C_{m_α}	-0.03025	-0.02525	-0.02025
C_{l_α}	0		0.05
$C_{m_{\delta_e}}$	-0.69		-0.49
C_{n_β}	0.0714	0.0614	

- The command signal consist of combined doublets on all three axes to excite the entire system. A command shaping filter has been applied to create a realistic reference signal.
- No sensors are modeled. Hence, the controller has a feedback of the true aircraft state at each point in time.

The most important parameters for the simulation and controller are summarized in Table 4-1

The response is plotted in Figure 4-3. It can be seen that the reference is tracked well by the NDI controller. At about $T = 10$ s, the rudder control is saturated, and the yaw and roll rate cannot be tracked well anymore. To show the controllers response to a tracking error, a second simulation has been plotted in the same figure. In this simulation, the control law does not include the time derivative of the reference signal, and the commanded rates are not filtered.

Effect of parametric uncertainties

The NDI control law is fully dependent on the model parameters. Therefore, simulations were performed with some aerodynamic uncertainties. Two cases have been considered. In case A, uncertainties in C_{m_α} and C_{n_β} are considered to show the effect of a bad parameter estimation of an aircraft in a nominal flight. In case B, some effects of an asymmetrical damage to the horizontal stabilizer have been considered, whereas the controller still uses the nominal parameters. The model parameters for this case are stated in Table 4-2

The uncertainties in the parameters mimic an asymmetrical damage in the horizontal stabilizer.

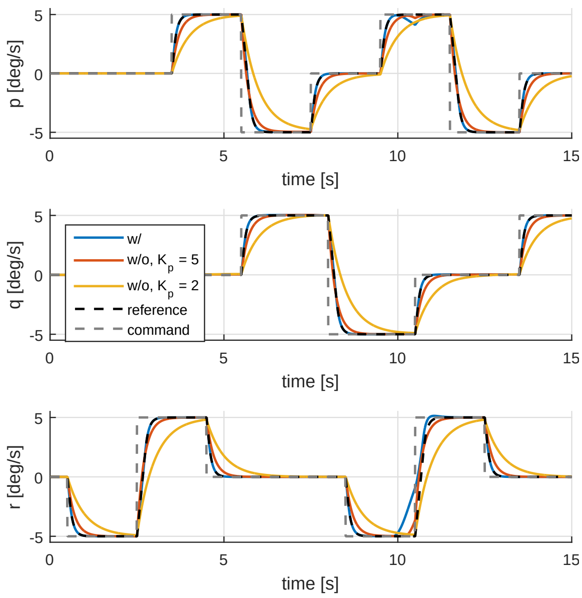

(a) Angular rates

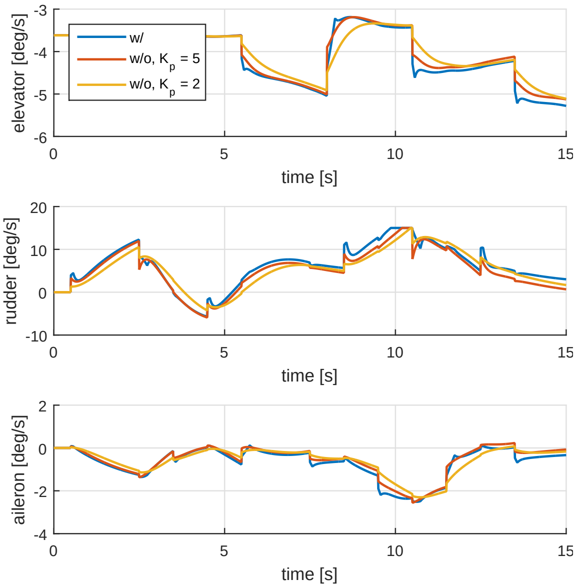

(b) Control surface deflections

Figure 4-3: NDI controller response with and without feed-forward of $\dot{\mathbf{x}}_3$, with different controller gain values K_p.

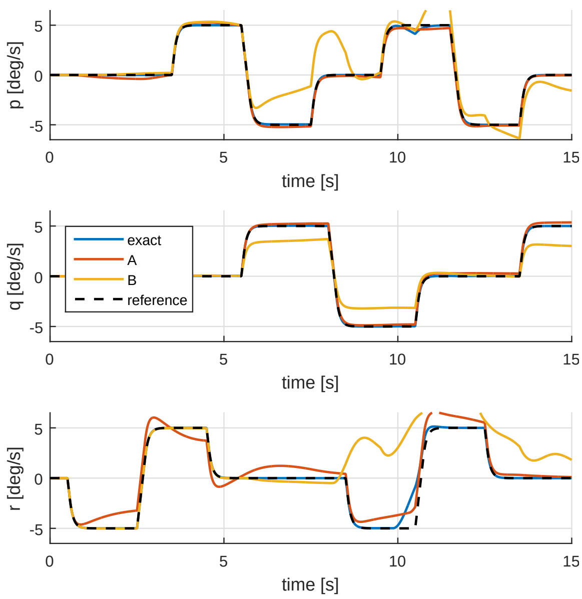

(a) Angular rates

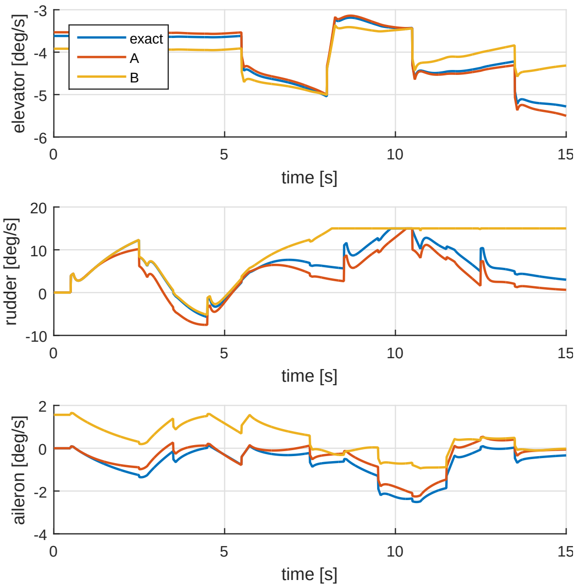

(b) Control surface deflections

Figure 4-4: NDI controller response with parametric uncertainties: small uncertainties (case A) and asymmetrical damage to the horizontal stabilizer (case B).

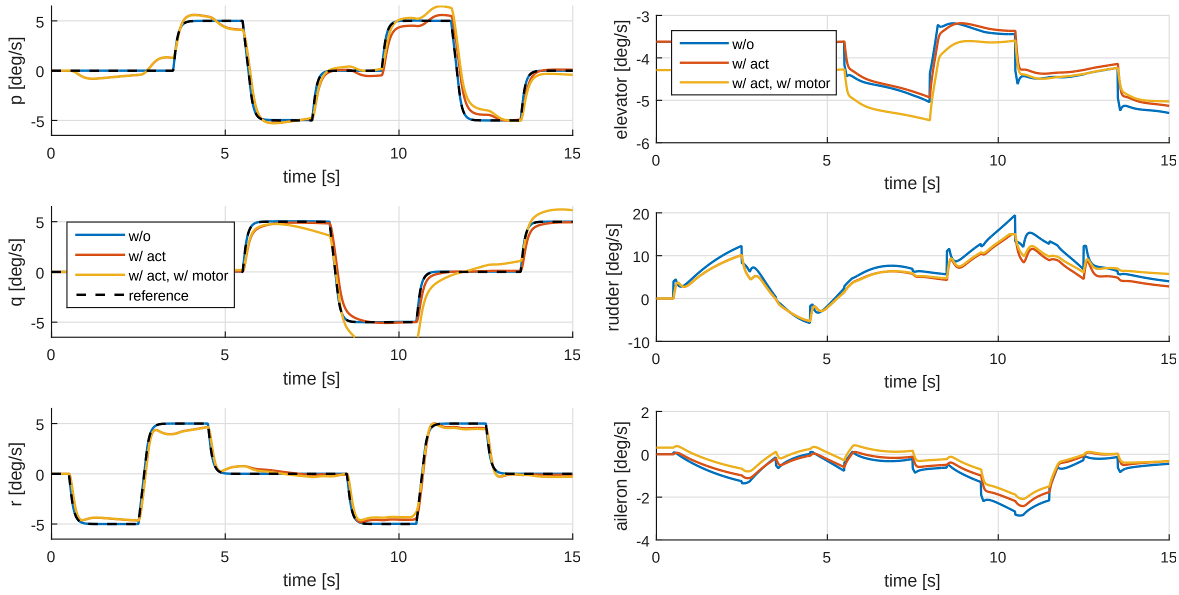

(a) Angular rates

(b) Control surface deflections

Figure 4-5: NDI controller response with unmodelled dynamics: only actuator dynamics (red) and actuator and motor inertia dynamics (yellow).

Effect of unmodelled actuator and motor dynamics

Figure 4-5 shows simulation results where actuator dynamics and motor inertia is included. The actuator effectively filters the control command and hence puts a delay on al control signals. Therefore, the control is not unstable or showing diverging effects, but has small steady errors. Motor inertia causes coupling moments in axes different than the controlled axis. The tracking errors resulting from an imperfect control signal need to be canceled by the linear controller.

4-3-2 INDI controller

The simulation results of the NDI controller presented above show that the NDI control laws are highly dependent on the model parameters. The INDI controller however, does not depend on any system dynamics parameters. It should therefore be robust or invariant to any changes to the system dynamics. In this section, simulation results for the INDI controller will be presented to show this robustness.

First, a simulation is performed to show the superiority of the INDI control law over NDI. The very same parameter uncertainty cases are considered, see Table 4-2. In Figure 4-6, simulation results are presented of four different cases:

- "exact": This is a simulation that is as close to the derived incremental control law in Equation 4-20. No actuator and motor dynamics are included, and true angular accelerations are fed back to the controller. Furthermore, the aerodynamics of the

Table 4-3: Parameters used for the simulations with INDI controllers in Figure 4-6.

Parameter	"exact"	"realistic"
Solver	ode3 Bogacki-Shampine	
Sample time	0.01 s	
Trim velocity	20 m/s	
Aerodynamics	Simplified polynomial model	lookup tables
Motor and propeller inertia	no	yes
Actuator dynamics	no	yes, bandwidth 2.5 Hz
Sensor noise	no	
Sensor dynamics	no	
Control law	NDI angular rate control, Equation 4-12	
Command shaping	$\omega_n = 10$ rad/s, rate limit 30 deg/s	
Angular accelerations	true accelerations	first order washout filter, $\omega_n = 30$ rad/s

aircraft are modeled by the simplified polynomial estimation, so that exact, constant control effectiveness coefficients can be used in the control law.

- "realistic": In this simulation, the aircraft's full model is used: actuator dynamics, motor dynamics and the full table-lookup aerodynamics are used to model the plant. Comparing this already with this NDI controller shows the advantage of INDI
- "uncertainty case A and B": these simulations are identical to the "realistic" simulation, but in this simulation also some parameter uncertainties are added. These are the same as those used for the NDI controller results and can be found in Table 4-2.

The most important parameters for these simulations are summarized in Table 4-3. The results in Figure 4-6 show that the INDI controller can easily cope with parameter uncertainties and is robust to different system dynamics. There are however some small steady tracking errors visible, especially in the roll rate. This error is correlated with the delay used for the incremental control. In the next paragraph we will further analyze the influence of this delay.

Effect of increment delay

The incremental control method relies on calculating a control increment with respect to a point in the recent past (see Equation 4-14). The time difference to this point is referred to as the increment delay. The increment delay must be designed such that the delayed control deflection $\mathbf{u}_0$ corresponds to the delay of the feedback signal of the angular accelerations. Therefore, if the angular accelerations are estimated by a washout filter on the angular rate sensors, a similar filter must be placed in the incremental control loop to compensate for this effect. Likewise, an additional delay may be placed if there is an extra transport delay in the control loop. The general incremental control diagram is shown in Figure 4-10.

Figs. 4-7 and 4-8 show the tracking response by varying the actuator bandwidth and washout filter frequency, hence by effectively varying the increment delay. It can be seen that the steady errors that were already apparent in Figure 4-6, now show to be clearly related to the actuator bandwidth and the washout filter frequency.

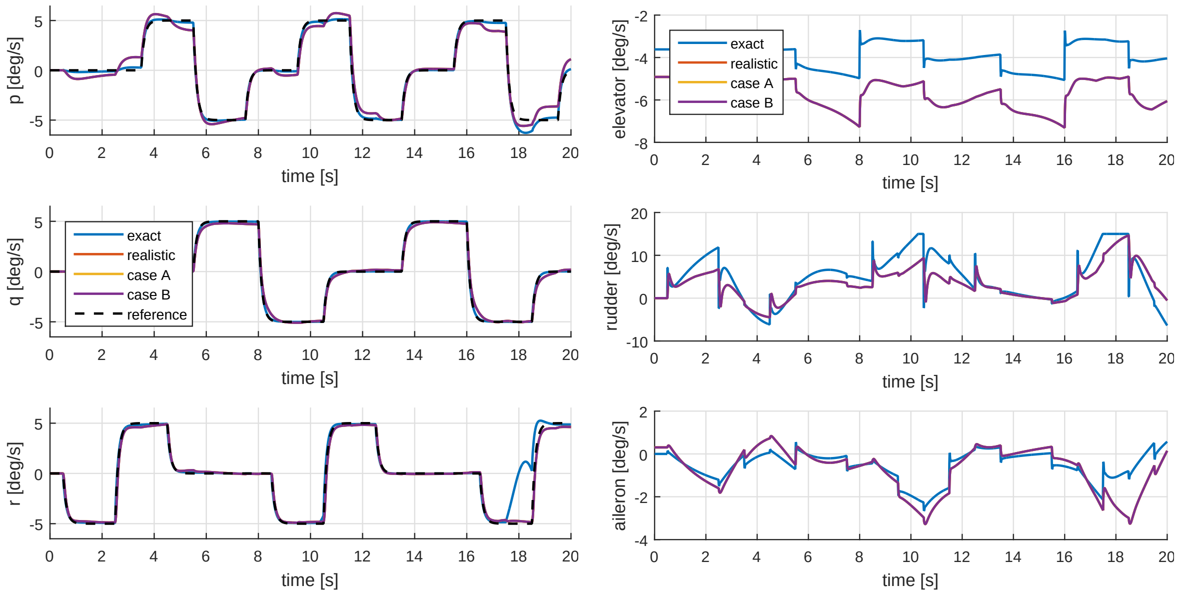

(a) Angular rates

(b) Control surface deflections

Figure 4-6: INDI controller response with unmodelled dynamics, plotted without uncertainties (blue), with realistic aircraft dynamics (red), small parameter uncertainties (yellow) and asymmetric horizontal stabilizer damage (purple). In fact, the "realistic" cases and both parameter uncertainty cases show nearly the same tracking response, hence the red and yellow plots are not visible.

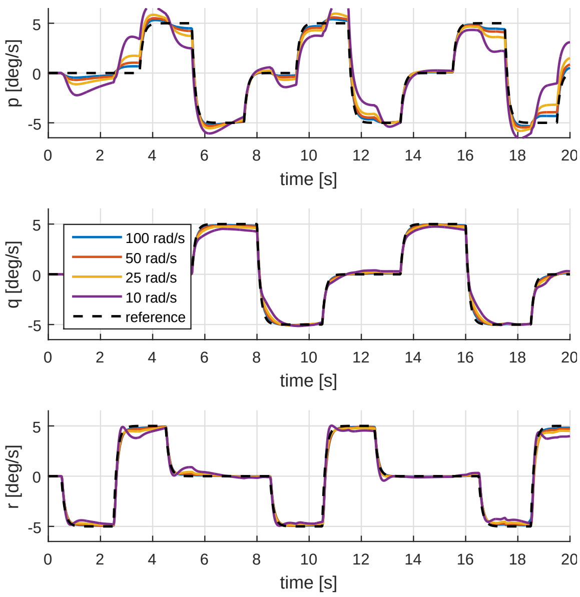

Figure 4-7: INDI angular rate responses for different washout filter bandwidths in rad/s.

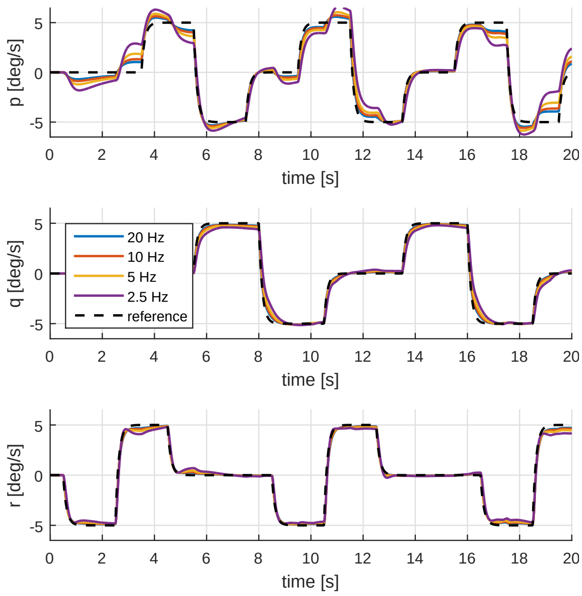

Figure 4-8: INDI angular rate responses for different actuator bandwidths in Hz.

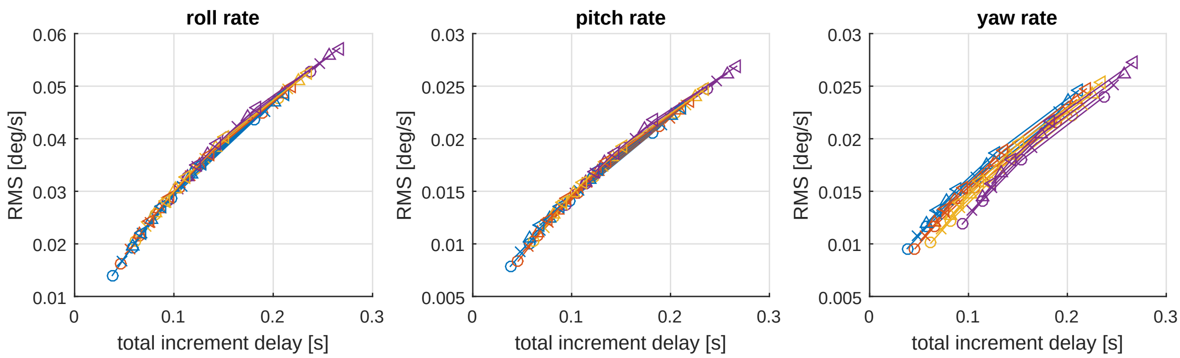

Figure 4-9: Root-mean-square of the tracking error, for simulations with varying actuator bandwidth, washout filter frequency and additional delay. Individual lines connecting the markers indicate the effect of the washout filter frequency (varied between 50-6.125 rad/s). Different colors indicate simulations with various actuator bandwidths (20-2.5 Hz). The markers ○, ×, △, ◁ indicate a transport delay of 1, 2, 3, 4 samples respectively.

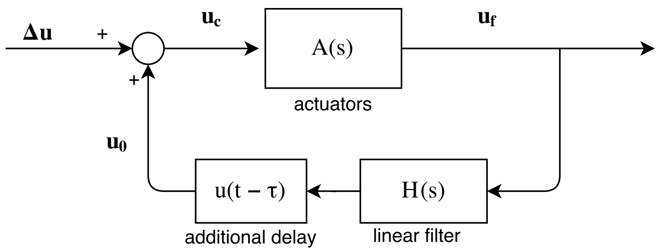

Figure 4-10: Control diagram of general incremental control, including actuator dynamics $A(s)$, a linear filter $H(s)$ and an additional delay τ .

In Figure 4-9, the RMS of the tracking errors are plotted against the estimated increment delay. An estimate of the increment delay is calculated by taking the sum of the actuator and washout filter time constants (rise time) and the additional delay. When the actuator and washout filter are first-order linear filters, the 63% rise time is simply $\tau = {}^{1}/_{\omega_n} = {}^{1}/_{2\pi f}$, with ω_n and f the filter frequency or bandwidth in respectively rad/s and Hz.

The results in Figure 4-9 clearly show that the tracking error is directly related to the increment delay. The only discrepancy is the effect of the transport delay to the yaw rate tracking error, although also in the yaw axis, the trend is that an increment delay directly causes an increase in the tracking error. It will be discussed in section 4-5 what parts of the controller and system dynamics cause these tracking errors.

4-4 Similar proportional-integral controller

In subsection 2-4-3 it was discussed and derived how, under some strict assumptions, incremental control laws can be brought down to a similar PI-controller by treating the incremental part as an integrator. In this section it will be shown that the the INDI control laws derived to track the angular rates indeed yield a similar response.

Incremental control without actuator dynamics

Referring to Equation 2-79 in Equation 2-74, the incremental control law in Equation 4-20 without actuator dynamics can be compared with the following PI control law:

$$\mathbf{u}(t) = K_p\mathbf{e}_3(t) + K_i\int_0^t \mathbf{e}_3(t)dt \tag{4-22}$$

with

- $K_p = \frac{B_{3,0}^{-1}}{T_s}$
- $K_i = C_3\frac{B_{3,0}^{-1}}{T_s}$

Figure 4-12a shows a comparison of this PI control law with the INDI control law, for different sample times. The INDI controller response has been simulated using true angular accelerations, delayed by one sample to prevent algebraic loops. Also, in Figure 4-12b, the RMS of the tracking error of both controllers, as well as the RMS of the error between both controllers is plotted for different sample times.

It can be seen that in all three axes, the PI controller performs slightly better. Their difference can result from a slightly different delay, as the PI controller has no feedback of the angular accelerations.

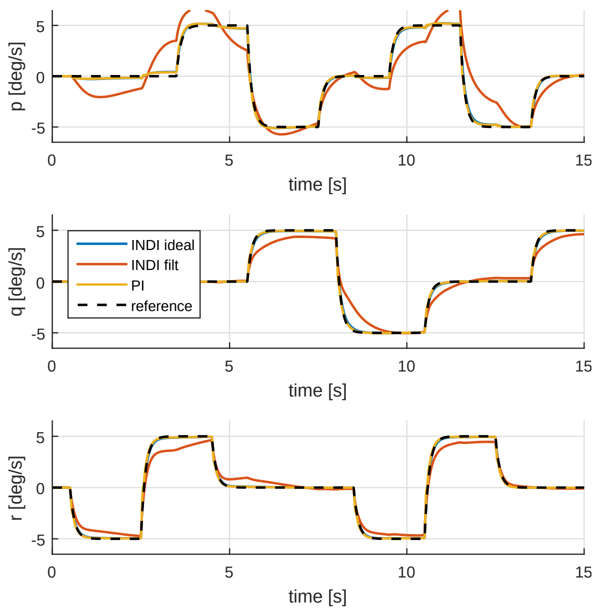

Figure 4-11: INDI and comparable PI control, at a sample time of $T_s = 0.01\,\mathrm{s}$. The ideal INDI controller uses true angular accelerations with a delay of one sample. The filtered INDI controller uses a washout filter to differentiate the angular rates. This filter is also included in the control increment loop.

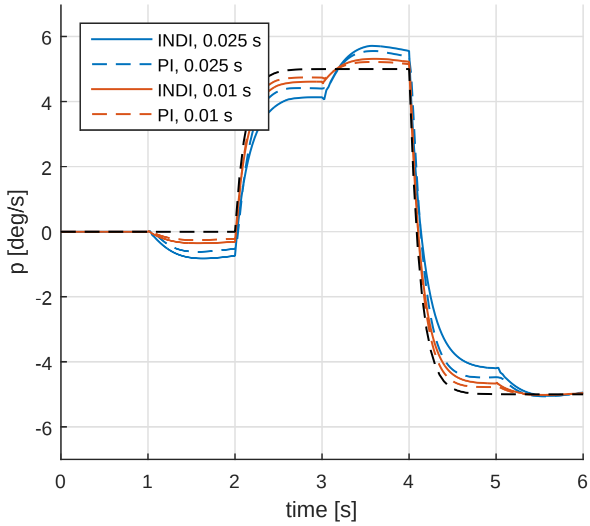

(a) Roll rate tracking response (Simultaneous yaw rate command starting at $t = 1\,\mathrm{s}$ not shown).

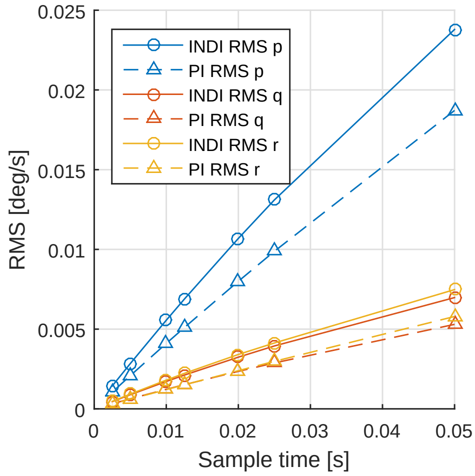

(b) RMS of the tracking error.

ó

Figure 4-12: Comparison INDI controller with a comparable PI-controller, for different sample times. In the RMS error plot, circles (○) and triangles (△) depict individual tracking errors.

Incremental control with actuator dynamics

When the INDI control law includes actuator dynamics, the feedback in the increment loop includes these actuator dynamics to feed back the actual actuator positions $\boldsymbol{\delta}$. In subsection 2-4-3 it was derived that this incremental control law can be compared to the following PI controller:

$$\mathbf{u}(t) = K_p \mathbf{e}_3(t) + K_i \int_0^t \mathbf{e}_3(t) dt \tag{4-23}$$

with

- $K_p = \frac{B_{3,0}^{-1}}{\tau_{act}}$
- $K_i = C_3 \frac{B_{3,0}^{-1}}{\tau_{act}}$

The only difference with the previously derived PI control law is the the exchange of T_s for τ_{act}. Because the sample time T_s is normally much lower than the actuator time constant τ_{act} we expect less aggressive control actions. Simulation results are shown in Figure 4-13. It must be noted that the PI control law does already include the actuator dynamics in the control law, hence a correct comparison is an INDI controller *with* actuator dynamics, and the PI controller *without* actuaor dynamics. Hence, this control law is not directly implementable, but only serves as a comparison with the INDI controller. Additional simulations are performed that include additional actuator dynamics with this PI controller. It can be seen that this results in a less damped system.

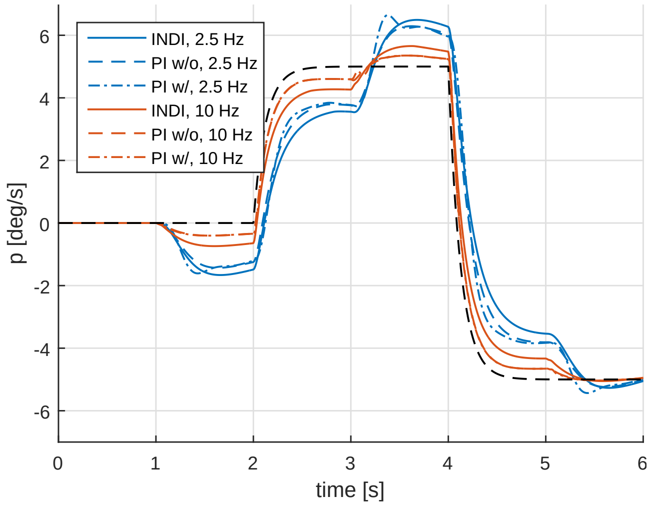

(a) Roll rate tracking response (Simultaneous yaw rate command starting at $t = 1\,\mathrm{s}$ not shown).

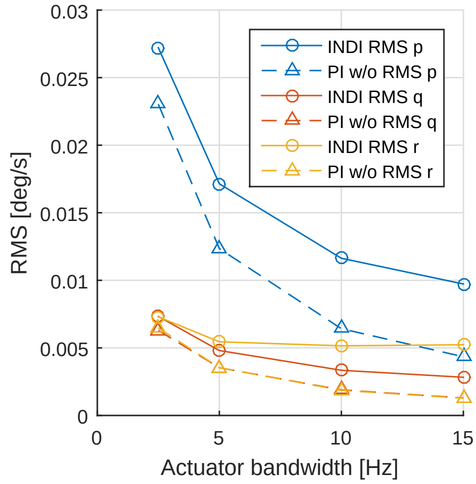

(b) RMS of the tracking error.

Figure 4-13: Comparison INDI controller with actuator dynamics with a comparable PI-controller, for different values for the actuator bandwidth. Simulation results for the comparable PI control law are shown with (w/) and without (w/o) actuator dynamics in the loop. In the RMS error plot, circles (○) and triangles (△) depict individual tracking errors.

Robustness

An indication for the robustness of the comparable PI control law can be given by performing simulations with different aerodynamic parameters. In Figure 4-14, simulation results are presented where the aerodynamic parameters C_{m_q} and C_{m_α} are varied. These are important pitch dynamic parameters that determine the longitudinal stability of the plant.

4-5 Analysis on neglecting system dynamics increments

The incremental control laws are based on a first-order taylor-series expansion of the state derivative around a previous point in time, as presented in Equation 4-14

$$\dot{\mathbf{x}}_3 \approx \dot{\mathbf{x}}_{3,0} + \underbrace{\left(\frac{\partial \mathbf{f}_3(\mathbf{x})}{\partial \mathbf{x}} + \frac{\partial \mathbf{g}_3(\mathbf{x},\mathbf{u})}{\partial \mathbf{x}} \right)\Bigg|_{\mathbf{x}_0,\mathbf{u}_0}}_{A_{3,0}} (\mathbf{x} - \mathbf{x}_0) + \underbrace{\frac{\partial \mathbf{g}_3(\mathbf{x},\mathbf{u})}{\partial \mathbf{u}}\Bigg|_{\mathbf{x}_0,\mathbf{u}_0}}_{B_{3,0}} (\mathbf{u} - \mathbf{u}_0) \tag{4-24}$$

When the assumptions of the locally linear model and the neglection of the system dynamiccs terms in Equation 4-14 are valid, no steady state errors are expected to occur with an INDI controller. This is because every time step the measured angular accelerations are compared with the expected accelerations, in contrast to normal NDI control, where angular rates are used as feedback. However, previous simulation results in Figs. 4-6 to 4-8 do show steady state tracking errors. Those errors are greater with a greater delay, as can be seen in Figure 4-9.

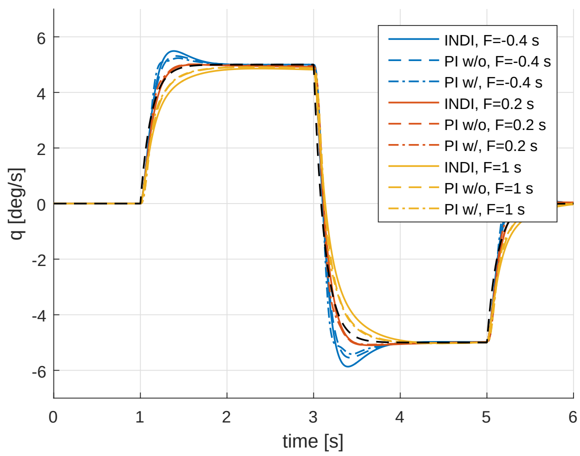

(a) Pitch rate tracking response of the different controllers and resizing factors F for C_{m_α} and C_{m_q} combined.

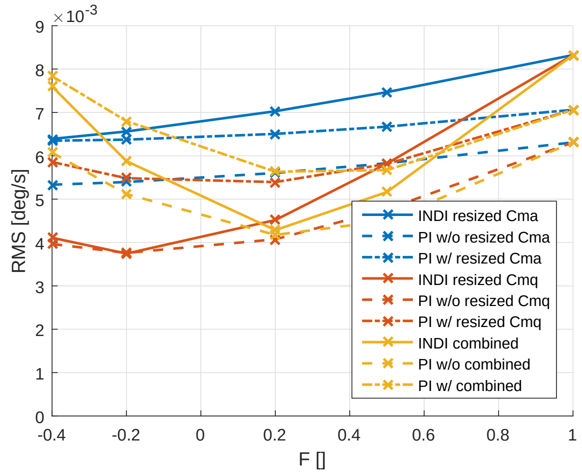

(b) RMS error pitch rate versus the coefficient resize factor F for coefficient C_{m_α}, C_{m_q} and both combined.

Figure 4-14: Tracking response of INDI controllers compared with similar PI controllers (with and without actuator dynamics in the loop), for different values of C_{m_q} and C_{m_α}. The coefficients are resized with factor F.

4-5-1 Component breakdown of system dynamics components

To validate the assumptions made, all the terms in the system dynamics have been calculated in the simulation. This includes the term $\mathbf{f}_3$ in Equation 4-2 and terms $A_{3,0}\Delta\mathbf{x}$ and $B_{3,0}\Delta\mathbf{u}$ in Equation 4-15. Those terms are plotted in Figure 4-15. . In this figure, it can be seen that at almost any moment the control is applied, the system dynamics increment $A_{3,0}\Delta\mathbf{x}$ is not small and the time-scale separation is not valid. The system dynamics increments do damp out quite quickly in the pitch direction, but in the yaw and roll, increments achieve a steady state value, and are continuously counteracted by a control increment. It can indeed be seen in the control deflections in Figure 4-6b that the rudder deflection (green) does not achieve steady state values, whereas the elevator deflection (blue) does. The increments $A_{3,0}\Delta\mathbf{x}$ and $B_{3,0}\Delta\mathbf{u}$ have also been calculated for the ideal INDI controller without actuator dynamics and without a filter to obtain angular accelerations, but using the true angular accelerations as feedback. The increments are plotted in Figure 4-17, and the difference in tracking response between the normal and the ideal controller is plotted in Figure 4-18. It can be seen that the increments $A_{3,0}\Delta\mathbf{x}$ and $B_{3,0}\Delta\mathbf{u}$ are both much smaller for the ideal controller. However, the ratio between $A_{3,0}\Delta\mathbf{x}$ and $B_{3,0}\Delta\mathbf{u}$ is still almost identical. Hence, the fact that the ideal controller does not show any steady state error, is only because the controller can respond much faster to system dynamics increments. This suggests that the steady state errors will scale proportionally with the increment delay $t - t_0$.

FiXme: Make this same plot for the case without incrment delays and with faster actuators//or just in the ideal case

Looking at the equations for the simplified aerodynamics in Equation 3-25, we see that the system dynamics increments $A_{3,0}\Delta\mathbf{x}$ can be split up in terms related to the aerodynamics angles α and β, and the angular rates $\hat{p}, \hat{q}, \hat{r}$. Those states capture the most important system dynamics. The system dynamics increments related to these states have been calculated.

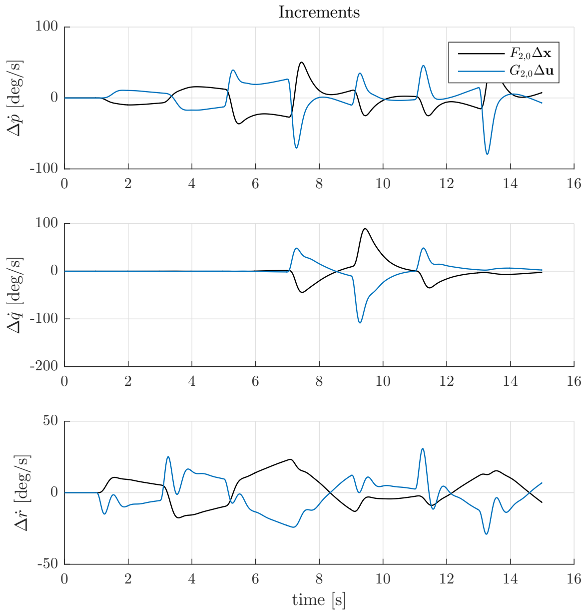

Figure 4-15: Comparison of incremental terms $A_{3,0}\Delta\mathbf{x}$ and $B_{3,0}\Delta\mathbf{u}$ from (4-15) while tracking angular rate references with the normal INDI controller.

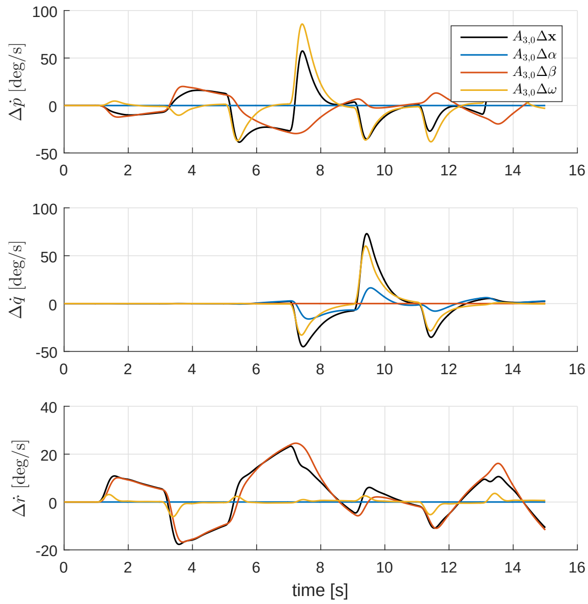

Figure 4-16: Breakdown of incremental term $A_{3,0}\Delta\mathbf{x}$ from (4-15) while tracking angular rate references with the normal INDI controller.

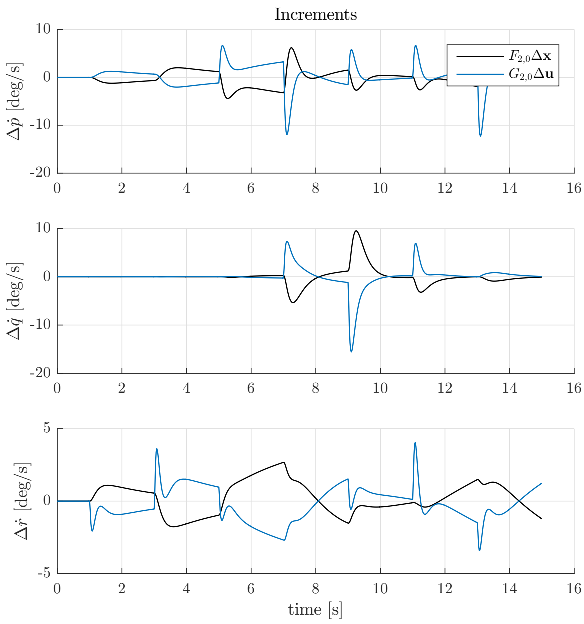

Figure 4-17: Comparison of incremental terms $A_{3,0}\Delta\mathbf{x}$ and $B_{3,0}\Delta\mathbf{u}$ from (4-15) while tracking angular rate references with the ideal INDI controller (no actuators, perfect angular acceleration feedback).

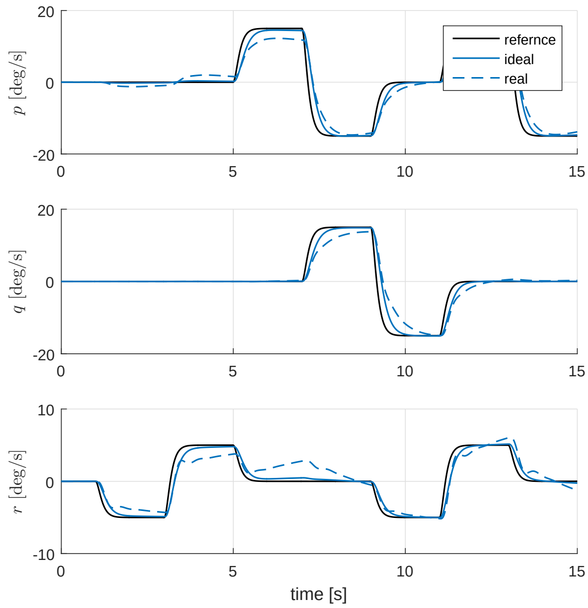

Figure 4-18: Tracking response of the INDI angular rate controller, both for the normal as the ideal (no actuators, perfect angular acceleration feedback) configuration.

Hence, we calculated:

$$\frac{\partial \mathbf{f}_3(\mathbf{x})}{\partial \alpha}\Delta\alpha = \frac{\partial}{\partial \alpha} I^{-1}(\mathbf{M}_0(\mathbf{x}) - \mathbf{x}_3 \times I\mathbf{x}_3)\Delta\alpha = \bar{q}S\frac{\partial}{\partial \alpha}\begin{bmatrix} bC_{l,\text{base+rate}} \\ cC_{m,\text{base+rate}} \\ bC_{n,\text{base+rate}} \end{bmatrix}\Delta\alpha \tag{4-25}$$

and the incremental terms related to sideslip and angular rates. When the aerodynamics are simulated with the simplified polynomial model the calculation of $A_{3,0}\Delta\mathbf{x}$ becomes straightforward:

$$A_{3,0}\Delta\mathbf{x} = \bar{q}S\begin{bmatrix} b & & \\ & c & \\ & & b \end{bmatrix}\begin{bmatrix} & C_{l_\beta} & \frac{2V}{b}C_{l_{\hat{p}}} & & \\ C_{m_\alpha} & & & \frac{2V}{c}C_{m_{\hat{q}}} & \\ & C_{n_\beta} & & & \frac{2V}{b}C_{n_{\hat{r}}} \end{bmatrix}\begin{bmatrix} \Delta\alpha \\ \Delta\beta \\ \Delta p \\ \Delta q \\ \Delta r \end{bmatrix} \tag{4-26}$$

Simulation results using the simplified polynomial model for the aerodynamics are performed, and a breakdown of the different system dynamics increments is plotteed in Figure 4-16. From these plotted terms we can conclude the following: during the tracking of step responses, the transient system dynamics increments are dominated by terms related to the angular rates, whereas steady state increments are dominated by the aerodynamic angles: in the longitudinal dynamics, the angle of attack has only little effect on the system dynamics increment and the sideslip has no effect at all. However, in the lateral dynamics, the increment related to the sideslip angle is dominant.

Simulations are performed where the specific stability derivatives $C_{m_\alpha}, C_{n_\beta}, C_{l_\beta}$ and dynamic damping coefficients $C_{n_p}, C_{m_q}, C_{l_r}$ are reduced. The tracking results are plotted in Figure 4-19. As expected, it can be seen that the tracking errors are reduced almost proportionaly to the coefficient reduction.

Concluding, Figs. 4-15 and 4-16 clearly show that the assumption of neglecting the system dynamics increments is not valid and causes steady state tracking errors. The simulation results in Figs. 4-16 and 4-19 indicate that by compensating for the system dynamics increments in the control law, the errors could be removed. This will be discussed in the next section.

4-5-2 Compensation for system dynamics increments in control law

Without actuators

When the aerodynamic model is fully known, compensation for the system dynamics terms is possible. The control law shown in (4-16) as derived from (4-15) while setting $A_{3,0}\Delta\mathbf{x}$ would yield in this case:

$$\Delta\mathbf{u} = B_{3,0}^{-1}\left(C_3\mathbf{e}_3 - \dot{\mathbf{x}}_{3,0} - A_{3,0}\Delta\mathbf{x} + \dot{\mathbf{x}}_{3,ref}\right) \tag{4-27}$$

Controllers have been implemented and simulations are performed with the simplified polynomial model for the aerodynamics.

We assume that the airspeed V appearing in the dynamic pressure $\bar{q}$ has no significant effect over the control increment time. The coefficients $C_{m_\alpha}, C_{l_\beta}, \ldots$ denote the partial derivatives to the particular states.

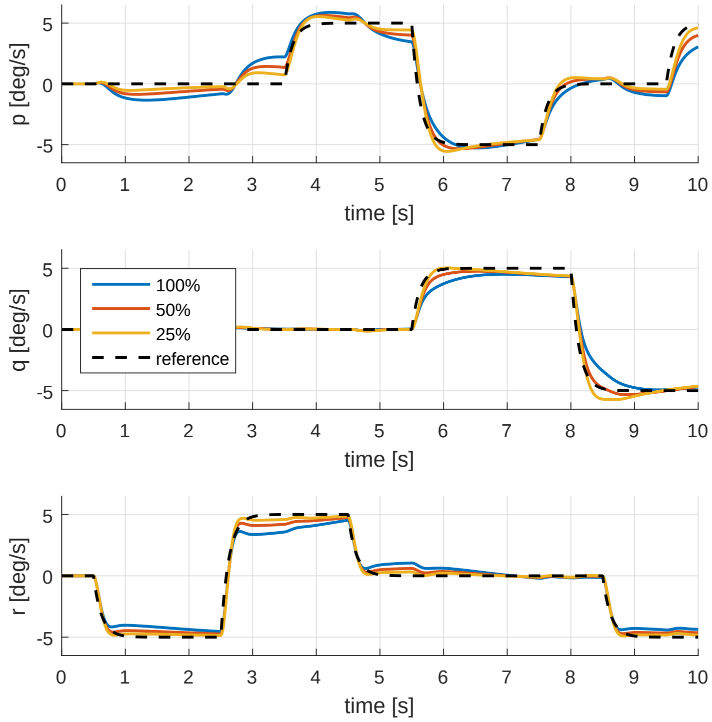

Figure 4-19: INDI angular rate response with reduced system dynamics coefficients $C_{m_\alpha}, C_{n_\beta}, C_{l_\beta}, C_{n_p}, C_{m_q}, C_{l_r}$.

With actuators

In the simulation, actuator dynamics for control surface deflections are described by a first order linear model:

$$\dot{\delta}_i = -\frac{1}{\tau_{act}}\delta_i + \frac{1}{\tau_{act}}u_i \tag{4-28}$$

where τ_{act} is the actuator time constant and δ_i the control surface deflection of control surface i. In discrete time, the actuator dynamics are:

$$\begin{aligned} \delta_{i,k+1} &= e^{-\frac{T_s}{\tau_{act}}}\delta_{i,k} + (1 - e^{-\frac{T_s}{\tau_{act}}})u_{i,k} \\ &= e^{-\frac{T_s}{\tau_{act}}}\delta_{i,k} + (1 - e^{-\frac{T_s}{\tau_{act}}})(\delta_{i,k} + \Delta u_{i,k}) \end{aligned} \tag{4-29}$$

which yields in incremental form:

$$\Delta\delta_{i,k} = \beta_{act}\Delta u_{i,k} \tag{4-30}$$

where $\beta_{act} = (1 - e^{-\frac{T_s}{\tau_{act}}})$ is the actuator filter constant with $0 < \beta_{act} < 1$. The result above shows that all increments commanded by the control are scaled as deflection increments. Now define the filter constant matrix for all control deflections as:

$$\beta_{act} = \begin{bmatrix} \beta_e & & \\ & \beta_r & \\ & & \beta_a \end{bmatrix} \tag{4-31}$$

Then, the system described by (4-15) including actuator dynamics and substituting for the incremental control law in (4-27) yields:

$$\begin{aligned}\dot{\mathbf{x}}_3 &= \dot{\mathbf{x}}_{3,0} + A_{3,0}\Delta\mathbf{x} + B_{3,0}\Delta\boldsymbol{\delta} \\ &= \dot{\mathbf{x}}_{3,0} + A_{3,0}\Delta\mathbf{x} + B_{3,0}\beta_{act}\Delta\mathbf{u} \\ &= \dot{\mathbf{x}}_{3,0} + A_{3,0}\Delta\mathbf{x} + B_{3,0}\beta_{act}B_{3,0}^{-1}\left(C_3\mathbf{e}_3 - \dot{\mathbf{x}}_{3,0} - A_{3,0}\Delta\mathbf{x} + \dot{\mathbf{x}}_{3,ref}\right) \\ &= (I-\beta_{act})\dot{\mathbf{x}}_{3,0} + (I-\beta_{act})A_{3,0}\Delta\mathbf{x} + \beta_{act}\left(C_3\mathbf{e}_3 + \dot{\mathbf{x}}_{3,ref}\right)\end{aligned} \tag{4-32}$$

The resulting equation shows that the compensation for system dynamics increments is never fully achieved, but depends on the sample time T_s and actuator time constant τ_{act}. For example, with $T_s = 0.01\,\mathrm{s}, \tau_{act} = 0.05\,\mathrm{s}$ we have $\beta_{act} = 0.18$. So, the compensation is achieved by only 18%.

When the actuator dynamics behaves indeed according to the first-order model and when there is a good estimate of time constants available, we can compensate for effect of the actuators by scaling the compensation term $A_{3,0}\Delta\mathbf{x}$ by $1/\beta_{act}$. The control law with a *scaled* compensation for the system dynamics increments then is (compare with (4-27)):

$$\Delta\mathbf{u} = B_{3,0}^{-1}\left(C_3\mathbf{e}_3 - \dot{\mathbf{x}}_{3,0} - \beta_{act}^{-1}A_{3,0}\Delta\mathbf{x} + \dot{\mathbf{x}}_{3,ref}\right) \tag{4-33}$$

This yields for the system dynamics:

$$\begin{aligned}\dot{\mathbf{x}}_3 &= \dot{\mathbf{x}}_{3,0} + A_{3,0}\Delta\mathbf{x} + B_{3,0}\beta_{act}\Delta\mathbf{u} \\ &= \dot{\mathbf{x}}_{3,0} + A_{3,0}\Delta\mathbf{x} + B_{3,0}\beta_{act}B_{3,0}^{-1}\left(-C_3\mathbf{z}_3 - \dot{\mathbf{x}}_{3,0} - \beta_{act}^{-1}A_{3,0}\Delta\mathbf{x} + \dot{\mathbf{x}}_{3,ref}\right) \\ &= (I-\beta_{act})\dot{\mathbf{x}}_{3,0} + \beta_{act}\left(C_3\mathbf{e}_3 + \dot{\mathbf{x}}_{3,ref}\right)\end{aligned} \tag{4-34}$$

Simulation results for the normal compensation and the scaled compensation are shown in Figure 4-20. The system dynamics increments $A_{3,0}\Delta\mathbf{x}$ are calculated according to Equation 4-26. The full FASER model has been used for the simulation, i.e. table lookup aerodynamics and motor inertia. Looking at the tracking errors, it is clearly shown that a normal compensation only has a marginal effect. When actuator dynamics are taken into account by scaling the compensation by $1/\beta_{act}$, the steady state tracking error indeed vanishes, although the yaw rate tracking response still has a significant error when actuator dynamics are included. Looking at Figure 4-21, it can be seen that simulations with the simplified polynomial model however, yield much lower tracking errors. The remaining tracking errors can therefore mainly be attributed by to differences in both models.

From the RMS error results in Figure 4-21, it is that in roll and pitch motion, the minimum errors are not achieved at $F = 1$, even with the simplified polynomial model. Rather, the plot shows that an overcompensation yields a better result. The reason for this is that during the transient part of the step inputs, the INDI controller typically has a small delay, due to uncompensated damping effects and an increment delay caused by actuator dynamics and the washout filter. An overcompensation effectively means that during this transient, the control is more aggressive and therefore reaches the final comman faster. This can be seen in the time-domain plot in Figure 4-20a.

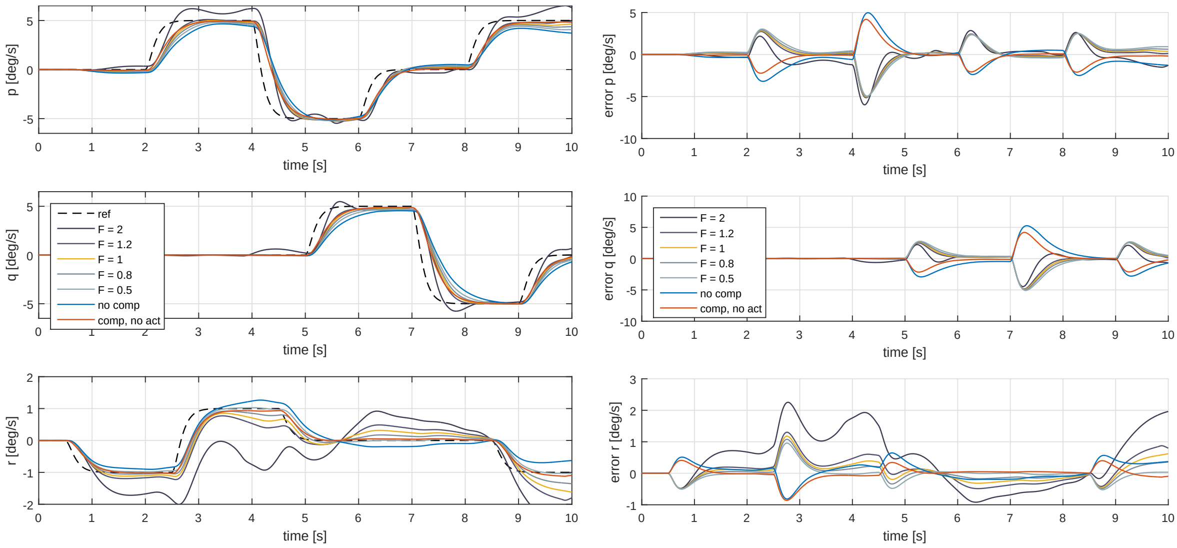

(a) Angular rates **(b)** Tracking errors

Figure 4-20: INDI controller tracking response, simulated with lookup table aerodynamics and motor dynamics, using no compensation (blue), unscaled compensation (red) without actuator dynamics and compensation with actuator dynamics. To show the effect of an imperfect estimation the entire increment compensation in the control law is scaled by F, so the compensation term equals $-F\beta_{act}^{-1}A_{3,0}$. Only roll and yaw rate tracking response are plotted.

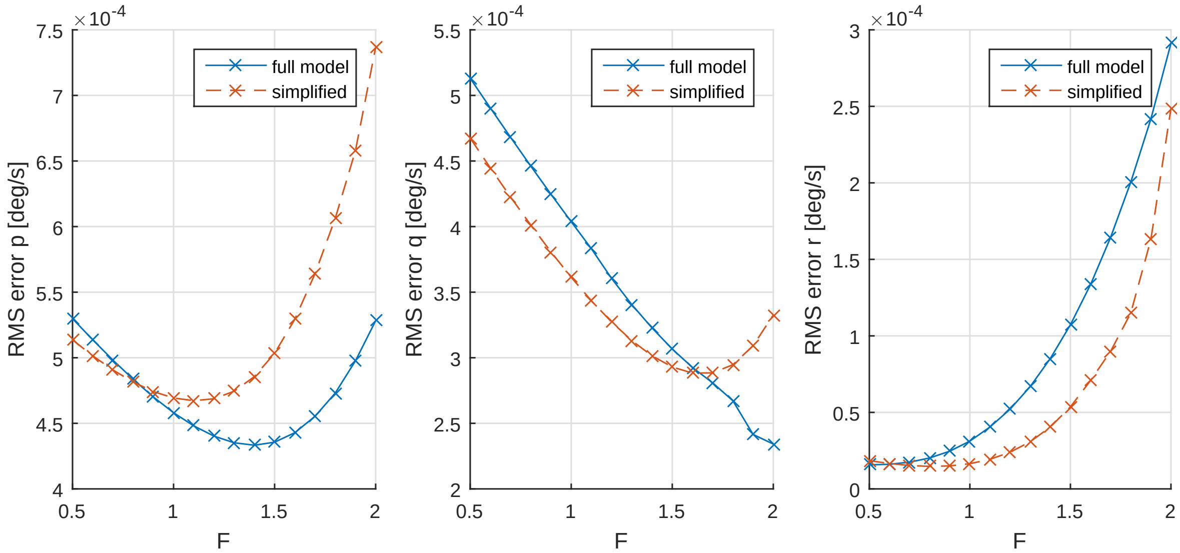

Figure 4-21: RMS tracking error for an INDI controller with compensation for system dynamics increments. Simulation results plotted both for full table look-up aerodynamics as for the simplified polynomial model.

4-6 Intermediate summary and conclusions

Up until this point, we have presented an analysis on the application of INDI controllers to the FASER UAV to track the angular rates. We have compared nominal NDI controllers with INDI controllers. The NDI control law was derived as:

$$\mathbf{u} = G_3^{-1}(\mathbf{x})\left(C_3\mathbf{e}_3 + \dot{\mathbf{x}}_{3,ref} - \mathbf{f}_3(\mathbf{x})\right) \tag{4-35}$$

The INDI control law was derived as:

$$\mathbf{u} = \mathbf{u}_0 + G_{3,0}^{-1}\left(C_3\mathbf{e}_3 + \dot{\mathbf{x}}_{3,ref} - \dot{\mathbf{x}}_{3,0}\right) \tag{4-36}$$

A comparable PI control law was presented:

$$\mathbf{u} = \frac{G_{3,0}^{-1}}{\tau_{pi}}\left(\mathbf{e}_3 + C_3\int_0^t \mathbf{e}_3 dt\right) \tag{4-37}$$

where $\tau_{pi} = T_s$ is the sample time when actuator dynamics are not included, and $\tau_{pi} = \tau_{act}$ is the actuator time constant when they are included. A control law with compensation for system dynamics increments was presented:

$$\Delta\mathbf{u} = G_{3,0}^{-1}\left(C_3\mathbf{e}_3 - \dot{\mathbf{x}}_{3,0} - \beta_{act}^{-1}F_{3,0}\Delta\mathbf{x} + \dot{\mathbf{x}}_{3,ref}\right) \tag{4-38}$$

with $\beta_{act} = (1 - e^{-\tau_{act}/T_s})$.

We are able to draw the following main conclusions about INDI control laws for fixed-wing aircraft that have dynamics comparable to the FASER UAV:

- According to our expectations, the INDI control laws show a higher robustness against uncertainties in the control effectiveness and furthermore are completely independent to system dynamics. See Figs. 4-3, 4-5 and 4-6.
- Non-zero transient and steady tracking errors are apparent, which are caused by the neglection of the system dynamics increments $F_{3,0}\Delta\mathbf{x}$. These errors scale with the increment delay time. Hence, a lower sample time will yield a better control response.
- A comparable PI-control yields responses with equal or even lower tracking errors in nominal cases, but also show similar robustness properties. This comparison can be beneficial or helpful in at least two ways: on one hand, it can give more insight in the INDI control laws, e.g. when investigating the influence of control effectiveness parameters in $G_{3,0}$. On the other hand, it can help to find proper gains for PI control laws. Results of the PI control law are not completely equilalent with INDI control laws. This might be caused by the fact that the assumption had to be made for the comparison, that the discrete implementation equals its continuous form, see subsection 2-4-3 and in particular Equation 2-77. It is mathematically more correct to compare it with an incremental PI control law, as discussed in subsection 2-4-4. The paper included as an appendix of this thesis (Acquatella B. et al., 2017) shows indeed this indeed reseults in identical responses.

- The system dynamics can be compensated for when estimates of stability derivatives are known, see Figure 4-20. However, actuator dynamics must be taken into account. Furthermore, simulations show that a simple compensation based on simplified aerodynamical model of the aircraft might not give a good compensation in all axes.

The next sections will cover the extension of these controllers for the attitude control. The core of these controllers is equivalent to the INDI control laws presented in the previous sections.

4-7 INDI for attitude flight control

Typical flight control laws include some cascaded control structure. Usually, the inner loop consists of an angular rate control law. Around this loop, the attitude of the aircraft is controlled. Examples of implementations with classical flight control laws can be found in (Stevens & Lewis, 2003). A typical pitch angle hold mode can follow a reference θ_r by giving commands for a pitch rate q_{cmd} based on the measured tracking error:

$$q_{cmd} = LC(\theta_{ref} - \theta_m) \tag{4-39}$$

Likewise, controlling the lateral modes involves a controller which gives references for the roll rate p, based on a roll tracking error. To follow a coordinated turn, i.e., one without a resultant lateral force, a yaw rate command can be designed in multiple ways.

The incremental control law presented in the previous section can be extended to an attitude control law using similar techniques. The problem with a controller in which the pitch and roll modes are separated, is that it relies on the assumption that the control laws do not have a coupling effect on each other. The underlying assumption actually is that $q \approx \dot{\theta}$ and $p \approx \dot{\phi}$. This approximation is only useful for small attitude angles. The true kinematic relation was presented in Equation 3-7:

$$\begin{bmatrix} \dot{\phi} \\ \dot{\theta} \\ \dot{\psi} \end{bmatrix} = \begin{bmatrix} 1 & \sin\phi\tan\theta & \tan\theta\cos\phi \\ 0 & \cos\phi & -\sin\phi \\ 0 & \sin\phi\sec\theta & \cos\phi\sec\theta \end{bmatrix} \begin{bmatrix} p \\ q \\ r \end{bmatrix} \tag{4-40}$$

There are two ways in which we can use NDI to control the attitude angles of the aircraft. First, two loops can be considered, much like the cascaded structure of a multi-loop PID controlled aircraft. The outer loop then contains a (true) kinematic inversion to convert Euler angle commands to angular rate commands. The inner loop then is exactly the same as the INDI angular rate controller presented in the previous chapter. The second method consists of a single loop, INDI controller by describing the system as a second order system with a relative degree of two. We will present both controllers.

4-7-1 Multi-loop NDI-INDI attitude control

When we consider the angular rates to be the commands for the attitude control loop, the equation shows that the dynamics are just a linear combination of the angular rates which has no uncertainties when the state is known. Hence its relative degree is 1. It is therefore perfectly suitable for a nonlinear dynamic inversion.

Define the outer loop state, reference and error as:

$$\mathbf{x}_2 = \begin{bmatrix} \phi \\ \theta \\ \psi \end{bmatrix}, \quad \mathbf{x}_{2,ref} = \begin{bmatrix} \phi \\ \theta \\ \psi \end{bmatrix}_{ref}, \quad \mathbf{e}_2 = \mathbf{x}_{2,ref} - \mathbf{x}_2 \tag{4-41}$$

Although, in fact, we are aiming to control merely the pitch and roll angle, while keeping a coordinated flight, i.e. without body side forces. To do this, we will set $\psi - \psi_{ref} = 0$ for this controller and hence leave the final heading angle uncontrolled. Instead, we only use a time derivative of the heading reference $\dot{\psi}$. The reason that we choose to define a reference for the time derivative of the heading is that the heading of fixed-wing aircraft is indirectly controlled by the bank or roll angle of the aircraft, given a (reasonable) coordinated turn. It means that a fixed roll angle corresponds to a fixed reference heading rate $\dot{\psi}$ by aiming for a coordinated turn in which the lateral force is generated completely by turning the lift vector of the aircraft. Normally, a reference for ψ and $\dot{\psi}$ will determine the reference for the roll angle ϕ or bank angle μ, hence the reference for the roll angle should normally be defined, such that no body side force is needed to turn the aircraft with a desired rate. However, at this point we are merely interested in finding an attitude control and we are not considering a navigational loop. Therefore, a reference roll angle ϕ will determine a reference heading rate $\dot{\psi}_{ref}$ as follows. From Equation 5-41 we have:

$$\dot{\chi} = \frac{1}{mV\cos\gamma}\left(Y\cos\mu + L\sin\mu + F_T(\sin\alpha\sin\mu - \cos\alpha\cos\mu\sin\beta)\right) \tag{4-42}$$

Where V is the airspeed (not the inertial or ground velocity). In a coordinated turn at small and constant side slip angles and with a cancellation of the (body) lateral aerodynamic force, this approximates to:

$$\dot{\psi} \approx \dot{\chi} \approx \frac{1}{mV\cos\gamma}\left(L\sin\phi + F_T(\sin\alpha\sin\phi)\right) \tag{4-43}$$

In which we identify the vertical load factor:

$$n_z = \frac{1}{mg}\left(L + F_T\sin\alpha\right) \tag{4-44}$$

which yields an equation to compute the heading rate reference from a roll angle:

$$\dot{\psi}_{ref} = \frac{n_z g}{V\cos\gamma}\sin\phi \tag{4-45}$$

To prevent effects on $\dot{\psi}_{ref}$ from turbulence and sharp control of the angle of attack which affect n_z, the load factor can be low-pass filtered.

Continuing with the derivation for the control law, write the state derivative presented in Equation 4-40 in vector notation as:

$$\begin{aligned} \dot{\boldsymbol{\theta}} &= N(\boldsymbol{\theta})\boldsymbol{\omega} \\ \dot{\mathbf{x}}_2 &= N(\mathbf{x}_2)\mathbf{x}_3 \end{aligned} \tag{4-46}$$

If the virtual control $\boldsymbol{\nu}_2$ is set equal to the derivative of the attitude $\boldsymbol{\theta}$, the commands for the angular rate can be calculated by a simple inversion of the equation above:

$$\mathbf{x}_{3,cmd} = N(\mathbf{x}_2)^{-1}\boldsymbol{\nu}_2 \tag{4-47}$$

The assumption must be made that the inner loop is time-scale separated from the attitude loop, so that for the equation above we can assume that $\boldsymbol{\omega} \approx \boldsymbol{\omega}_{cmd}$. The virtual control $\boldsymbol{\nu}_2$ is a linear controller using the tracking error plus the first derivative of the attitude reference:

$$\boldsymbol{\nu}_2 = K_p\mathbf{e}_2 + K_d\dot{\mathbf{e}}_2 + \dot{\mathbf{x}}_{2,ref} \tag{4-48}$$

so that:

$$\mathbf{x}_{3,cmd} = N(\mathbf{x}_2)^{-1}\left(K_p\mathbf{e}_2 + K_d\dot{\mathbf{e}}_2 + \dot{\mathbf{x}}_{2,ref}\right) \tag{4-49}$$

with:

$$N^{-1}(\boldsymbol{\theta}) = \begin{bmatrix} 1 & 0 & -\sin\theta \\ 0 & \cos\phi & \cos\theta\sin\phi \\ 0 & -\sin\phi & \cos\theta\cos\phi \end{bmatrix} \tag{4-50}$$

A command shaping filter is used to provide the signal $\dot{\mathbf{x}}_{2,ref}$ and to impose constraints to prevent saturation. The commands for the angular rates $\mathbf{x}_{3,cmd}$ are passed to the inner loop angular rate controller, which is identical to the angular rate controller presented in the previous section. Hence, the final control law equals:

$$\Delta\mathbf{u} = B_{3,0}^{-1}\left(K_p\mathbf{e}_3 - \dot{\mathbf{x}}_{3,0} + \dot{\mathbf{x}}_{3,ref}\right) \tag{4-51}$$

An control diagram of this control law to control the attitude is given in Figure 4-22.

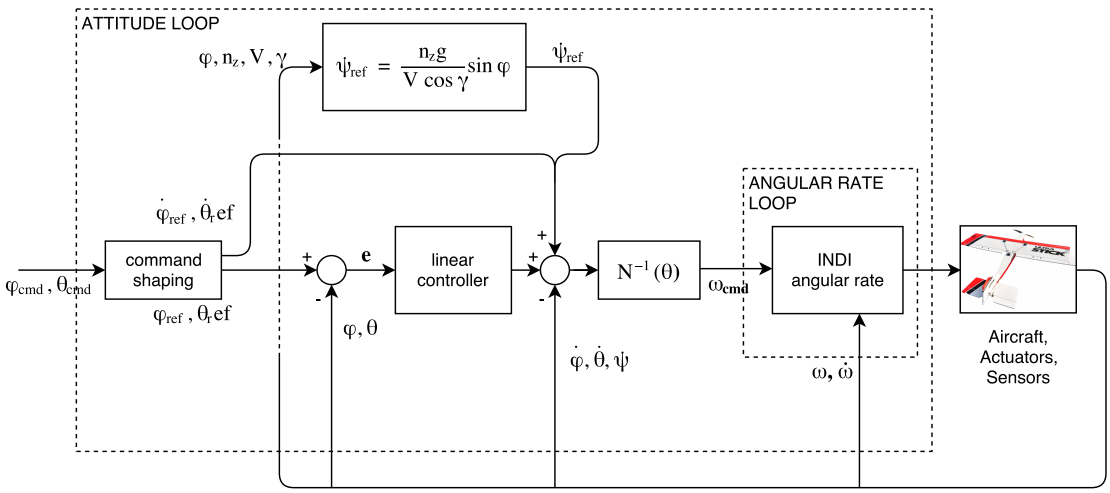

Figure 4-22: Multi-loop INDI control structure for attitude control.

4-7-2 Single loop INDI attitude control

Define the outer loop state, reference and error again as:

$$\mathbf{x}_2 = \boldsymbol{\theta} = \begin{bmatrix} \phi \\ \theta \\ \psi \end{bmatrix}, \quad \mathbf{x}_{2,ref} = \begin{bmatrix} \phi \\ \theta \\ \psi \end{bmatrix}_{ref}, \quad \mathbf{e}_2 = \mathbf{x}_{2,ref} - \mathbf{x}_2 \tag{4-52}$$

And write Equation 4-40 again in vector notation as:

$$\dot{\boldsymbol{\theta}} \quad = N(\boldsymbol{\theta})\boldsymbol{\omega} \tag{4-53}$$

Now, consider the angular rates $\boldsymbol{\omega} = \mathbf{x}_3$ as a real state and do not assume time-scale separation. In that case we have to continue the feedback linearization process by taking the second derivative of the output $\mathbf{x}_2$. However, to simplify the equations later on, note that the time derivative of the angular rates $\dot{\boldsymbol{\omega}}$ is kinematically related to the first and second time derivatives of the Euler angles:

$$\begin{aligned} \boldsymbol{\omega} \quad &= N^{-1}(\boldsymbol{\theta})\dot{\boldsymbol{\theta}} \\ \dot{\boldsymbol{\omega}} \quad &= [\tfrac{d}{dt}N^{-1}(\boldsymbol{\theta})]\dot{\boldsymbol{\theta}} + N^{-1}(\boldsymbol{\theta})\ddot{\boldsymbol{\theta}} \end{aligned} \tag{4-54}$$

Similarly, a direct eqution for $\ddot{\boldsymbol{\theta}}$ can be found by taking the time derivative of (4-53) directly:

$$\ddot{\boldsymbol{\theta}} = [\tfrac{d}{dt}N(\boldsymbol{\theta})]\boldsymbol{\omega} + N(\boldsymbol{\theta})\dot{\boldsymbol{\omega}} \tag{4-55}$$

This equation can be rewritten for $\dot{\boldsymbol{\omega}}$ as:

$$\dot{\boldsymbol{\omega}} = N^{-1}(\boldsymbol{\theta})\ddot{\boldsymbol{\theta}} - N^{-1}[\tfrac{d}{dt}N(\boldsymbol{\theta})]\boldsymbol{\omega} \tag{4-56}$$

Note that, by comparison of terms with (4-54):

$$-N^{-1}[\tfrac{d}{dt}N(\boldsymbol{\theta})]\boldsymbol{\omega} = [\tfrac{d}{dt}N^{-1}(\boldsymbol{\theta})]\dot{\boldsymbol{\theta}} \tag{4-57}$$

Now, continue the feedback linearization process by taking the second time derivative of $\mathbf{x}_2 = \boldsymbol{\theta}$ and subsitute angular accelerations in incremental form as written in (4-15):

$$\begin{aligned} \ddot{\mathbf{x}}_2 \quad &= [\tfrac{d}{dt}N(\mathbf{x}_2)]\mathbf{x}_3 + N(\mathbf{x}_2)\dot{\mathbf{x}}_3 \\ \ddot{\mathbf{x}}_2 \quad &= [\tfrac{d}{dt}N(\mathbf{x}_2)]\mathbf{x}_3 + N(\mathbf{x}_2)\left(\dot{\mathbf{x}}_{3,0} + A_{3,0}\Delta\mathbf{x} + B_{3,0}\Delta\mathbf{u}\right) \end{aligned} \tag{4-58}$$

The dynamics can be inverted to describe a control law which linearizes a virtual command $\boldsymbol{\nu}_2$:

$$\begin{aligned} \dot{\mathbf{x}}_{3,0} + A_{3,0}\Delta\mathbf{x} + B_{3,0}\Delta\mathbf{u} \quad &= N^{-1}(\mathbf{x}_2)\left(\boldsymbol{\nu}_2 - \tfrac{d}{dt}N(\mathbf{x}_2)\mathbf{x}_3\right) \\ \Delta\mathbf{u} \quad &= B_{3,0}^{-1}\left\{N^{-1}(\mathbf{x}_2)\left(\boldsymbol{\nu}_2 - \tfrac{d}{dt}N(\mathbf{x}_2)\mathbf{x}_3\right) - \dot{\mathbf{x}}_{3,0} - A_{3,0}\Delta\mathbf{x}\right\} \end{aligned} \tag{4-59}$$

Note that we can substitute (4-57) which yields:

$$\Delta\mathbf{u} = B_{3,0}^{-1}\left\{\underbrace{N^{-1}(\mathbf{x}_2)\boldsymbol{\nu}_2 + [\tfrac{d}{dt}N^{-1}(\mathbf{x}_2)]\dot{\mathbf{x}}_2}_{\text{objective }\dot{\mathbf{x}}_3}\ \underbrace{-\dot{\mathbf{x}}_{3,0} - A_{3,0}\Delta\mathbf{x}}_{\text{system dynamics }\dot{\mathbf{x}}_3}\right\} \tag{4-60}$$

This control law yields a system which is linear between the output $\mathbf{x}_2$ and the virtual control $\boldsymbol{\nu}_2$:

$$\ddot{\mathbf{x}}_2 = \boldsymbol{\nu}_2 \tag{4-61}$$

If we select a virtual control as:

$$\boldsymbol{\nu}_2 = K_d\dot{\mathbf{e}}_2 + K_p\mathbf{e}_2 + \ddot{\mathbf{x}}_{2,ref} \tag{4-62}$$

which yields:

$$0 = \ddot{\mathbf{e}}_2 + K_d \dot{\mathbf{e}}_2 + K_p \mathbf{e}_2 \tag{4-63}$$

then, we can design K_d and K_p to yield stable tracking error dynamics. The control law in (4-60) still contains a system dynamics increment term. We may assume that those increments are small with respect to the control increments $B_{3,0}\Delta\mathbf{u}$ and hence can be neglected in the control law. Hence, the final total control is:

$$\mathbf{u} = \mathbf{u}_0 + B_{3,0}^{-1}\left\{ \underbrace{N^{-1}(\mathbf{x}_2)\boldsymbol{\nu}_2 + [\tfrac{d}{dt}N^{-1}(\mathbf{x}_2)]\dot{\mathbf{x}}_2}_{\text{objective } \dot{\mathbf{x}}_3} \underbrace{-\dot{\mathbf{x}}_{3,0} - A_{3,0}\Delta\mathbf{x}}_{\text{system dynamics } \dot{\mathbf{x}}_3} \right\} \tag{4-64}$$

with:

$$N^{-1}(\boldsymbol{\theta}) = \begin{bmatrix} 1 & 0 & -\sin\theta \\ 0 & \cos\phi & \cos\theta\sin\phi \\ 0 & -\sin\phi & \cos\theta\cos\phi \end{bmatrix} \tag{4-65}$$

and:

$$\tfrac{d}{dt}N^{-1}(\boldsymbol{\theta})\dot{\boldsymbol{\theta}} = \begin{bmatrix} 0 & 0 & -\cos\theta\dot{\theta} \\ 0 & -\sin\phi\dot{\phi} & -\sin\theta\dot{\theta}\sin\phi + \cos\theta\cos\phi\dot{\phi} \\ 0 & -\cos\phi\dot{\phi} & -\sin\theta\dot{\theta}\cos\phi - \cos\theta\sin\phi\dot{\phi} \end{bmatrix} \begin{bmatrix} \dot{\phi} \\ \dot{\theta} \\ \dot{\psi} \end{bmatrix} \tag{4-66}$$

We can again identify the great similarity with the INDI angular rate controller by noting that the first two terms inside the brackets form the objective for the angular accelerations $\dot{\mathbf{x}}_3$. The difference between this single-loop attitude control law and the previously presented multi-loop control law is that the kinematic inversion is now integrated with the incremental control law. In the multi-loop controller, the reference signal for the angular rates and accelerations $\mathbf{x}_{3,ref}$ and $\dot{\mathbf{x}}_{3,ref}$ was generated by a command shaping filter.

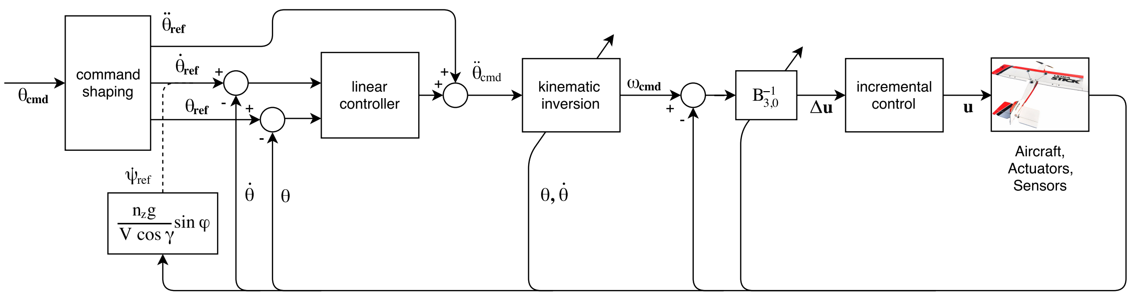

Figure 4-23: Single-loop INDI control structure for attitude control.

4-7-3 Simulation results

We will now present simulation results for the attitude INDI controllers presented in the previous sections. These controllers are also compared against a baseline PI control law, for which the gains have been tuned completely independent from the INDI control laws. The PI controller consists of seperate control loops for the pitch and roll motion, giving inputs to the elevator and aileron, respectively. The specific tuning of the gains of this controller is not discussed here. It can be expected that for each different aircraft configuration (trim state,

Table 4-4: Changed aerodynamic parameters for case A (small uncertainties) and case B (to mimic an asymmetrical damage in the horizontal stabilizer).

parameter	old value	case B	case C
C_{m_α}	-0.3025	-0.2025	0.0975
C_{l_α}	0	0.05	0
$C_{m_{\delta_e}}$	-0.69	-0.49	

aerodynamic parameters), a tuning of this PI controller can be made that gives a satisfactory response.

The following simulation results are presented in this section:

- A nominal simulation without parameter uncertainties (Figure 4-24)
- A simulation with simulated horizontal stabilizer dammage, according to case B in Table 4-4 (Figure 4-25)
- A simulation with a statically unstable aircraft (positive C_{m_α}, according to case C in Table 4-4 (Figure 4-25)

The parameter used for these simulation are stated in Table 4-5. Tuning was done manually, by first tuning the inner loop, and thereafter the outer loop.

A degraded elevator has no visible effect on the performance of the PI controller like is the case with both INDI control loops. Furthermore, other than a difference in tuning, the single and multi-loop INDI controllers perform similar. During the acceleration in pitch and roll, we do not see large differences between the controllers. This indicates that with the current control task and controller set-up, time-scale separation can be assumed.

The robustness of the INDI controllers is best visible in the simulation with the statically unstable aircraft. As the INDI controller does use acceleration feedback to measure system dynamics, the tuned controllers have a similar performance even if the aerodynamics change drastically. The PI controller would have to be re-tuned for the specific case.

4-8 Conclusion

In this chapter we presented INDI control laws for two control problems. The main part of this chapter focused on the angular rate control problem. The INDI angular rate controller is the core control law used for all control laws in this thesis and hence needed extensive analysis on robustness and verification.

A summary and conclusion on the first part has already been given in section 4-6. We have shown that system dynamics increments can not always be neglected to reduce the steady state tracking error in the angular rates, especially when considering the yawing motion of the aircraft. Furthermore, the INDI control law has been successfully compared with PI control. Finally, the angular rate controller shows good performance and indicates its applicability for real flight tests.

Table 4-5: Parameters used for the simulations with attitude INDI controllers in Figure 4-6.

Parameter	value
Solver	ode3 Bogacki-Shampine
Sample time	0.01 s
Trim velocity	20 m/s
Aerodynamics	lookup tables
Motor and propeller inertia	yes
Actuator dynamics	yes, bandwidth 2.5 Hz
Sensor noise	no
Sensor dynamics	no
Control law	Equation 4-64 and Equation 4-49
Attitude command shaping	$\omega_n = 10\,\mathrm{rad/s}, \zeta = 0.7$, rate limit 40 deg/s
Angular accelerations	first order washout filter, $\omega_n = 20\,\mathrm{rad/s}$
Multi-loop control gains	$K_{p_\theta} = 2, K_{p_\phi} = 2, K_{d_\theta} = 1, K_{d_\phi} = 1.5, K_{p_\omega} = \mathrm{diag}([4, 4, 2])$
Single-loop control gains	$K_{p_\theta} = 4, K_{d_\theta} = [10, 20, 10]$

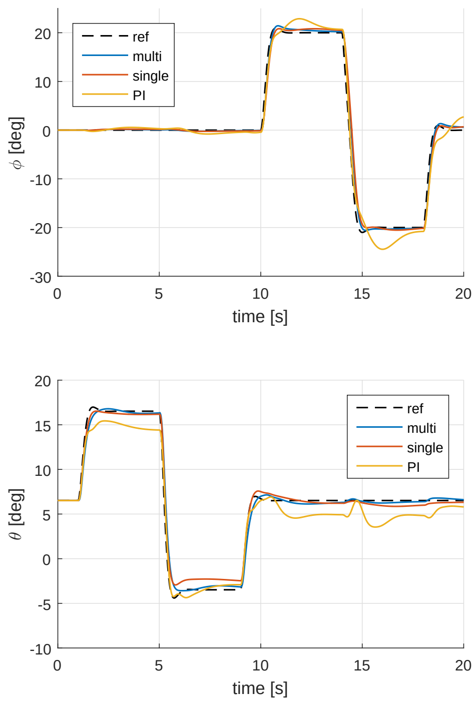

(a) Euler angles ϕ, θ

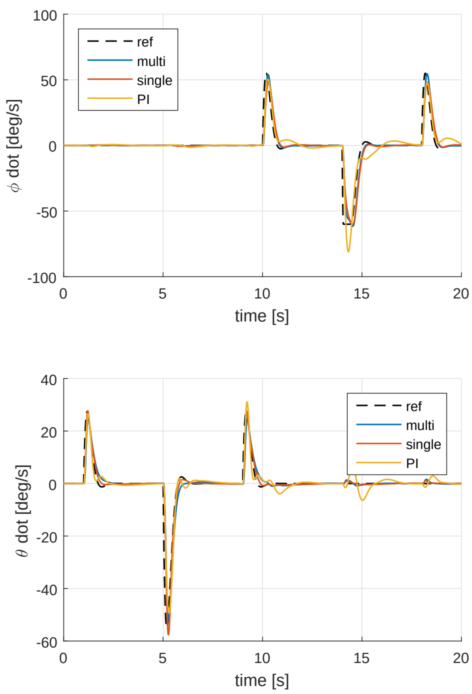

(b) Euler angle derivatives $\dot{\phi}, \dot{\theta}$

Figure 4-24: Tracking response of INDI the multi and single loop control laws for attitude control in the nominal situation without parameter uncertainties.

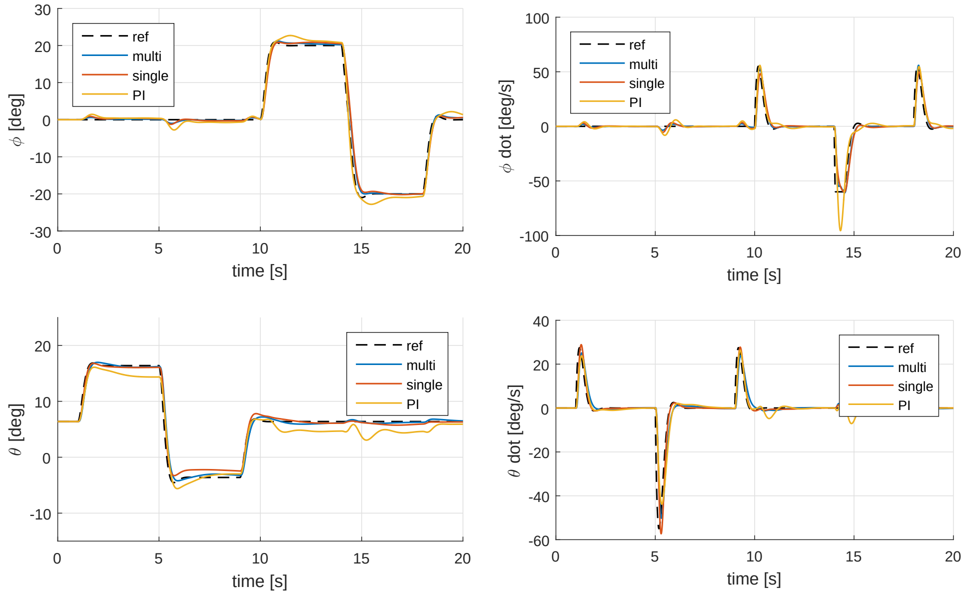

(a) Euler angles ϕ, θ **(b)** Euler angle derivatives $\dot{\phi}, \dot{\theta}$

Figure 4-25: Tracking response of INDI the multi and single loop attitude control laws with parameter uncertainties case B.

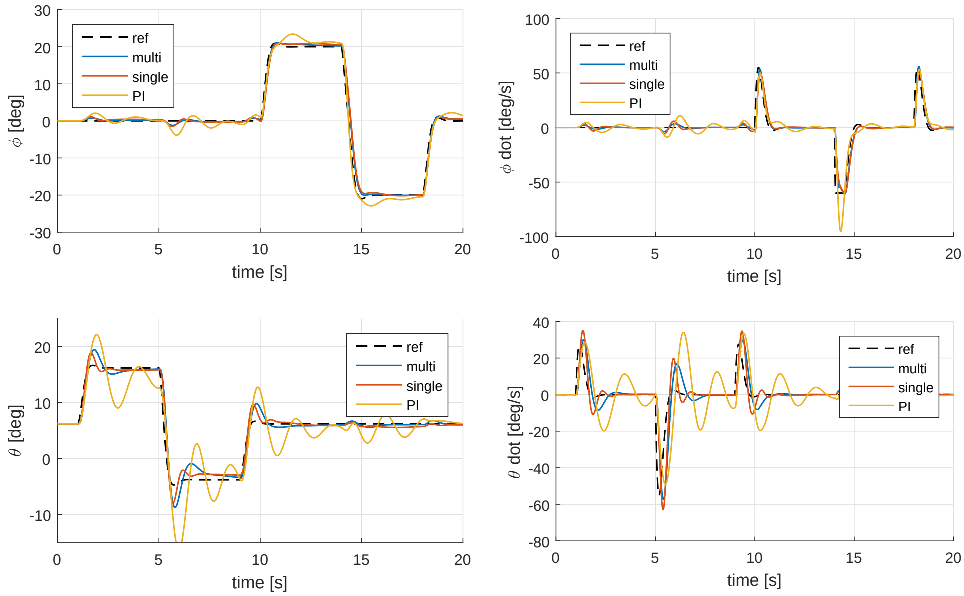

(a) Euler angles ϕ, θ **(b)** Euler angle derivatives $\dot{\phi}, \dot{\theta}$

Figure 4-26: Tracking response of INDI the multi and single loop attitude control laws with parameter uncertainties case C.

As the attitude control problem essentially is an extension to the angular rate control problem without unknown parts (only a kinematic relationship), the analyses done in the first part also apply for the attitude control law, and not much extra analysis was needed to show its applicability. We have presented both a multi-loop as well as an integrated feedback linearization control structure, which have similar performance under the simulation conditions used in this chapter. Simulation results show that even when the aircraft is statically *unstable*, still a stable tracking response is achieved, hence proving its independence to system dynamics.

Chapter 5

Incremental Backstepping for Attitude and Trajectory Flight Control

Backstepping control is a Lyapunov-based method to design a controller for a cascaded non-linear system that has a mathematical foundation for its stability. As backstepping is always performed on a system in strict-feedback form (an affine-in-control cascaded system), it is especially suitable for outer loop flight control designs. This chapter presents both an aerodynamic attitude controller (section 5-1) and a longitudinal trajectory controller (section 5-2). Essentially, the latter is an extension of the former, but it is different compared to a usual approach because the outer loop dynamics have been written in an incremental form.

5-1 Attitude control of aerodynamic angles

When dealing with fixed-wing aircraft, it is more appropriate to control the aerodynamic angle of attack α rather than its body pitch angle θ. The angle of attack directly influences the amount of lift generated by the wings, hence it determines the load factor and the change of flight path. In the lateral direction, the bank angle μ determines the part of the lift used for lateral acceleration.

A backstepping control law will be derived to track angle of attack α, roll angle ϕ and side slip angle β (which needs to be kept zero). Instead of the bank angle μ, the roll angle ϕ will be tracked. Tracking the aerodynamic bank angle involves complex kinematic transformations and hence makes the control law unnecessarily complex. However, the bank angle ϕ is in most cases very similar to the roll angle ϕ.

We define the output state and reference signal by:

$$\mathbf{x}_2 = \begin{bmatrix} \phi \\ \alpha \\ \beta \end{bmatrix}, \quad \mathbf{x}_{2,ref} = \begin{bmatrix} \phi \\ \alpha \\ \beta \end{bmatrix}_{ref} \tag{5-1}$$

5-1-1 Equations of motion

To derive the dynamics from the model dynamics presented in section 3-2, we need to apply a coordinate transformation:

$$
\begin{aligned}
V &= \sqrt{u^2+v^2+w^2} & & u &= V\cos\alpha\cos\beta \\
\alpha &= \arctan\frac{w}{u} & \Leftrightarrow\quad & v &= V\sin\beta \\
\beta &= \arcsin\frac{v}{V} & & w &= V\sin\alpha\cos\beta
\end{aligned}
\tag{5-2}
$$

Time derivatives are:

$$
\begin{aligned}
\dot{V} &= \frac{u\dot{u}+v\dot{v}+w\dot{w}}{V} \\
\dot{\alpha} &= \frac{u\dot{w}-w\dot{u}}{u^2+w^2} \\
\dot{\beta} &= \frac{\dot{v}V-v\dot{V}}{V^2\cos\beta}
\end{aligned}
\tag{5-3}
$$

Substituting $\dot{u},\dot{v},\dot{w}$ from Equation 3-8 yields:

$$
\begin{aligned}
\dot{V} &= u\Big(rv-qw+\frac{F_T}{m}+\frac{\bar{X}^b}{m}-g\sin\theta\Big)+w\Big(qu-pv+\frac{\bar{Z}^b}{m}+g\cos\phi\cos\theta\Big)+ \\
&\quad +v\Big(pw-ru+\frac{\bar{Y}^b}{m}+g\cos\theta\sin\phi\Big) \\
\dot{\alpha} &= -\frac{1}{u^2+w^2}\Bigg(w\big[rv-qw+\frac{F_T}{m}+\frac{\bar{X}^b}{m}-g\sin\theta\big]- \\
&\quad -u\big[qu-pv+\frac{\bar{Z}^b}{m}+g\cos\phi\cos\theta\big]\Bigg) \\
\dot{\beta} &= \frac{-1}{V^2\cos\beta}\Bigg(v\Big[u\big(rv-qw+\frac{F_T}{m}+\frac{\bar{X}^b}{m}-g\sin\theta\big)+w\big(qu-pv+\frac{\bar{Z}^b}{m}+g\cos\phi\cos\theta\big)+ \\
&\quad +v\big(pw-ru+\frac{\bar{Y}^b}{m}+g\cos\theta\sin\phi\big)\Big]-V\Big[pw-ru+\frac{\bar{Y}^b}{m}+g\cos\theta\sin\phi\Big]\Bigg)
\end{aligned}
$$

Which can be simplified to yield the equations of motion in the transformed coordinates:

$$
\dot{V} = \frac{1}{m}\big[\bar{X}^b\cos\alpha\cos\beta+\bar{Y}^b\sin\beta+\bar{Z}^b\sin\alpha\cos\beta+F_T\cos\alpha\cos\beta+mg_1\big] \tag{5-4a}
$$

$$
\dot{\alpha} = q-p\cos\alpha\tan\beta-r\sin\alpha\tan\beta+\frac{1}{mV\cos\beta}\big[-\bar{X}^b\sin\alpha+\bar{Z}^b\cos\alpha-F_T\sin\alpha+mg_3\big] \tag{5-4b}
$$

$$
\dot{\beta} = p\sin\alpha-r\cos\alpha+\frac{1}{mV}\big[-\bar{X}^b\cos\alpha\sin\beta+\bar{Y}^b\cos\beta-\bar{Z}^b\sin\alpha\sin\beta-F_T\cos\alpha\sin\beta+mg_2\big] \tag{5-4c}
$$

where g_1, g_2, g_3 are the gravity components, given by:

$$\begin{aligned} g_1 &= g\left(-\cos\alpha\cos\beta\sin\theta + \sin\beta\sin\phi\cos\theta + \sin\alpha\cos\beta\cos\phi\cos\theta\right) \\ g_2 &= g\left(\cos\alpha\sin\beta\sin\theta + \cos\beta\sin\phi\cos\theta - \sin\alpha\sin\beta\cos\phi\cos\theta\right) \\ g_3 &= g\left(\sin\alpha\sin\theta + \cos\alpha\cos\phi\cos\theta\right) \end{aligned} \tag{5-5}$$

The equations in (5-4) are effectively the force equations in the aerodynamic reference frame. The terms between brackets are the sum of forces in the aerodynamic reference frame in x, z and y direction, respectively. Those forces can be measured by the accelerometers in the body reference frame:

$$\begin{aligned} A_x &= \frac{\bar{X}^b + F_T}{m} - g\sin\theta \\ A_y &= \frac{\bar{Y}^b}{m} + g\cos\theta\sin\phi \\ A_z &= \frac{\bar{Z}^b}{m} + g\cos\theta\cos\phi \end{aligned} \tag{5-6}$$

The thrust acts in the body x-direction and is primarily used to control the airspeed V. The airspeed is not considered to be a control variable in this section. Also, the airspeed is controlled much slower compared to α and β. Because of these reasons, the thrust F_T appearing in the equations for $\dot{\alpha}$ and $\dot{\beta}$ can be considered as system dynamics rather than control terms. With this definition, the system dynamics of α and β can be fully measured by the accelerometers.

The time derivative of the roll angle was derived in (3-7):

$$\dot{\phi} = p + q\sin\phi\tan\theta + r\tan\theta\cos\phi \tag{5-7}$$

The time derivatives can be gathered to form $\dot{\mathbf{x}}_2$ and the terms can be grouped, while substituting specific forces in the equations for α and β:

$$\begin{aligned} \begin{bmatrix} \dot{\phi} \\ \dot{\alpha} \\ \dot{\beta} \end{bmatrix} = & \begin{bmatrix} 0 \\ \frac{1}{V\cos\beta}\left(A_x\sin\alpha + A_z\cos\alpha\right) \\ \frac{1}{V}\left(A_x\cos\alpha\sin\beta + A_y\cos\beta - A_z\sin\alpha\sin\beta\right) \end{bmatrix} + \\ & \begin{bmatrix} 1 & \sin\phi\tan\theta & \tan\theta\cos\phi \\ -\cos\alpha\tan\beta & 1 & -\sin\alpha\tan\beta \\ \sin\alpha & 0 & -\cos\alpha \end{bmatrix} \begin{bmatrix} p \\ q \\ r \end{bmatrix} \end{aligned} \tag{5-8}$$

This can be rewritten in the form:

$$\dot{\mathbf{x}}_2 = \mathbf{f}_2(\mathbf{x}) + G_2(\mathbf{x})\mathbf{x}_3 \tag{5-9}$$

with:

$$\mathbf{f}_2 = \begin{bmatrix} 0 \\ \frac{1}{V\cos\beta}\left(A_x\sin\alpha + A_z\cos\alpha\right) \\ \frac{1}{V}\left(A_x\cos\alpha\sin\beta + A_y\cos\beta - A_z\sin\alpha\sin\beta\right) \end{bmatrix} \tag{5-10}$$

$$G_2 = \begin{bmatrix} 1 & \sin\phi\tan\theta & \tan\theta\cos\phi \\ -\cos\alpha\tan\beta & 1 & -\sin\alpha\tan\beta \\ \sin\alpha & 0 & -\cos\alpha \end{bmatrix} \tag{5-11}$$

The state $\mathbf{x}_3$ are the rotational rates, for which the dynamics are already described in (4-2) in its full form as:

$$\dot{\mathbf{x}}_3 = \mathbf{f}_3(\mathbf{x}) + \mathbf{g}_3(\mathbf{x}, \mathbf{u}) \tag{5-12}$$

and in incremental form as:

$$\dot{\mathbf{x}}_3 \cong \dot{\mathbf{x}}_{3,0} + A_{3,0}\Delta\mathbf{x} + B_{3,0}\Delta\mathbf{u} \tag{5-13}$$

5-1-2 Incremental backstepping control law

The task of the bacsktepping control law is to track a reference $\mathbf{x}_{2,ref}$, using thrust $F_{T,c}$ and control deflection commands u_e, u_r, u_a as inputs. For the moment, assume the thrust F_T is reached by giving thrust command inputs $F_{T,c}$. On the Ultrastick UAV, throttle commands in the range $[0, 1]$ must be given which translates to a power level for the electrically driven propeller. The system dynamics described by Eqs. (5-9) and (5-12) is in an affine-in-control form. Therefore, a 2-step backstepping control can be derived as follows.

Define the tracking error of the output as:

$$\mathbf{z}_2 = \mathbf{x}_2 - \mathbf{x}_{2,ref} \tag{5-14}$$

The error dynamics are:

$$\dot{\mathbf{z}}_2 = \mathbf{f}_2(\mathbf{x}) + G_2(\mathbf{x})\mathbf{x}_3 - \dot{\mathbf{x}}_{2,ref} \tag{5-15}$$

For the first step, a CLF is defined:

$$V_2 = \frac{1}{2}\mathbf{z}_2^T\mathbf{z}_2 \tag{5-16}$$

Its derivative is:

$$\begin{aligned} \dot{V}_2 &= \mathbf{z}_2^T\dot{\mathbf{z}}_2 \\ &= \mathbf{z}_2^T\left(\mathbf{f}_2 + G_2\mathbf{x}_3 - \dot{\mathbf{x}}_{2,ref}\right) \end{aligned} \tag{5-17}$$

If we define stabilizing functions for F_T and $\mathbf{x}_3$ as

$$\mathbf{x}_{3,ref} = G_2^{-1}\left(-C_2\mathbf{z}_2 - \mathbf{f}_2 + \dot{\mathbf{x}}_{2,ref}\right) \tag{5-18}$$

then the derivative $\dot{V}_2$ yields:

$$\dot{V}_2 = -\mathbf{z}_2^T C_2\mathbf{z}_2 + \mathbf{z}_2^T G_2\mathbf{z}_3 \tag{5-19}$$

The second step is very similar to the INDI control law derived in section 4-2. Augment the CLF to V_3:

$$V_3 = V_2 + \frac{1}{2}\mathbf{z}_3^T\mathbf{z}_3 \tag{5-20}$$

When subsystem 3 is described in incremental form the derivative of V_3 equals:

$$\begin{aligned} \dot{V}_3 &= \dot{V}_2 + \mathbf{z}_3^T\left(\dot{\mathbf{x}}_{3,0} + A_{3,0}\Delta\mathbf{x} + B_{3,0}\Delta\mathbf{u} + \dot{\mathbf{x}}_{3,ref}\right) \\ &= -\mathbf{z}_2^T C_2\mathbf{z}_2 + \mathbf{z}_3^T\left(\dot{\mathbf{x}}_{3,0} + A_{3,0}\Delta\mathbf{x} + B_{3,0}\Delta\mathbf{u} + \dot{\mathbf{x}}_{3,ref} + G_2^T\mathbf{z}_2\right) \end{aligned} \tag{5-21}$$

under the assumption that the system is locally linear so that the Taylor series expansion holds. Then, an incremental control law at this step defined by:

$$\Delta\mathbf{u} = B_{3,0}^{-1}\left(-C_3\mathbf{z}_3 - \dot{\mathbf{x}}_{3,0} - A_{3,0}\Delta\mathbf{x} + \dot{\mathbf{x}}_{3,ref} - G_2^T\mathbf{z}_2\right) \tag{5-22}$$

renders the last CLF negative definite.

5-1-3 Command-filtered incremental backstepping control law

The 2-step backstepping control law in (5-22) is not augmented with command-filters. As such, derivatives of the reference signal $\dot{\mathbf{x}}_{3,ref}$ must be analytically calculated from Equation 5-18. However, this is impossible as the term $\mathbf{f}_3$ depends on accelerometer measurements. Command-filters can be used to obtain time derivatives of the reference signals. The thrust command $F_{T,c}$ does not need to be filtered, as the time derivative is not needed. For the reference signal $\mathbf{x}_{3,ref}$ we define a raw reference $\mathbf{x}^0_{3,ref}$, which is filtered with a second order filter:

$$\mathbf{x}_{3,ref} = \mathrm{CF}\{\mathbf{x}^0_{3,ref}\} \tag{5-23}$$

CF{.} denotes the command-filter, in this case a second order filter:

$$\begin{aligned} \begin{bmatrix} \dot{q}_1 \\ \dot{q}_2 \end{bmatrix} &= \begin{bmatrix} q_2 \\ S_R\big\{2\zeta\omega_n\big(\frac{\omega_n^2}{2\zeta\omega_n} S_M(x^0_{3i,ref} - q_1)\big)\big\} \end{bmatrix} \\ x_{3i,ref} &= q_1 \\ \dot{x}_{3i,ref} &= q_2 \end{aligned} \tag{5-24}$$

With $i = 1, 2, 3$ denoting the elements of $\mathbf{x}_{3,ref}$. Define the compensated tracking error of the attitude state as

$$\bar{\mathbf{z}}_2 = \mathbf{z}_2 - \boldsymbol{\chi}_2 \tag{5-25}$$

where $\boldsymbol{\chi}_2$ is the estimated effect of the command-filter on the tracking error $\mathbf{z}_2$. Its dynamics are defined by a stable filter as

$$\dot{\boldsymbol{\chi}}_2 = -C_2\boldsymbol{\chi}_2 + G_2\left(\mathbf{x}_{3,ref} - \mathbf{x}^0_{3,ref}\right) \tag{5-26}$$

where G_{2,x_3} is again the control effectiveness matrix of the angular rates to the attitude state, defined by the last three rows of G_2. The dynamics of $\bar{\mathbf{z}}_2$ are then given by:

$$\begin{aligned} \dot{\bar{\mathbf{z}}} &= \dot{\mathbf{z}}_2 - \dot{\boldsymbol{\chi}}_2 \\ &= \dot{\mathbf{x}}_2 - \dot{\mathbf{x}}_{2,ref} - \dot{\boldsymbol{\chi}}_2 \\ &= \mathbf{f}_2(\mathbf{x}) + G_2(\mathbf{x})\mathbf{x}_3 - \dot{\mathbf{x}}_{2,ref} + C_2\boldsymbol{\chi}_2 - G_2\left(\mathbf{x}_{3,ref} - \mathbf{x}^0_{3,ref}\right) \end{aligned} \tag{5-27}$$

To derive the raw reference signal $\mathbf{x}^0_{3,ref}$ in the first step using the command-filtered approach, the energy of the compensated tracking errors are considered instead of the real tracking errors. Hence, the CLF from (5-16) is now defined as

$$V_2 = \frac{1}{2}\bar{\mathbf{z}}_2^T\bar{\mathbf{z}}_2 \tag{5-28}$$

and its derivative yields by substitution of (5-27):

$$\begin{aligned} \dot{V}_2 &= \bar{\mathbf{z}}_2^T\dot{\bar{\mathbf{z}}}_2 \\ &= \bar{\mathbf{z}}_2^T\left(\mathbf{f}_2 + G_2\mathbf{x}_3 - \dot{\mathbf{x}}_{2,ref} + C_2\boldsymbol{\chi}_2 - G_2\left(\mathbf{x}_{3,ref} - \mathbf{x}^0_{3,ref}\right)\right) \\ &= \bar{\mathbf{z}}_2^T\left(\mathbf{f}_2 + G_2\mathbf{z}_3 - \dot{\mathbf{x}}_{2,ref} + C_2\boldsymbol{\chi}_2 + G_2\mathbf{x}^0_{3,ref}\right) \\ &= \bar{\mathbf{z}}_2^T\left(\mathbf{f}_2 + G_2\mathbf{x}^0_{3,ref} - \dot{\mathbf{x}}_{2,ref} + C_2\boldsymbol{\chi}_2 + G_2\mathbf{z}_3\right) \end{aligned} \tag{5-29}$$

If the (raw) reference signals for F_T and $\mathbf{x}_3$ are defined as

$$\mathbf{x}_{3,ref}^0 = G_2^{-1}\left(-C_2\mathbf{z}_2 - \mathbf{f}_2 + \dot{\mathbf{x}}_{2,ref}\right) \tag{5-30}$$

then $\dot{V}_2$ yields by substitution:

$$\begin{aligned} \dot{V}_2 &= \bar{\mathbf{z}}_2^T\left(-C_2\mathbf{z}_2 + C_2\boldsymbol{\chi}_2 + G_{2,x_3}\mathbf{z}_3\right) \\ &= -\bar{\mathbf{z}}_2^T C_2\bar{\mathbf{z}}_2 + \bar{\mathbf{z}}_2^T G_2\mathbf{z}_3 \end{aligned} \tag{5-31}$$

If we compare the result with (5-19), it can be seen that the remaining term $\bar{\mathbf{z}}_2^T G_2\mathbf{z}_3$ which has to be compensated for in the second step, has changed. As the control signal of the inner loop is not fed through a command-filter, the derivation for the inner loop remains unchanged. Therefore, the final incremental control law for the control deflection yields:

$$\Delta\mathbf{u} = B_{3,0}^{-1}\left(-C_3\mathbf{z}_3 - \dot{\mathbf{x}}_{3,0} - A_{3,0}\Delta\mathbf{x} + \dot{\mathbf{x}}_{3,ref} - G_2^T\bar{\mathbf{z}}_2\right) \tag{5-32}$$

5-1-4 Simulation results

In Figure 5-1, simulation results are presented, of which the used parameters are stated in Table 5-2. Parameters are varied for the cases that are previously described in Table 4-2 and Table 4-4. It can be seen that the control response for the unstable case (case C) is not well damped, although it should be expected that the system is more or less independent to changing system dynamics because of the acceleration feedback. However, simulations with faster actuators, accelerations filters and with a higher sample rate. Parameters are shown in Table 5-1 and the simulation results are presented in Figure 5-2. It can be seen that the tracking performance is closely related with the speed of the control actions, without changing any tuning parameters of the controller.

Table 5-1: Control parameter changes for the simulation in Figure 5-2

	sim 1 (nominal)	sim 2	sim 3
Sample time T_s [s]	0.02	0.01	0.005
Actuator bandwidth [Hz]	2.5	5	10
Washout filter bandwidth $\omega_{n,f}$[rad/s]	12	20	25

5-2 Trajectory control

For the trajectory control problem, the velocity variables χ, V, γ are the defining variables for the velocity of the aircraft. The aircraft has to be steered in such a way that it will track reference in these variables appropriately. By deriving the time derivatives of these variables, one obtains the force equations, as the time derivative of velocity variables is proportional to a force in the same direction. A schematic showing these variables is given in Figure 5-3.

Table 5-2: Parameters used for the simulations with attitude IBS controllers in Figure 5-1 and Figure 5-2.

Parameter	value
Solver	ode3 Bogacki-Shampine
Sample time	0.02 s
Trim velocity	25 $^{\mathrm{m}}/_{\mathrm{s}}$
Aerodynamics	lookup tables
Motor and propeller inertia	yes
Actuator dynamics	yes, bandwidth 2.5 Hz
Sensor noise	no
Sensor dynamics	no
Control law	Equation 4-64 and Equation 4-49
Attitude command shaping	$\omega_n = 10\,{}^{\mathrm{rad}}/_{\mathrm{s}}, \zeta = 0.7$, rate limit 40 $^{\mathrm{deg}}/_{\mathrm{s}}$
Angular accelerations	first order washout filter, $\omega_n = 12\,{}^{\mathrm{rad}}/_{\mathrm{s}}$
C_2	$\mathrm{diag}([3, 5, 1])$
$C_{2,d}$	$\mathrm{diag}([1, 1, 0])$
C_3	$\mathrm{diag}([6, 8, 2])$

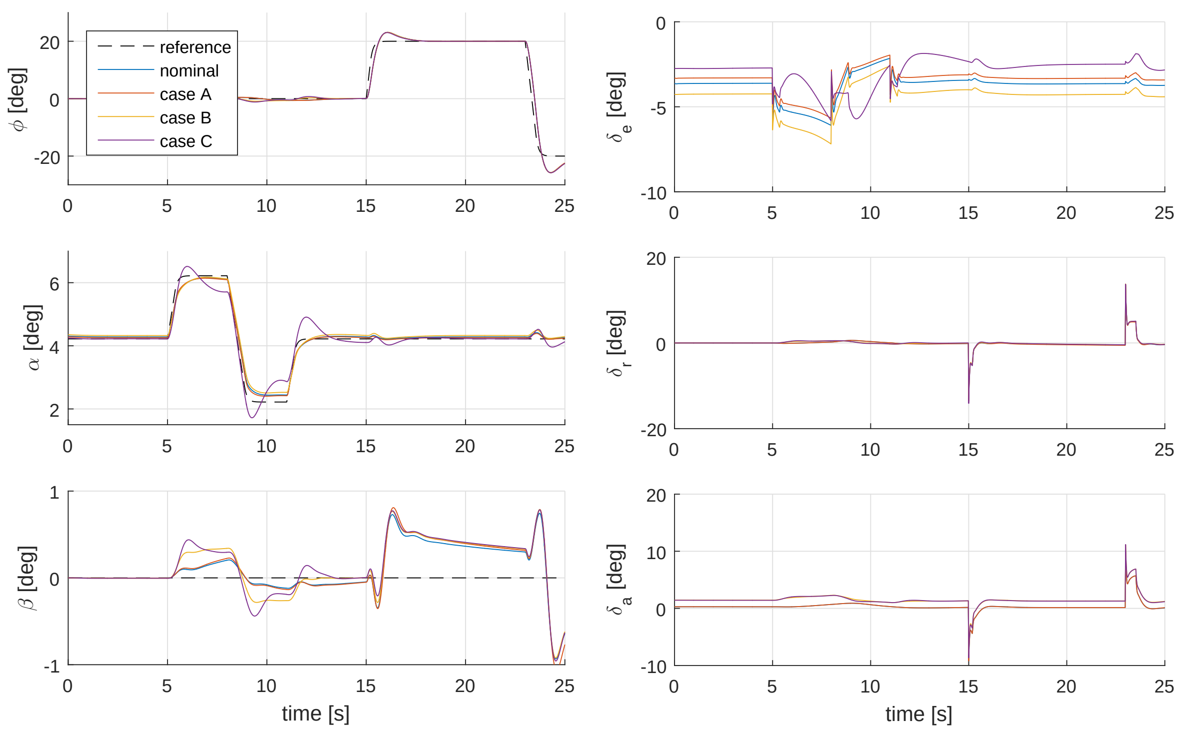

Figure 5-1: IBS aerodynamic attitude controller response

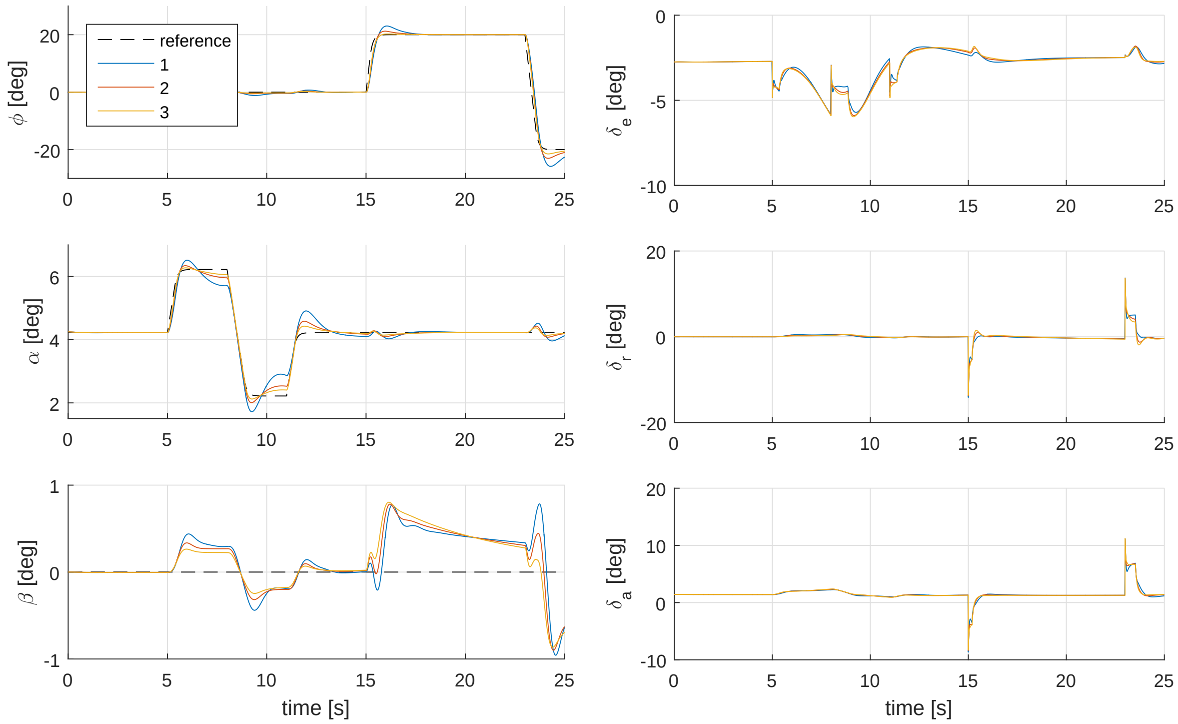

Figure 5-2: IBS aerodynamic attitude controller response for parameter uncertainty case C, with increasing sampling rate, faster actuators and faster acceleration filter (but with identical gains)

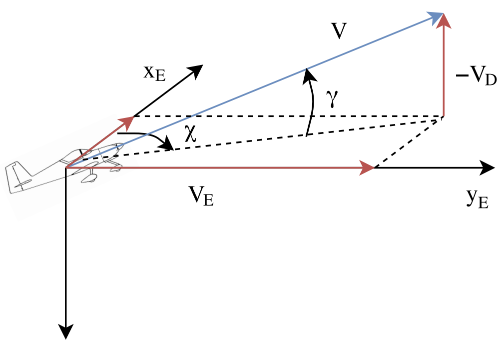

Figure 5-3: Flight path angles γ and χ (course) and total speed V_T, setting up the aircrafts speed vector to be controlled in outer loop control.

5-2-1 Equations of motion

In the NED reference frame we apply the general equations of motion for a constant mass:

$$\frac{\mathbf{F}^e}{m} = \frac{d\mathbf{V}^e}{dt} \tag{5-33}$$

And we transform the coordinates to the velocity frame (denoted by superscript v), obtained by the Euler angle rotations from the NED reference frame over χ and γ:

$$\frac{\mathbf{F}^v}{m} = \mathbb{T}_{ve}(\gamma, \chi)\frac{d\mathbf{V}^e}{dt} \tag{5-34}$$

Because the velocity vector is always aligned with the x-axis of the velocity frame, an increment $d\mathbf{V}^e$ yields dV, $d\gamma$, $d\chi$. It follows that:

$$\begin{bmatrix} dV \\ V\cos\gamma d\chi \\ -V d\gamma \end{bmatrix} = \mathbb{T}_{ve}(\gamma, \chi) d\mathbf{V}^e \tag{5-35}$$

Therefore, the time derivatives follow:

$$\begin{bmatrix} \dot{V} \\ \dot{\chi} \\ \dot{\gamma} \end{bmatrix} = \begin{bmatrix} 1 & & \\ & \frac{1}{V\cos\gamma} & \\ & & -\frac{1}{V} \end{bmatrix} \mathbb{T}_{ve}(\gamma, \chi)\frac{d\mathbf{V}^e}{dt} \tag{5-36}$$

Substituting (5-34) yields:

$$\begin{bmatrix} \dot{V} \\ \dot{\chi} \\ \dot{\gamma} \end{bmatrix} = \begin{bmatrix} 1 & & \\ & \frac{1}{V\cos\gamma} & \\ & & -\frac{1}{V} \end{bmatrix} \frac{\mathbf{F}^v}{m} \tag{5-37}$$

Where $\mathbf{F}^v = \begin{bmatrix} F_x^v & F_y^v & F_z^v \end{bmatrix}^T$ is the sum of forces expressed in the velocity frame components. The aerodynamic forces are split up in lift, drag and side force in the aerodynamic frame:

$$\mathbf{F}_a^v = \mathbb{T}_{vw}(\mu) \begin{bmatrix} -D \\ Y \\ -L \end{bmatrix} = \begin{bmatrix} 1 & 0 & 0 \\ 0 & \cos\mu & -\sin\mu \\ 0 & \sin\mu & \cos\mu \end{bmatrix} \begin{bmatrix} -D \\ Y \\ -L \end{bmatrix} \tag{5-38}$$

The thrust force is assumed to act in the body x-axis:

$$\mathbf{F}_T^v = \mathbb{T}_{vw}(\mu)\mathbb{T}_{wb}(\alpha, \beta) \begin{bmatrix} F_T \\ 0 \\ 0 \end{bmatrix} \tag{5-39}$$

And the gravitational force:

$$\mathbf{F}_g^v = \mathbb{T}_{ve}(\chi, \gamma) \begin{bmatrix} 0 \\ 0 \\ mg \end{bmatrix} \tag{5-40}$$

This yields by substition in (5-37)

$$\begin{aligned}
\begin{bmatrix}\dot{V}\\ \dot{\chi}\\ \dot{\gamma}\end{bmatrix} &= \begin{bmatrix}\frac{1}{m} & & \\ & \frac{1}{mV\cos\gamma} & \\ & & -\frac{1}{mV}\end{bmatrix}\left(\mathbf{F}_a^v + \mathbf{F}_T^v + \mathbf{F}_g^v\right)\\
&= \begin{bmatrix}\frac{1}{m} & & \\ & \frac{1}{mV\cos\gamma} & \\ & & -\frac{1}{mV}\end{bmatrix}\left(\mathbb{T}_{vw}(\mu)\begin{bmatrix}-D\\ Y\\ -L\end{bmatrix} + \mathbb{T}_{vw}(\mu)\mathbb{T}_{wb}(\alpha,\beta)\begin{bmatrix}F_T\\ 0\\ 0\end{bmatrix} + \mathbb{T}_{ve}(\chi,\gamma)\begin{bmatrix}0\\ 0\\ mg\end{bmatrix}\right)\\
&= \begin{bmatrix}\frac{1}{m}\left(-D + F_T\cos\alpha\cos\beta\right) - g\sin\gamma\\ \frac{1}{mV\cos\gamma}\left(Y\cos\mu + L\sin\mu + F_T(\sin\alpha\sin\mu - \cos\alpha\cos\mu\sin\beta)\right)\\ -\frac{1}{mV}\left(L\cos\mu - Y\sin\mu + F_T(\cos\mu\sin\alpha + \cos\alpha\sin\beta\sin\mu)\right) - \frac{g}{V}\cos\gamma\end{bmatrix}
\end{aligned} \tag{5-41}$$

Alternatively, we can express (5-37) into a form to calculate the derivatives using accelerometer measurments. This is possible because linear accelerometers measure the specific forces in body frame, excluding the gravity:

$$\mathbf{A}^b_{x,y,z} = \frac{\sum \mathbf{F}^b}{m} - \mathbf{g} = \frac{\mathbf{F}^b_{a+T}}{m} \tag{5-42}$$

This yields

$$\begin{bmatrix}\dot{V}\\ \dot{\chi}\\ \dot{\gamma}\end{bmatrix} = \begin{bmatrix}1 & & \\ & \frac{1}{V\cos\gamma} & \\ & & -\frac{1}{V}\end{bmatrix}\left(\mathbb{T}_{vb}(\mu,\alpha,\beta)\mathbf{A}^b_{x,y,z} + \mathbb{T}_{ve}(\gamma,\chi)\begin{bmatrix}0\\ 0\\ g\end{bmatrix}\right) \tag{5-43}$$

5-2-2 Command-filtered incremental backstepping control law for longitudinal control

In this section, an incremental control law will be derived to control the aircrafts airspeed, V and the flight path angle γ. It uses command filters between each step in order to constrain the intermediate reference signals and to retrieve the time derivatives of those reference signals. The heading angle remains uncontrolled, but the roll angle ϕ and side slip angle β are controlled similar to the attitude backstepping control law presented in section 5-1.

Represent the state and tracking error to be controlled as:

$$\mathbf{y} = \begin{bmatrix}V\\ \gamma\\ \phi\\ \beta\end{bmatrix}, \quad \mathbf{y}_{ref} = \begin{bmatrix}V\\ \gamma\\ \phi\\ \beta\end{bmatrix}_{ref} \tag{5-44}$$

We start of by considering only the outer loop states V and γ. The control of the other two outputs ϕ and β will be treated in the second step.

Outer loop

The state and tracking error of the outer loop is defined as:

$$\mathbf{x}_1 = \begin{bmatrix}V\\ \gamma\end{bmatrix}, \quad \mathbf{z}_1 = \mathbf{x}_1 - \mathbf{x}_{1,ref} \tag{5-45}$$

The compensated tracking error is:

$$\bar{\mathbf{z}}_1 = \mathbf{z}_1 - \boldsymbol{\chi}_1 \tag{5-46}$$

The term $\boldsymbol{\chi}_1$ is a compensation for the effect the command-filter has on the tracking error. The dynamics of $\boldsymbol{\chi}_1$ will be defined later. Write the system dynamics of $\mathbf{x}_1$ in its general form as:

$$\dot{\mathbf{x}}_1 = \mathbf{f}_1(\mathbf{x}) + \mathbf{g}_1(\mathbf{x}, \delta_t, \alpha) \tag{5-47}$$

Where $\mathbf{x}$ represents the total state of the aircraft. The (virtual) inputs considered in this loop are the throttle δ_t and the aerodynamic angle of attack α. From Equation 5-41 $\mathbf{f}_1$ and $\mathbf{g}_1$ can be identified. For this, the lift force is split up into a static part L_0, and a part dependant on α, denoted by L_α, such that $L = L_0 + L_\alpha(\alpha)$.

$$\mathbf{f}_1 = \begin{bmatrix} \frac{1}{m}(-D) - g\sin\gamma \\ \frac{1}{mV}(L_0\cos\mu - Y\sin\mu) - \frac{g}{V}\cos\gamma \end{bmatrix} \tag{5-48a}$$

$$\mathbf{g}_1 = \begin{bmatrix} \frac{1}{m}F_T\cos\alpha\cos\beta \\ \frac{1}{mV}(L_\alpha(\alpha)\cos\mu + F_T(\cos\mu\sin\alpha + \cos\alpha\sin\beta\sin\mu)) \end{bmatrix} \tag{5-48b}$$

The thrust F_T is controlled by the throttle setting δ_t. Those dynamics can be approximated by first order actuator dynamics and are modeled as such. The bandwidth of these dynamics is around 1.7 Hz, depending on the airspeed and air density. When the actuator dynamics are neglected in a similar way as with the actuator dynamics of the control surface deflection, we can describe the thrust as some nonlinear function of the throttle setting, $F_T = f(\delta_t)$. This relationship also depends on the airspeed and the air density.

When aiming to control the airspeed and flight path angle $[V, \gamma]$ using the throttle δ_t and the angle of attack α, there are two reasons why the system described by Equation 5-47 might benefit from a description into an incremental form. First of all, the system is (in general) non-affine in control, as $L(\alpha)$ and $F(\delta_t)$ are not necessarily linear functions, hence $\mathbf{g}_1(\mathbf{x}, \delta_t, \alpha)$ is non-linear. It is possible to use an algebraic inverse of $\mathbf{g}_1$, but for NDI this requires accurate knowledge of the nonlinearity. By using an incremental description, only an estimate of the local partial derivatives $\frac{\partial \mathbf{g}_1}{\partial \delta_t}$ and $\frac{\partial \mathbf{g}_1}{\partial \alpha}$ are necessary. Secondly, writing the system in incremental form poses the possibility to use the time-scale-separation principle to neglect system dynamics increments, like what is done by the incremental control law in the inner loop. In this way, no knowledge of the static lift L_0 or the aerodynamic drag D is needed.

Writing Equation 5-47 in incremental form by using a taylor series expansion around a recent point t_0 yields:

$$\dot{\mathbf{x}}_1 \approx \dot{\mathbf{x}}_{1,0} + \underbrace{\left(\frac{\partial \mathbf{f}_1}{\partial \mathbf{x}} + \frac{\partial \mathbf{g}_1}{\partial \mathbf{x}}\right)\bigg|_{\mathbf{x}_0, t_0}}_{A_{1,0}} \Delta\mathbf{x} + \underbrace{\begin{bmatrix} \frac{\partial \mathbf{g}_1}{\partial \delta_t} & \frac{\partial \mathbf{g}_1}{\partial \alpha} \end{bmatrix}\bigg|_{\mathbf{x}_0, t_0}}_{B_{1,0}} \begin{bmatrix} \Delta\delta_t \\ \Delta\alpha \end{bmatrix} \tag{5-49}$$

Then, perform the following simplifications:

- Neglect the system dynamics increments $A_{1,0}\Delta\mathbf{x}$ that are due to the increments $\Delta\gamma$ and ΔV.
- Assume that the longitudinal control has only a small effect on the lateral dynamics such that it can be assumed that $\mu \approx \mu_0$, $Y \approx Y_0$ and $\beta \approx \beta_0$. In fact, the only direct effect the longitudinal dynamics have on the lateral dynamics are the gyroscopic effects of the angular momentum of the motor and propeller.

- Lastly, also assume that increments the aerodynamic drag D and the static part of the lift L_0 are small and or slow in comparison to the control increments. It is not immediately clear that this assumption holds, as the static lift is continuously influenced by the elevator deflection δ_e. It must be checked afterwards whether it is valid to make such an assumption.

By applying the assumptions, the entire system dynamics increments $A_{1,0}\Delta\mathbf{x}$ can be considered small in comparison with $B_{1,0}[\Delta\delta_t, \Delta\alpha]^T$. (5-49) can then be written as:

$$\dot{\mathbf{x}}_1 \approx \dot{\mathbf{x}}_{1,0} + B_{1,0}\begin{bmatrix}\Delta\delta_t \\ \Delta\alpha\end{bmatrix} \tag{5-50}$$

Referring again to (5-49), the elements of $B_{1,0}$ are given by partial derivatives of $\mathbf{g}_1$:

$$\frac{\partial \mathbf{g}_1}{\partial \delta_t} = \begin{bmatrix} \frac{1}{m}\frac{\partial F_T}{\partial \delta_t}\cos\alpha\cos\beta \\ \frac{1}{mV}\frac{\partial F_T}{\partial \delta_t}(\cos\mu\sin\alpha + \cos\alpha\sin\beta\sin\mu) \end{bmatrix} \tag{5-51a}$$

$$\frac{\partial \mathbf{g}_1}{\partial \alpha} = \begin{bmatrix} -\frac{1}{m}F_T\sin\alpha\cos\beta \\ \frac{1}{mV}\frac{\partial L_\alpha(\alpha)}{\partial \alpha}\cos\mu + F_T(\cos\mu\cos\alpha - \sin\alpha\sin\beta\sin\mu) \end{bmatrix} \tag{5-51b}$$

$$\begin{aligned} B_{1,0} &= \left.\begin{bmatrix}\frac{\partial \mathbf{g}_1}{\partial \delta_t} & \frac{\partial \mathbf{g}_1}{\partial \alpha}\end{bmatrix}\right|_{\mathbf{x}_0,t_0} \\ &= \left.\begin{bmatrix} \frac{1}{m}\frac{\partial F_T}{\partial \delta_t}\mathrm{c}\alpha\mathrm{c}\beta & -\frac{1}{m}F_T\mathrm{s}\alpha\mathrm{c}\beta \\ \frac{1}{mV}\frac{\partial F_T}{\partial \delta_t}(\mathrm{c}\mu\mathrm{s}\alpha + \mathrm{c}\alpha\mathrm{s}\beta\mathrm{s}\mu) & \frac{1}{mV}\frac{\partial L_\alpha(\alpha)}{\partial \alpha}\mathrm{c}\mu + F_T(\mathrm{c}\mu\mathrm{c}\alpha - \mathrm{s}\alpha\mathrm{s}\beta\mathrm{s}\mu) \end{bmatrix}\right|_{\mathbf{x}_0,t_0} \end{aligned} \tag{5-52}$$

in which we used $\mathrm{c}x = \cos x$ and $\mathrm{s}x = \sin x$ as shorthand notation. The model-dependent parts of this matrix must be estimated in order to be able to use this matrix in the control law. The model-dependent parts are:

- The throttle-to-thrust term $\partial F_T/\partial\delta_t$.
- The lift-curve slope $\partial L_\alpha(\alpha)/\partial\alpha$, determined by its nondimensional coefficient C_{L_α}. Usually, this value is fairly constant over α.
- The total thrust F_T. It is often not so easy to have accurate knowledge of the total thrust.

The backstepping control law is derived by defining the first CLF as:

$$V_1(\bar{\mathbf{z}}_1) = \frac{1}{2}\bar{\mathbf{z}}_1^T\bar{\mathbf{z}}_1 \tag{5-53}$$

Where V_1 should not be confused with the airspeed V. Its time derivative can be approximated by substituting Equation 5-50:

$$\dot{V}_1 = \bar{\mathbf{z}}_1^T\left(\dot{\mathbf{x}}_1 - \dot{\mathbf{x}}_{1,ref} - \dot{\boldsymbol{\chi}}_1\right) \tag{5-54}$$

Now, define the tracking error compensation term $\boldsymbol{\chi}_1$ as:

$$\dot{\boldsymbol{\chi}}_1 = -C_1\boldsymbol{\chi}_1 + B_{1,0}\left(\begin{bmatrix}\delta_t\\ \alpha\end{bmatrix}_{ref} - \begin{bmatrix}\delta_t\\ \alpha\end{bmatrix}_{cmd}\right) \tag{5-55}$$

In which C_1 is the gain of the outer loop. Then, substition into (5-54) yields:

$$\begin{aligned}
\dot{V}_1 &= \bar{\mathbf{z}}_1^T\left\{\dot{\mathbf{x}}_1 - \dot{\mathbf{x}}_{1,ref} + C_1\boldsymbol{\chi}_1 - B_{1,0}\left(\begin{bmatrix}\Delta\delta_t\\ \Delta\alpha\end{bmatrix}_{ref} - \begin{bmatrix}\Delta\delta_t\\ \Delta\alpha\end{bmatrix}_{cmd}\right)\right\}\\
&\approx \bar{\mathbf{z}}_1^T\left\{\dot{\mathbf{x}}_{1,0} + B_{1,0}\begin{bmatrix}\Delta\delta_t\\ \Delta\alpha\end{bmatrix} - \dot{\mathbf{x}}_{1,ref} + C_1\boldsymbol{\chi}_1 - B_{1,0}\left(\begin{bmatrix}\Delta\delta_t\\ \Delta\alpha\end{bmatrix}_{ref} - \begin{bmatrix}\Delta\delta_t\\ \Delta\alpha\end{bmatrix}_{cmd}\right)\right\}\\
&= \bar{\mathbf{z}}_1^T\left\{\dot{\mathbf{x}}_{1,0} + B_{1,0}\begin{bmatrix}\Delta\delta_t\\ \Delta\alpha_{ref}\end{bmatrix} + B_{1,0}\begin{bmatrix}0\\ z_\alpha\end{bmatrix} - \dot{\mathbf{x}}_{1,ref} + C_1\boldsymbol{\chi}_1 - B_{1,0}\left(\begin{bmatrix}\Delta\delta_t\\ \Delta\alpha\end{bmatrix}_{ref} - \begin{bmatrix}\Delta\delta_t\\ \Delta\alpha\end{bmatrix}_{cmd}\right)\right\}\\
&= \bar{\mathbf{z}}_1^T\left\{\dot{\mathbf{x}}_{1,0} + B_{1,0}\begin{bmatrix}\Delta\delta_{t_{cmd}}\\ \Delta\alpha_{cmd}\end{bmatrix} + B_{1,0}\begin{bmatrix}0\\ z_\alpha\end{bmatrix} - \dot{\mathbf{x}}_{1,ref} + C_1\boldsymbol{\chi}_1\right\}
\end{aligned} \tag{5-56}$$

Where we used:

$$\begin{aligned}
\Delta\alpha &= \alpha - \alpha_0\\
&= z_\alpha + \alpha_{ref} - \alpha_0\\
&= z_\alpha + \Delta\alpha_{ref}
\end{aligned} \tag{5-57}$$

And because the throttle δ_t is a real input to the system and not a virtual input like α, we have $\delta_t = \delta_{t_{ref}}$ and only a term with z_α appears in the last equation.

Stabilizing functions for $\Delta\delta_{t_{cmd}}$ and $\Delta\alpha_{cmd}$ to provide asymptotic stability can now be designed:

$$\begin{bmatrix}\Delta\delta_{t_{cmd}}\\ \Delta\alpha_{cmd}\end{bmatrix} = B_{1,0}^{-1}\left(-C_1\mathbf{z}_1 - \dot{\mathbf{x}}_1 + \dot{\mathbf{x}}_{1,ref}\right) - \boldsymbol{\chi}_1 \tag{5-58}$$

with C_1 a diagonal matrix with each element positive definite. In this intermediate control law, an estimate of $B_{1,0}$ must be used. Furthermore, a measurement of $\dot{\mathbf{x}}_1$ must be available. It can be calculated using (5-43), which means that $\dot{\mathbf{x}}_1$ is dependent on accelerometer measurements and knowledge of the aerodynamic attitude. when we use $\alpha_{ref} = \alpha_0 + \Delta\alpha_{ref}$ as intermediate control law. Substition of the stabilizing functions into (5-56) then yields:

$$\begin{aligned}
\dot{V}_1 &= \bar{\mathbf{z}}_1^T\left\{-C_1\mathbf{z}_1 + B_{1,0}\begin{bmatrix}0\\ z_\alpha\end{bmatrix} + C_1\boldsymbol{\chi}_1 - B_{1,0}\boldsymbol{\chi}_1\right\}\\
&= \bar{\mathbf{z}}_1^T\left\{-C_1\bar{\mathbf{z}}_1 + B_{1,0}\begin{bmatrix}0\\ z_\alpha\end{bmatrix} - B_{1,0}\boldsymbol{\chi}_1\right\}\\
&= \bar{\mathbf{z}}_1^T\left\{-C_1\bar{\mathbf{z}}_1 + B_{1,0}\begin{bmatrix}0\\ \bar{z}_\alpha\end{bmatrix}\right\}\\
&= -\bar{\mathbf{z}}_1^T C_1\bar{\mathbf{z}}_1 + \bar{\mathbf{z}}_1^T B_{1,0}\begin{bmatrix}0\\ \bar{z}_\alpha\end{bmatrix}\\
&= -\bar{\mathbf{z}}_1^T C_1\bar{\mathbf{z}}_1 + \bar{\mathbf{z}}_1^T B_{1,0_\alpha}\bar{z}_\alpha
\end{aligned} \tag{5-59}$$

Where $B_{1,0_\alpha}$ is the second column of $B_{1,0}$.

Middle loop

For the middle loop, the state and tracking errors are defined the same as in section 5-1:

$$\mathbf{x}_2 = \begin{bmatrix} \phi \\ \alpha \\ \beta \end{bmatrix}, \quad \mathbf{x}_{2,ref} = \begin{bmatrix} \phi_{ref} \\ \alpha_{ref} \\ \beta_{ref} \end{bmatrix}, \quad \mathbf{z}_2 = \mathbf{x}_2 - \mathbf{x}_{2,ref}, \quad \bar{\mathbf{z}}_2 = \mathbf{z}_2 - \boldsymbol{\chi}_2 \tag{5-60}$$

Referring to (5-9), the dynamics are written as:

$$\dot{\mathbf{x}}_2 = \mathbf{f}_2(\mathbf{x}) + G_2(\mathbf{x})\mathbf{x}_3 \tag{5-61}$$

Continue the backstepping procedure by augmenting the CLF from the previous step:

$$V_2 = V_1 + \frac{1}{2}\bar{\mathbf{z}}_2^T\bar{\mathbf{z}}_2 \tag{5-62}$$

The time derivative equals:

$$\begin{aligned}
\dot{V}_2 &= \dot{V}_1 + \bar{\mathbf{z}}_2^T\left\{\mathbf{f}_2(\mathbf{x}) + G_2\mathbf{x}_3 - \dot{\mathbf{x}}_{2,ref} - \dot{\boldsymbol{\chi}}_2\right\} \\
&= -\bar{\mathbf{z}}_1^T C_1\bar{\mathbf{z}}_1 + \bar{\mathbf{z}}_1^T B_{1,0_\alpha}\bar{z}_\alpha + \bar{\mathbf{z}}_2^T\left\{\mathbf{f}_2(\mathbf{x}) + G_2\mathbf{x}_3 - \dot{\mathbf{x}}_{2,ref} + C_2\boldsymbol{\chi}_2 - G_2\left(\mathbf{x}_{3,ref} - \mathbf{x}_{3,cmd}\right)\right\} \\
&= -\bar{\mathbf{z}}_1^T C_1\bar{\mathbf{z}}_1 + \bar{z}_\alpha B_{1,0_\alpha}^T\bar{\mathbf{z}}_1 + \bar{\mathbf{z}}_2^T\left\{\mathbf{f}_2(\mathbf{x}) + G_2\mathbf{x}_{3,cmd} + G_2\mathbf{z}_3 - \dot{\mathbf{x}}_{2,ref} + C_2\boldsymbol{\chi}_2\right\} \\
&= -\bar{\mathbf{z}}_1^T C_1\bar{\mathbf{z}}_1 + \bar{\mathbf{z}}_2^T\begin{bmatrix} 0 \\ B_{1,0_\alpha}^T \\ 0 \end{bmatrix}\bar{\mathbf{z}}_1 + \bar{\mathbf{z}}_2^T\left\{\mathbf{f}_2(\mathbf{x}) + G_2\mathbf{x}_{3,cmd} + G_2\mathbf{z}_3 - \dot{\mathbf{x}}_{2,ref} + C_2\boldsymbol{\chi}_2\right\} \\
&= -\bar{\mathbf{z}}_1^T C_1\bar{\mathbf{z}}_1 + \bar{\mathbf{z}}_2^T\left\{\mathbf{f}_2(\mathbf{x}) + G_2\mathbf{x}_{3,cmd} + G_2\mathbf{z}_3 - \dot{\mathbf{x}}_{2,ref} + C_2\boldsymbol{\chi}_2 + \begin{bmatrix} 0 \\ B_{1,0_\alpha}^T \\ 0 \end{bmatrix}\bar{\mathbf{z}}_1\right\}
\end{aligned} \tag{5-63}$$

Stabilizing functions for the angular rates $\mathbf{x}_3$ can now be designed:

$$\mathbf{x}_{3,ref} = G_2^{-1}\left(-C_2\mathbf{z}_2 - \mathbf{f}_2 + \dot{\mathbf{x}}_{2,ref} - \begin{bmatrix} 0 \\ B_{1,0_\alpha}^T \\ 0 \end{bmatrix}\bar{\mathbf{z}}_1\right) - \boldsymbol{\chi}_3 \tag{5-64}$$

Similar to (5-31), substitution into (5-63) yields:

$$\dot{V}_2 = -\bar{\mathbf{z}}_1^T C_1\bar{\mathbf{z}}_1 - \bar{\mathbf{z}}_2^T C_2\bar{\mathbf{z}}_2 + \bar{\mathbf{z}}_2^T G_2\bar{\mathbf{z}}_3 \tag{5-65}$$

As the control gain C_2 is again a diagonal matrix with positive definite elements, only the last term in this result needs to be canceled out in the next step. This term is exactly the same as for the backstepping control law in section 5-1. Therefore, the last step of this backstepping procedure is the same.

Inner loop

The inner loop state and tracking errors and inputs are defined equivalent to the definitions in previous sections:

$$\mathbf{x}_3 = \begin{bmatrix} p \\ q \\ r \end{bmatrix}, \quad \mathbf{x}_{3,ref} = \begin{bmatrix} p \\ q \\ r \end{bmatrix}_{ref}, \quad \mathbf{z}_3 = \mathbf{x}_3 - \mathbf{x}_{3,ref}, \quad \mathbf{u} = \begin{bmatrix} \delta_e \\ \delta_r \\ \delta_a \end{bmatrix} \tag{5-66}$$

so that the incremental backstepping control law for the control surface deflections has the same structure as in (5-22):

$$\Delta \mathbf{u} = B_{3,0}^{-1} \left(-C_3 \mathbf{z}_3 - \dot{\mathbf{x}}_{3,0} + \dot{\mathbf{x}}_{3,ref} - G_2^T \bar{\mathbf{z}}_2 \right) \tag{5-67}$$

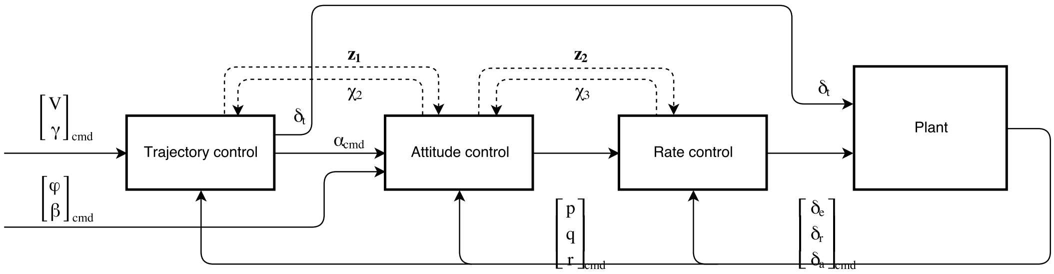

Figure 5-4: Overview of the total IBS control loop for longitudinal trajectory control

5-2-3 Simulation results

In Figure 5-5 and Figure 5-5 simulation results of the incremental backstepping flight path angle controller is shown, at an aispeed of 25 m/s. The first figure displays the effect of uncertainties in the lift curve slope, by scaling this parameter in the control law with a factor F. Underestimation of the lift curve slope leads to instability, although overestimation merely causes the control law to behave less aggressive. This effect is in line with the effect of scaling the inner loop control effectiveness for incremental angular rate control. The second figure shows the effect of parameter uncertainties, again by the different cases discussed in the previous sections. It can be seen that the flight path angle is tracked while while maintaining airspeed.

5-3 Conclusion

Backstepping control laws for the attitude stabilization and flight path control of fixed wing aicraft are derived, using an incremental control loop, very similar to the inner loop of the INDI control laws presented in chapter 4.

Simulation results of the aerodynamic attitude control law show that robustness is achieved that is similar to the euler attitude control responses shown in chapter 4. This indicates the applicability of the control laws for flight tests on the FASER UAV, if the aerodynamic state can be measured. It also shows that backstepping is a convenient procedure to design stable cascaded control structures without the need to assume time-scale separation between the control loops.

The incremental form can also be used in outer control loops, such as the incremental control of velocity and flight path angle via throttle and angle of attack, so that stable, nonlinear flight control laws with complete cancelling of system dynamics can be derived without requiring much extra knowledge of the model parameters.

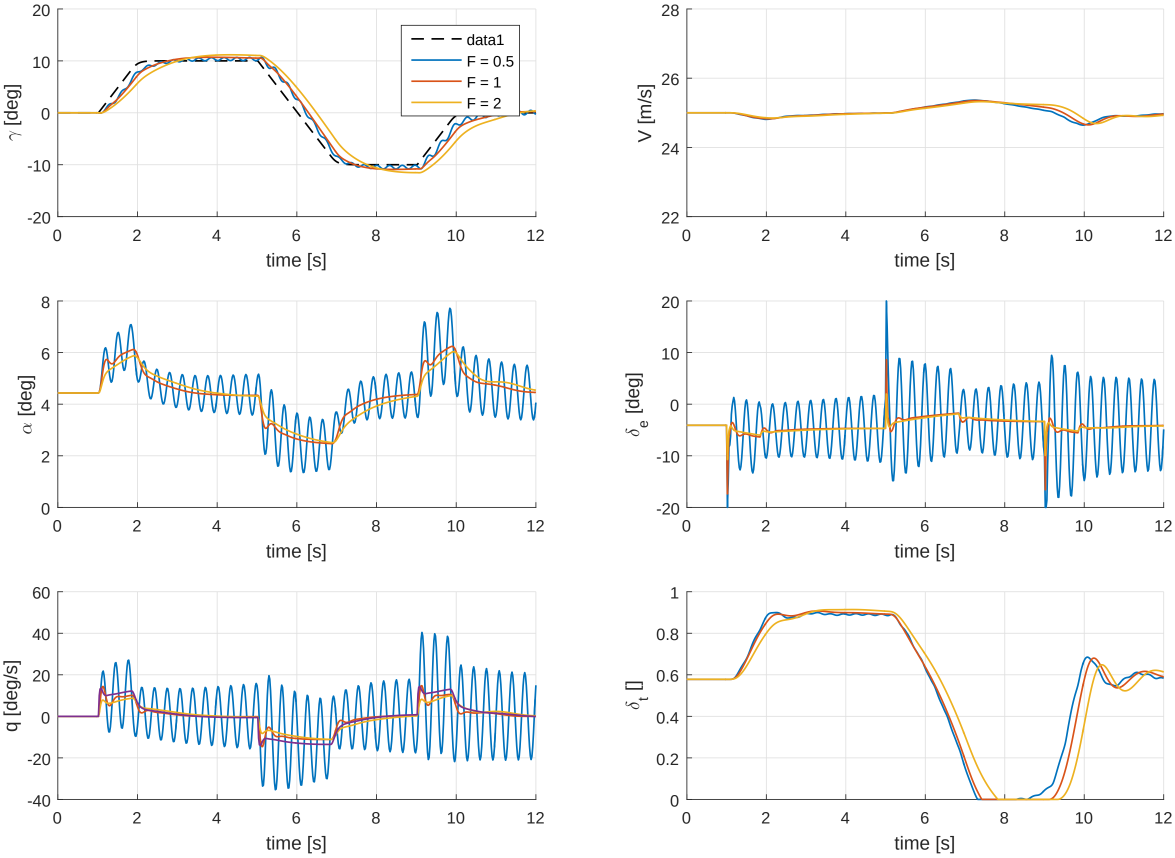

Figure 5-5: Nominal flight path angle tracking response with scaled estimates of C_{L_α} in the controller. F is the scaling factor.

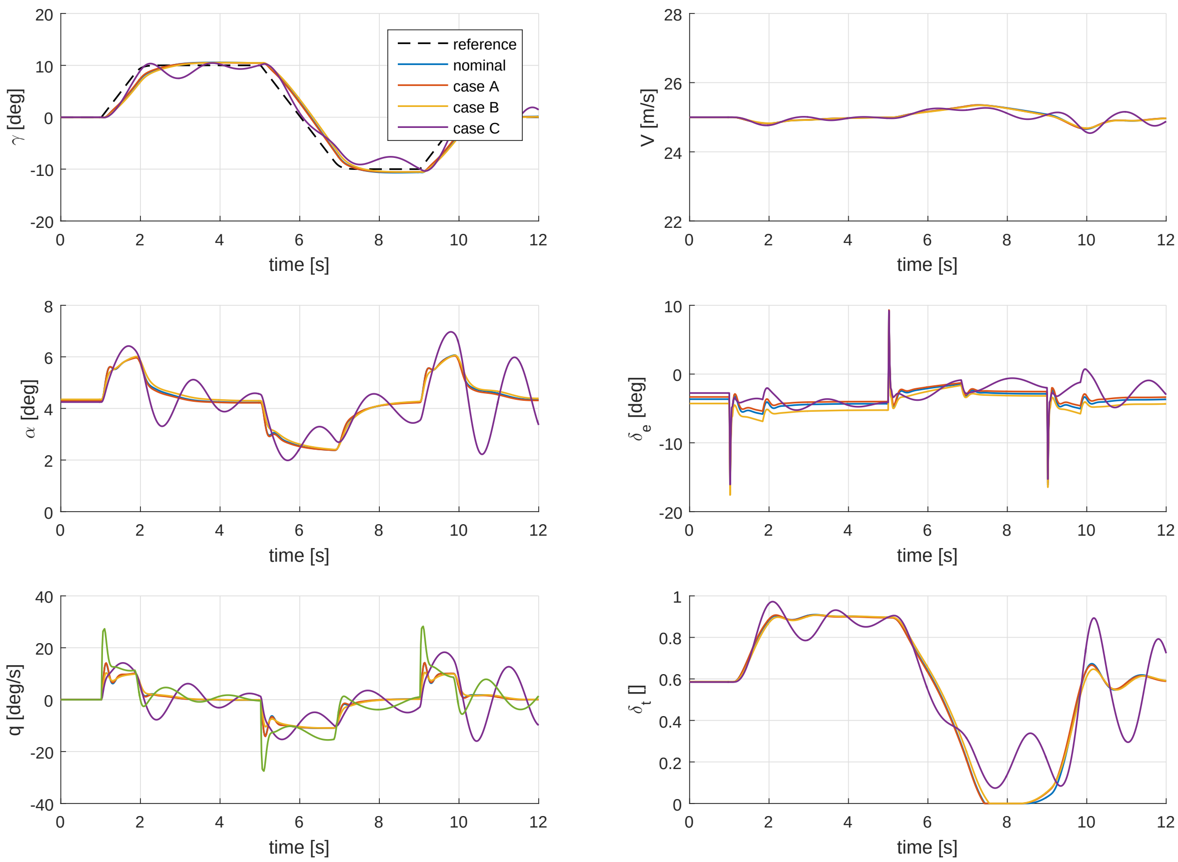

Figure 5-6: Flight path angle tracking response with with aerodynamic parameter variations according to the cases of Table 4-4.

Chapter 6

Conclusion and Recommendations

6-1 Conclusion

In the context of fault-tolerant flight control (FTFC), incremental control methods have been proposed previously in literature for the stabilization of the aircraft attitude or angular rates. Both IBS and INDI control techniques show high potential by simulation on fixed wing aircraft. The work presented in this thesis brings the scientific community a small step further on the road to resilient, fault-tolerant flight control methods, by presenting the design, analysis, implementation and flight testing of INDI and IBS methods. Based on the analysis presented the preliminary thesis, the following conclusions can be drawn

- Focusing on the inner loop angular rate control, it can be concluded that incremental control methods do not perfectly invert the system dynamics when the system dynamics increment is not taken into account. This is shown by steady state tracking errors that occur as a result of these system dynamics increments. Because the effect is directly related to the aerodynamic stability and damping parameters of the aircraft, this should apply to all fixed-wing aircraft that have similar configurations.
- The tracking errors due to an imperfect dynamic inversion are directly correlated with the total increment delay. With the current design, the increment delay contains the delay of the angular acceleration measurement, an additional controller delay, and the actuator delays. Decreasing these delays, by for example increasing the bandwidth of the actuators, shows the same positive effect on the tracking errors in all cases. This is shown in simulation examples for the inner loop angular rate control, but also for the IBS aerodynamic attitude controller on a statically unstable aircraft. Hence, faster actuators, higher sample rates and shorter measurement delays are key factors for a better tracking performance.
- Similarities of incremental NDI with classical PI(D) control exist. First of all, when not considering actuators, the gains of a PI control law in incremental form can be related to parameters of an INDI control law. They can also be related to incremental

feedback linearization, which is essentially a nonlinear dynamic inversion control of a second-order system with a relative degree of two. Secondly, an intuitive derivation that can be supported by block diagrams shows a similar (but mathematically less sound) result. This derivation uses the total, non-incremental form of a PID controller. When actuators are included and can be approximated by first-order dynamics, very similar results can be obtained.

- The backstepping procedure in combination with incremental control is a systematic method, very useful for the typical cascaded control structure appearing in flight control applications. Using the backstepping method, stable control laws are derived. Using incremental forms of the system dynamics, its dependency on model is reduced at the cost of requiring a feedback of the state derivative. From simulations of flight path angle control it can be concluded that the use of an incremental control method is not restricted to the inner control loop.

Additionally, the work in the scientific paper completes the thesis by presenting the design, implementation and flight testing of the discussed control laws. Based on these flight test results, additional conclusions can be made.

- Successful, qualitative flight tests are performed with IBS and INDI attitude control laws. Results clearly show that both controllers perform well. It is for the first time that results of real flight tests with IBS attitude control laws for fixed-wing aircraft are reported in literature.
- The presented design of IBS and INDI control laws for the attitude control of fixed-wing aircraft has been validated by showing that the controller response is according to its specifications: with nominal estimates of the control effectiveness parameters, the observed closed loop system has the capability of tracking the imposed reference dynamics and hence canceling its system dynamics.
- The INDI Euler attitude control flight results show stable and decoupled responses with an accurate tracking. The IBS aerodynamic attitude control flight results validate the longitudinal mode to a limited manner. Small doublets in angle of attack can be followed clearly. Both control laws show that they can be used over a wide range of airspeeds. Flight test results on the lateral mode also indicate that the control laws behave as expected, but are not tested yet with nominal settings.
- For the presented design and experiment set-up and with the imposed aerodynamic parameter variations, the tracking response of the INDI and IBS control laws are almost identical. It is suspected that the feed-forward of the outer loop tracking error does have little effect.

6-2 Recommendations

As subsequent steps towards incremental nonlinear flight control laws as a successful fault-tolerant flight control system, recommendations are suggested. Also, general points of improvement are proposed regarding the design and implementation of the analyzed control laws.

- The useful properties of incremental control methods rely on high-quality state and state derivative measurements, knowledge of the true actuator position and a fast control action. The value of the current controller design can be increased, by improving the quality of the state measurements. Specifically, this includes a better estimation of the aerodynamic angles α and β, smaller delays of angular acceleration measurement and a higher actuator bandwidth.

- The incremental control law is still dependent on the control effectiveness of the aircraft. The current design can be extended with a model identification module that estimates the control derivatives appearing in the control effectiveness matrix. An adaptation strategy can be implemented to reconfigure the control laws online in the event of system faults. When the control laws are tested in flight with successful parameter adaptations, the aircrafts control laws become (up to certain limitations) entirely independent to its system dynamics.

- Flight tests with realistic fault cases have a great scientific value in terms of validation of the applicability of the incremental control laws as a fault-tolerant flight control system. Faults can include control surface jamming or changed stability properties such as shifts in center of gravity or changes in the lift curve slope determined by C_{L_α}.

- The presented control laws are nonlinear control laws. It has already been shown in this thesis that the control laws behave well over a variety of flight conditions (different airspeeds), but the control laws have been used mainly in the linear regime of the aircraft, at low angles of attack. Different previous studies, e.g. in Van Gils (2015), indicate that the control laws perform well also in the nonlinear regimes. Flight tests in the nonlinear regimes can therefore give a meaningful contribution to the research on these control laws.

- Quantitative flight tests that proof the superiority of IBS and INDI control methods should be done by comparing the methods to their non-incremental equivalents or to conventional linear control methods.

- For the presented design and experiment and with the imposed aerodynamic parameter variations, the tracking response of the INDI and IBS control laws are almost identical, as already mentioned in the conclusion. It is suspected that the feed-forward of the outer loop tracking error does have little effect in general. In fact, the outer loop error is already appearing indirectly in the inner loop. For the presented attitude control designs it can be mathematically shown that the feed-forward term introduced in the backstepping controller has little effect, by comparing this term with the propagation of the outer loop error to the inner loop. It could be interesting to know to which extent this feed-forward term may be neglected. This may lead to a better comparison study between multi-loop NDI and backstepping.

Appendix A

Aerodynamic Model

For the aerodynamic model of the FASER Ultrastick120 UAV, the force and moment coefficients are measured using wind-tunnel testsHoe et al. (2012); Owens et al. (2006) and stored in look-up tables. The coefficients are split up into a base, control and a dynamic part dependent on the angular rates:

$$\begin{aligned} \mathbf{C}_F &= \mathbf{C}_{F,\text{base}}(\alpha,\beta) + \Delta\mathbf{C}_{F,\text{ctrl}}(\boldsymbol{\delta},\alpha,\beta) + \Delta\mathbf{C}_{F,\text{rate}}(\hat{\boldsymbol{\omega}},\alpha,\beta) \\ \mathbf{C}_M &= \mathbf{C}_{M,\text{base}}(\alpha,\beta) + \Delta\mathbf{C}_{M,\text{ctrl}}(\boldsymbol{\delta},\alpha,\beta) + \Delta\mathbf{C}_{M,\text{rate}}(\hat{\boldsymbol{\omega}},\alpha,\beta) \end{aligned} \tag{A-1}$$

with

$$\hat{\boldsymbol{\omega}} = \begin{bmatrix} \frac{pb}{2V} \\ \frac{qc}{2V} \\ \frac{rb}{2V} \end{bmatrix}. \tag{A-2}$$

In the look-up tables, only the most important effects of the states on the coefficients are considered. Therefore, most force-moment coefficients are only dependent on a small set of states. An overview of those dependencies is given in Tab. A-1. The pitch rate damping was not measured in wind-tunnel tests. Instead, an estimation of C_{m_q} is obtained from a digital DATCOM estimationWilliams and Vukelich (1979).

Table A-1: Overview of dependency of the different force and moment coefficients on the aircraft states in the aerodynamic look-up tables.

Coefficient part	C_D	C_Y	C_L	C_l	C_m	C_n
Base $\mathbf{C}_{\text{base}}$	α,β	α,β	α,β	α,β	α,β	α,β
Elevator $\Delta\mathbf{C}_{\text{base},\delta_e}$	α,δ_e		α,δ_e		α,δ_e	
Rudder $\Delta\mathbf{C}_{\text{base},\delta_r}$		α,β,δ_r				α,β,δ_r
Aileron $\Delta\mathbf{C}_{\text{base},\delta_a}$				α,β,δ_a		
Roll rate $\Delta\mathbf{C}_{\text{rate},\hat{p}}$		$\alpha,\beta,\hat{p}$				$\alpha,\beta,\hat{p}$
Pitch rate $\Delta\mathbf{C}_{\text{rate},\hat{q}}$					fixed C_{m_q}	
Yaw rate $\Delta\mathbf{C}_{\text{rate},\hat{r}}$		$\alpha,\beta,\hat{r}$				$\alpha,\beta,\hat{r}$

A polynomial model estimation has been performed on the look-up tables using a least-squares approach. The polynomials have been fitted for $\alpha < 12\,\mathrm{deg}$ and $\beta < 20\,\mathrm{deg}$. The general form of all regressor terms that build up the polynomial is:

$$\begin{aligned}\mathbf{C}_F &= \sum_{i=0}^{2}\sum_{j=0}^{2}\mathbf{c}_{\mathrm{base}_{ij}}\alpha^i\beta^j + \mathbf{c}_{\mathrm{base}_{03}}\beta^3 + \sum_{k=1}^{3}\sum_{i=0}^{2}\sum_{j=0}^{2}\mathbf{c}_{\mathrm{ctrl}_{kij}}\delta_k\alpha^i\beta^j \\ \mathbf{C}_M &= \sum_{i=0}^{2}\sum_{j=0}^{2}\mathbf{c}_{\mathrm{base}_{ij}}\alpha^i\beta^j + \mathbf{c}_{\mathrm{base}_{03}}\beta^3 + \sum_{k=1}^{3}\sum_{i=0}^{2}\sum_{j=0}^{2}\mathbf{c}_{\mathrm{ctrl}_{kij}}\delta_k\alpha^i\beta^j + \sum_{l=1}^{3}\sum_{j=0}^{2}\mathbf{c}_{\mathrm{dyn}_{lij}}\hat{\omega}_l\alpha^i\beta^j \quad .\end{aligned} \tag{A-3}$$

In Tables A-2 to A-7, the estimated coefficients are presented.

Table A-2: Polynomial coefficients of $\mathbf{C}_{\mathrm{base}}$

Regressor	C_D	C_Y	C_L	C_l	C_m	C_n
1	0.042	0	-0.04	0	-0.0174	0
α	-0.1443	0	4.419	0	-0.3025	0
α^2	1.88	0	-0.5226	0	-1.041	0
β	0	-0.4126	0	-0.0401	0	0.0714
β^2	-0.0254	0	-0.1194	0	0.2538	0
$\alpha\beta$	0	0.2347	0	-0.3039	0	-0.1015
$\alpha\beta^2$	0.2094	0	-4.066	0	0.0438	0
$\alpha^2\beta$	0	-0.4635	0	0.6848	0	0.1074
$\alpha^2\beta^2$	-0.9064	0	8.988	0	-0.9023	0
β^3	0	0	0	0	0	0
RMS error	0.003181	0.002441	0.003648	0.0004296	0.001873	0.001132

Table A-3: Polynomial coefficients of $\mathbf{C}_{\mathrm{ctrl},\delta_e}$

Regressor	C_D	C_L	C_m
δ_e	-0.01634	0.3048	-0.6894
$\delta_e\alpha$	0.2513	0.04222	0.1263
$\delta_e\alpha^2$	-0.2364	-1.306	-0.1516
δ_e^2	0.01406	-0.06121	0.347
$\delta_e^2\alpha$	-0.3158	-0.8089	0.1992
$\delta_e^2\alpha^2$	2.937	9.372	-6.877
RMS error	0.002189	0.002245	0.002122

Table A-4: Polynomial coefficients of $\Delta\mathbf{C}_{\mathrm{ctrl},\delta_a}$

Regressor	C_l
δ_a	-0.1865
$\delta_a\beta$	0.02747
$\delta_a\beta^2$	0.3395
$\delta_a\alpha$	-0.2408
$\delta_a\alpha\beta$	0.0004451
$\delta_a\alpha\beta^2$	-0.007027
$\delta_a\alpha^2$	-0.4716
$\delta_a\alpha^2\beta$	-0.00231
$\delta_a\alpha^2\beta^2$	0.02938
δ_a^2	0.08956
$\delta_a^2\beta$	-0.06551
$\delta_a^2\beta^2$	-0.6522
$\delta_a^2\alpha$	0.6373
$\delta_a^2\alpha\beta$	-0.001652
$\delta_a^2\alpha\beta^2$	0.01204
$\delta_a^2\alpha^2$	1.238
$\delta_a^2\alpha^2\beta$	0.008538
$\delta_a^2\alpha^2\beta^2$	0.02858
RMS error	0.000163

Table A-5: Polynomial coefficients of $\Delta\mathbf{C}_{\mathrm{ctrl},\delta_r}$

Regressor	C_Y	C_m
δ_r	0.02083	-0.03606
$\delta_r\beta$	-0.0008474	0.001889
$\delta_r\beta^2$	0.4348	-0.1394
$\delta_r\alpha$	-0.5212	0.1071
$\delta_r\alpha\beta$	0.0001723	-5.398e-05
$\delta_r\alpha\beta^2$	-0.001939	0.0005968
$\delta_r\alpha^2$	1.067	-0.2127
$\delta_r\alpha^2\beta$	-0.000909	0.0002646
$\delta_r\alpha^2\beta^2$	0.01374	-0.003882
δ_r^2	-0.2249	0.01942
$\delta_r^2\beta$	-0.1142	0.04648
$\delta_r^2\beta^2$	0.4667	-0.08927
$\delta_r^2\alpha$	-1.194	0.2455
$\delta_r^2\alpha\beta$	0.0003391	-0.0001046
$\delta_r^2\alpha\beta^2$	-0.006994	0.001909
$\delta_r^2\alpha^2$	2.443	-0.487
$\delta_r^2\alpha^2\beta$	-0.001159	0.0002877
$\delta_r^2\alpha^2\beta^2$	0.07808	-0.01896
RMS error	0.0007614	0.001191

Table A-6: Polynomial coefficients of $\Delta\mathbf{C}_{\mathrm{rate},p}$

Regressor	C_Y	C_l	C_n
$\hat{p}$	-0.07032	-0.3976	0.001675
$\hat{p}\alpha$	0.838	0.0364	-0.5065
$\hat{p}\alpha^2$	-2.243	-1.711	0.2688
RMS error	0.0003317	0.0002019	0.0003126

Table A-7: Polynomial coefficients of $\Delta\mathbf{C}_{\mathrm{rate},r}$

Regressor	C_Y	C_l	C_n
$\hat{r}$	0.3091	0.04467	-0.1366
$\hat{r}\alpha$	0.1376	0.6087	-0.04955
$\hat{r}\alpha^2$	-1.738	0.1337	1.684
RMS error	0.0002849	0.0002891	0.0006108

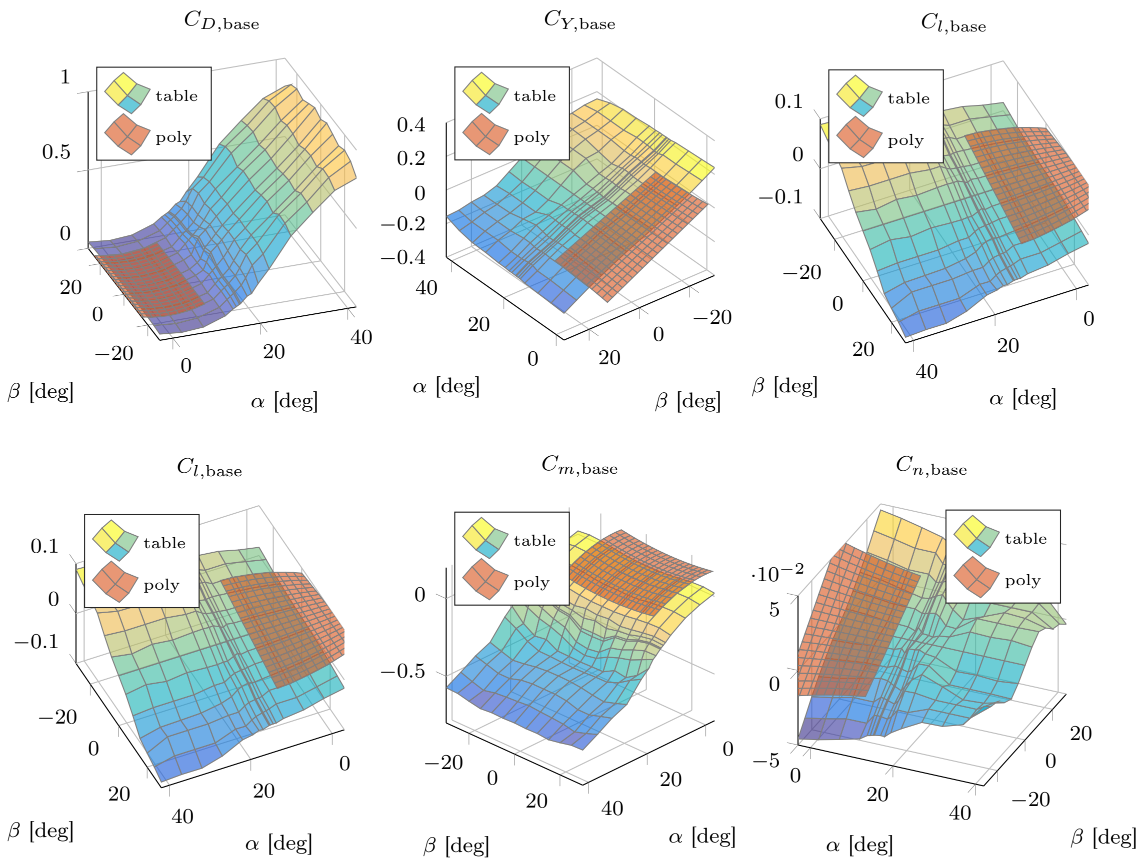

Figure A-1: Base force/moment coefficient $C_{i,\text{base}}$ versus α and β.

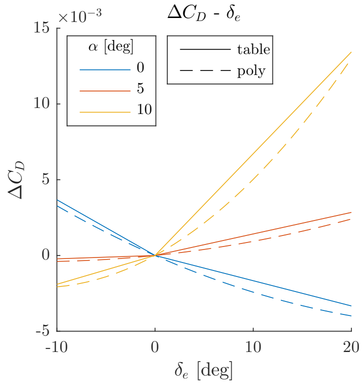

Figure A-2: $\Delta C_{D_{\text{ctrl}}}$ versus elevator deflection

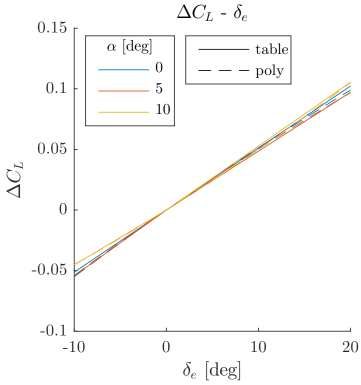

Figure A-3: $\Delta C_{L_{\text{ctrl}}}$ versus elevator deflection

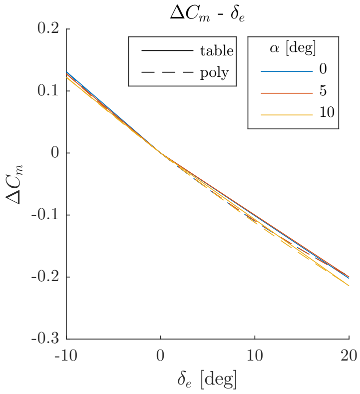

Figure A-4: $\Delta C_{m_{\text{ctrl}}}$ versus elevator deflection

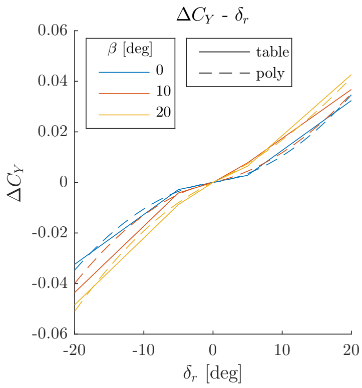

Figure A-5: $\Delta C_{Y_{\text{ctrl}}}$ versus rudder deflection

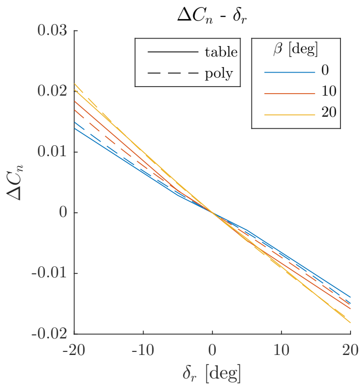

Figure A-6: $\Delta C_{n_{\text{ctrl}}}$ versus rudder deflection

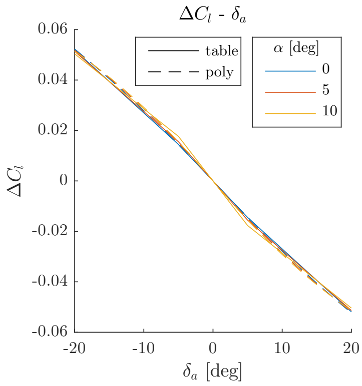

Figure A-7: $\Delta C_{l_{\text{ctrl}}}$ versus aileron deflection

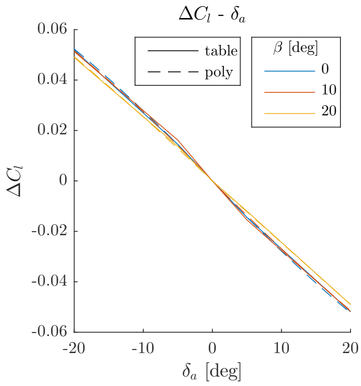

Figure A-8: $\Delta C_{l_{\text{ctrl}}}$ versus aileron deflection

Appendix B

Flight Results

This appendix contains more detailed figures on the tracking responses during all experiments, displayed on the next pages. Stabilization tracking tasks are not included. The following table depicts the presented experiments and the corresponding figure number. Flight videos of a small selection of the experiment runs can be viewed at the following link: `https://youtu.be/PRnHx8323Ts`.

Table B-1: List of detailed tracking response figures

#	Figure	Description	Doublet magnitude
INDI Euler attitude control experiments			
1A	Fig. B-1	Pitch control only, manual roll/yaw and velocity control. conservative parameters	$\theta_{ref} = 10\,\text{deg}$
1B	Fig. B-2, Fig. B-3	Add auto-throttle control	$\theta_{ref} = 10\,\text{deg}$
1C	Fig. B-4	Add roll/yaw control	$\phi_{ref} = 20\,\text{deg}$
	Fig. B-5		$\phi_{ref} = 30\,\text{deg}$
2A	Fig. B-6	Fully automatic control, nominal gains	$\theta_{ref} = 10\,\text{deg}$
	Fig. B-7		$\theta_{ref} = 15\,\text{deg}$
	Fig. B-8		$\phi_{ref} = 20\,\text{deg}$
	Fig. B-7		$\phi_{ref} = 45\,\text{deg}$
IBS aerodynamic attitude control experiments			
4	Fig. B-10	Pitch and velocity control only, manual roll/yaw control.	$\alpha_{ref} = 1\,\text{deg}$
	Fig. B-11	conservative parameters	$\alpha_{ref} = 2\,\text{deg}$
5	Fig. B-12	Fully automatic control, nominal gains	$\alpha_{ref} = 1\,\text{deg}$
	Fig. B-13		$\alpha_{ref} = 2\,\text{deg}$
6	Fig. B-14	Add roll/yaw control, conservative parameters	$\phi_{ref} = 15\,\text{deg}$

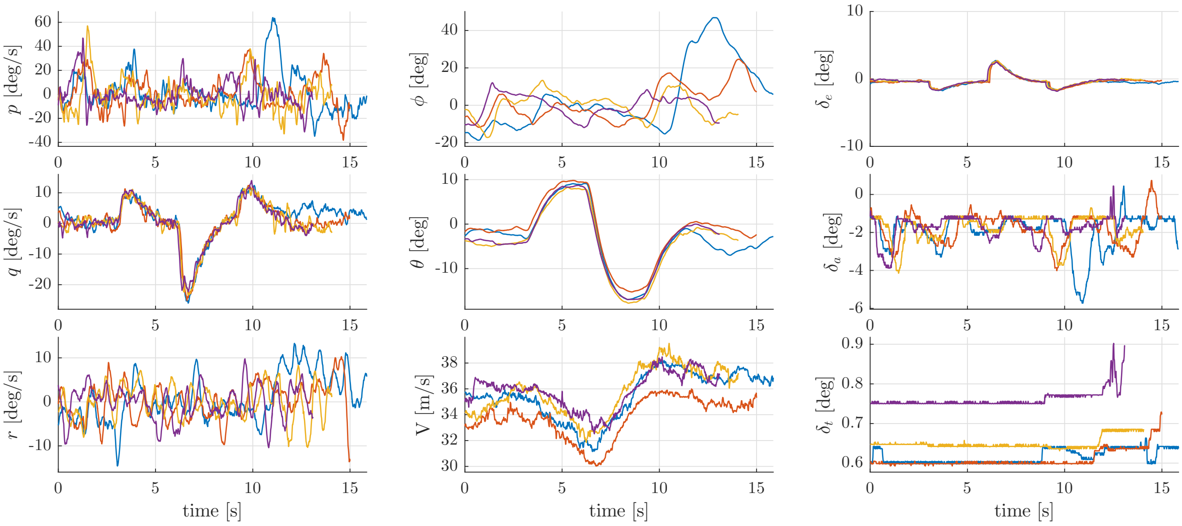

Figure B-1: Experiment 1A, $\theta_{ref} = \pm 10\,\mathrm{deg}$, Run 1 to 4

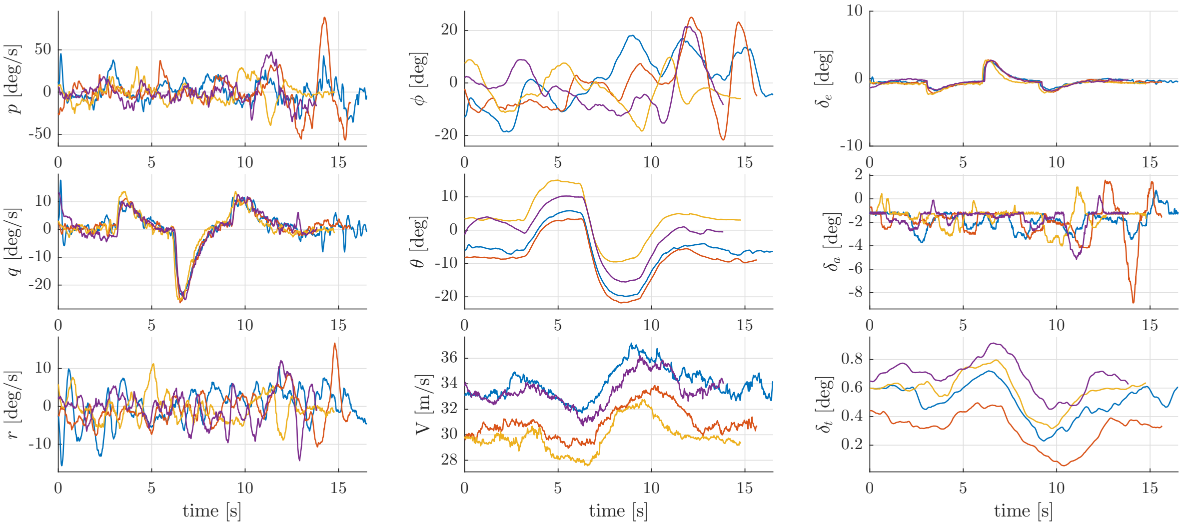

Figure B-2: Experiment 1B, $\theta_{ref} = \pm 10\,\mathrm{deg}$, throttle gain 0.10, Run 1 to 4

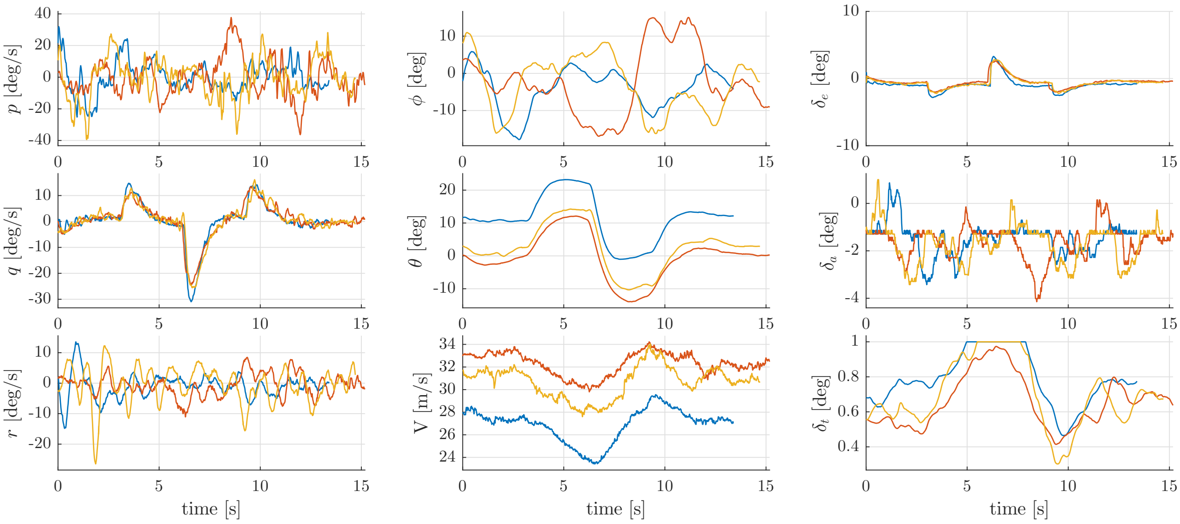

Figure B-3: Experiment 1B, $\theta_{ref} = \pm 10\,\mathrm{deg}$, throttle gain 0.15, Run 1 to 3

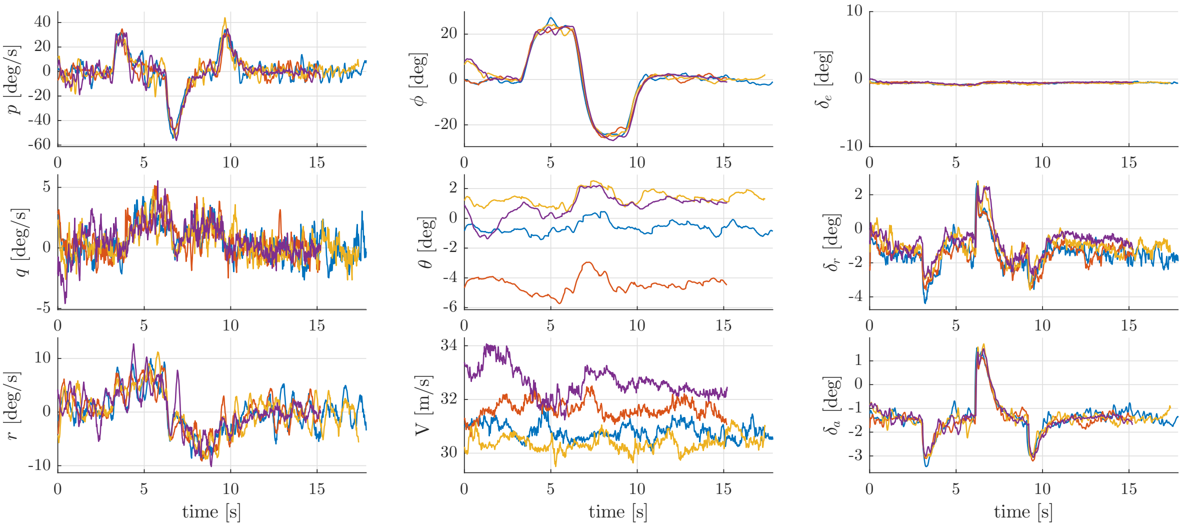

Figure B-4: Experiment 1C, $\phi_{ref} = \pm 20\,\text{deg}$, Run 1 to 4

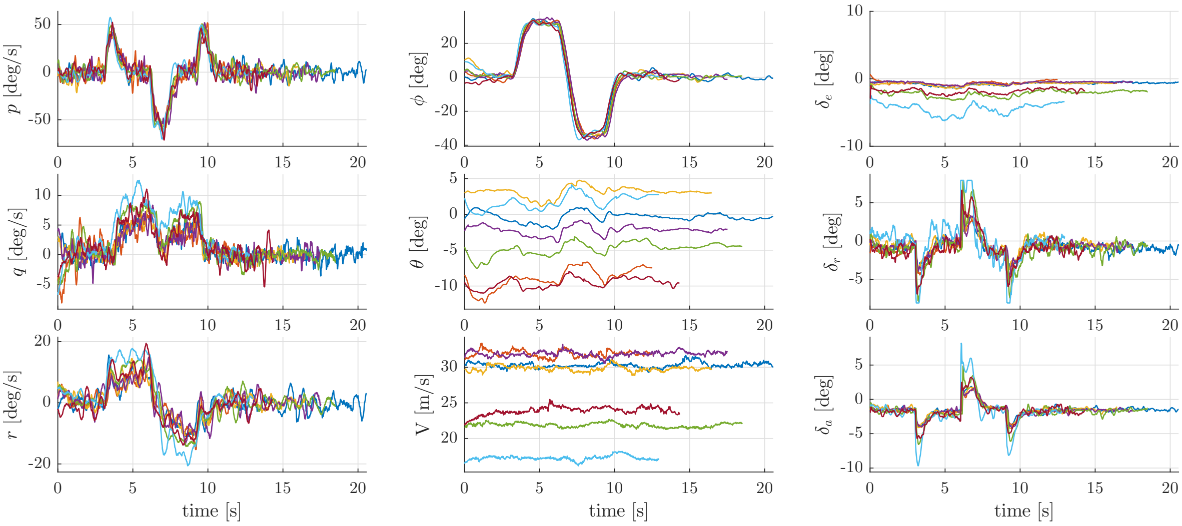

Figure B-5: Experiment 1C, $\phi_{ref} = \pm 30\,\text{deg}$, Run 1 to 7

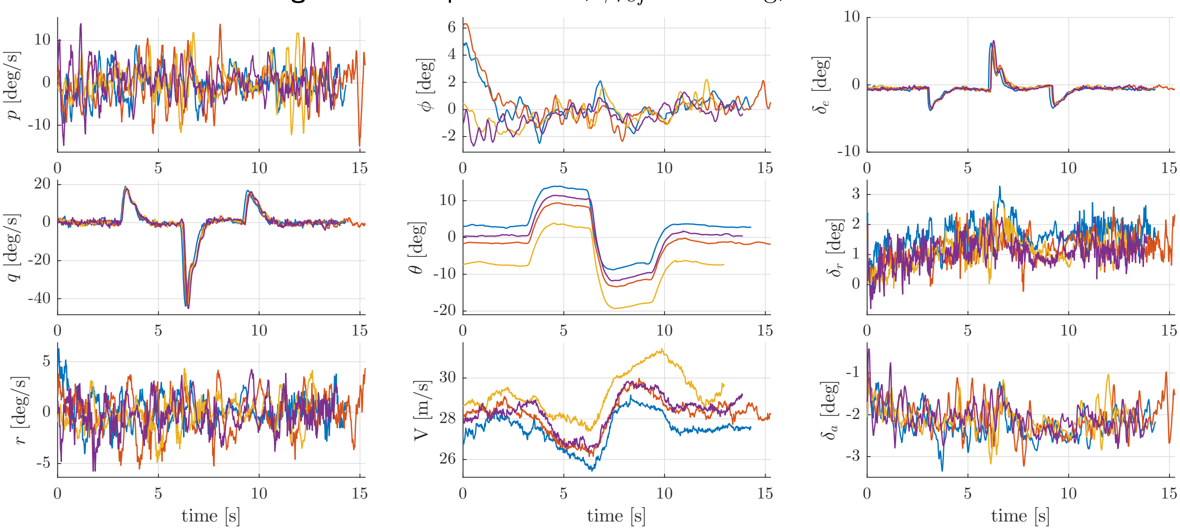

Figure B-6: Experiment 2A, $\theta_{ref} = \pm 10\,\text{deg}$, Run 1 to 4

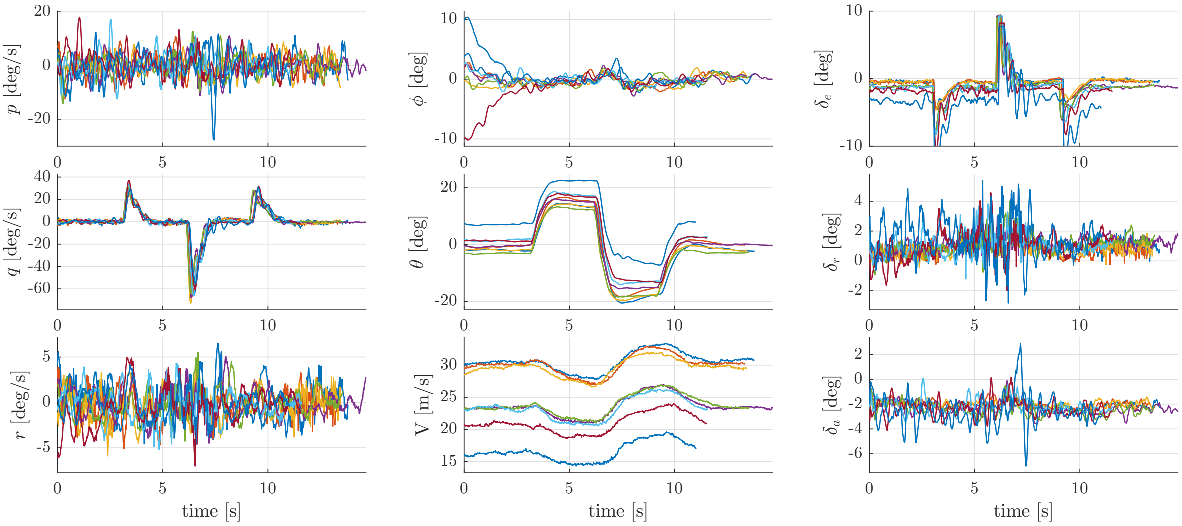

Figure B-7: Experiment 2A, $\theta_{ref} = \pm 15\,\mathrm{deg}$, Run 1 to 8

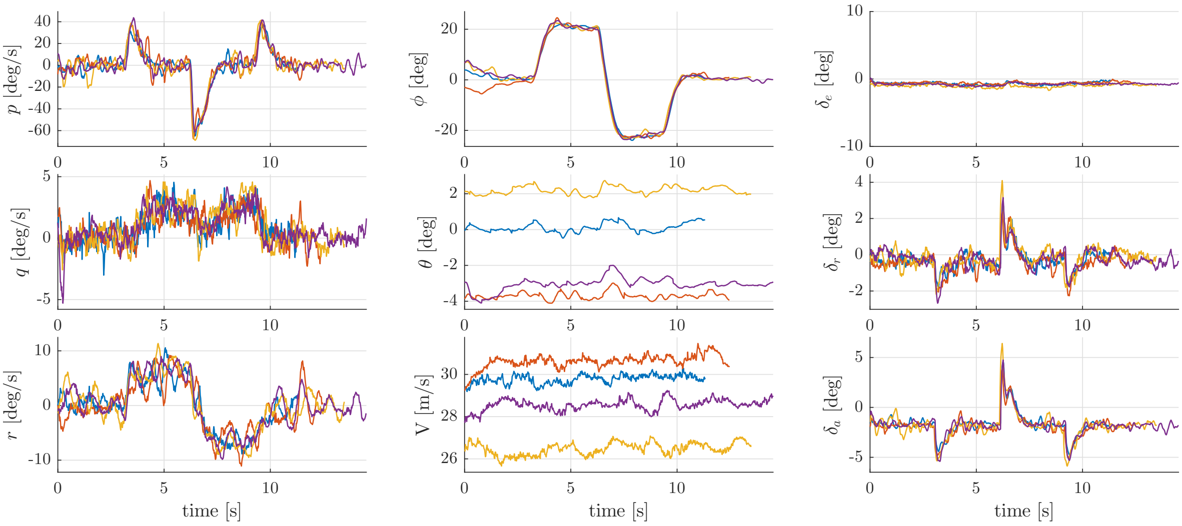

Figure B-8: Experiment 2A, $\phi_{ref} = \pm 20\,\mathrm{deg}$, Run 1 to 4

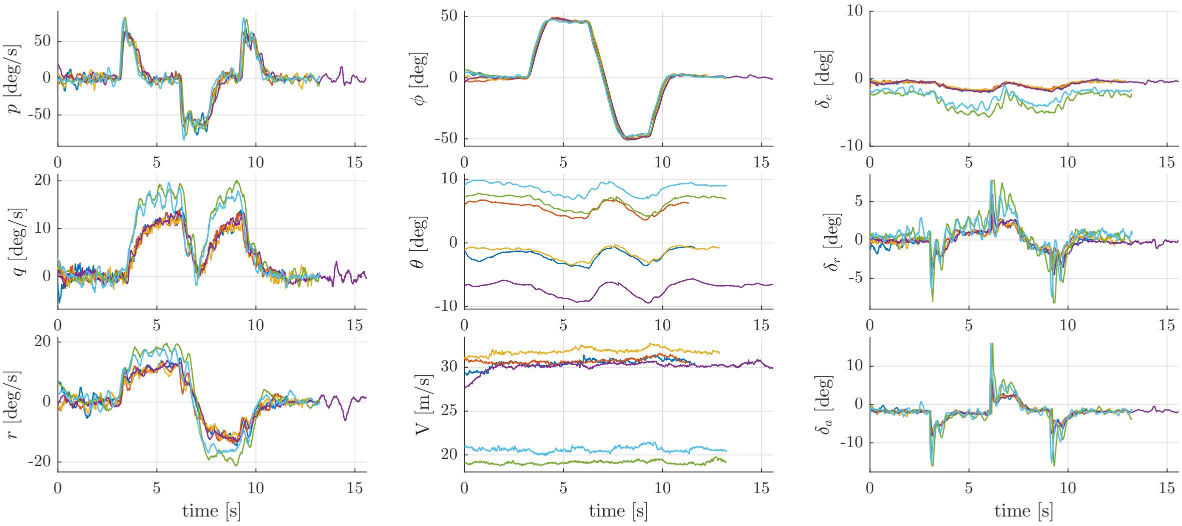

Figure B-9: Experiment 2A, $\phi_{ref} = \pm 45\,\mathrm{deg}$, Run 1 to 4

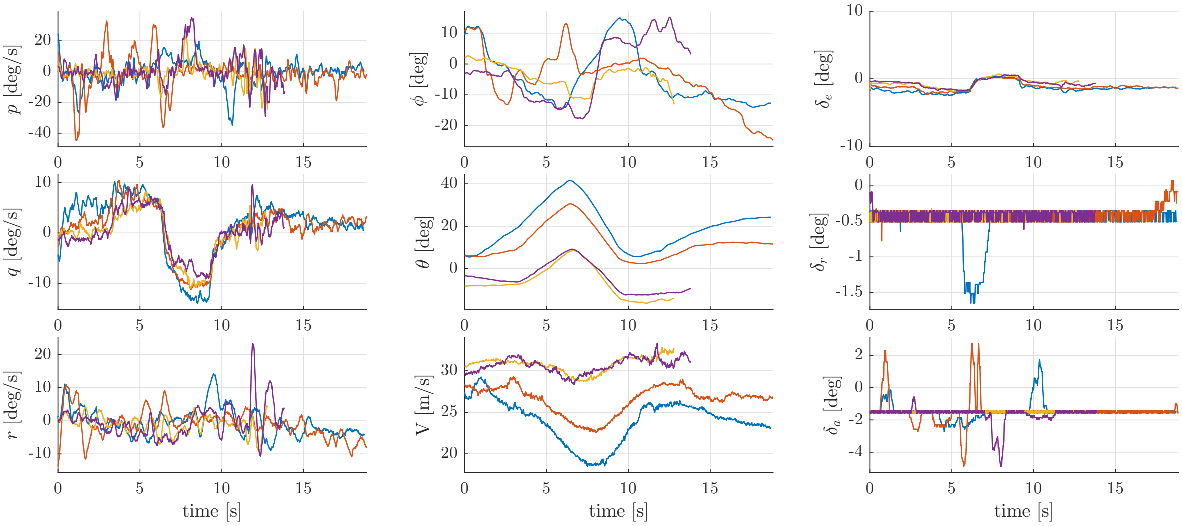

Figure B-10: Experiment 4, $\alpha_{ref} = \pm 1\,\text{deg}$, Run 1 to 4

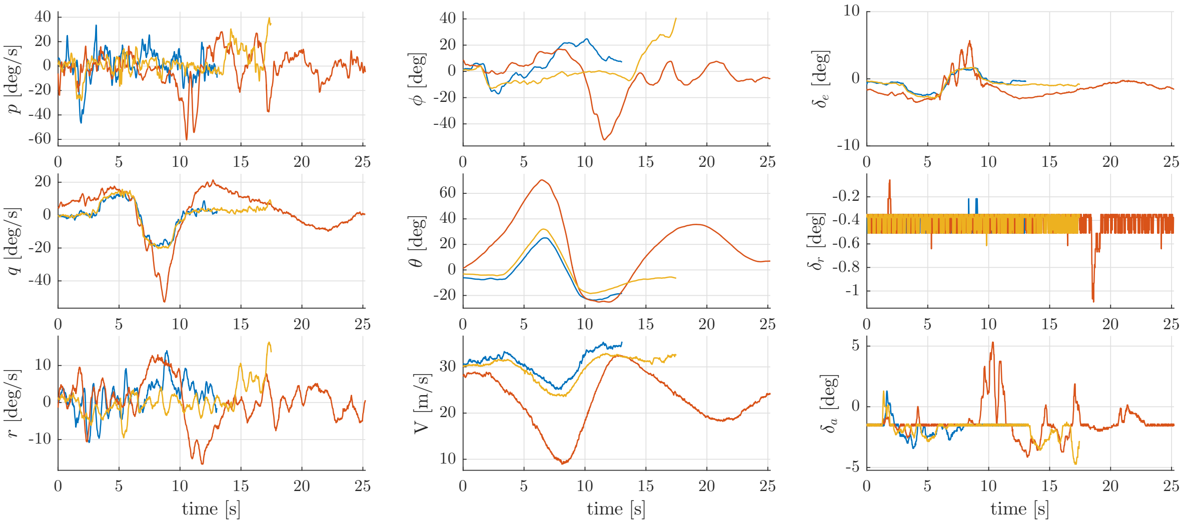

Figure B-11: Experiment 4, $\alpha_{ref} = \pm 2\,\text{deg}$, Run 1 to 4

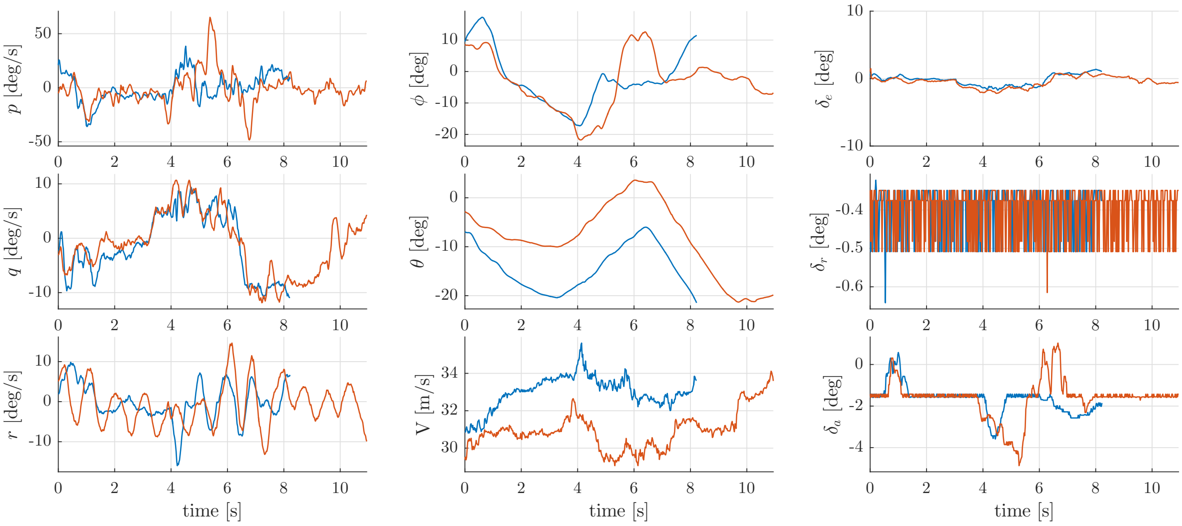

Figure B-12: Experiment 5, $\alpha_{ref} = \pm 1\,\text{deg}$, Run 1 to 2

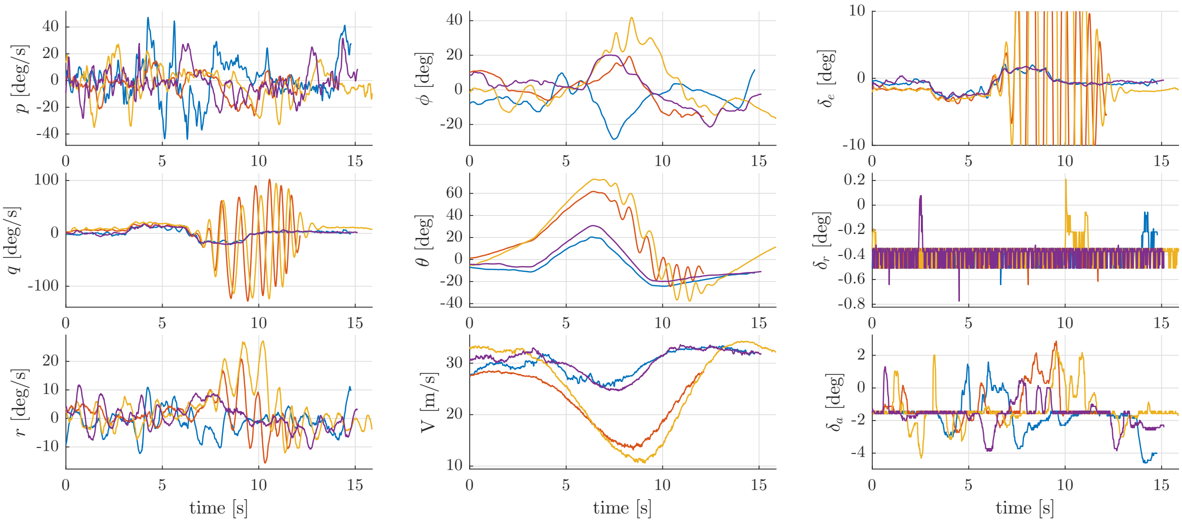

Figure B-13: Experiment 5, $\alpha_{ref} = \pm 2\,\text{deg}$, Run 1 to 4

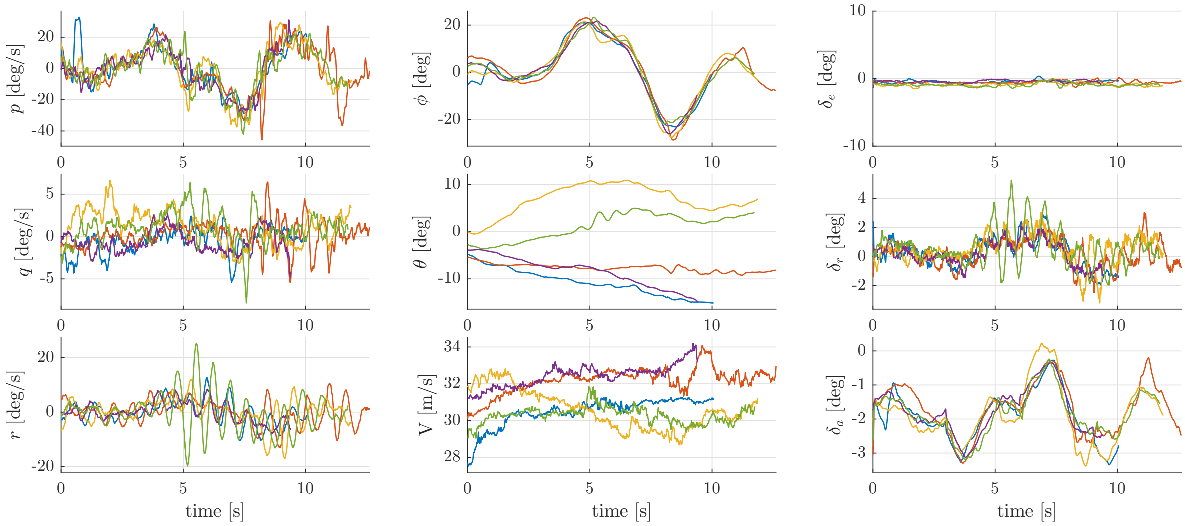

Figure B-14: Experiment 6, $\phi_{ref} = \pm 15\,\text{deg}$, Run 1 to 5

Appendix C

Model Validation

This appendix presents more flight data results supported with simulations for the model validation discussed in section II of the paper. For three different maneuvers, all relevant measured flight states are plotted together with open-loop simulation results in which identical inputs are given. Furthermore, for each maneuver additional simulations have been performed where aerodynamic parameters of the model are scaled. Scaling factors scale part of the aerodynamic moment coefficents. They are defined as:

$$\begin{aligned} C_{i,\text{base,scaled}} &= F_{i,\text{base}} C_{i,\text{base}} \\ \Delta C_{i,\text{ctrl,scaled}} &= F_{i,\text{ctrl}} \Delta C_{i,\text{ctrl}} \qquad \text{for} \quad i = l, m, n \\ \Delta C_{i,\text{rate,scaled}} &= F_{i,\text{rate}} \Delta C_{i,\text{rate}} \end{aligned} \tag{C-1}$$

Where F_* are scaling factors for each component of the aerodynamic model. By varying each scaling factor over a mimimum, nominal and maximum value, simulations of each possible combination set of factors is performed. The limits are set to $F_* = \pm 25\,\%$ for each scaling factor.

In Figs. C-1 to C-12 all results are presented. It can be seen that the total attitude shows considerable offsets, which is expected as acceleration errors between the model and flight propagate through the integration.

Results of the pitch maneuver are presented in Figs. C-1 to C-4. The pitch accelerations are slightly out of bounds at acceleration peaks. This indicates that the aircraft has a lower control effectiveness $C_{m_{\delta_e}}$ than expected, or a higher pitch inertia I_{yy}. In this maneuver, the roll accelation measurements contains strong vibrations and an oscillation in the yaw rate is present which is not predicted by the model. These effects could be attributed to turbulence.

Results of the roll maneuver are presented in Figs. C-5 to C-8. At its peaks, the roll accelerations measured in flight are significantly lower than what is predicted by the model, which could also be attributed to aerodynamic model mismatches or to different flight conditions (winda and angles of attack). It is unlikely that the aircraft contains nonlinearities in the aileron effectiveness that may bring the effectiveness down at high aileron angles, as the measured effectiveness in windtunnel tests showed a very linear and comparable result for all angles of attack and angles of sideslip (see Fig. A-7). In contrast with measurements, the simulation also predicts a stronger coupling between the roll and yaw motion, and between the longitudinal and lateral mode.

Results of the yaw maneuver are presented in Figs. C-9 to C-12. In this axis, accelerations seem to correspond quite accurately. Yaw accelerations lie within the uncertainty bounds for the major part of the measurements, and the yaw rate measurements align well with simulations results.

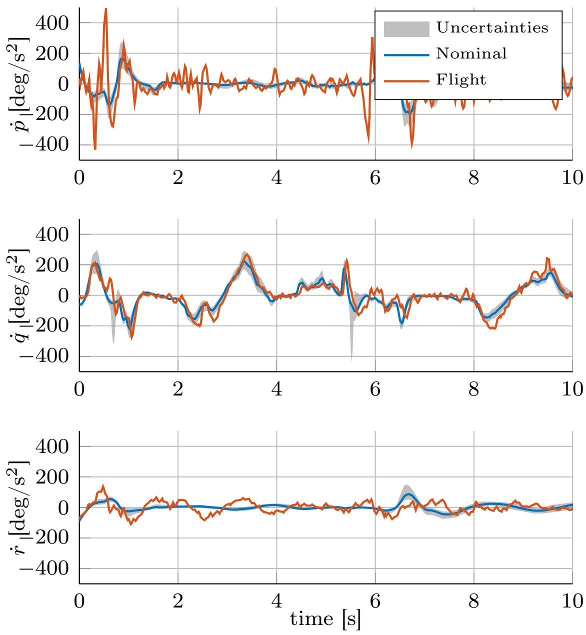

Figure C-1: Pitch maneuver angular accelerations

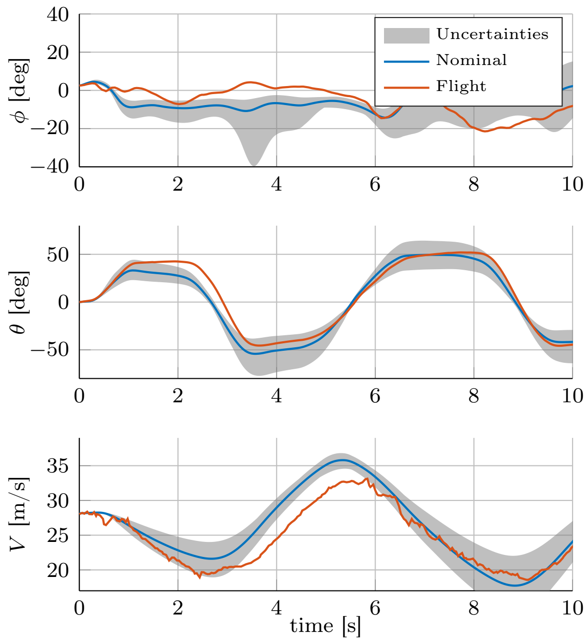

Figure C-2: Pitch maneuver attitude and airspeed

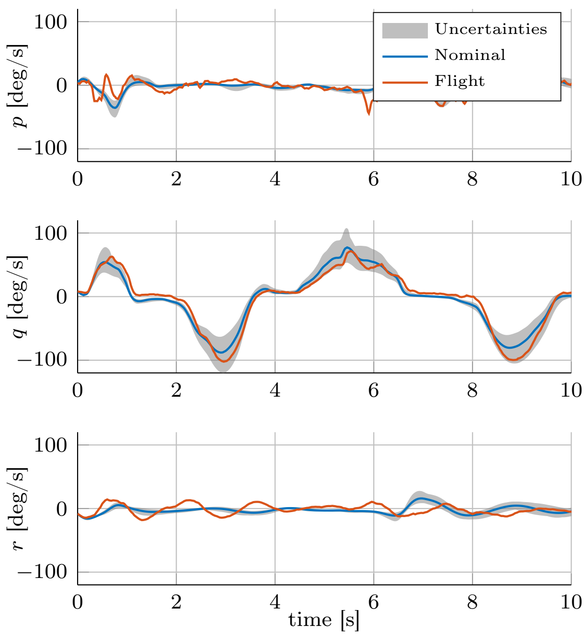

Figure C-3: Pitch maneuver angular rates

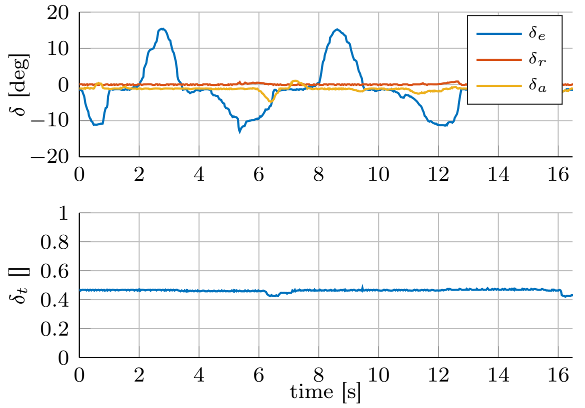

Figure C-4: Pitch maneuver inputs

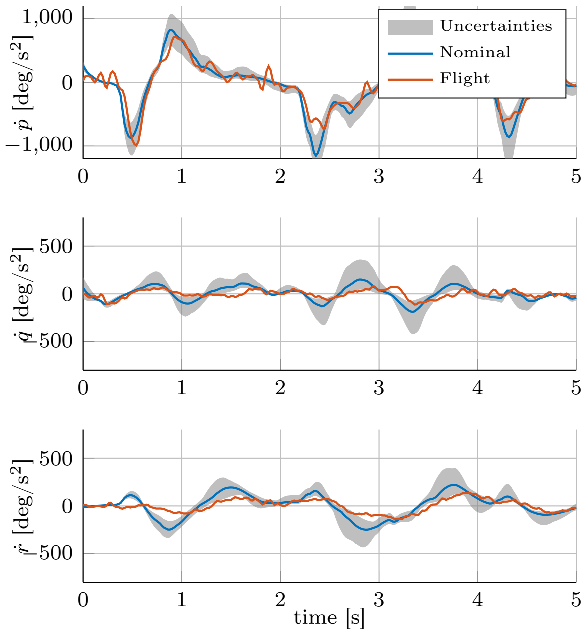

Figure C-5: Roll maneuver angular accelerations

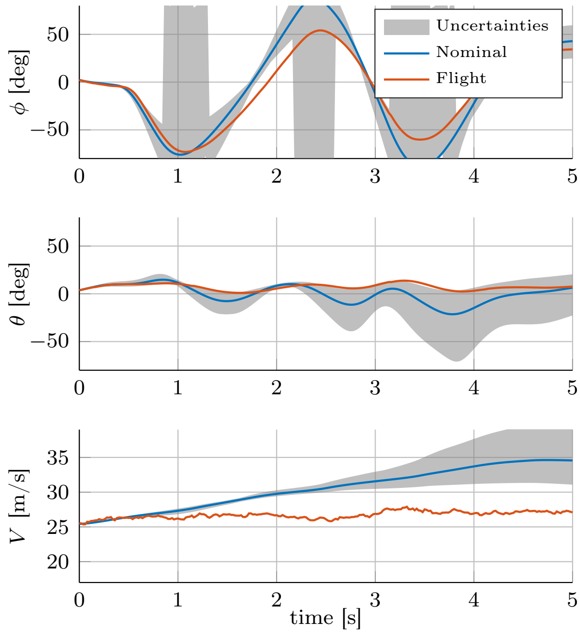

Figure C-6: Roll maneuver attitude and airspeed

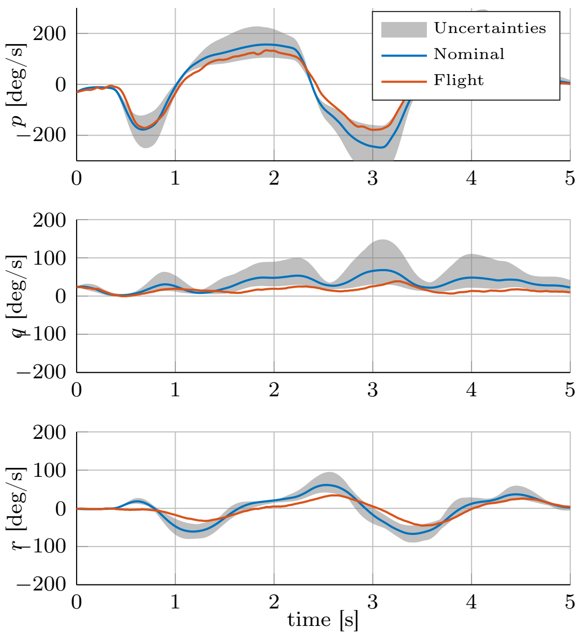

Figure C-7: Roll maneuver angular rates

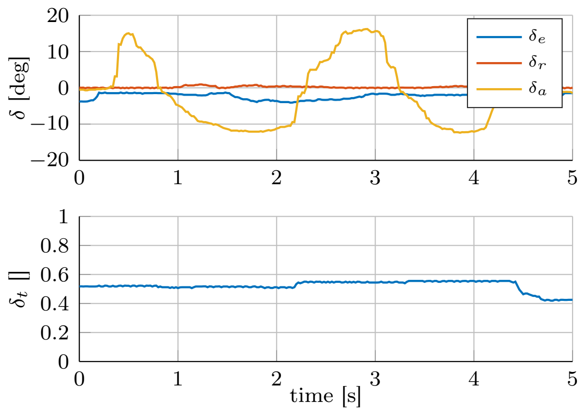

Figure C-8: Roll maneuver inputs

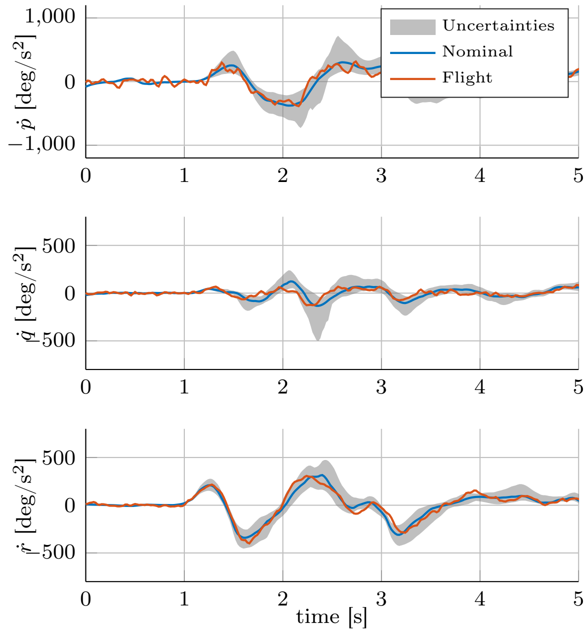

Figure C-9: Yaw maneuver angular accelerations

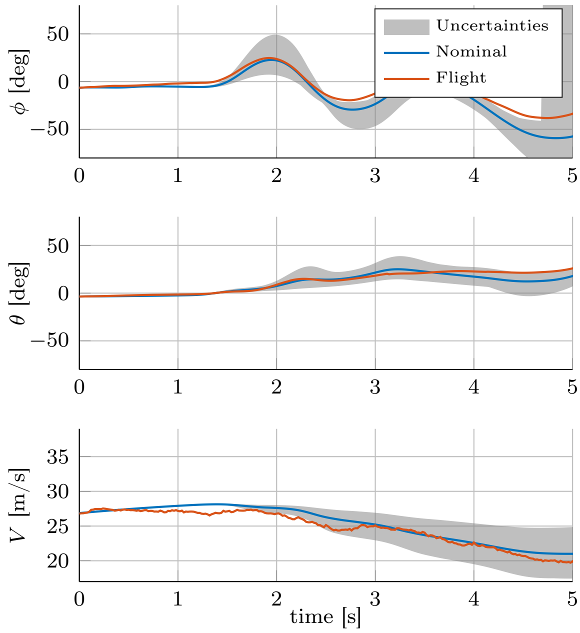

Figure C-10: Yaw maneuver attitude and airspeed

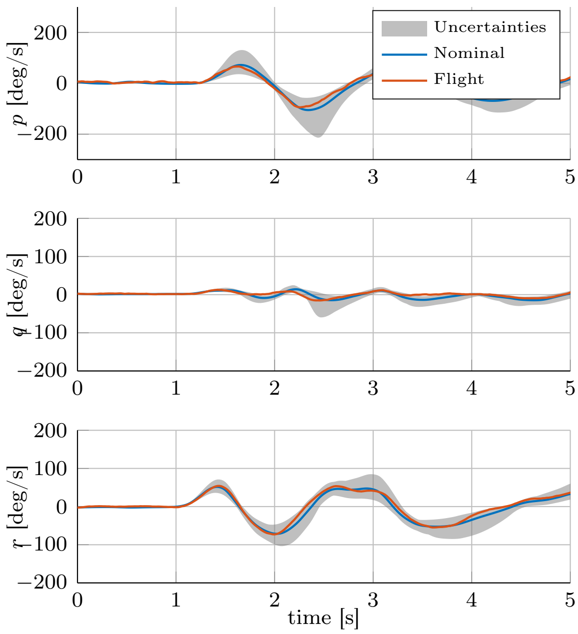

Figure C-11: Yaw maneuver angular rates

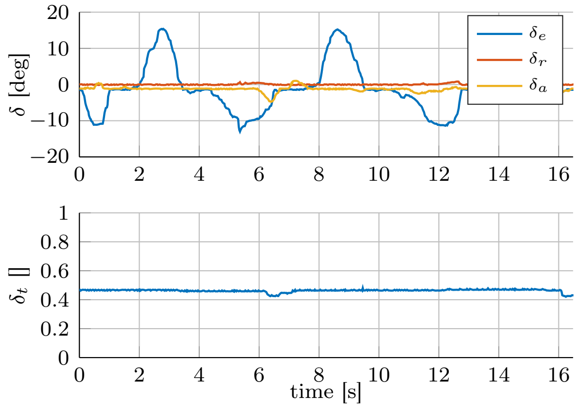

Figure C-12: Yaw maneuver inputs

PI(D) tuning for Flight Control Systems via Incremental Nonlinear Dynamic Inversion

Paul Acquatella B. [*,1] **Wim van Ekeren** [*,**,2] **Qi Ping Chu** [**,3]

[*] *DLR, German Aerospace Center*
Institute of System Dynamics and Control
Oberpfaffenhofen, Germany
[**] *Delft University of Technology, Faculty of Aerospace Engineering*
Delft, The Netherlands

Abstract: Previous results reported in the robotics literature show the relationship between *time-delay control* (TDC) and *proportional-integral-derivative control* (PID). In this paper, we show that incremental nonlinear dynamic inversion (INDI) — more familiar in the aerospace community — are in fact equivalent to TDC. This leads to a meaningful and systematic method for PI(D)-control tuning of robust nonlinear flight control systems via INDI. We considered a reformulation of the plant dynamics inversion which removes effector blending models from the resulting control law, resulting in robust model-free control laws like PI(D)-control.

Keywords: aerospace, tracking, application of nonlinear analysis and design

1. INTRODUCTION

Ensuring stability and performance in between operational points of widely-used gain-scheduled linear PID controllers motivates the use of nonlinear dynamic inversion (NDI) for flight control systems. NDI cancels out nonlinearities in the model via state feedback, and then linear control can be subsequently designed to close the systems' outer-loop, hence eliminating the need of linearizing and designing different controllers for several operational points as in gain-scheduling.

In this paper we consider nonlinear flight control strategies based on incremental nonlinear dynamic inversion (INDI). Using sensor and actuator measurements for feedback allows the design of an incremental control action which, in combination with nonlinear dynamic inversion, stabilizes the *partly*-linearized nonlinear system *incrementally.* With this result, dependency on exact knowledge of the system dynamics is greatly reduced, overcoming this major robustness issue from conventional nonlinear dynamic inversion. INDI has been considered a sensor-based approach because sensor measurements were meant to replace a large part of the vehicle model.

Theoretical development of increments of nonlinear control action date back from the late nineties and started with activities concerning 'implicit dynamic inversion' for inversion-based flight control (Smith (1998); Bacon and Ostroff (2000)), where the architectures considered in this paper were firstly described. Other designations for these developments found in the literature are 'modified NDI' and 'simplified NDI', but the designation 'incremental NDI', introduced in (Chen and Zhang (2008)), is considered to describe the methodology and nature of these type of control laws better (Chen and Zhang (2008); Chu (2010); Sieberling et al. (2010)). INDI has been elaborated and applied theoretically in the past decade for advanced flight control and space applications (Sieberling et al. (2010); Smith (1998); Bacon and Ostroff (2000); Bacon et al. (2000, 2001); Acquatella B. et al. (2012); Simplicio et al. (2013)). More recently, this technique has been applied for quadrotors and adaptive control (Smeur et al. (2016b,a)).

In this paper, we present three main contributions in the context of nonlinear flight control system design.

1) We revisit the NDI/INDI control laws and we establish the equivalence between INDI and *time-delay control* (TDC).

2) Based on previous results reported in the robotics literature showing the relationship between discrete formulations of TDC and *proportional-integral-derivative control* (PID), we show that an equivalent PI(D) controller with gains $< K,\ T_i,\ (T_d,) >$ tuned via INDI/TDC is more meaningful and systematic than heuristic methods, since one considers *desired* error dynamics given by Hurwitz gains $< k_P,\ (k_D,) >$. Then, tuning the remaining effector/decoupled blending gain is much less cumbersome than designing a whole set of gains iteratively.

3) We also consider a reformulation of the plant dynamics inversion as it is done in TDC which removes the effector blending model (control derivatives) from the resulting control law, which has not been the case so far in the reported INDI controllers, causing robustness problems because of the susceptibility on their uncertainties.

[1] Research Engineer, Space Systems Dynamics Department. paul.acquatella@dlr.de.
[2] Graduate Student, Control & Simulation Department. w.vanekeren@student.tudelft.nl.
[3] Associate Professor, Control & Simulation Department. q.p.chu@tudelft.nl.

2. FLIGHT VEHICLE MODELING

We are interested in Euler's equation of motion representing flight vehicles' angular velocity dynamics

$$I\,\dot{\omega} + \omega \times I\,\omega = M_B \tag{1}$$

where $M_B \in \mathcal{R}^3$ is the external moment vector in body axes, $\omega \in \mathcal{R}^3$ is the angular velocity vector, and $I \in \mathcal{R}^{3\times3}$ the inertia matrix of the rigid body assuming symmetry about the plane $x - z$ of the body.

Furthermore, we will be interested in the time history of the angular velocity vector, hence the dynamics of the rotational motion of a vehicle in Eq. (1) can be rewritten as the following set of differential equations

$$\dot{\omega} = I^{-1}\big(\, M_B - \omega \times I\,\omega \,\big) \tag{2}$$

where

$$\omega = \begin{bmatrix} p \\ q \\ r \end{bmatrix}, \quad M_B = \begin{bmatrix} L \\ M \\ N \end{bmatrix} = SQ\begin{bmatrix} b\,C_l \\ \bar{c}\,C_m \\ b\,C_n \end{bmatrix},$$

$$I = \begin{bmatrix} I_{xx} & 0 & I_{xz} \\ 0 & I_{yy} & 0 \\ I_{xz} & 0 & I_{zz} \end{bmatrix},$$

with p, q, r, the body roll, pitch, and yaw rates, respectively; L, M, N, the roll, pitch, and yaw moments, respectively; S the wing surface area, Q the dynamic pressure, b the wing span, $\bar{c}$ the mean aerodynamic chord, and C_l, C_m, C_n the moment coefficients for roll, pitch, and yaw, respectively. Furthermore, let M_B be the sum of moments partially generated by the aerodynamics of the airframe M_a, and moments generated by control surface deflections M_c, assumed to be linear in the deflection angles δ, as

$$M_B = M_a + M_c\delta \tag{3}$$

where

$$M_a = \begin{bmatrix} L_a \\ M_a \\ N_a \end{bmatrix}, \; M_c = \begin{bmatrix} L_c \\ M_c \\ N_c \end{bmatrix}, \; \delta = \begin{bmatrix} \delta_a \\ \delta_e \\ \delta_r \end{bmatrix}$$

and δ corresponding to the control inputs: aileron, elevator, and rudder deflection angles, respectively. Hence the dynamics in Eq. (2) can be rewritten as

$$\dot{\omega} = f(\omega) + G(\omega)\delta \tag{4}$$

with

$$f(\omega) = I^{-1}\big(M_a - \omega \times I\,\omega\big), \; G(\omega) = I^{-1}M_c.$$

For practical implementations, we consider first-order actuator dynamics represented by the following transfer function

$$\frac{\delta}{\delta_c} = G_a(s) = \frac{K_a}{\tau_a s + 1}, \tag{5}$$

and furthermore, we don't consider these actuator dynamics in the control design process as it is usually the case for dynamic inversion-based control. For that reason, we assume that these actuators are *sufficiently fast* in the control-bandwidth sense, meaning that $1/\tau_a$ is higher than the control system closed-loop bandwidth.

3. FLIGHT CONTROL LAW DESIGN

3.1 Nonlinear Dynamic Inversion

Let's define the control parameter to be the angular velocities, hence the output is simply $y = \omega$. We then consider an error vector defined as $e = y_d - y$ where y_d denotes the *smooth* desired output vector (at least one time differentiable).

Nonlinear dynamic inversion is designed to linearize and decouple the rotational dynamics in order to obtain an *explicit* desired closed loop dynamics to be followed. Introducing the virtual control input $\nu = \dot{\omega}_{\text{des}}$, if the matrix $G(\omega)$ is non-singular (i.e., invertible) in the domain of interest for all ω, the nonlinear dynamic inversion (NDI) control consists in the following input transformation (Slotine and Li (1990); Chu (2010))

$$\delta = G(\omega)^{-1}\big[\nu - f(\omega)\big] \tag{6}$$

which cancels all the nonlinearities, and a simple input-output linear relationship between the output y and the new input ν is obtained as

$$\dot{y} = \nu \tag{7}$$

Apart from being linear, an interesting result from this relationship is that it is also decoupled since the input ν_i only affects the output y_i. From this fact, the input transformation (6) is called a *decoupling control law*, and the resulting linear system (7) is called the *single-integrator* form. This single-integrator form (7) can be rendered exponentially stable with

$$\nu = \dot{y}_d + k_P e \tag{8}$$

where $\dot{y}_d$ is the feedforward term for tracking tasks, and $k_P \in \mathcal{R}^{3\times3}$ a constant diagonal matrix, whose $i-$th diagonal elements k_{P_i} are chosen so that the polynomials

$$s + k_{P_i} \qquad (i = p, q, r) \tag{9}$$

may become Hurwitz, i.e., $k_{P_i} < 0$. This results in the exponentially stable and decoupled *desired* error dynamics

$$\dot{e} + k_P e = 0 \tag{10}$$

which implies that $e(t) \to 0$. From this typical tracking problem it can be seen that the entire control system will have two control loops (Chu (2010); Sieberling et al. (2010)): the inner linearization loop based on Eq. (6), and the outer control loop based on Eq. (8). This resulting NDI control law depends on accurate knowledge of the aerodynamic model contained in both M_a and M_c, hence susceptible to model uncertainties.

In NDI control design, we consider outputs with relative degrees of one (rates), meaning a first-order system to be controlled, see Fig. 1. Extensions of input-output linearization for systems involving higher relative degrees are done via *feedback linearization* (Slotine and Li (1990); Chu (2010)).

3.2 Incremental Nonlinear Dynamic Inversion

The concept of incremental nonlinear dynamic inversion (INDI) amounts to the application of NDI to a system expressed in an incremental form. This improves the robustness of the closed-loop system as compared with conventional NDI since dependency on the accurate knowledge of the plant dynamics is reduced. Unlike NDI, this control design technique is *implicit* in the sense that desired closed-loop dynamics do not reside in some explicit model to be followed but result when the feedback loops are closed (Bacon and Ostroff (2000); Bacon et al. (2000)).

To obtain an incremental form of system dynamics, we consider a first-order Taylor series expansion of $\dot{\omega}$ (Smith

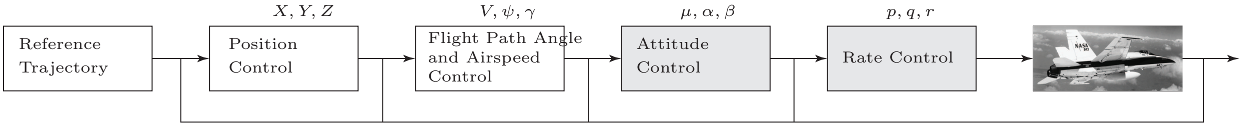

Fig. 1. Four loop feedback design for nonlinear flight control. We are focused on nonlinear dynamic inversion of the rate control loop in the following. Image credits: Sonneveldt (2010).

(1998); Bacon and Ostroff (2000); Bacon et al. (2000, 2001); Sieberling et al. (2010); Acquatella B. et al. (2012, 2013)), not in the geometric sense, but with respect to a *suffiently small* time-delay λ as

$$\begin{aligned}\dot{\omega} =\ & \dot{\omega}_0 + \frac{\partial}{\partial\omega}\big[f(\omega) + G(\omega)\delta\big]\Big|_{\substack{\omega=\omega_0\\ \delta=\delta_0}} (\omega - \omega_0)\\ & + \frac{\partial}{\partial\delta}\big[G(\omega)\delta\big]\Big|_{\substack{\omega=\omega_0\\ \delta=\delta_0}} (\delta - \delta_0) + \mathcal{O}(\Delta\omega^2, \Delta\delta^2)\\ \cong\ & \dot{\omega}_0 + f_0\,(\omega - \omega_0) + G_0\,(\delta - \delta_0)\end{aligned}$$

with

$$\dot{\omega}_0 \equiv f(\omega_0) + G(\omega_0)\delta_0 \tag{11a}$$

where $\omega_0 = \omega(t-\lambda)$ and $\delta_0 = \delta(t-\lambda)$ are the time-delayed signals of the current state ω and control δ, respectively. This means an approximate linearization about the $\lambda-$delayed signals is performed *incrementally.*

For such sufficiently small time-delay λ so that $f(\omega)$ does not vary significantly during λ, the following approximation holds

$$\epsilon(t) = f_0(\omega(t)) - f_0(\omega(t-\lambda)) \cong 0 \tag{12}$$

which leads to

$$\dot{\omega} \cong \dot{\omega}_0 + G_0 \cdot \Delta\delta \tag{13}$$

Here, $\Delta\delta = \delta - \delta_0 = \delta - \delta(t-\lambda)$ represents the so-called incremental control input. For the obtained approximation, NDI is applied to obtain a relation between the incremental control input and the output of the system

$$\delta = \delta_0 + G_0^{-1}\big[\nu - \dot{\omega}_0\big] \tag{14}$$

Note that the deflection angle δ_0 that corresponds to $\dot{\omega}_0$ is taken from the output of the actuators, and it has been assumed that a commanded control is achieved *sufficiently fast* according to the assumptions of the actuator dynamics in Eq. (5). The total control command along with the obtained linearizing control $\Delta\delta$ can be rewritten as

$$\delta(t) = \delta(t-\lambda) + G_0^{-1}\Big[\nu - \dot{\omega}(t-\lambda)\Big]. \tag{15}$$

Remark 1: By using the measured $\dot{\omega}(t-\lambda)$ and $\delta(t-\lambda)$ incrementally we practically obtain a robust, model-free controller with the self-scheduling properties of NDI.

The dependency of the closed-loop system on accurate knowledge of the dynamics in $f(\omega)$ is largely decreased, improving robustness against model uncertainties contained therein. Therefore, this implicit control law design is more dependent on accurate measurements or accurate estimates of $\dot{\omega}_0$, the angular acceleration, and δ_0, the deflection angles, respectively.

Notice, however, that typical INDI control laws are nevertheless also depending on effector blending models reflected in G_0, which makes this implicit controller susceptible to uncertainties in these terms. Instead, consider the following transformation as in (Chang and Jung (2009))

$$\dot{\omega} = H + \bar{g}\cdot\delta \tag{16}$$

with

$$H(t) = f(\omega) + (G(\omega) - \bar{g})\delta,$$

and with the following (but not limited) options for $\bar{g}$ (Chang and Jung (2009)), where $n = 3$ in our case

$$\bar{g}_1 = k_G{\cdot}\mathcal{I}_n = k_G\begin{bmatrix}1 & 0 & \cdots & 0\\ 0 & 1 & & \\ \vdots & & \ddots & \\ 0 & & & 1\end{bmatrix},\ \bar{g}_2 = \begin{bmatrix}k_{G_1} & 0 & \cdots & 0\\ 0 & k_{G_2} & & \\ \vdots & & \ddots & \\ 0 & & & k_{G_n}\end{bmatrix}.$$

Applying nonlinear dynamic inversion (NDI) to Eq. (16) results in an expression for the control input of the vehicle as

$$\delta(t) = \bar{g}^{-1}\big[\nu(t) - H(t)\big]. \tag{17}$$

Considering $H_0 = \dot{\omega}_0 - \bar{g}\cdot\delta_0$, the incremental counterpart of Eq.(17) results in a control law that is not depending on the aerodynamic model nor effector blending moments

$$\delta(t) = \delta(t-\lambda) + \bar{g}^{-1}\Big[\nu - \dot{\omega}(t-\lambda)\Big]. \tag{18}$$

Remark 2: The self-scheduling properties of INDI in Eq.(15) due to the term G_0 are now lost, suggesting that $\bar{g}$ should be an scheduling variable.

3.3 Time Delay Control and Proportional Integral control

Time delay control (TDC) (Chang and Jung (2009)) departs from the usual dynamic inversion input transformation of Eq.(16)

$$\delta = \bar{g}^{-1}\big[\nu - \bar{H}(t)\big] \tag{19}$$

where $\bar{H}$ denotes an estimation of H, being the nominal case when $\bar{H} = H$ which results in perfect inversion. Instead of having an estimate, the TDC takes the following assumption (Chang and Jung (2009))

$$\epsilon(t) \equiv H(t-\lambda) - H(t) \cong 0. \tag{20}$$

This relationship is used together with Eq.(16) to obtain what is called *time-delay estimation* (TDE) as the following

$$\bar{H} = H(t-\lambda) = \dot{\omega}(t-\lambda) - \bar{g}\cdot\delta(t-\lambda) \tag{21}$$

In addition, $\epsilon(t)$ is called TDE *error* at time t. Combining the equations we obtain the following TDC law

$$\delta(t) = \delta(t-\lambda) + \bar{g}^{-1}\big[\nu - \dot{\omega}(t-\lambda)\big] \tag{22}$$

which is in fact *equivalent* to the INDI control law obtained in Eq.(18). Appropriate selection of $\bar{g}$ must ensure stability

Preprint submitted to 20th IFAC World Congress. Received October 31, 2016.

according to (Chang and Jung (2009)), and ideally, this term should be tuned according to the best estimate of the true effector blending moment $\hat{g}(\tilde{\omega})$ for measured angular velocities $\tilde{\omega}$.

So far we have considered these derivations in continuous form. For practical implementations of these controllers and for the matters of upcoming discussions, sampled-time formulations involving continuous and discrete quantities as in (Chang and Jung (2009)) are more convenient. For that, considering that the smallest λ one can consider is the equivalent of the sampling period t_s of the digital device. The sampled formulation of Eq.(22) may be expressed as

$$\delta(k) = \delta(k-1) + \bar{g}^{-1}\big[\nu(k-1) - \dot{\omega}(k-1)\big] \tag{23}$$

where it has been necessary to consider ν at sample $k-1$ for causality reasons. Replacing the sampled virtual control ν according to Eq. (8) we have

$$\delta(k) = \delta(k-1) + \bar{g}^{-1}\big[\dot{e}(k-1) + k_P e(k-1)\big] \tag{24}$$

and we can consider the following finite difference approximation of the error derivatives as angular accelerations are not directly measured

$$\dot{e}(k) = [e(k) - e(k-1)]/t_s \tag{25}$$

Consider now the standard *proportional-integral* (PI) control

$$\delta(t) = K\big(e(t) + T_I^{-1}\int_0^t e(\sigma)\mathrm{d}\sigma\big) + \delta_{DC}, \tag{26}$$

where $K \in \mathcal{R}^{3\times3}$ denotes a diagonal (possibly time-varying) proportional gain matrix, $T_I \in \mathcal{R}^{3\times3}$ a constant diagonal matrix representing a reset or integral time, and $\delta_{DC} \in \mathcal{R}^3$ denotes a constant vector representing a trim-bias, which acts as a trim setting and is computed by evaluating the initial conditions. The number of PI gains is 6 except for δ_{DC}. The discrete form of the PI is given by

$$\delta(k) = K\big(e(k-1) + T_I^{-1}\sum_{i=0}^{k-1} T_s e(i)\big) + \delta_{DC} \tag{27}$$

When substracting two consecutive terms of this discrete formulation, we can remove the integral sum and achieve the so-called PI controller in incremental form

$$\delta(k) = \delta(k-1) + K\cdot t_s\big(\dot{e}(k-1) + T_I^{-1}\cdot e(k-1)\big) \tag{28}$$

Following the same steps, and for completeness, we also present the PID extension by simply considering the extra derivative term $\ddot{e}$

$$\delta(k) = \delta(k-1) + K\cdot t_s\big(T_D\ddot{e}(k-1) + \dot{e}(k-1) + T_I^{-1}\cdot \mathrm{e}(k-1)\big),$$

where $T_D \in \mathcal{R}^{3\times3}$ a constant diagonal matrix representing derivative time.

3.4 Equivalence of INDI/TDC/PI(D)

Having in mind the found the equivalence between INDI and TDC, and comparing terms from Eq. (24) with Eq. (28), we have the following relationships as originally found in (Chang and Jung (2009)) which are the relationship between the discrete formulations of TDC and PI in incremental form

$$K = (\bar{g}\cdot t_s)^{-1}, \quad T_I = k_P^{-1} \tag{29}$$

Whenever the system under consideration is of second-order controller canonical form, we will have error dynamics of the form $\ddot{e} + k_D\dot{e} + k_P e = 0$, and considering the newly introduced derivative gain k_D related to $\ddot{e}$ we have

$$K = k_D\cdot(\bar{g}\cdot t_s)^{-1}, \quad T_I = k_D\cdot k_P^{-1}, \quad T_D = k_D^{-1}, \tag{30}$$

This suggests not only that an equivalent discrete PI(D) controller with gains $< K,\, T_i,\, (T_d,) >$ can be obtained via INDI/TDC, but doing so is more meaningful and systematic than heuristic methods. This is because we begin the design from *desired* error dynamics given by Hurwitz gains $< k_P,\, (k_D,) >$ and what follows is finding the remaining effector blending gain $\bar{g}$ either analytically, whenever G is well known, or by tuning according with a proper estimate. As already mentioned, details on a sufficient condition for closed-loop stability under discrete TDC, and therefore applicable to its equivalent INDI, can be found in (Chang and Jung (2009)).

In essence, this procedure is more efficient and much less cumbersome than designing a whole set of gains iteratively. Moreover, for flight control systems, the self-scheduling properties of inversion-based controllers have suggested superior advantages with respect to PID controls since these must be gain-scheduled according to the flight envelope variations. The relationships here outlined suggests that PID-scheduling shall be done at the proportional gain K via the effector blending gain $\bar{g}$, and *not* over the whole set of gains $< K,\, T_i,\, (T_d,) >$.

4. LONGITUDINAL FLIGHT CONTROL SIMULATION

In this section, robust PI tuning via INDI is demonstrated with an example consisting of the tracking control design for a longitudinal launcher vehicle model. The second-order nonlinear model is obtained from (Sonneveldt (2010); Kim et al. (2004)), and it consists on longitudinal dynamic equations representative of a vehicle traveling at an altitude of approximately 6000 meters, with aerodynamic coefficients represented as third order polynomials in angle of attack α and Mach number M.

The nonlinear equations of motion in the pitch plane are given by

$$\dot{\alpha} = q + \frac{\bar{q}S}{mV_T}\Big[C_z(\alpha, M) + b_z(M)\delta\Big], \tag{31a}$$

$$\dot{q} = \frac{\bar{q}Sd}{I_{yy}}\Big[C_m(\alpha, M) + b_m(M)\delta\Big], \tag{31b}$$

where

$$\begin{aligned} C_z(\alpha, M) &= \varphi_{z1}(\alpha) + \varphi_{z2}(\alpha)M, \\ C_m(\alpha, M) &= \varphi_{m1}(\alpha) + \varphi_{m2}(\alpha)M, \\ b_z(M) &= 1.6238M - 6.7240, \\ b_m(M) &= 12.0393M - 48.2246, \end{aligned}$$

and

$$\begin{aligned} \varphi_{z1}(\alpha) &= -288.7\alpha^3 + 50.32\alpha\,|\alpha| - 23.89\alpha, \\ \varphi_{z2}(\alpha) &= -13.53\alpha\,|\alpha| + 4.185\alpha, \\ \varphi_{m1}(\alpha) &= 303.1\alpha^3 - 246.3\alpha\,|\alpha| - 37.56\alpha, \\ \varphi_{m2}(\alpha) &= 71.51\alpha\,|\alpha| + 10.01\alpha. \end{aligned}$$

These approximations are valid for the flight envelope of $-10° \le \alpha \le 10°$ and $1.8 \le M \le 2.6$. To facilitate the control design, the nonlinear missile model is rewritten in the more general state-space form as

$$\dot{x}_1 = x_2 + f_1(x_1) + g_1 u \tag{32a}$$
$$\dot{x}_2 = f_2(x_1) + g_2 u \tag{32b}$$

where:

$$x_1 = \alpha, \qquad x_2 = q$$
$$g_1 = C_1 b_z, \qquad g_2 = C_2 b_m$$

and

$$f_1(x_1) = C_1\big[\varphi_{z1}(x_1) + \varphi_{z2}(x_1)M\big], \qquad C_1 = \frac{\bar{q}S}{mV_T},$$
$$f_2(x_1) = C_2\big[\varphi_{m1}(x_1) + \varphi_{m2}(x_1)M\big], \qquad C_2 = \frac{\bar{q}Sd}{I_{yy}}.$$

The control objective considered here is to design a PI autopilot via INDI that tracks a smooth command reference y_r with the pitch rate x_2. It is assummed that the aerodynamic force and moment functions are accurately known and the Mach number M is treated as a parameter available for measurement. Moreover, for this second-order system in non-lower triangular form due to $g_1 u$ and $f_2(x_1)$, pitch rate control using INDI is possible due to the time-scale separation principle (Chu (2010); Sieberling et al. (2010)). With respect to actuator dynamics, we consider $K_a = 1$, and $\tau_a = 1e^{-2}$ in Eq.(5).

4.1 Pitch rate control design

First, introduce the rate-tracking error

$$z_2 = x_2 - x_{2_{ref}} \tag{33}$$

the z_2-dynamics satisfy the following error

$$\dot{z}_2 = \dot{x}_2 - \dot{x}_{2_{ref}} \tag{34}$$

for which we design the following exponentially stable *desired* error dynamics

$$\dot{z}_2 + k_{P_2} z_2 = 0, \quad k_{P_2} = 50 \text{ rad/s}. \tag{35}$$

According to the results previously outlined, the incremental nonlinear dynamic inversion control law design follows from considering the approximate dynamics around the current reference state for the dynamic equation of the pitch rate as in Eq. (13)

$$\dot{q} \cong \dot{q}_0 + \bar{g} \cdot \Delta\delta \tag{36}$$

assuming that pitch acceleration is available for measurement and the scalar $\bar{g}$ to be a factor of the accurately known estimate of g_2

$$\bar{g} = k_G \hat{g}_2, \quad k_G = 1.$$

This is rewritten in our formulation as

$$\dot{x}_2 \cong \dot{x}_{2_0} + \bar{g}\Delta u \tag{37}$$

where recalling that $\dot{x}_{2_0}$ is an incremental instance before $\dot{x}_2$, and therefore the incremental nonlinear dynamic inversion law is hence obtained as

$$u = u_0 + \bar{g}^{-1}\big(\nu - \dot{x}_{2_0}\big), \tag{38}$$

with

$$\nu = -k_{P_2} z_2 + \dot{x}_{2_{ref}}, \tag{39}$$

or more compactly

$$u = u_0 + \bar{g}^{-1}\big(- k_{P_2} z_2 - \dot{x}_{2_0} + \dot{x}_{2_{ref}}\big) \tag{40}$$

This results as desired, in the following z_2-dynamics

$$\dot{z}_2 = \dot{x}_{2_0} + \bar{g} \cdot \Delta u - \dot{x}_{2_{ref}}. \tag{41}$$

Notice that we are replacing the accurate knowledge of f_2 by a measurement (or an estimate) as $f_2 \cong \dot{x}_{2_0}$, which will result in a control law which is not entirely dependent on a model, hence more robust.

So far the incremental control laws are in continuous form, but these are usually implemented with *sampled*-time formulations. To that end, we replace the small λ with the sampling period t_s so that $t_k = k \cdot t_s$ is the $k-$th sampling instant at time k, and therefore

$$\begin{aligned} u(k) = u(k-1) + \\ \bar{g}^{-1}\big[- k_{P_2} z_2(k-1) - \dot{x}_2(k-1) + \dot{x}_{2_{ref}}(k-1)\big], \end{aligned} \tag{42}$$

where due to causality relationships we need to consider the independent variables at the same sampling time $k-1$.

Referring back to the derived relationship between INDI and PI control, the equivalent PI control in incremental form is

$$u(k) = u(k-1) + K \cdot t_s\big[\dot{z}_2(k-1) + T_I^{-1} z_2(k-1)\big], \tag{43}$$

with

$$K = (\bar{g} \cdot t_s)^{-1}, \quad T_I = k_{P_2}^{-1} \tag{44}$$

The nature of the desired error dynamics (proportional) gain k_{P_2} is therefore of an integral control action, whereas the effector blending gain $\bar{g}$ act as proportional control. Having designed for desired error dynamics, and for a given sampling time t_s, tuning a pitch rate controller is only a matter of selecting a proper effector blending gain $\bar{g}$ according to performance requirements.

Remark 3: Notice at this point that having the PI control in incremental form introduces a finite difference of the error state, which is the equivalent counterpart of what has been considered the acceleration or state derivative $\dot{x}_{2_0}$ in INDI controllers.

Remark 4: Notice also that designing the PI control gains via INDI is highly beneficial, since only the effector blending gain is the tuning variable. This strongly suggests that robust adaptive control can be achieved by scheduling this variable online during flight and not the whole set of gains.

Simulation results for the INDI/PI control are presented in Figure 2, considering smooth rate doublets for a nominal longitudinal dynamics model at Mach 2.0. The designed INDI gains of $k_{P_2} = 50$ rad/s and $k_G = 1$ are mapped to PI gains resulting in $K = 100\ \hat{g}_2^{-1}$ and $T_I = 0.02$ s, both controller showing the exact same performance and closed-loop response as expected.

With this example demonstrate how a self-scheduled PI can be tuned via INDI by departing from desired error dynamics with the gain k_{P_2}, and considering an accurate effector blending model estimate $\bar{g} = \hat{g}_2$.

5. CONCLUSIONS

This paper presented a meaningful and systematic method for PI(D) tuning of robust nonlinear flight control systems based on results previously reported in the robotics literature (Chang and Jung (2009)) regarding the relationship between *time-delay control* (TDC) and *proportional-*

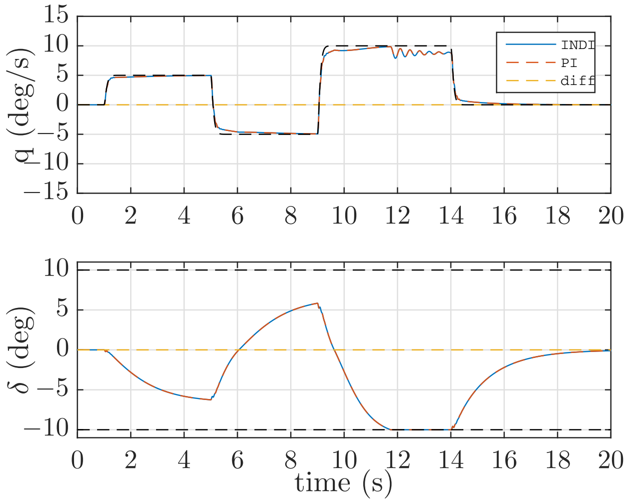

Fig. 2. INDI/PI tracking control numerical simulation of the nominal longitudinal flight model for $k_{P_2} = 50$ rad/s and $k_G = 1$

integral-derivative control (PID). The method was demonstrated in the context of an example for the longitudinal pitch rate tracking of a conventional nonlinear flight model, showing the same tracking performance under nominal conditions.

Being incremental nonlinear dynamic inversion (INDI) equivalent to TDC clearly suggests that imposing *desired* error dynamics, as usual for INDI control laws, and then mapping these into an equivalent incremental PI(D)-controller together with control derivatives leads to a meaningful and systematic PI(D) gain tuning method, which is very difficult to do heuristically.

We considered a reformulation of the plant dynamics inversion which reduces knowledge of the effector blending model (control derivatives) from the resulting control law, reducing feedback control dependency on accurate knowledge of both the aircraft/engine and effector blending models, hence resulting in robust and model-free control laws like the PI(D) control. Since usual flight control systems involves gain scheduling over the flight envelope, another key benefit of this result is that scheduling only the gain corresponding to the effector blending seems promising for adaptive control systems. Since the decoupling $\bar{g}$ is just dependent on the non-dimensional control derivatives scaled by dynamic pressure, this already yields a scheduling procedure of this term.

ACKNOWLEDGEMENTS

Markus Ruf and Gertjan Looye are acknowledged for discussions leading to improvements of this paper.

REFERENCES

Acquatella B., P., Falkena, W., van Kampen, E., and Chu, Q.P. (2012). Robust Nonlinear Spacecraft Attitude Control using Incremental Nonlinear Dynamic Inversion. In *AIAA Guidance, Navigation, and Control Conference*. American Institute of Aeronautics and Astronautics, Inc. (AIAA-2012-4623).

Acquatella B., P., van Kampen, E., and Chu, Q.P. (2013). Incremental Backstepping. In *EUROGNC Guidance, Navigation, and Control Conference*. American Institute of Aeronautics and Astronautics, Inc. (AIAA-2012-4623).

Bacon, B.J. and Ostroff, A.J. (2000). Reconfigurable Flight Control using Nonlinear Dynamic Inversion with a Special Accelerometer Implementation. In *AIAA Guidance, Navigation, and Control Conference and Exhibit*. American Institute of Aeronautics and Astronautics, Inc. (AIAA-2000-4565).

Bacon, B.J., Ostroff, A.J., and Joshi, S.M. (2000). Nonlinear Dynamic Inversion Reconfigurable Controller utilizing a Fault-tolerant Accelerometer Approach. Technical report, NASA Langley Research Center.

Bacon, B.J., Ostroff, A.J., and Joshi, S.M. (2001). Reconfigurable NDI Controller using Inertial Sensor Failure Detection & Isolation. *IEEE Transactions on Aerospace and Electronic Systems*, 37, 1373–1383.

Chang, P.H. and Jung, J.H. (2009). A Systematic Method for Gain Selection of Robust PID Control for Nonlinear Plants of Second-Order Controller Canonical Form. *IEEE Transactions on Control Systems Technology*, 17(2), 473–483.

Chen, H.B. and Zhang, S.G. (2008). Robust Dynamic Inversion Flight Control Law Design. In *ISSCAA 2008, 2nd International Symposium on Systems and Control in Aerospace and Astronautics*. doi: 10.1109/ISSCAA.2008.4776382.

Chu, Q.P. (2010). *Advanced Flight Control*. Lecture notes, Delft University of Technology, Faculty of Aerospace Engineering.

Kim, S.H., Kim, Y.S., and Song, C. (2004). A Robust Adaptive Nonlinear Control Approach to Missile Autopilot Design. *Control Engineering Practice*, 33(6), 1732–1742.

Sieberling, S., Chu, Q.P., and Mulder, J.A. (2010). Robust Flight Control Using Incremental Nonlinear Dynamic Inversion and Angular Acceleration Prediction. *Journal of Guidance, Control and Dynamics*, 33(6), 1732–1742.

Simplicio, P., Pavel, M., van Kampen, E., and Chu, Q.P. (2013). An Acceleration Measurements-based Approach for Helicopter Nonlinear Flight Control using Incremental Nonlinear Dynamic Inversion. *Control Engineering Practice*, 21(8), 10651077.

Slotine, J.J. and Li, W. (1990). *Applied Nonlinear Control*. Prentice Hall Inc.

Smeur, E.J., Chu, Q.P., and de Croon, G.C. (2016a). Adaptive Incremental Nonlinear Dynamic Inversion for Attitude Control of Micro Air Vehicles. *Journal of Guidance, Control and Dynamics*, 39(3), 450–461.

Smeur, E.J., de Croon, G.C., and Chu, Q.P. (2016b). Gust Disturbance Alleviation with Incremental Nonlinear Dynamic Inversion. In *IEEE/RSJ IROS*. IEEE.

Smith, P.R. (1998). A Simplified Approach to Nonlinear Dynamic Inversion Based Flight Control. In *AIAA Atmospheric Flight Mechanics Conference*, 762–770. American Institute of Aeronautics and Astronautics, Inc. (AIAA-98-4461).

Sonneveldt, L. (2010). *Adaptive Backstepping Flight Control for Modern Fighter Aircraft*. PhD thesis, Delft University of Technology, Faculty of Aerospace Engineering.

Bibliography

Acquatella B., P. (2011). *Robust Nonlinear Spacecraft Attitude Control: An Incremental Backstepping Approach.* MSc thesis, Delft University of Technology.

Acquatella B., P., Falkena, W., van Kampen, E.-J., & Chu, Q. P. (2012). Robust Nonlinear Spacecraft Attitude Control using Incremental Nonlinear Dynamic Inversion. *AIAA Guidance, Navigation, and Control Conference*(August). doi: 10.2514/6.2012-4623

Acquatella B., P., van Ekeren, W., & Chu, Q. (2017). PI (D) tuning for Flight Control Systems via Incremental Nonlinear Dynamic Inversion (unpublished). *20th International Federation of Automatic Control (IFAC) World Congress*.

Acquatella B., P., van Kampen, E.-j., & Chu, Q. (2013). Incremental Backstepping for Robust Nonlinear Flight Control. *Proceedings of the EuroGNC 2013, 2nd CEAS Specialist Conference on Guidance, Navigation & Control*, 1444–1463. doi: 10.2541/1.49978

Ali, A., Chu, Q., van Kampen, E., & de Visser, C. (2014). Exploring Adaptive Incremental Backstepping using Immersion and Invariance for an F-16 aircraft. In *Aiaa guidance, navigation, and control conference.* doi: 10.2541/6.2014-0084

Bacon, B., Ostroff, A. J., & Joshi, S. (2001). Reconfigurable NDI Controller Using Inertial Sensor Failure Detection & Isolation. *Aerospace and Electronic Systems, IEEE Transactions on*, *37*(4), 1373–1383. doi: 10.1109/7.976972

Belcastro, C. M., & Foster, J. V. (2010). Aircraft Loss-of-Control Accident Analysis. *AIAA Guidance, Navigation and Control Conference*. doi: 10.2514/6.2010-8004

Boeing Commercial Airplanes. (2010). *Statistical Summary of Commercial Jet Airplane Accidents* (Tech. Rep.).

Bugajski, D. J., Enns, D. F., & Elgersma, M. R. (1990). A Dynamic Inversion Based Control Law With Application To The High Angle-of-Attack Research Vehicle. *Guidance, Navigation and Control Conference*, 826–839. doi: 10.2514/6.1990-3407

Chang, P. H., & Jung, J. H. (2009). A systematic method for gain selection of robust PID control for nonlinear plants of second-order controller canonical form. *IEEE Transactions on Control Systems Technology*, *17*(2), 473–483. doi: 10.1109/TCST.2008.2000989

Chen, H. B., & Zhang, S. G. (2008). Robust Dynamic Inversion Flight Control Law Design. *2nd International Symposium on Systems and Control in Aerospace and Astronautics*(7), 1–6. doi: 10.1109/ISSCAA.2008.4776382

Chu, Q. (2014). *Advanced Flight Control.* Course lecture slides, Delft University of Technology.

da Costa, R. R., Chu, Q. P., & Mulder, J. A. (2003). Reentry Flight Controller Design Using Nonlinear Dynamic Inversion. *Journal of Spacecraft and Rockets*, *40*(1), 64–71. doi: 10.2514/2.3916

Doman, D. B., & Ngo, A. (2002). Dynamic Inversion-Based Adaptive/Reconfigurable Control of the X-33. *Journal of Guidance, Control and Dynamics*, *25*(2), 275–284.

Dong, W., Farrell, J. A., Polycarpou, M. M., Djapic, V., & Sharma, M. (2012). Command filtered adaptive backstepping. *IEEE Transactions on Control Systems Technology*, *20*(3), 566–580. doi: 10.1109/TCST.2011.2121907

Edwards, C., Lombaerts, T., & Smaili, H. (2010). *Fault Tolerant Flight Control.* Springer. doi: 10.1007/978-3-642-11690-2

European Aviation Safety Agency (EASA). (2014). *Annual Safety Review 2013* (Tech. Rep.). European Aviation Safety Agency. doi: 10.2822/50513

Farrell, J., Polycarpou, M., & Sharma, M. (2003). Adaptive Backstepping With Magnitude, Rate, and Bandwidth Constraints: Aircraft Longitude Control. *Proceedings of the 2003 American Control Conference, 2003.*, *5*, 3898–3904. doi: 10.1109/ACC.2003.1240444

Farrell, J., Sharma, M., & Polycarpou, M. (2005). Backstepping-Based Flight Control with Adaptive Function Approximation. *Journal of Guidance, Control, and Dynamics*, *28*(6), 1089–1102. doi: 10.2514/1.13030

Farrell, J. A., Polycarpou, M., Sharma, M., & Dong, W. (2008). Command Filtered Backstepping. In *American control conference* (Vol. 54, pp. 1391–1395). doi: 10.1109/ACC.2008.4586773

Hoe, G., Owens, D. B., & Denham, C. (2012). Forced Oscillation Wind Tunnel Testing for FASER Flight Research Aircraft. *AIAA Atmospheric Flight Mechanics Conference*, 1–12. doi: 10.2514/6.2012-4645

Kanellakopoulos, I., Kokotovic, P., & Morse, A. (1991). Systematic Design of Adaptive Controllers For Feedback Linearizables Systems. *IEEE Transactions on Automatic Control*, *36*(11), 1241–1253. doi: 10.1109/9.100933

Khalil, H. K. (1996). *Nonlinear Systems.* Prentice Hall. doi: 10.1007/978-1-4757-3108-8

Klamer, J. (2007). *UAV Helicopter Nonlinear Flight Control.* MSc thesis, Delft University of Technology.

Kokotovic, P. (1992). *The joy of feedback: nonlinear and adaptive* (Vol. 12). doi: 10.1109/37.165507

Krstić, M. (1995). *Nonlinear and Adaptive Control Design.* Wiley.

Krstić, M., Kanellakopoulos, I., & Kokotovic, P. V. (1994). Nonlinear design of adaptive controllers for linear systems. *IEEE Transactions on Automatic Control*, *39*(4), 738–752. doi: 10.1109/9.286250

Mulder, J., van Staveren, W., van der Vaart, J., de de Weerdt, E., in 't Veld, A., & Mooij, E. (2011). *Flight Dynamics.* AE3202 Course lecture reader, Delft University of Technology.

Ochi, Y., & Kanai, K. (1991). Design of Restructurable Flight Control Systems Using Feedback Linearization. *Journal of Guidance, Control, and Dynamics*, *14*(5), 903–911. doi: 10.2541/3.20730

Owens, B., Cox, D. E., & Morelli, E. A. (2006). Development of a Low-Cost Sub-Scale Aircraft for Flight Research: The FASER Project. *AIAA Aerodynamic Measurement Technology and Ground Testing Conference*, 1–11. doi: 10.2514/6.2006-3306

Sieberling, S., Chu, Q. P., & Mulder, J. A. (2010). Robust Flight Control Using Incremental Nonlinear Dynamic Inversion and Angular Acceleration Prediction. *Journal of Guidance, Control, and Dynamics*, *33*(6), 1732–1742. doi: 10.2514/1.49978

Slotine, L. (1991). *Applied Nonlinear Control.* Prentice Hall.

Smeur, E. J. J. (2016). Adaptive Incremental Nonlinear Dynamic Inversion for Attitude Control of Micro Aerial Vehicles. *Journal of Guidance, Control, and Dynamics*, *39*(3), 450–461. doi: 10.2514/1.G001490

Smith, P. R. (1998). A Simplified Approach to Nonlinear Dynamic Inversion Based Flight Control. In *Aiaa atmospheric flight mechanics conference and exhibit* (pp. 762–770).

Steinberg, M. (2005). Historical Overview of Research in Reconfigurable Flight Control. *Proceedings of the Institution of Mechanical Engineers, Part G: Journal of Aerospace Engineering*, *219*(4), 263–275. doi: 10.1243/095441005X30379

Stevens, B. L., & Lewis, F. L. (2003). *Aircraft Control and Simulation.* Wiley.

Van Gils, P. (2015). Adaptive Incremental Backstepping Flight Control for a High-Performance Aircraft with Uncertainties. *AIAA Guidance, Navigation, and Control Conference*. doi: 10.2541-6.2016/1380

Vlaar, C. (2014). *Incremental Nonlinear Dynamic Inversion flight control.* MSc thesis, Delft University of Technology.

Williams, J. E., & Vukelich, S. R. (1979). *The USAF Stability and Control Digital DATCOM. Volume I. Users Manual.*

Zhang, Y., & Jiang, J. (2008). Bibliographical review on reconfigurable fault-tolerant control systems. *Annual Reviews in Control*, *32*(2), 229–252. doi: 10.1016/j.arcontrol.2008.03.008